

UNIVERSITY OF BELGRADE  
FACULTY OF MECHANICAL ENGINEERING

Muamar M. Benisa

**INTEGRATED PROCESS PLANNING,  
DIE-DESIGN AND SIMULATION IN  
SHEET METAL RUBBER FORMING**

Doctoral Dissertation

Beograd, 2013

UNIVERZITET U BEOGRADU  
MAŠINSKI FAKULTET

Muamar M. Benisa

**INTEGRISANO PROJEKTOVANJE  
TEHNOLOŠKOG PROCESA, ALATA I  
SIMULACIJA PROCESA IZRADA  
DELOVA OD LIMA U ALATIMA SA  
GUMENIM JEZGROM**

doktorska disertacija

Beograd, 2013

## EXAMINATION COMMITTEE

**Supervisor:** Dr Bojan Babić, professor  
University of Belgrade, Faculty of Mechanical  
Engineering

**Members:** Dr Zoran Stefanović, professor  
University of Belgrade, Faculty of Mechanical  
Engineering

Dr Aleksandar Sedmak, professor  
University of Belgrade, Faculty of Mechanical  
Engineering

Dr Aleksandar Grbović, assistant professor  
University of Belgrade, Faculty of Mechanical  
Engineering

Dr Marko Rakin, associate professor  
University of Belgrade, Faculty of Technology and  
Metallurgy

**Date of defence**

**Комисија за оцену и одбрану дисертације:**

**Ментор:**

Др Бојан Бабић, редовни професор  
Универзитет у Београду, Машински факултет

**Чланови комисије:**

Др Зоран Стефановић, редовни професор  
Универзитет у Београду, Машински факултет

Др Александар Седмак, редовни професор  
Универзитет у Београду, Машински факултет

Др Александар Грбовић, доцент  
Универзитет у Београду, Машински факултет

Др Марко Ракин, ванредни професор  
Универзитет у Београду, Технолошко металуршки

факултет

**Датум одбране:**

## DEDICATION

To my parents, my wife and my kids Mariam Mohamed, Maha, Mihad and Abdulgader

# Acknowledgment

First of all I would like to express my praises and sincere thanks to Almighty Allah, start with no end and end will never start, for his divine assistance and guidance, which gave me the ability to succeed.

I would like to express my deep appreciation and gratitude to my supervisor professor Dr. **Bojan Babic** for his guidance, advise, interest, encouragement and assistance in this work.

I want to thank Dr. **Aleksandar Grbovic** for all his continues help, support, interest and valuable hints

My sincere appreciation, thanks and gratitude to the academic staff members of my faculty , all are my friends.

My sincere appreciation, thanks and gratitude to the laboratory staff members of my faculty, all are my friends.

My sincere appreciation, thanks and gratitude to the Libyan General People's Committee of higher education which gave me scholarship and have supported me to my further education.

My sincere appreciation, thanks and gratitude to my family, specially my parents - to my mother being with Allah, may peace upon her - , for their suport and incorage me throughout all my study life.

My sincere appreciation, thanks and gratitude to my wife for her patience during the period of my study.

# INTEGRATED PROCESS PLANNING, DIE-DESIGN AND SIMULATION IN SHEET METAL RUBBER FORMING

## **Abstract**

To produce a new component there is a trial and error stage to obtain a sheet metal part without defects, which strongly depends on an operator's skill and experience. At the design stage, the experience of the designer and manufacturers should give an important aid to reduce trials to enable the minimization of response time and cost with the maximization of the product quality. Rubber pad forming highly improves the formability of the blank because the contact surfaces between the rigid die and the rubber pad are flexible. This method enables production of sheet metal components with the complex contour at relatively low cost because only one rigid die is required. However, in the aerospace field, parts are produced in small sheet metal bending and small number of components. It means that large investments are cost-effective for the production of structures formed by the sheet metal press. For these reasons it is recommendable to use finite element (FE) simulation of the manufacturing process during the conceptual design [1]. Moreover, it could give important answers in the analyses of the processes and could predict the defects that may occur. Therefore, the modifications can be easily done before the tool manufacturing and part production.

This thesis is concerned with a forming simulation of aluminum alloy parts and investigation of significant parameters (such as forming force and stress, and strain distribution in a blank) associated with the rubber-pad forming process and the capabilities of this process regarding the manufacturing of the aircraft tail ribs. These finite element models of rubber pad forming process are studied in this dissertation to investigate the effect of tool geometry for supporting ribs with the lightening hole of the aircraft tail. The different tool geometries for supporting ribs with the lightening hole are

used to optimize the tool geometry and to find out the right design of the tool for a defect free product. The simulation and investigation carried out identifies the stress and strain distributions in a blank as well as the forming force. This research shows a good correlation between FE simulations and experimental results.

The springback and wrinkling phenomena have been taken into account during sheet metal forming using rubber pad forming process in order to get the right final product. The prediction of the springback angle is presented, with the focus on the straight rib and the rib with the lightening hole in different tool geometries. The numerical simulations using Finite Element Method (FEM) have been performed for different bend radii. The FEM simulation in 2D and 3D have been used to analyze both the springback and wrinkling phenomena in order to reduce influence of these phenomena on the final shape of the horizontal tail ribs.

The study conducted within this thesis shows that FE simulations results watched with experimental results in term of the springback angle prediction and wrinkling phenomena.

**Keywords:** Rubber pad forming, sheet metal forming, FE M simulation, Optimization, springback, wrinkling

**Scientific field:**

Technical science, Mechanical Engineering

**Narrow scientific field:**

Production Engineering

UDC 621.98:621.73 (043.3)

# ИНТЕГРИСАНО ПРОЈЕКТОВАЊЕ ТЕХНОЛОШКОГ ПРОЦЕСА, АЛАТА И СИМУЛАЦИЈА ПРОЦЕСА ИЗРАДЕ ДЕЛОВА ОД ЛИМА У АЛАТИМА СА ГУМЕНИМ ЈЕЗГРОМ

## Абстракт

При производњи делова од лима без дефеката користи се приступ покушаја и грешака, који значајно зависи од искуства и вештине оператора. У фази пројектовања искуство пројектанта и пројектанта технолошког процеса би требало да допринесе смањењу броја покушаја потребних за минимизацију времена одзива и трошкова уз максимизацију производности и квалитета. Обрада у алатима са језгром од гуме значајно унапређује обрадљивост дела од лима зато што су контактне површине између крутог дела калупа и гуменог језгра флексибилне. Овај метод омогућује израду комплексних делова од лима уз ниске трошкове јер је потребан смо један део калупа од чврстог материјала. У области аерокосмонаутике делови се производе у малим серијама. То значи да није исплативо да се не исплате веће инвестиције за алате у производњи делова од лима. Из тог разлога препоручује да се током концептуалног пројектовања примењује метода коначних елемената за симулацију технолошког процеса. На тај начин се могу добити значајни одговори у вези анализе процеса и могу се предвидети дефекти који могу настати током обраде. На тај начин се могу направити потребне модификације пре израде алата и израде делова.

Ова теза се бави симулацијом израде делова од легура алуминијума и истраживањем фактора обраде као што су деформациона сила, напони и деформације повезане са процесом обраде у алату са гуменим језгром, као и могућностима овог процеса за израду делова који представљају ребра репа авиона.

Модели процеса израде делова у алатима од гуме засновани на методи коначних елемената проучени у овој тези су коришћени за истраживање утицаја ефекта геометрије алата за израду ребара са отвором. Различите геометрије алата су коришћене у циљу оптимизације геометрије алата у циљу израде делова без дефеката. На основу симулационих експеримента је идентификована расподела напона и деформација у делу од лима. У истраживању је демонстрирана добра корелације између симулација коначним елементима и експерименталних резултата.

Посебно су истраживани ефекти еластичног враћања и гужвања током израде делова од лима. Приказано је предвиђање угла еластичног враћања посебно за обично ребро и за ребро са отвором. Нумеричке симулације засноване на методи коначних елемената (МКЕ) су изведене за различите радијусе савијања. МКЕ симулације у 2D и 3D су коришћене за анализу еластичног враћања и гужвања у циљу смањења утицаја ових феномена на коначни облик хоризонталних репних ребара.

Спроведена истраживања у оквиру тезе су показале висок степен поклапања између резултата добијених експериментално и симулацијом методом коначних елемената, а везано за предвиђање угла еластичног враћања и феномена гужвања.

**Кључне речи:** Обрада лима у алатима са гуменим језгром, Симулација методом коначних елемената, Оптимизација, Еластично враћање

**Научна област:**

Техничке науке, Машинство

**Ужа научна област:**

Производно машинство

UDC 621.98:621.73 (043.3)

## TABLE OF CONTANT

|   |    |
|---|----|
| 1. INTRODUCTION .....                                     | 1  |
| 1.1 METHODOLOGY AND HYPOTHESES OF THE THESIS .....        | 3  |
| 1.2 RESEARCH OBJECTIVE AND APPROACH .....                 | 6  |
| 1.4 ORGANIZATION OF THE DISSERTATION.....                 | 7  |
| 2. STATE OF THE ART REVIEW.....                           | 10 |
| 3. SHEET METAL FORMING .....                              | 20 |
| 3.1 SIGNIFICANT MATERIAL PROPERTIES IN SHEET FORMING..... | 23 |
| 3.2 METAL BEHAVIOUR IN SHEET FORMING: .....               | 25 |
| 3.3 FLEXIBLE SHEET METAL FORMING PROCESSES: .....         | 26 |
| 3.3.1 Hydroforming: .....                                 | 27 |
| 3.3.2 Hot Metal Gas Forming .....                         | 30 |
| 3.3.3 Viscous Pressure Forming.....                       | 32 |
| 3.3.4 Rubber-Pad Forming:.....                            | 34 |
| 4. OVERVIEW OF SHEET METAL RUBBER FORMING.....            | 37 |
| 4.1 THE GUERIN PROCESS .....                              | 37 |
| 4.2 THE MARFORM PROCESS .....                             | 40 |
| 4.3 THE VERSON-WHEELON PROCESS.....                       | 41 |
| 4.4 THE DEMAREST PROCESS .....                            | 43 |
| 4.5 THE VERSON HYDROFORM PROCESS.....                     | 44 |
| 4.6 SAAB RUBBER-DIAPHRAGM PROCESS .....                   | 46 |
| 4.7 BULGING PUNCHES .....                                 | 47 |
| 4.8 MASLENNIKOV'S PROCESS .....                           | 49 |
| 4.9 TUBE BULGING .....                                    | 50 |
| 4.10 FLEXIBLE TOOL MATERIALS .....                        | 52 |
| 4.11 INDUSTRIAL APPLICATION OF RUBBER PAD FORMING .....   | 52 |

|  |     |
|--|-----|
| 5. DIE DESIGN IN CAD -CAM ENVIRONMENT IN SHEET METAL FORMING.....  | 54  |
| 5.1 CATIA IN RUBBER PAD FORMING PROCESS .....  | 54  |
| 6. FINITE ELEMENT ANALYSES OF SHEET METAL RUBBER PAD FORMING PROCESS .....   | 71  |
| 6.1. MAJOR STEPS IN FEA .....  | 72  |
| 6.2. TYPES OF STRUCTURAL PROBLEMS THAT CAN BE ANALYZED BY FEM.....   | 73  |
| 6.3. NONLINEARITY.....   | 74  |
| 6.3.1. Geometric Nonlinearity .....  | 74  |
| 6.3.2. Material Nonlinearity.....  | 75  |
| 6.3.3. Changing-Status Nonlinearity .....  | 76  |
| 6.4. MESH DENSITY .....  | 77  |
| 6.5. COMPUTER AIDED ENGINEERING WITH ANSYS .....   | 79  |
| 6.5.1. Organization of ANSYS Software .....  | 79  |
| 6.5.1.1 ANSYS Analysis Approach.....   | 79  |
| 6.5.1.2. ANSYS Preprocessor .....  | 80  |
| 6.5.1.3. ANSYS Solution Processor .....  | 80  |
| 6.5.1.4. ANSYS General Postprocessor .....   | 81  |
| 6.5.1.5 ANSYS Time History Postprocessor.....  | 81  |
| 6.6. ANSYS WORKBENCH INTERFACE .....   | 81  |
| 6.6.1. Elastic versus Plastic Materials .....  | 85  |
| 6.6.2. Test Data Needed for Hyperelasticity: .....   | 86  |
| 7. NUMERICAL MODELING OF RUBBER PAD FORMING PROCESS... 88  |     |
| 7.1. FINITE ELEMENT MODELLING OF THREE DIFFERENT SHEET METAL ELEMENTS .... 88  |     |
| 7.1.1. Results obtained in FEM Simulations and Discussion:.....  | 94  |
| 7.2. OPTIMIZATION OF THE SHEET METAL FORMING TOOL GEOMETRY IN A RUBBER PAD FORMING PROCESS WITH FLEXIBLE PUNCH- NUMERICAL APPROACH. .... | 100 |
| 7.2.1 Results and Discussion: .....  | 104 |

|   |     |
|---|-----|
| 7.3. USING FEA IN SPRINGBACK SIMULATIONS.....                       | 117 |
| 7.3.1. Finite Element Analysis of Springback.....                   | 120 |
| 7.4. WRINKLING IN FORMED RIBS USING RUBBER PAD FORMING PROCESS..... | 135 |
| 8. EXPERIMENTAL VALIDATION OF NUMERICAL RESULTS.....                | 145 |
| 9. CONCLUSIONS AND RECOMMENDATIONS:.....                            | 170 |
| 9.1 CONCLUSIONS: .....  | 170 |
| 9.2 RECOMMENDATIONS.....  | 174 |
| LIST OF REFERENCES: .....   | 175 |

## List of figures:

|  |    |
|--|----|
| FIGURE 1. 1 GENERAL PERCEPTION OF FLOWCHART FOR METHODOLOGY AND<br>HYPOTHESES OF THESIS.....                                     | 5  |
| FIGURE2. 1 SCHEMATIC REPRESENTATION OF RUBBER-PAD FORMING PROCESS B)<br>GEOMETRY MODEL OF RUBBER PAD FORMING.....                | 11 |
| FIGURE3. 1 BULGES FORMING OF TUBES USING HYDRO FORMING PROCESS.....  | 28 |
| FIGURE3. 2 SHEET HYDRO FORMING PROCESS .....   | 29 |
| FIGURE3. 3 HYDRO-FORMED BELLOWS USING A CIRCULAR INSERT RING WITH AXIAL<br>FEEDING .....   | 29 |
| FIGURE3. 4 HYDRO-FORMED TUBE DOUBLE SHEET COMPONENT .....  | 30 |
| FIGURE3. 5 HOT METAL GAS FORMING PROCESS .....   | 31 |
| FIGURE3. 6 MAGNESIUM ALLOY TUBE AFTER HOT METAL GAS FORMING .....  | 32 |
| FIGURE3. 7 VISCIOUS PRESSURE FORMING PROCESS .....   | 33 |
| FIGURE3. 8. CORRUGATED SURFACE SHAPE OF A NICKEL-BASED SUPER ALLOY<br>SPECIMEN FORMED BY VISCIOUS PRESSURE FORMING PROCESS ..... | 34 |
| FIGURE3. 9 DIFFERENT RUBBER-PAD FORMING OPERATIONS.....  | 36 |
| FIGURE4. 1 GUERIN PROCESS TOOL .....   | 38 |
| FIGURE4. 2 TYPICAL CROSS SECTIONS OF FORM BLOCKS WITH AUXILIARY TOOLS.....   | 40 |

|   |    |
|---|----|
| FIGURE4. 3 TOOLING AND SETUP FOR RUBBER-PAD FORMING BY THE MARFORM<br>PROCESS .....                                 | 41 |
| FIGURE4. 4 VERNON-WHEELON PROCESSES .....   | 43 |
| FIGURE4. 5 DEMAREST FORMING PROCESS .....   | 44 |
| FIGURE4. 6 VERNON HYDROFORM PROCESS.....  | 45 |
| FIGURE4. 7 SAAB RUBBER-DIAPHRAGM PROCESS .....  | 47 |
| FIGURE4. 8 STAGES OF THE SAAB FLUID-FORM METHOD OF PRESS WORKING .....  | 47 |
| FIGURE4. 9 BULGING PUNCHES PROCESS .....  | 49 |
| FIGURE4. 10 MASLENNIKOV'S DEEP DRAWING PROCESS.....   | 50 |
| FIGURE4. 11 BULGING T JOINT WITH RUBBER ROD .....   | 51 |
| FIGURE4. 12 FREE BULGES FORMING OF TUBE USING RUBBER ROD .....  | 51 |
| FIGURE4. 13 EXAMPLES FORMED RIBS USING RUBBER PAD FORMING PROCESS.....  | 53 |
| FIGURE5. 1 CREATION OF UPPER SURFACE OF AIRFOIL USING CATIA'S OPTION<br>SPLINE.....                                 | 57 |
| FIGURE5. 2 CREATION OF LOWER SURFACE OF AIRFOIL USING CATIA'S OPTION<br>SPLINE.....                                 | 57 |
| FIGURE5. 3 DESIGN OF SURFACES OF AIRFOIL USING COMMAND EXTRUDE .....  | 58 |
| FIGURE5. 4 BASIC WALL OF THE RIB CREATED USING COMMAND WEB .....  | 58 |
| FIGURE5. 5 SURFACIC FLANGE DEFINED BY THE LOWER SURFACE OF AIRFOIL .....  | 60 |
| FIGURE5. 6 SURFACIC FLANGE DEFINED BY THE UPPER SURFACE OF AIRFOIL .....  | 60 |
| FIGURE5. 7 FLANGE OBTAINED USING COMMAND FLANGE.....  | 61 |
| FIGURE5. 8 TWO JOGGLES DEFINED ON SURFACIC FLANGES USING COMMAND<br>JOGGLE.....                                     | 62 |
| FIGURE5. 9 EXACT POSITION OF THE FLANGED HOLE MUST BE DEFINED FIRST .....   | 63 |
| FIGURE5. 10 PARAMETERS NECESSARY TO DEFINE FLANGED HOLE.....  | 63 |
| FIGURE5. 11 FINAL SHAPE OF THE RIB WITH LIGHTENING HOLE USED IN 3D FEM<br>SIMULATIONS AS DESIGNED IN CATIA v5 ..... | 64 |
| FIGURE5. 12 SHAPE OF THE BLANK OBTAINED USING COMMAND UNFOLD.....   | 64 |
| FIGURE5. 13 CREATION OF SURFACES EQUIVALENT TO INTERNAL FACES OF RIB,<br>USING COMMAND OFFSET SURFACE .....         | 65 |

|   |    |
|---|----|
| FIGURE5. 14 SHAPE OF THE SURFACE AFTER USING COMMANDS FILL AND JOIN .....   | 65 |
| FIGURE5. 15 FINAL SHAPE OF THE TOOL FOR RIB WITH LIGHTENING HOLE.....   | 66 |
| FIGURE5. 16 RIB WITH LIGHTENING HOLE AND APPROPRIATE TOOL.....  | 66 |
| FIGURE5. 17 CUT VIEW OF THE RIB WITH LIGHTENING HOLE AND APPROPRIATE TOOL.  | 67 |
| FIGURE5. 18 DIMENSIONS OF THE RIB WITH LIGHTENING HOLE .....  | 67 |
| FIGURE5. 19 MACHINING OPERATIONS USED IN SIMULATION OF RIB TOOL<br>MANUFACTURING:.....  | 70 |
| FIGURE6. 1 THREE-DIMENSIONAL FINITE ELEMENT MESH OF THE BLANK FOR RIB<br>WITH A LIGHTENING HOLE .....   | 72 |
| FIGURE6. 2 STRESS STRAIN CURVES PRESENTED IN ANSYS IN ENGINEERING DATA .....  | 75 |
| FIGURE6. 3 2D SYMMETRICAL MESH OF RIB WITH A LIGHTENING HOLE USING RUBBER<br>PAD FORMING PROCESS .....  | 79 |
| FIGURE6. 4 CLASSIC ANSYS INTERFACE .....  | 81 |
| FIGURE6. 5 COMMAND FILE.....  | 82 |
| FIGURE6. 6 ANSYS WORKBENCH .....  | 82 |
| FIGURE6. 7 STATIC STRUCTURAL COMPONENTS.....  | 84 |
| FIGURE6. 8 THE TESTS DATA FOR DICRIE HYPERLESTIC MODEL ,A) UNIAXIAL<br>TENSILE TEST ,B) UNIAXIAL COMPRESSIVE TEST C) SHEAR TEST .....                               | 87 |
| FIGURE7. 1: GEOMETRICAL MODELS USED IN INVESTIGATION: STRAIGHT RIB (A),<br>STRINGER (B) AND RIB WITH A LIGHTENING HOLE (C).....                                     | 89 |
| FIGURE7. 2: CONSTRAINTS USED IN FE SIMULATION .....   | 90 |
| FIGURE7. 3: EXPERIMENTAL TENSILE STRESS- STRAIN CURVE FOR ALUMINUM BLANK<br>SHEET .....   | 91 |
| FIGURE7. 4: FORMING STEPS DURING THE RUBBER-PAD FORMING: A) STRAIGHT RIB, ....  | 94 |
| FIGURE7. 5: CONVERGENCE OF FORMING FORCE FOR A) STRAIGHT RIB,B) STRINGER<br>AND C) RIB WITH A LIGHTENING HOLE .....   | 95 |
| FIGURE7. 6: FORMING FORCES IN THREE MODELS .....  | 96 |
| FIGURE7. 7: EQUIVALENT STRESS (LEFT COLUMN) AND PLASTIC STRAIN (RIGHT<br>COLUMN) IN STRAIGHT RIB, STRINGER AND RIB WITH A LIGHTENING HOLE (FROM<br>THE TOP).. ..... | 98 |

|   |     |
|---|-----|
| FIGURE7. 8: GEOMETRY PARAMETERS VARIED IN FE SIMULATIONS OF RUBBER PAD FORMING.....   | 101 |
| FIGURE7. 9: CONSTRAINTS AS APPLIED IN SYMMETRY FE MODEL OF RIB WITH LIGHTEN HOLE.....   | 102 |
| FIGURE7. 10: RIGID PUNCH, SHEET METAL AND RUBBER PAD MODELS.....  | 103 |
| FIGURE7. 11: INFLUENCE OF GEOMETRY PARAMETERS ON PLASTIC STRAIN DURING RUBBER PAD FORMING PROCESS: A) CASE ONE, B) CASE TWO.....                  | 105 |
| FIGURE7. 12: RI=1 MM A) FIRST CASE (RII, RIII, AND H EQUAL 2 MM) B) SECOND CASE (RII, RIII, AND H EQUAL 3 MM).....                                | 110 |
| FIGURE7. 13 :RI=1.5 MM A) FIRST CASE (RII, RIII, AND H EQUAL 2MM) B) SECOND CASE (RII, RIII, AND H EQUAL 3MM).....                                | 110 |
| FIGURE7. 14: H=4.5 MM A) FIRST CASE (RI, RII AND RIII EQUAL 2 MM) B) SECOND CASE (RI, RII AND RIII EQUAL 3 MM).....                               | 111 |
| FIGURE7. 15: RI=2.5 MM A) FIRST CASE (RII, RIII AND H EQUAL 2 MM) B) SECOND CASE (RII, RIII AND H EQUAL 3 MM).....                                | 111 |
| FIGURE7. 16: RII=3 MM A) FIRST CASE (RI, RIII, AND H EQUAL 2 MM) B) SECOND CASE (RI, RIII, AND H EQUAL 3 MM).....                                 | 112 |
| FIGURE7. 17: H=1.5 MM A) FIRST CASE (RI, RII, AND RIII EQUAL 2 MM) B) SECOND CASE (RI, RI, AND RIII EQUAL 3 MM).....                              | 112 |
| FIGURE7. 18: THE INFLUENCE OF RIII ON THE FILLING THE CAVITY OF THE TOOL RIB  | 113 |
| FIGURE7. 19: RANDOMLY SELECTED GEOMETRY PARAMETERS.....   | 114 |
| FIGURE7. 20: MORE RANDOMLY SELECTED GEOMETRY PARAMETERS.....  | 116 |
| FIGURE7. 21: SPRINGBACK PARAMETERS.....   | 119 |
| FIGURE7. 22: DEFINITION OF DIE PARAMETERS.....  | 122 |
| FIGURE7. 23: VON MISSES STRESS IN RUBBER FORMING PROCESS FOR STRAIGHT RIB DURING A) LOADING FORMING PROCESS AND B) UNLOADING FORMING PROCESS..... | 124 |
| FIGURE7. 24: INFLUENCE OF THE BEND RADIUS IN STRAIGHT RIB ON THE SPRINGBACK FACTOR.....   | 125 |
| FIGURE7. 25: OVERBENDING IN RUBBER PAD FORMING PROCESS FOR STRAIGHT RIB ...   | 126 |

|  |     |
|--|-----|
| FIGURE7. 26: SPRINGBACK IS NOT PRESENTED IN RIB WITH LIGHTEN HOLE WHEN A) RI= 1MM AND B) RI=1.5MM .....  | 127 |
| FIGURE7. 27 INFLUENCE OF THE BEND RADII RI AND RII IN RIB WITH LIGHTEN HOLE ON THE SPRINGBACK FACTOR K.....  | 128 |
| FIGURE7. 28: SPRINGBACK IS NOT PRESENTED WHEN RII= 1MM IN RIB WITH LIGHTEN HOLE .....  | 129 |
| FIGURE7. 29: CONSTRAINS APPLIED IN SYMMETRICAL 3D MODEL FOR THE SIMULATION OF THE FORMING OF STRAIGHT RIB USING RUBBER PAD TECHNIQUE.....                | 131 |
| FIGURE7. 30: 3D FE MESH OF SYMMETRICAL MODEL USED IN SIMULATION OF THE FORMING OF STRAIGHT RIB USING RUBBER PAD TECHNIQUE.....                           | 132 |
| FIGURE7. 31: 3D FEM SIMULATION OF RUBBER PAD FORMING PROCESS OF SYMMETRICAL MODEL OF STRAIGHT RIB: A) LOAD STEP B) UNLOAD STEP.....                      | 133 |
| FIGURE7. 32: FEM SIMULATION OF ONE HALF OF THE RIB OF LIGHT AIRCRAFT HORIZONTAL TAIL USING RUBBER PAD FORMING PROCESS: A) LOAD STEP, B) UNLOAD STEP..... | 134 |
| FIGURE7. 33 CONSTRAINTS APPLIED IN 3D MODEL FOR THE SIMULATION OF THE FORMING OF RIB WITH LIGHTENING HOLE USING RUBBER PAD TECHNIQUE.....                | 136 |
| FIGURE7. 34: FE MESH USED IN ANALYSIS OF SYMMETRICAL MODEL OF THE RIB FORMING USING RUBBER PAD.....  | 137 |
| FIGURE7. 35: FE SIMULATION OF FORMING THE RIB WITH LIGHTENING HOLE USING RUBBER PAD FORMING PROCESS: A) FIRST STEP, B) FINAL STEP .....                  | 138 |
| FIGURE7. 36: FE SIMULATION OF FORMING A BLANK OF RIB WITH LIGHTENING HOLE  | 139 |
| FIGURE7. 37: WRINKLING IN FEM MODEL OF FORMED RIB WITH LIGHTENING HOLE .   | 140 |
| FIGURE7. 38: UNDESIRABLE 3D MODEL RESULT RIB.....  | 141 |
| FIGURE7. 39: OPTIMIZATION OF THE BLANK SHAPE.....  | 142 |
| FIGURE7. 40: 3D MODEL OF THE RIB AFTER REDESIGN .....  | 142 |
| FIGURE8. 1 HYDRAULIC PRESS MACHINE AND EXPERIMENTAL RUBBER PAD FORMING SET-UP .....  | 145 |
| FIGURE8. 2: A) SCHEMATIC REPRESENTATION OF THE ASSEMBLY OF A DIE SET B) EXPERIMENTAL SET-UP .....  | 146 |

|   |     |
|---|-----|
| FIGURE8. 3: FORCE TRANSDUCER OF TYPE U10M 125KN.....  | 147 |
| FIGURE8. 4: POSITION OF THE DISPLACEMENT TRANSDUCER PM2S 150MM USED IN<br>EXPERIMENTS.....  | 148 |
| FIGURE8. 5 :POSITION OF STRAIN GAUGES USED ON THE BLANK FOR RIB WITH<br>LIGHTENING HOLE.....  | 148 |
| FIGURE8. 6 CABLES AND CONNECTORS USED TO TRANSMIT MEASURED VALUES TO THE<br>ACQUISITION SYSTEM .....  | 149 |
| FIGURE8. 7:SPIDER8 ACQUISITION SYSTEM .....   | 150 |
| FIGURE8. 8: SCREENSHOT OF MACH3 SOFTWARE WINDOWS.....   | 151 |
| FIGURE8. 9: CNC MACHINE USED FOR WOODEN TOOLS MANUFACTURING.....  | 151 |
| FIGURE8. 10: MACHINING OPERATIONS USED IN RIB TOOL MANUFACTURING: .....   | 152 |
| FIGURE8. 11: WOODEN TOOLS FOR RIBS OF HORIZONTAL TAIL.....  | 153 |
| FIGURE8. 12:UNFOLDED RIBS (BLANKS) PREPARED FOR CUTTING .....   | 154 |
| FIGURE8. 13: CUTTING THE BLANKS ON FLEXICAM MACHINE .....   | 155 |
| FIGURE8. 14: BLANKS MADE OF ALUMINUM 2024-T3 USED IN EXPERIMENTS.....   | 155 |
| FIGURE8. 15: BLANKS FIXED IN TOOLS FOR EXPERIMENTS.....   | 156 |
| FIGURE8. 16: SHAPES OF RIBS FORMED BY RUBBER PAD ON EXPERIMENTAL SET-UP .....   | 157 |
| FIGURE8. 17: SPRINGBACK IN TWO RIBS FORMED BY RUBBER PAD .....  | 158 |
| FIGURE8. 18: SPRINGBACK OBTAINED IN (A) EXPERIMENT AND (B) FEM SIMULATION .....   | 159 |
| FIGURE8. 19: SMALL CRACK INITIATED IN AREA WITH OUTER RADIUS $R_{II}$ .....   | 160 |
| FIGURE8. 20: THE CRACK APPEARED IN THE AREA OF RADIUS $R_{II}$ (A) AS PREDICTED BY<br>FE CALCULATIONS (B).....  | 161 |
| FIGURE8. 21: NEW STEEL TOOL FOR RIB WITH LIGHTENING HOLE .....  | 162 |
| FIGURE 8. 22: RIB WITH LIGHTENING HOLE FORMED ON STEEL TOOL.....  | 162 |
| FIGURE8. 23: SEVERAL HORIZONTAL TAIL RIBS MANUFACTURED ON STEEL TOOLS .....   | 163 |
| FIGURE8. 24: ELIMINATION OF WRINKLES ON RIB'S FLANGE .....  | 164 |
| FIGURE8. 25: COMPARISON OF THE WRINKLES OBTAINED ON RIB WITH LIGHTENING<br>HOLE IN (A) FEM SIMULATION AND (B) EXPERIMENT WITH RUBBER PAD FORMING<br>PROCESS ..... | 165 |

|  |     |
|--|-----|
| FIGURE8. 26 COMPARISON OF THE WRINKLES OBTAINED ON STRAIGHT RIB IN (A) FEM SIMULATION AND (B) EXPERIMENT WITH RUBBER PAD FORMING PROCESS.....  | 166 |
| FIGURE8. 27: MATERIAL OVERLAPPING ON RIB IN (A) FEM SIMULATION AND (B) EXPERIMENT WITH RUBBER PAD FORMING PROCESS. SOME AMOUNT OF SPRINGBACK IS ALSO OTICEABLE.....                      | 167 |
| FIGURE8. 28 ACCEPTABLE WRINKLING ON REDESIGNED RIB OBTAINED IN (A) FEM SIMULATION AND (B) EXPERIMENT WITH RUBBER PAD FORMING PROCESS. SOME AMOUNT OF SPRINGBACK IS ALSO NOTICEABLE ..... | 169 |

## LIST OF TABLES

|  |     |
|--|-----|
| TABLE7. 1 INTERFACE CONTACT .....  | 92  |
| TABLE7. 2 NUMBER OF NODES AND ELEMENTS FOR THREE MODELS .....  | 93  |
| TABLE 7. 3 SUMMARIZATION OF RESULTS OBTAINED IN THE RUBBER-PAD SHEET METAL FORMING SIMULATIONS.....  | 97  |
| TABLE 7. 4 VALUES OF EQUIVALENT STRESS, PLASTIC STRAIN AND REACTION FORCE OBTAINED IN FE SIMULATIONS WITH FIXED VALUES OF $R_{II}$ , $R_{III}$ AND $H$ (FIRST CASE 2 MM, SECOND CASE 3 MM) AND CHANGEABLE VALUE OF $R_I$ ..... | 106 |
| TABLE 7. 5 VALUES OF EQUIVALENT STRESS, PLASTIC STRAIN AND REACTION FORCE OBTAINED IN FE SIMULATIONS WITH FIXED VALUES OF $R_I$ , $R_{III}$ AND $H$ (FIRST CASE 2 MM, SECOND CASE 3 MM) AND CHANGEABLE VALUE OF $R_{II}$ ..... | 107 |
| TABLE 7. 6 VALUES OF EQUIVALENT STRESS, PLASTIC STRAIN AND REACTION FORCE OBTAINED IN FE SIMULATIONS WITH FIXED VALUES OF $R_I$ , $R_{II}$ AND $H$ (FIRST CASE 2 MM, SECOND CASE 3 MM) AND CHANGEABLE VALUE OF $R_{III}$ ..... | 108 |
| TABLE 7. 7 VALUES OF EQUIVALENT STRESS, PLASTIC STRAIN AND REACTION FORCE OBTAINED IN FE SIMULATIONS WITH FIXED VALUES OF $R_I$ , $R_{II}$ AND $R_{III}$ (FIRST CASE 2 MM, SECOND CASE 3 MM) AND CHANGEABLE VALUE OF $H$ ..... | 109 |
| TABLE 7. 8 VALUES OF SPRINGBACK FACTOR $K$ AND OVERBEND ANGLE FOR STRAIGHT RIB WHEN BEND RADIUS $R$ IS CHANGEABLE WHERE THE OTHER GEOMETRY PARAMETERS ARE FIXED .....  | 129 |

TABLE 7. 9 VALUES OF SPRINGBACK FACTOR  $K$  AND OVERBEND ANGLE FOR RIB WITH LIGHTENING HOLE WHEN BEND RADIUS  $R_{II}$  IS CHANGEABLE WHERE THE OTHER GEOMETRY PARAMETERS ARE FIXED ..... 130

TABLE 7. 10 VALUES OF SPRINGBACK FACTOR  $K$  AND OVERBEND ANGLE FOR RIB WITH LIGHTENING HOLE WHEN BEND RADIUS  $R_{II}$  IS CHANGEABLE WHERE THE OTHER GEOMETRY PARAMETERS ARE FIXED ..... 130

## 1. Introduction

There are other alternatives to form complex shape beside conventional forming processes such as deep drawing, bending, stretching, stamping and blanking. Sheet metal rubber pad forming, also known as flexible die forming, uses a rubber diaphragm as one half of a tool in sheet metal forming. This method requires only one solid tool half, which is usually the punch. The rubber pad is used to distribute equal pressure on all work piece surfaces as it is pressed around the form block. Rubber pad forming is designed for the use of fabricating parts with relatively complex shape.[1]

In aircraft industry most of the sheet metal parts such as frames, seat parts, ribs, windows, and doors are produced using rubber pad forming process. In other industries, for instance automotive industry and military application, this process is mainly used for prototypes or pilot productions. Therefore, it is suitable mostly for small series (typical of aircraft industry)[1, 2, 3].

In most cases, the formability of the various parts is determined experimentally or based on the empirical experience of the designer. This often led to formability problems even in common parts, and when new materials or totally new parts were introduced, the designer did not have any experience to rely on. For these parts, prototype tools were made based on the experience of tool design engineers. The prototype tools and parts were tested until an acceptably good part was formed. This required many changes and adjustments to provide the hard tooling, which should also go through a series of try-outs involving minor (or in many cases major) modifications until the final good part was produced. This methodology in stamping practice resulted in considerable time and cost with long lead times.

Most of industrial companies are very keen on reducing the time for the manufacturing of new stamping tool sets with the consequent saving of costs

and resources. It can be stated that the expected role of finite element simulation is to meet these requirements. The simulation may be effectively performed at different stages of design and manufacturing to support decision-making. The first simulation need arises at the design stage. The purpose of the simulation at this stage is to make a rough estimation as to whether the parts to be manufactured can be formed or not. If the answer is “no”, the design must be modified. However, at this stage the geometry of the parts is not fully described in a CAD system and no tool data exist. A so-called one-step simulation codes are particularly suited for these purposes. One-step FEM simulation is also easy to use and provides quick results, which allows the product designer to make the necessary changes at the right time.

As the product has been designed and validated as „formable“ the development cycle enters the process and die design stage where a more precise simulation is required. At this stage, the die geometry is modeled by a CAD surface description and thus the modification of die data can be made quite easily according to the simulation results. The performance of an integrated CAD and simulation system is crucial for obtaining well optimized stamping steps and die shapes in the very limited time allocated to the production tool design.

Simulation is also required at the try-out stage to find a solution to avoid forming defects such as fracture, springback and wrinkling appearing during the try-out. In order to study the mechanism of origination and propagation of defects, a systematic series of simulations should be performed and the information obtained should be used efficiently in the next new model. Assuming that the finite element simulation is powerful enough to predict all the forming defects and provide optimum stamping tools and conditions, the prototype tools may be completely eliminated from the design and manufacturing procedure, and the number of trials and modifications can be significantly reduced. Thus, the process might be shortened dramatically. This

is the most ideal scenario for finite element simulation in sheet metal forming in industry.

In sheet metal forming, modeling and simulation can be used for other purposes, for example to predict material flow, to analyse stress-, strain- and temperature-distribution, to determine forming forces, to forecast potential sources of defects and failures, to improve part quality and complexity and to reduce manufacturing costs. Nowadays, modeling and simulation are often integrated parts of product and process design in an integrated manufacturing environment.

The finite element (FE) simulations of a sheet metal forming process help the manufacturing engineer to design the forming process by shifting the costly press shop try-outs to the computer-aided design environment.

One of the main drawbacks in industrial practice, hindering the (even more wide) application of simulation techniques, is that the output results of simulation packages are usually not directly and easily usable for computer aided die design. Obviously, there are tremendous efforts to successfully link CAD and FEM systems. However, there is still a lot to do in this field. It is important to emphasize that good solutions require a fully integrated approach of computer aided product design, process planning and die design, as well as the finite element simulation of the forming processes. It means that simulation tools should be efficiently used throughout the whole product development cycle.

### **1.1 Methodology and Hypotheses of the Thesis**

Numerical simulations of manufacturing processes of rubber pad forming have been introduced in the past for the purpose of finding and solving the problems encountered in production. Better understanding of rubber pad forming process (included in the numerical simulations for instance) may have significant contributions with respect to the prediction of defects of this process and obtaining a defect-free part, which mainly depends on the operator's skill

and experience. When the number of product parts is small, it is necessary to use finite element simulations of manufacturing process during the conceptual design. In order to perform simulations, models must be built first and then modification can be easily done before the tool manufacturing and part production. In this thesis CATIA V5 will be used to create geometry models of the light aircraft ribs and tools, while ANSYS 14.5 will be used to simulate the rubber pad forming process. The theoretical models will also be experimentally validated.

Computer aided engineering (CAE) has a vital and central role in the recent developments in rubber pad forming, concerning the whole product development cycle. The application of various methods and techniques of CAE activities resulted in significant developments. The CAE tool provides significant advantages both in the design and in the manufacturing phase. Today, sheet metal forming simulation results are already reliable and accurate enough that even tryout tools and the time consuming tryout processes may be eliminated or at least significantly reduced. An increase in productivity can be achieved if the part geometry, the fabrication method, the die design and the material properties are specified during the design stage.

To meet these requirements, computer-aided engineering systems are being developed and applied to sheet metal forming. This allows for a scientific approach combined with the know-how of experienced designers to develop a novel design methodology and process control strategy in rubber pad forming. The CAE system development for this purpose should be able to simulate the specific rubber pad forming process accurately and study the sheet metal behavior during the process. This would require the system to have a mathematical model which describes the process and necessary modules to incorporate the experience-based knowledge into the system. Such a system would serve as a powerful design aid tool for designers to explore alternative

designs, evaluate trade-off and arrive at optimal designs at the lowest cost and shortest lead times (Figure1.1).

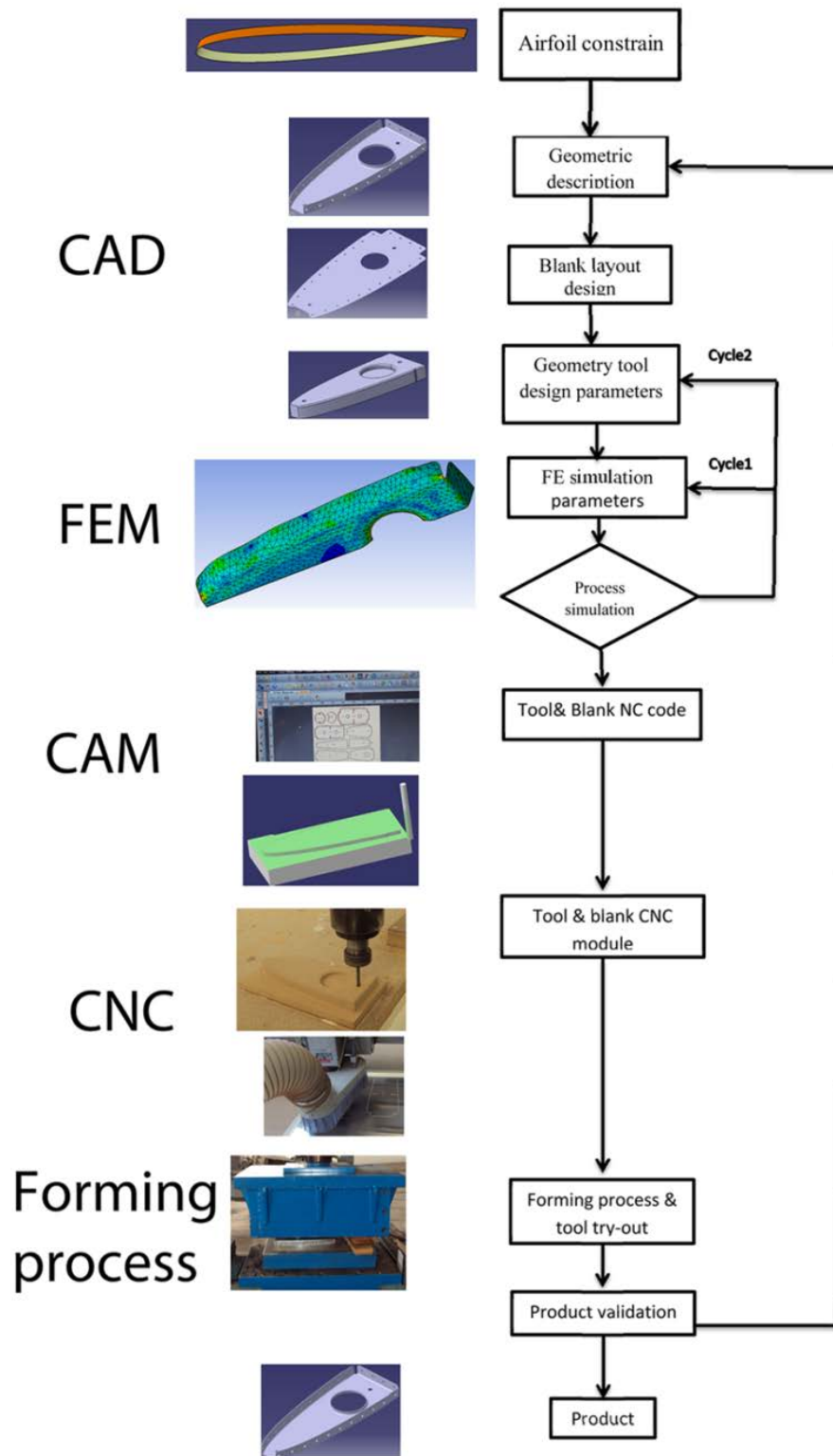


Figure1. 1 General perception of flowchart for Methodology and Hypotheses of thesis

## 1.2 Research Objective and Approach

This dissertation deals with the application of rubber pad forming process and description of this process regarding the manufacturing of aircraft tail ribs. The main aims of investigations were development of numerical models which would be able to successfully simulate the rubber pad forming process, development of the methodology for process planning and die design in a CAD environment, as well as the methodology of die tool optimization in the rubber forming process.

Finite element method was used for blank and rubber behavior analysis during the forming process. The study was concerned with the simulation and investigation of the significant parameters (such as forming force and stress and strain distributions in a blank), associated with the rubber-pad forming process and capabilities of this process regarding the manufacturing of aircraft tail ribs.

For the purpose of achieving the main goal of the dissertation, CATIA V5 was used for supporting the process planning and die design tasks, while FEM software ANSYS v14.5 was used for numerical simulations. The selection of these two program packages can be explained by several reasons. On the one hand, both the CATIA V5 and the ANSYS 14.5 are among the most widely applied packages in the aircraft industry in the world. On the other hand, these two systems are among the first who offered a special interface module to enhance the information and data exchange between CAD modeling and FEM simulations in both directions, making possible the most efficient integration during the whole product development cycle.

Based on few existing solutions, new methodology was developed in two main modules: a mathematical-based analysis module (ANSYS 14.5), and design-rule and knowledge-based module (a parametric CAD package CATIA V5).

The overall objective is to improve sheet metal forming using the rubber pad forming process through the use of process simulation, by: (a) improving

existing sheet material characterization techniques, (b) understanding the influence of tool variables in rubber pad forming and (c) investigating the effect of tool geometry for supporting ribs of a tail, for the purpose of optimizing the tool geometry and finding out the right design of the blank and solid tool geometry.

#### **1.4 Organization of the Dissertation**

This dissertation is divided into eight chapters. The contents of each chapter are as follows:

- Chapter 1 This chapter presents basic information about the need to design the methodology and simulation of the technological process of sheet metal rubber pad forming and the organization of the dissertation.
- Chapter 2: This chapter presents a state-of-the-art review of the sheet metal plastic deformation with the emphasis on the sheet of rubber pad forming technology.
- Chapter 3 This chapter gives a brief overview of a fixable sheet metal forming technology. This chapter also analyzes the characteristics of materials under plastic deformation. It provides an overview of the influential factors on the choice of materials. It also analyzes the behavior of materials in processing plastic deformation that significantly affects the quality and accuracy of manufactured parts from sheet metal. In this way, there are basic elements for the design of the technological process of sheet metal parts as well as the modeling and simulation process.
- Chapter 4: This chapter presents the methods of sheet metal rubber pad forming, and illustrates the basic principles of each method. The emphasis is given to the industrial application of the methods of sheet metal rubber pad forming process, especially for the production of parts in the aerospace industry.

Chapter 5 In this chapter the dissertation is given the concept design of sheet metal parts and tools for their development in the CAD/CAM environment. Through relevant examples this chapter presents steps in modeling the parts, the design of solid work tools, and generated NC programs for its development. The details of simulation development tools are also added.

Chapter 6: This chapter is devoted to the analysis of the finite element method (FEM) of sheet metal rubber pad forming. It also explains the main steps of the analysis. The FEM analysis has defined objectives and structural problems that are analyzed. In particular, the application of ANSYS software package for engineering analysis and calculations, and analyzed aspects of the application of elastic, plastic, as well as hyperelastic materials are discussed.

Chapter 7: This chapter is focused on numerical modeling of the rubber pad forming process with discussion. Using commercial software ANSYS.FEM the finite of three different sheet metal elements were introduced in the simulation to optimize the sheet metal forming process and the effect of tool geometry. It also presents the FEM analysis of the springback and wrinkling phenomena in formed ribs using the rubber pad forming process.

Chapter8:This chapter illustrates experimental set-up of the rubber pad forming process. The experimental verification of the results from the numerical simulation presented in the previous chapter is illustrated. For experiments hard part tools (molds) are made of wood from CAD models and NC programs generated by the CAM, as it has already been shown in previous chapters. A hydraulic press is used in the production of parts. The experimental verification of the results from the previous chapter is presented. A comparison is made of numerical results obtained by simulations and experimental

results obtained by measuring the appropriate parameters during the production of real parts. According to the previous comparison, the results obtained by the simulation are fully verified results obtained by experiments.

Chapter 9: This chapter presents some conclusions based on the previously presented experimental and FEM simulation results and discussion, while there is also a proposal for further research.

## 2. State of the art review

Stamping is a metal-forming process, with which the sheet metal is punched using a press tool that is mounted on a machine or a stamping press forming the sheet into the desired shape. The conventional stamping process is performed through a punch, which, together with a blank holder, forces the sheet metal to slide into a die and comply with the shape of the die itself.

Rubber-pad forming, also known as flexible-die forming, employs a rubber pad or a flexible diaphragm as one tool half, requiring only one solid tool half to form a part to final shape. The solid tool half is usually similar to the punch in a conventional die, but it can be the die cavity. The rubber acts somewhat like a hydraulic fluid in exerting nearly equal pressure on all workpiece surfaces as it is pressed around the form block. Rubber-pad forming is designed to be used on moderately shallow, recessed parts having simple flanges and relatively simple configurations. Form block height is usually less than 100 mm. The production rates are relatively high, with cycle times averaging 1 min or less [1.2].

This forming process is a metalworking process where sheet metal is pressed between a die and a rubber block. In general, an elastic upper die, usually made of rubber, is connected to a hydraulic press. A rigid lower die, often called a form block, provides the mold for the sheet metal to be formed. Because the upper (male) die can be used with separate lower (female) dies, the process is relatively cheap and flexible. However, rubber-pads exert less pressure in the same circumstances than non-elastic parts, which may lead to less definition in forming.

In the rubber-pad forming process the blank is placed between the die and rubber-pad (flexible punch), which is later held in a container to enclose the flexible punch (Figure 2.1). At this stage, the flexible punch (rubber-pad) is fixed on the arm of a pressing machine and the punch is on a machine table. As the rubber-pad is moving down, the rubber deforms elastically and offers a counter

pressure. Due to this pressure the rubber-pad and the blank flow into the cavity of the die.

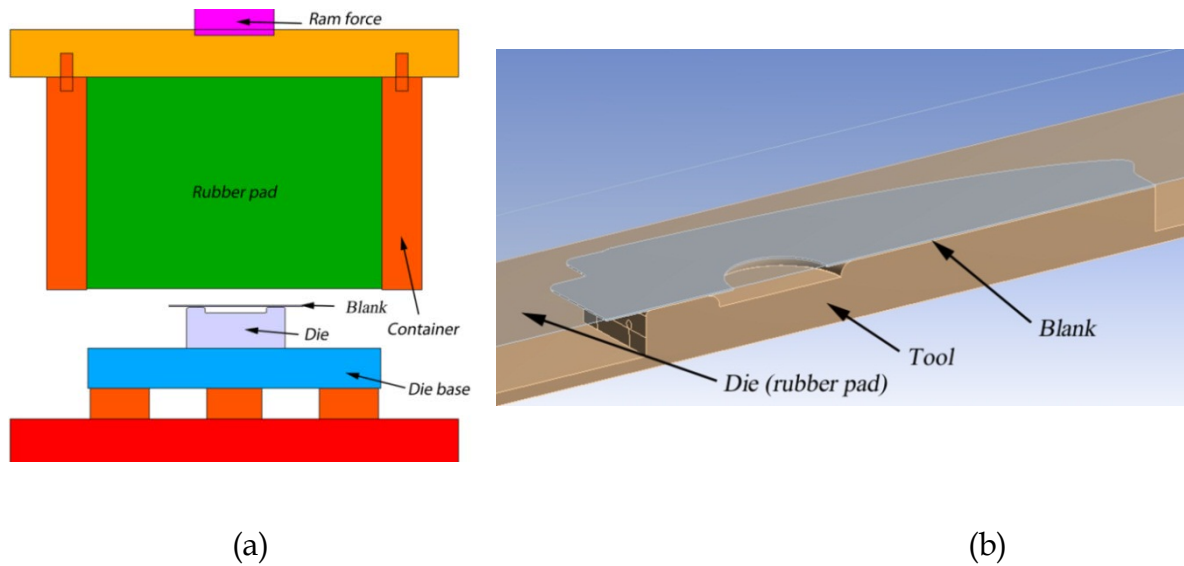


Figure2. 1 Schematic representation of rubber-pad forming process b) Geometry model of rubber pad forming

The sheet metal parts formed using rubber-pad forming can take a more severe formed shape compared to the conventional tools because the direction of the force is not limited to one direction as in the case of conventional metal forming. The multi-directional nature of the force from the rubber pad produces variable radius during forming and this enhances uniform elongation of the workpiece. This characteristic of rubber-pad forming makes it a cost effective process and flexible for low volume product series such as in aircraft structural parts and skin components. More than half of all formed aircraft structural metal parts are made using the rubber-pad forming techniques such as ribs, frames, doors and windows. The large variation in terms of size, geometry and thickness and the small quantity of the product series typical of the aircraft manufacturing industry, are the reasons for the adoption of flexible and low cost production processes such as rubber pad forming. This process is also used

in the manufacturing of home appliance parts, curved panels for buildings, moldings, utensils and parts drawn from pre-finished sheets [1,2].

The advantages of using the rubber-pad forming processes instead of conventional forming processes are that:

- Only a single rigid tool half is required to form a part
- One rubber pad or diaphragm takes the place of many different die shapes, returning to its original shape when the pressure is released
- Tools can be made of low cost, easy-to-machine materials due to the hydrostatic pressure exerted on the tools
- The forming radius decreases progressively during the forming stroke, unlike the fixed radius on conventional dies
- Thinning of the work metal, as occurs in conventional deep drawing, is reduced considerably
- Different metals and thicknesses can be formed in the same tool
- Parts with excellent surface finish can be formed as no tool marks are created

Set-up time is considerably shorter as no lining-up of tools is necessary

However the rubber pad forming process has certain disadvantages such as:

- The pad or diaphragm has a limited lifetime that depends on the severity of the forming in combination with the pressure level
- Lack of sufficient forming pressure results in parts with less sharpness or with wrinkles, which may require subsequent hand work
- The production rate is relatively slow, making the process suitable primarily for prototype and low volume production work.

- The process cannot be used at elevated temperatures due to the restricted temperature range within which rubber can be used.

Numerous studies have been conducted on traditional sheet metal forming methods such as deep drawing and mechanical stretch, where both methods required a male and a female die for proper forming of a part. Much less literature is available on rubber pad forming process, which uses flexible punch (only one solid tool half to form a part in the final shape). In this chapter a review of the literature focusing on the most recent experimental and numerical studies related to rubber pad forming process will be presented.

Thiruvarudchelvan[2] (1993) presented in this overview, highlighted the role of urethanes that are considered to be the best material for flexible tools because of their good oil and solvent resistance, good wear resistance, high thermal stability and load bearing capacity.

Sala [3] (2001) optimized the Guerin rubber pad forming process of an aluminum alloy fuselage frame belonging to AerMacchi MB-339 trainer aircraft using own finite element code. Several effects, depending on stamping velocity, component geometry, heat treatment of sheet metal, and rubber-pad parameters have been investigated. His work shows how the preliminary tuning of these parameters leads to minimizing defects, increasing component quality and reducing set-up times.

Browne and Battikha [4] (1995) presented the capability of the rubber pad forming process and optimized the process parameters to find out a product without defects. They analyzed the use of different types of lubricants at the blank and its interfaces. The dependence of the clamping force for the prevention of wrinkling and cracking on the type of blank material was also investigated

Thiruvarudchelvan [5] (2002) and Thiruvarudchelvan and Tan [6] (2005) have introduced several techniques for the use of flexible tools in metal forming

and developed the role of urethane in the design of metal forming tool such as sheet metal ashtray, plates, a tube bulging technique, a novel blank holding technique for deep drawing of cups of different shapes and redrawing of cups. They presented the principals involved in friction-aided sheet metal forming techniques, the design of the flexible tools, the actual prototype devices fabricated and tested, and the experimental data from forming operations.

Dirikolu and Akdemir [7] (2004) Investigated the influence of rubber hardness and blank material type on stress distribution using a 3D finite element simulation study concerning the flexible forming process. The investigation showed that variation of pad thickness would not impart a big change on forming stress in the blank. The influences of the rubber pad hardness and the stress distribution during the forming process in different blank material types have been presented. They also investigated contact friction, die design crucial parameters that required adjustment before actual operation.

Peng et al. (2009) [8] presented the micro/meso sheet soft punch stamping process to fabricate the micro channel via numerical simulation and experiments. They have analyzed in details the significant parameters related to this process, such as grain size, hardness of soft punch and lubrication condition. The numerical results have partially been validated experimentally. They found that sheet metal with small grain size is prone to obtain high formability. Larger friction coefficient (up to 0.3) between the sheet and the rigid die may increase the sheet thinning, which decreases the formability, and makes the metal sheet more difficult to flow as the friction coefficient increases, while the friction between the sheet metal and the soft punch is not an important factor. They also reported that the hardness of soft punch is not a decisive parameter to the final quality of the workpiece.

Fabrication of a metallic bipolar plate for the use in PEM fuel cells is presented in Yanxiong Liu, Lin Hua 2010 [9]. The FE analyses were used to

---

describe the rubber-pad forming process and to investigate main parameters such as rubber hardness and dimensions of the rigid die (the draft angle  $\alpha$ , outer radius  $R$ , and internal radius  $r$ ). It was found that the smaller internal radius is, the harder it is to fill the cavity of a rigid die. The formability of the blank increases as the outer radius and draft angle increases. The smaller the internal radius, the more difficult it is to fill the die cavity. The authors examined whether the blank filled the cavity of the rigid die or not by using 3D laser scanning measurements system. The hardness of the rubber pad is not an important parameter for the formation of a bipolar plate. The thickness distribution of the formed bipolar plate is uneven. The product had high surface quality because the die material has low stiffness. The amount of springback is very small. They found out the overall cost to producing bipolar plates can be reduced by using rubber pad forming process. Furthermore, the estimated cost of a double bipolar plate manufactured by rubber pad forming process with a non-coated SS304 is \$1.9.

Antonio [10](2011) presented numerical simulation of the rubber pad forming process of an aluminum alloy aeronautic component. Several effects, depending on stamping strategy, component geometry and rubber pad characterization were taken in account. His work showed the capability to produce shallow formed parts with a reduced metal thinning. Based on the FE analysis, the minimum available fillet radii for aluminum sheet have been found in term of the proposed measure. To decrease the minimum concave fillet radius, the fillet radius of the punch should be increased. A rubber hardness effect on the blank deformation becomes prominent when the concave radii increase.

M.W. Fu and H. Li[11] (2009) presented 3D-FE simulations and investigated the deformation behavior of the flexible die forming process (FDF). The comparison between the conventional deep drawing and viscoplastic pressure carrying medium (VPCM) based on flexible die forming was

conducted in terms of wall thickness reduction, hydrostatic pressure variation, principle stress distribution and damage factor. The deformation behavior is revealed for three typical workpiece including barrel, conic, and parabolic geometries. The FE simulation for three parts has been connected to predict and explore the deformation characteristics of the VPCM-based FDF process.

Ramezani [12](2010) presented an experimental study for the rubber-pad forming process to stamp aluminum blank and investigated the effect of the rubber type and stamping velocity on the process. Finite element simulation was used to analyze the process and deformation mechanics during the rubber pad forming process and compared with experimental measurements to validate the finite element model. He found that silicone rubber had shorter lifetime compared to polyurethane and natural rubber. As a result, it cannot be used to form blank with sharp edges. Rubber pad forming process reduced the thinning phenomena in the formed part, compared to conventional forming process. The maximum thinning in the specimen is 11.7% using the natural rubber while the thinning decreases to 10.4% for using polyurethane rubber and 10.6% using silicon rubber as a flexible punch. No significant change in the blank thinning was discovered for 5 different stamping velocities. This is a case of a good agreement between the experimental and finite element result.

Fabrizio and Loredana [13] (2010) presented the flexible forming of thin sheet from aluminum alloy using different flexible die geometries and materials (silicone rubber, SR, Styrene butadiene rubber, SBR, and polyamide66, PA). As a result of the comparison between different die materials, only PA dies have a complete formation without tearing. They have investigated the forming force during the forming process for different die materials and evaluated them together with the part springback. These investigations showed the sufficient agreement between numerical and experimental data.

Ramezani et al. [14] (2009) presented a theoretical model for static and kinetic friction in rubber pad forming process. They applied these models to

finite element simulation of an axisymmetric rubber pad forming operation. Experiments of rubber pad forming were carried out using a flexible punch. The coefficient of kinetic friction decreases with the increase of the sliding velocity and normal load. The result of finite element simulation using the new models (static friction model) instead of Coulomb friction model and kinetic friction model illustrated better agreement between experiments and numerical simulation. The maximum error prediction for punch load of FE simulation is 8% using Coulomb model and 5.6% using the kinetic model

J.W.Lee,H,C. Known(2003) [15] have investigated the deformation characteristics using the rubber-pad bending of an extruded rectangular aluminum tube. 3D finite element analysis was used to examine the effect of the process parameters on the deformation characteristics of an extruded aluminum tube and the influence of a formable radius of curvature of the tube on a bending resistance. The ratio of the second moment of inertia of the initial and deformed cross-sections of the tube was introduced as a measure of cross-sectional deformation to represent the variation of bending rigidity of the bent tube. The relation between the bent profile of the material and a roller stroke was defined. Rubber hardness was a dominant process parameter that affected the cross-sectional deformation of the rectangular tube. Its effect on the tube deformation became prominent when the radius of the bent tube decreased.

Madoat and Narimani[16] (2005) presented sheet forming by using the rubber-pad forming process. The main aim in theoretical investigation was to find a computer model, which was able to simulate the process and therefore to find the right design for a tooling set. The finite element method is used also to investigate both rubber pad and blank behavior during the process .The experimental and numerical results showed that the magnitude of the stress applied on the rubber is not as high as to cause damage in the rubber pad. Therefore the rubber pad can be used for forming different parts. This work shows that there is a limitation of the blank thickness, because the maximum

---

equivalent stress increases as the blank thickness increases. The investigation of the forming load, thickness variation of the formed plate and variations in the channel width to rib width ratio were also performed.

Two different deformation styles for rubber pad forming process used for manufacturing metallic bipolar plates are presented in Yaniong Liu and Lin Hua Jian Lan ,Xi Wei [17](2010), the finite element simulation and experiment methods were analyzed in detail in the concave and convex rubber-pad forming process. The forming load, thickness variation of formed plate and variations in the channel width to rib width ratio on the parts formation for the two deformation styles were also performed .The ratio of channel width to rib width determines which deformation style is suitable for bipolar plate fabrication. For  $w/s > 1$ , the concave style is more appropriate, otherwise the convex one is preferred ( $w/s < 1$ ). They found out in the convex deformation style that the value of  $h/w$  increase leads to the maximum thickness as the reduction decreases, while in the concave style the maximum thickness reduction increases as the  $h/w$  increases. The forming load of concave deformation style increases more sharply than that of the convex deformation style. Furthermore, the peak forming load in the concave style is larger than that of the convex deformation style.

The rubber pad bending of aluminum structural frames with five flanges has been investigated experimentally by H.C. Kwona, Y.T. Ima , D.C. Jib, M.H. R heeb [18](2001). A prototype bending machine was developed using hydraulic actuators. The influences of the number of cycles and the stroke on bending were determined experimentally. Furthermore, the relation between the bent profile of the material and the roller stroke were investigated. The authors found out that the number of process cycles has a minimal influence on the bent profiles when it is compared to the effect of the roller path. Thus an additional cycle following the initial roller path is not desirable. For the process

design of the arbitrary shaped profiles, the relation between the roller stroke and the curvature value at the profile center was obtained.

---

### 3. Sheet Metal Forming

Sheet metal forming is one of the most important technologies in the industry. In recent years, the demand for sheet metal parts with different shapes and properties has increased dramatically, due to the development of modern industries. Different techniques for forming high strength, low plasticity and difficult-to-form materials and complex-shaped parts have been developed in the past decades. In the manufacturing industry, four main conventional methods are used to fabricate a metallic product, i.e. casting, cutting, joining and metal forming. In casting, the molten material is poured into a mold, which contains a hollow cavity of the desired shape, and is then allowed to solidify. So the product can be shaped in one step. Nevertheless, it is not easy to make complex shapes with this method. Metal cutting involves removing material from the original piece through machining operations. In this method a lot of material is wasted. Moreover, it might be difficult to achieve complex geometries, and tools must be appropriately selected for successful machining.[1,19]

Manufacturing can also be carried out by joining techniques, such as welding and brazing. Joining can be defined as the process of bringing two or more surfaces into contact in order to establish continuity of the resulting product. This process cannot be applied to all types of materials and complex failure modes may occur in the final products.[1,20]

For sheet metal forming processes, different parameters such as tools, machines, material properties and tribology influence the product quality and cost. Some of these parameters have a direct influence on each other. The manufacturability of producing of sheet metal part depends on many factors such as material properties, applied forming technique and its

---

process parameters. The material properties can be evaluated by means of standard material characteristics such as tensile yield strength, ultimate elongation and tensile strength obtained from testing. The main challenge is to find the best way of producing the part most effectively and economically with the existing machines and forming techniques. Different types of sheet metal forming processes that are commonly used in manufacturing industries are described below.[1,19,20]

**Bending:** Pressing the punch gradually on to the sheet, the sheet can deform plastically and obey the shape of the punch. Bending is a flexible process by which a wide variety of shapes can be fabricated. The sheet metal is stressed beyond the yield strength but below the ultimate tensile strength. The material around the punch can move freely, so bending forces are the only forces that occur and the surface area of the sheet metal does not change much.[1,19]

**Roll forming:** A flat long strip of metal is power fed through successive sets of rollers, which shape the metal as it passes through them. A roll forming machine consists of pairs of rollers that continuously form or bend sheet or strip metal into the desired cross-sectional shape. Each roller performs only an incremental part of the forming process, until the desired cross-section profile is obtained. Roll forming is ideal for producing parts with long lengths or in large quantities [1, 19, and 21].

**Spinning:** A flat circular sheet is pressed against a rotating mandrel using a rigid tool. The mandrel and sheet metal are clamped together and secured between the headstock and tailstock of the lathe to be rotated at high speed by the spindle. While the sheet and mandrel rotate, force is applied to the sheet by a tool, causing the sheet metal to flow and lay down onto the mandrel which possesses the shape of the final product. Metal spinning is the process of making three-dimensional seamless, axisymmetrical geometries from flat circles of metal by a combination of rotational motion and force. . [1, 19, 21].

**Stretching:** In this process the sheet is clamped at its circumference over the die cavity and the punch is brought down to deform the sheet and make it take the shape of the die. Because the sheet metal is clamped around its edges, the material stretches and thins as it is formed. The deformation of the sheet is obtained from radial strain. Stretch formed parts are typically large and possess large radius bends. The shapes that can be produced vary from a simple curved surface to complex non-uniform cross sections. Stretch forming is capable of shaping parts with very high accuracy and smooth surfaces [1, 19, and 21].

**Deep drawing:** The sheet metal is clamped down by the blank-holder over the die, which has a cavity in the external shape of the part. The punch pushes the sheet metal downward, drawing it into a die cavity. The tensile force applied to the sheet causes it to deform plastically into a cup-shaped part. This process requires a blank, blank-holder, punch, and dies. The blank-holder prevents wrinkling of the sheet and controls the sliding of the sheet during the process. Deep drawn parts are characterized by a depth equal to more than half of the diameter of the part. Stretching and deep drawing are the most frequently used Sheet metal forming processes in manufacturing industry. The difference between these two processes is that in stretch forming, the sheet metal is prevented from deformation under the blank-holder while in deep drawing the sheet is able to move under the blank-holder [1, 19, 20, and 22].

Sheet metal forming processes have been classified into conventional and unconventional forming processes. The main difference between conventional and unconventional forming is the type of tools used in the process. In a conventional metal forming process, a rigid punch made of hard steel is normally used to push the part into the die. In unconventional forming processes, flexible tools are used to punch the work piece. In this type of forming, a flexible medium such as rubber, fluid or highly-viscous semi-solid material is replaced with conventional rigid tools, to form a component into its final shape. Some of the unconventional processes include hydro forming,

rubber-pad forming, gas forming, and viscous pressure forming processes to name a few. In the next section, different types of flexible-die forming processes are introduced.

### 3.1 Significant Material Properties in Sheet Forming.

Sheet metal production plays an important role in the manufacturing world. It is used to make everything, from hinges to automobiles. There are a lot of types of sheet metal fabrication for engineers to choose from. Deep drawing, stamping, rubber forming, and hydro forming are all different methods used for creating desired shapes out of a sheet metal. It is a responsibility of a design engineer to determine mechanical properties of the material, select the material that meets these requirements, and select the best fabrication process for the job. Before the material is selected for a design project, engineers have to determine the mechanical properties of the material. Designing for strength, material class and mode of loading are important considerations. Several factors have to be considered when selecting material, such as ductility; yield strength, ultimate tensile strength. When designing, all these factors are weighed against the properties of the available materials and it is a job of the design engineer to select the material that best fits the application [1, 21, 23].

- **Ductility:** Metal used in the sheet metal work must be ductile. If we use a brittle metal it can easily undergo failure during forming. That's why metal ductility is very important in sheet metal working.[23,24]
- **Yield Strength:** Yield strength of a material used in sheet metal forming must be low. High strength metals have reduced stretch distribution characteristics, making them less stretchable and drawable than lower strength metals. Stretch distribution characteristics determine the steel's ability to distribute stretch over a large surface area. The better the stretch distribution, the more the steel can stretch over the draw punch to create the final geometry.[23,24]

- 
- **Elastic Modulus:** Stretch distribution affects not only stretchability, but also elastic recovery, or springback, and the metal's total elongation.[23]
  - **Discontinuous Yielding:** Low carbon steels show a discontinuous yielding accompanied with the formation of Luder bands, which reduces the surface quality of the end product. In order to remove the discontinuous yield point, temper-rolling (rolling where a few percent of reduction is applied) can be applied [6, 23].
  - **Work Hardening Rate (n):** Work hardening rate is a very important sheet metal forming parameter. When  $n$  increases, the material's resistance to necking also increases. The work hardening is the mechanism that prevents local yielding and increases the uniform elongation - "elongation in a tensile test up to necking". This is why a reasonable work hardening is desired in sheet metal forming if the principal stresses are in the tensile mode (stretching). But as the work hardening rate increases, the applied force must also be increased.[23,24]
  - **Grain Size:** In general, a fine-grained metal is preferred in the fabricating of sheet metals. The individual crystal grains of the metal flow differently and in most cases the grain boundaries are visible on the surface. The surface consequently becomes rough and uneven. If the grain size exceeds a certain limit the roughness becomes noticeable and a condition termed "orange peel" should be assumed. Depending on the surface requirements, the grain size of the sheet is limited to a maximum value. On the other hand, it is undesirable to use a material with extremely small grains, as the yield stress increases with decreasing grain size.[23,24]
  - **Surface Finish:** The sheet metal must have good surface properties to provide minimum friction during forming. If the metal is very rough, mould life becomes shorter.[24]

### 3.2 Metal Behaviour in Sheet Forming:

- **Strain hardening:** Work hardening or strain hardening refers to the fact that as a metal deforms it undergoes changes in its atomic and crystalline structures resulting in increased resistance of the material to further deformation. Thus, additional strain increase requires more stress increment and the strain is spread throughout the sheet. Strain hardening then results in more uniform deformation. For materials with deformation behaviour described by the equation  $\sigma = K \epsilon^n$ , the rate of strain hardening is indicated by the strain-hardening exponent  $n$ .

In shearing operations, the punching force depends on the material, the amount of work-hardening during deformation, the thickness of the sheet metal and the punching speed. The rate of deformation is described by the strain rate [20, 21,23and24].

- **Necking:** At some point in the deformation, the strain suddenly localizes and necking, or localized thinning, begins. When this occurs, little further overall deformation of the sheet can be obtained without its fracturing in the necked region. As we noted in the previous section, the strain at necking for a  $\sigma = K \epsilon^n$  material is equal to strain hardening exponent  $n$ . [23,24]
- **Anisotropy (Directionality):** Anisotropy is another factor that affects formability. One consequence of directionality is a change in mechanical properties with direction. When forming sheet metal, practical consequences of directionality include such phenomena as excess wrinkling, puckering, ear-formation, local thinning, or actual rupture.[20,23]
- **Springback:** In the tensile test unloading occurs along a line parallel to the elastic deformation line. Analogously, when a part being formed is unloaded when it is removed from the die, elastic recovery or springback occurs. Elastic recovery results in the final shape of the part being different from the die shape or part shape in the die. If the elastic

recovery is relatively large compared to the deformation needed to form the part, large deviations from desired part shape result. Shallow or large curvature parts such as some automobile body panels can be difficult to form. The solution to springback problems is to over bend the parts. This raises the question of how much over-deformation should be imposed. Prediction of the amount of springback in terms of material properties and process characteristics is needed. This kind of deformation prediction requires accurate material behavior descriptions and process models [1, 3, 21, 23, and 24].

- **Wrinkling:** Although in sheet forming the metal is generally subjected to tensile stresses, the method of forming may be such that compressive stresses are developed in the plane of the sheet. We can imagine a circular blank being drawn into a circular die by a circular punch to form a can. Tensile stresses are produced in the can wall during drawing and compressive stresses in the blank flange as its length is being decreased as it moves toward the die cavity. Terms used to describe this kind of phenomena are buckling, folding, and collapsing. Wrinkling can be controlled by holding the flange down, but hold down force will restrain movement of the blank into the die and increase the tensile stress in the can wall. The wall fracture or tearing can result [1, 3, 21 and 23].

### 3.3 Flexible Sheet Metal Forming Processes:

As mentioned before, unlike the conventional metal forming process, flexible-die forming process uses a flexible pressure-carrying medium to replace a rigid punch or die. The medium might be liquid (water, oil), gas (pressured or expanding air), viscous elastic material, or elastic body (a rubber pad). In recent years, sheet flexible-die forming processes have been widely used in industries such as automotive and aerospace factories. Compared with the conventional sheet metal forming processes, the flexible-die forming processes have many advantages, such as low cost, high flexibility, good surface quality, and dimensional accuracy.[1,19]

Different pressure-carrying mediums possess assorted characteristics and can be used in different processes. Each process has its own advantages and disadvantages. Liquid and viscous materials are used for hydro forming and viscous-pressure forming. Despite their wide application in manufacturing industry, there are some drawbacks such as liquid splash when forming fails and difficulty in controlling the liquid or viscous pressure during forming. It is also difficult to perform the pressing operation due to concerns about the risk of leakage. Gas is used as the pressure-carrying medium for super plastic bulging and explosive forming, but its efficiency is low and its thickness reduction is great. [1, 3]

Rubber can also be used as pressure-carrying medium for rubber-pad forming process. However, deep-drawing parts and complicated work pieces cannot be produced by this technology because of the deformation limit of rubber itself. In the following sections, each process is introduced briefly. [1, 3]

### **3.3.1 Hydroforming:**

The hydroforming process uses liquid as a pressure medium instead of a conventional punch to form the part into the desired shape of the die.

This process is capable of forming complex geometries with concavities in one step, which would be difficult or impossible with conventional forming processes and would otherwise be made from multiple stamping parts joined together. It provides remarkable weight savings due to the elimination of flanges required for welding and using thinner metals. Hydroforming is currently used widely in industries such as the automotive industry, where the complex geometries that can be produced by this method are used to make stronger, lighter and more rigid structures for vehicles. The main defect of the process is excessive thinning which may occur in some parts during hydro forming. Thinning problems in tube hydroforming can be reduced by applying axial pressure to push the [1, 3, 19].

Compared with conventional stamped parts, hydro forming is better in respect of both tolerances and repeatability. The dimensional accuracy of hydro-formed parts is much better and it has less springback as it is released from the die, and residual stresses are significantly lower.

Hydro forming can be classified into two main categories, namely tube hydroforming and sheet hydro forming. The schematic of simple tube and sheet hydro forming processes are shown in Figures 3.1 and 3.2 respectively. In tube hydroforming, internal hydraulic pressure is applied to a tube that is surrounded by dies with the desired geometry. The die should be two-pieces to allow opening and closing. When the dies are closed, high pressure hydraulic pistons inject a liquid at very high pressure inside the tube which causes it to expand until it matches the die [19, 25, and 26].

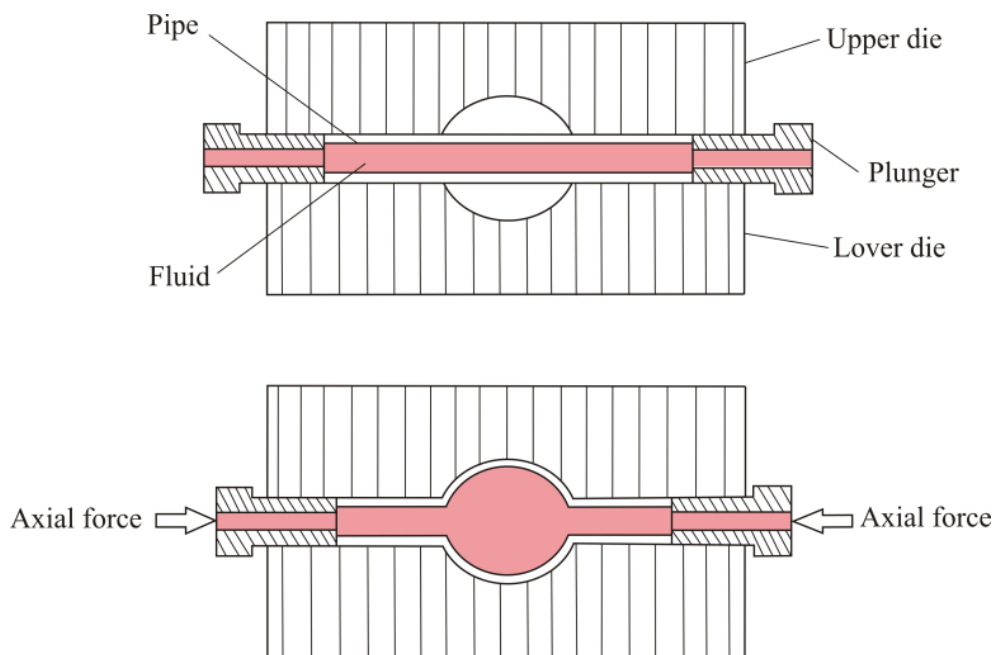


Figure 3.1 Bulge forming of tubes using hydro forming process

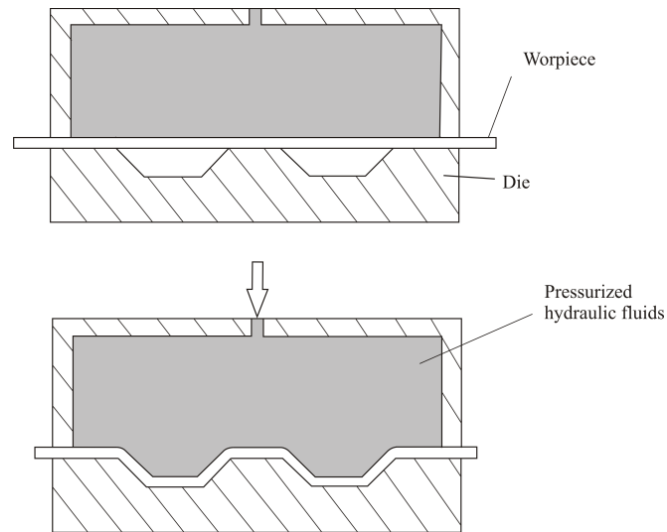


Figure3. 2 Sheet hydro forming process

Hydro forming is used widely for creating automotive components in order to produce good quality products, and to reduce the number of parts and thus the weight of automobiles. Tubes with changing diameters, stepped tubes, tubes with square or complex cross-sections, tubes with cross-sectional shapes that can vary continuously throughout the length of the part, and tubes with branches (such as T-joints and ball joints) can all be formed by the process. A hydro-formed bellows with complex geometry is shown in Figure3. 3[27].

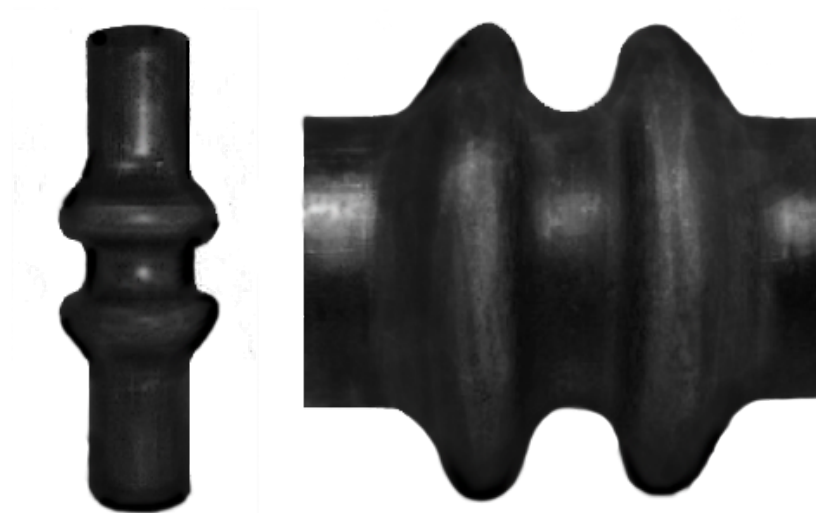


Figure3. 3 Hydro-formed bellows using a circular insert ring with axial feeding [Kang et al.,2007,[27])

In sheet hydro forming, the sheet metal is placed on blank-holder over a male punch. A hydraulic chamber then surrounds the sheet and a relatively low initial pressure presses the sheet against the punch. The punch then is raised into the hydraulic chamber, forcing the sheet to assume the shape of the punch under the pressure of the fluid. Some complex-shaped parts such as longitudinally curved boxes with a regular polygonal cross section are fabricated by hydroforming and are very difficult to form using the conventional deep-drawing process. Complex parts can also be fabricated using combined tube and sheet hydroforming. Figure 3.4, shows a part which is formed with the combination of the tube and double sheet hydro forming in one step [1, 19, 28,29].

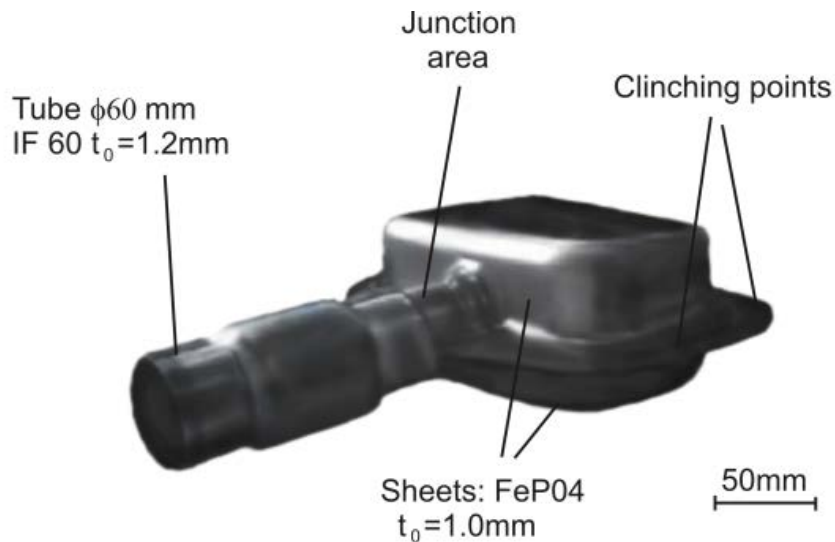


Figure 3. 4 Hydro-formed tube double sheet component (Merklein et al.,2005[29])

### 3.3.2 Hot Metal Gas Forming

Hot metal gas forming is a development that further improved upon the cost effectiveness and applicability of hydroforming process. In this process, an inner gas pressure replaces hydraulic fluid that permits fabricating tubular metal structures at high temperature, overcoming the existing limitations of hydroforming of these components. The metallic part is heated by

placing it in an inductive field and using the electrical current induced by the field to a pliable state, near but below its melting point. It is then pressurized internally by a gas in order to push the part outward into the enclosing die cavity to assume the shape defined by the die. Due to the decrease of yield stress of metal parts at high temperature, the parts can be fabricated into a complex shape using low-pressure gas introduced to the interior of the part and so a lower capacity of press machine is needed compared to hydro forming. Forming at high temperature allows the metal to elongate, or stretch much further without rupture than is possible in cold and warm hydroforming. Moreover, the component can be formed into finer details and requires less press capacity compared to traditional methods[1,19,26,27,30,31]. The schematic of the process is shown in Figure 3.5

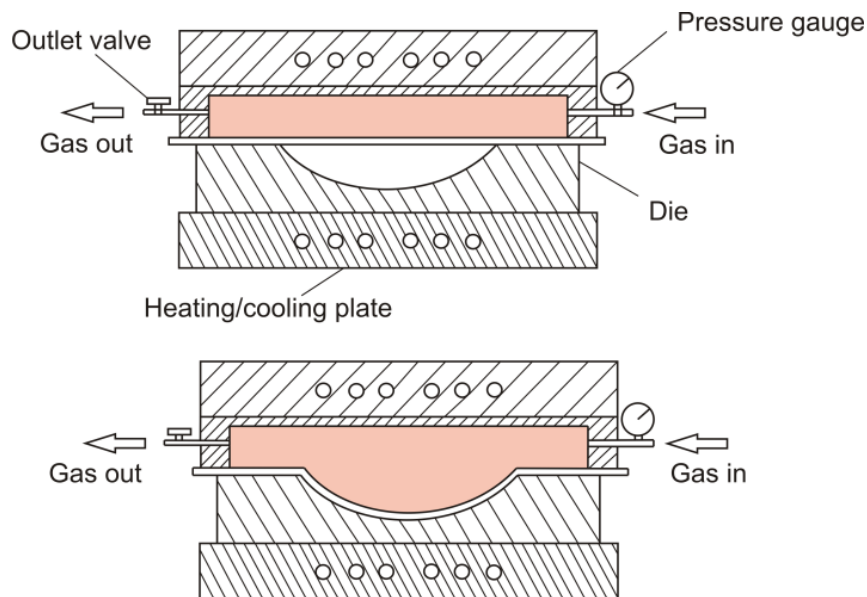


Figure3. 5 Hot metal gas forming process

Hot metal gas forming is capable of producing all tubular sections currently made by hydro forming, while eliminating some subsequent band working required due to the limitations of hydro forming. A magnesium alloy tube formed by both metal gas forming process is shown in Figure 3.6[30].

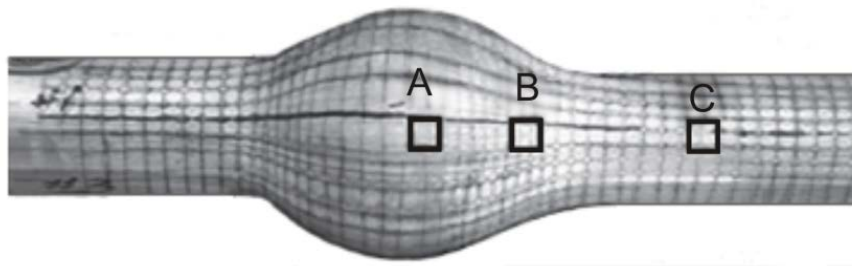


Figure 3.6 Magnesium alloy tube after hot metal gas forming (Liu and Wu, 2007[30])

### 3.3.3 Viscous Pressure Forming

The viscous medium is usually used in both sides of the work piece. During the viscous-pressure forming process, the viscous material is pumped under pressure into a medium chamber on one side of the workpiece, while the medium in the other side of the sheet is ejected through single or multiple ports. Thus, the viscous pressure forming operation is a combination of the bulk deformation of the viscous medium and shear metal forming processes [25,26]. This process is mostly used in the defense industry to form complicated shape parts in difficult-to-form materials. Unlike the conventional sheet metal forming, the viscous medium can fill complex-shaped surfaces very well, and parts with good surface quality and high dimensional accuracy can be formed using this method. The viscous pressure forming sequence is illustrated in Figure 3.7. Firstly the sheet metal is laid over the mouth of the die and the chamber is closed followed by the engagement of the blank binder as shown in Figure 3.7 (a). The viscous medium is pumped into the cavity of both sides of the sheet until it is full and overflowing into the diffuse cavities. With the constant volume achieved, the isostatic pressure is now raised to the set level. In order to create pressure differential, some of the viscous medium is removed from the die cavity below the sheet through outflow control valve and more viscous medium is added at the top cavity. The pressure differential

distribution over the whole sheet surface is maintained and controlled to the desired level Figure3.7 (b). This whole process continues while at the same time the blank-holder pressure is regulated in such a way that the sheet material is forced against the die. The pressure must be sufficient to enable the sheet to deform plastically and follow the derail of the die form Figure3.7(c). Once this is achieved, pressure is removed and the chamber is opened with the formed part completed Figure3.7 (d)[1,19,25,33,34] .

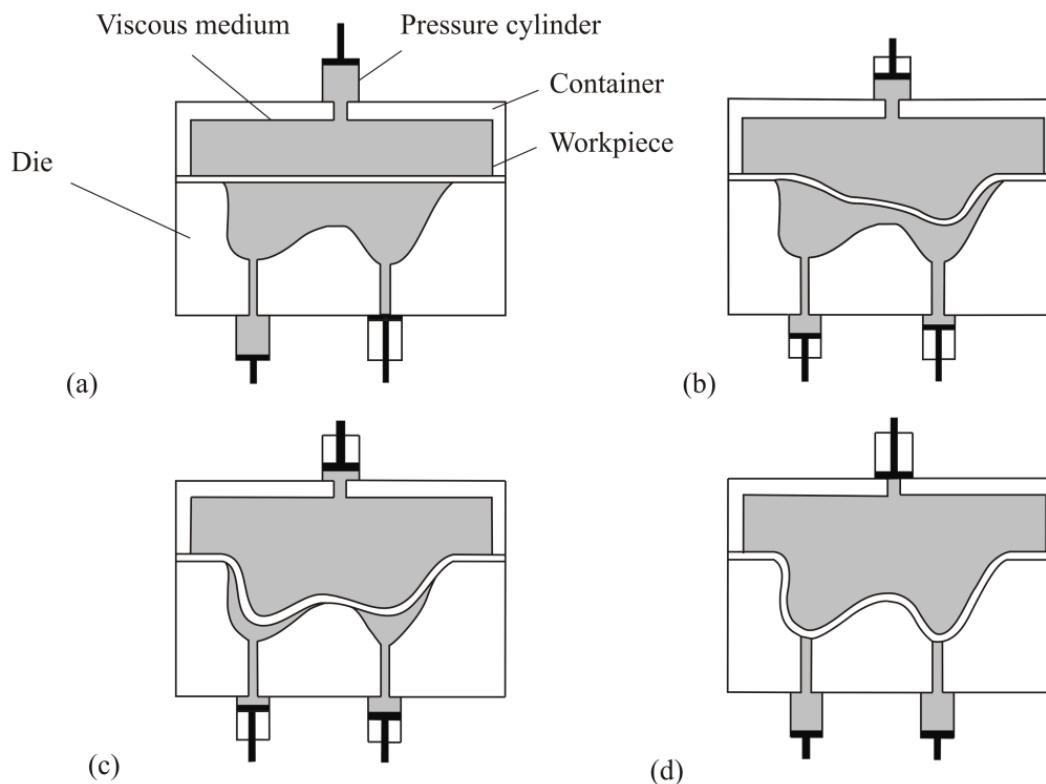


Figure3. 7Viscous pressure forming process

Due to the controlling of the value and the distribution of viscous medium pressure and blank-holder pressure in viscous-pressure forming, the work piece can be formed in a definite sequence. Non-uniform pressure distribution in the work piece can be achieved by controlling the position of the inlet and outlet ports of the viscous medium and the blank-holder pressure. This pressure non-uniformity is advantageous for forming of complex-shaped parts. The shape of

the part formed using viscous pressure forming depends on the direction of the flow of the medium; as such the flow can be controlled by specific location of the outlet ports. The sheet metal is pushed to the location of the outlet ports, for example by specifying the outlet port at the corner of the die, and more pressure can be focused on the sheet metal in the direction of the outlet port at the corner of the die. The force applied to the blank-holder is also important as low force of the blank-holder allows the sheet metal to be drawn in, reducing the yielding of the sheet metal at that particular instance. This ensures a more uniform thickness of the formed sheet metal product [19, 25, 32 and 34]. A thin-walled corrugated component formed by viscous pressure forming technique is shown in Figure 3.8

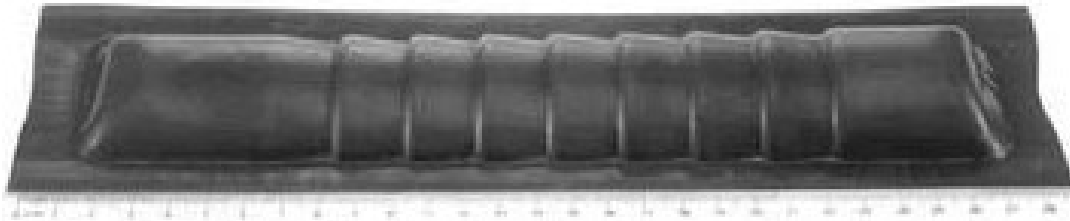


Figure 3. 8. Corrugated surface shape of a nickel-based super alloy specimen formed by viscous pressure forming process [32])

### 3.3.4 Rubber-Pad Forming:

Rubber-pad forming was developed before the other three flexible-die forming methods described previously and is a product of the nineteenth century. Adolph Delkescamp in 1872 used rubber pad for cutting and shearing of thin sheet materials, such as paper and foil. In 1888 Fred C. Cannon used rubber over metal dies to eliminate scratching of the work piece surface during forming. Leonard Beuroth used a rubber bulging technique to form metal barrels in 1912 and dental plates were formed by Friedrich Hamptemeyer in

---

1922 by rubber pads. Thus, by 1922 all the potentialities of rubber forming techniques such as shearing, embossing and forming had been applied to manufacturing processes. However, it was the three patents of Henry Guerin in 1938, 1939 and 1940 that led to the wide introduction and use of rubber forming techniques in industry. In the Guerin process, the incompressible nature of the rubber is used as a medium to transmit pressure to the sheet metal. The rubber pad when deformed acts as a female die forcing the sheet metal to form around a male die. There are many ways of applying the rubber-pad forming and, with the progress of technology the area of application has also increased. The rubber-pad forming is usually accomplished with a rubber upper die and a lower die made of steel, known as form block, acting as the mold. A few applications of rubber-pad forming techniques are shown in Figure 3.9. The separate upper and lower dies resulted in a relatively flexible and cost effective process. Due to the low hardness of the rubber pad, the sheet metal does not suffer from wear when compared to deep drawing. Since the amount of pressure exerted by the rubber is limited by the strength of the rubber itself, forming of the sheet metal parts with small forming radius may not be possible and the wear of the rubber is an issue in large quantity manufacturing [1, 2, and 19].

Rubber-pad forming, also known as flexible-die forming, employs a rubber pad or a flexible diaphragm as one tool half, requiring only one solid tool half to form a part to final shape. The solid tool half is usually similar to the punch in a conventional die, but it can be the die cavity. The rubber acts somewhat like hydraulic fluid in exerting nearly equal pressure on all workpiece surfaces as it is pressed around the form block (figure 3.9). [1, 2, 3]

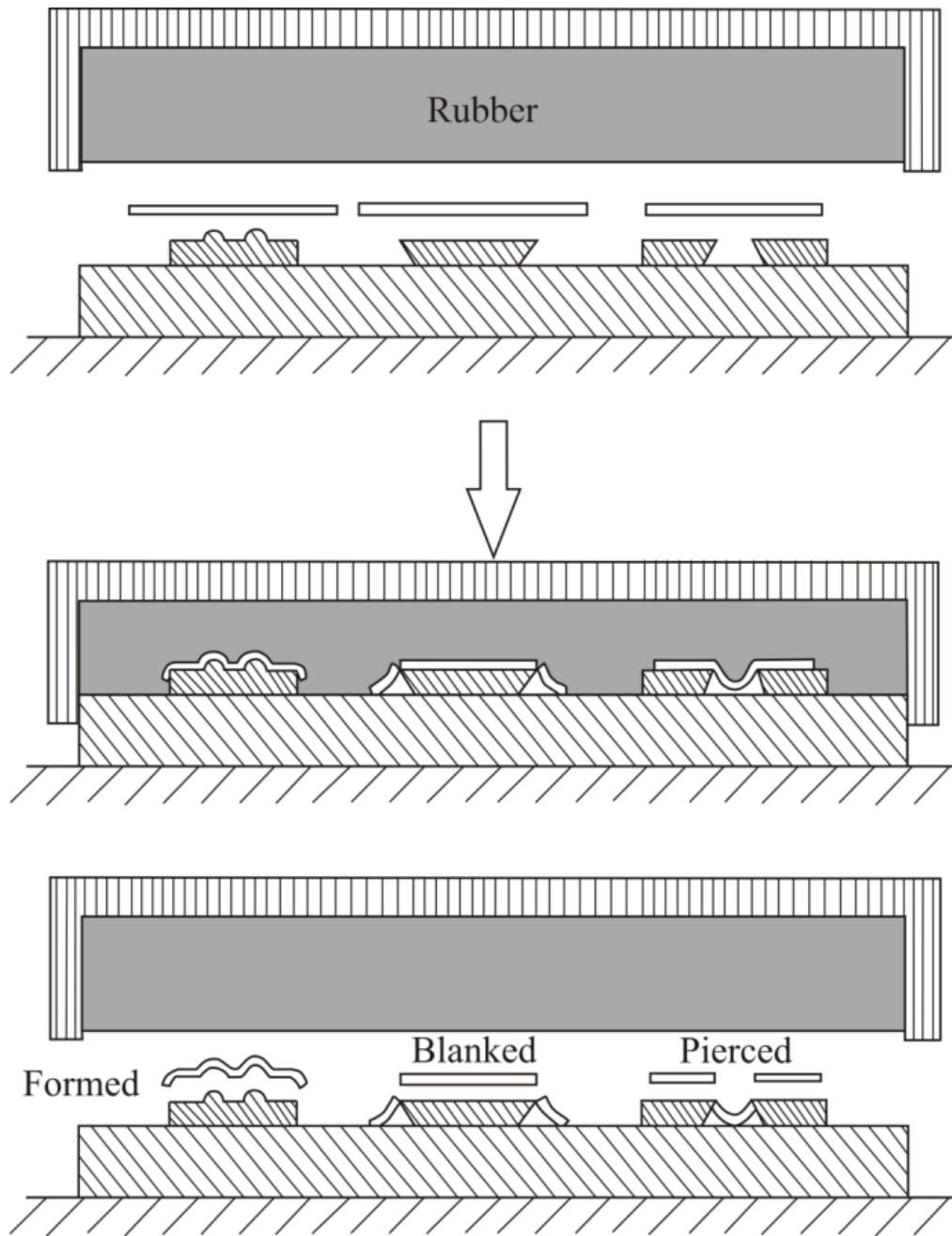


Figure3. 9Different rubber-pad forming operations

## 4. Overview of Sheet Metal Rubber Forming

Rubber forming dates back to the second half of the 19th century. Rubber was used over metal dies to eliminate scratching of the sheet-metal surfaces during blanking or forming. In the early part of the 20th century rubber *pads* were used to bulge metal barrels. By 1925 various options of rubber forming such as shearing, forming, bulging and embossing, had been explored. In the past, flexible-die forming methods were designated by specific processes: Guerin process, Verson-Wheelon process, trapped-rubber process, Marform process, Hydroform process, SAAB process, and Demarest process. Modern technology has reduced this list, categorizing the methods into three basic groups: rubber pad, fluid cell, and fluid forming. A general overview of the process is given below [1, 2, and 3].

### 4.1 The Guerin Process

A simple way of forming sheet metal using a flexible tool is shown in Figure 4.1. The Guerin process was named after Henry Guerin, a head of the department of Douglas Aircraft California, the USA, who discovered the technique of using rubber as the half die instead of metallic part in the late 1930s. This process is commonly used to form short runs of light metal parts [1, 2, and 19].

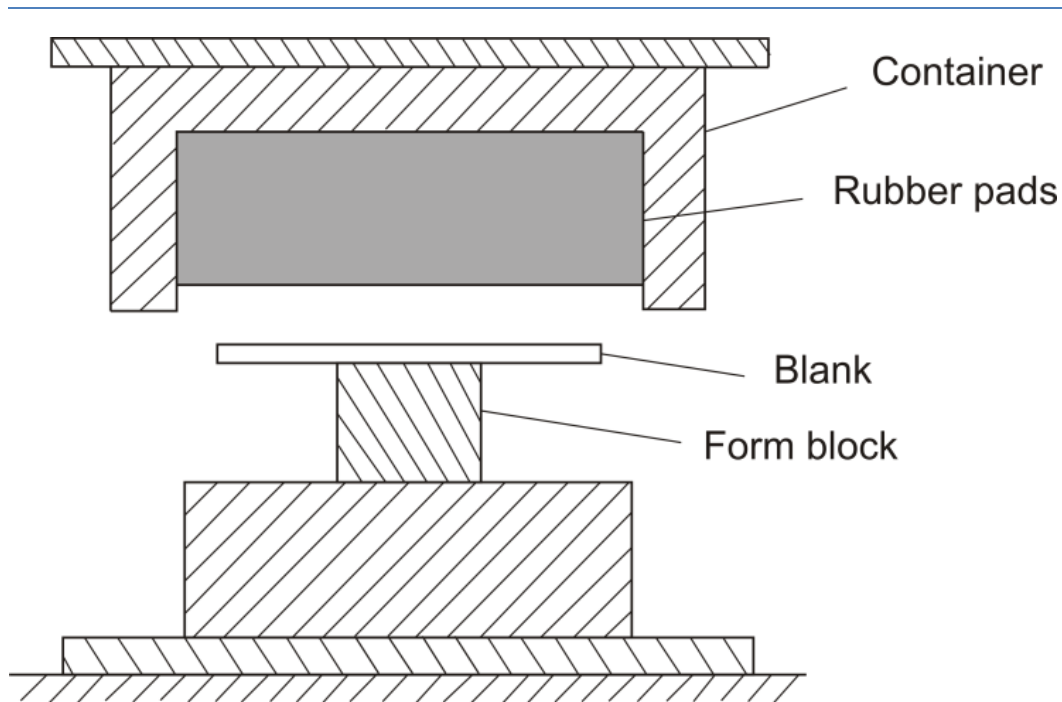


Figure4. 1Guerin process tool

The presses ram carrying the rubber pad moves down deforming the sheet metal. The punch is a solid block (a forming block) or a former. In the process the sheet metal takes its shape after forming. The former should have rounded corners; otherwise the work piece might be cut, instead of being formed. The flexible pad is contained in a retainer mounted on the press ram. A male punch (or a female die) is mounted on the press table. The press plate fits closely into the retainer, and prevents the pad from squeezing out through the space between the press plate and the pad retainer. As the press ram lowers, the pressure on the flexible pad builds up and deforms the sheet metal to take the shape of the former (a male punch or a female die). The press ram then retracts carrying the pad with it in the retainer, and the formed component is removed. This process is suitable for forming shallow components; with deeper components, the process may produce wrinkles. The reason for this is the fact that pressure in the rubber is not high enough to stop wrinkle forming in deeper formed parts due to low compressive strength of rubber. The minimum pad thickness is 30 percent bigger than the height of the form block, and generally varies from 150 to 300 mm [1]. The rubber pad is made of soft

---

elastomer (50-75 Shore hardness). Maximum stamping depth rarely exceeds 50 mm, which can be increased by using thicker pads and more powerful presses. The rubber chamber and the form block are made of steel or cast iron and are approximately 25 mm deeper than the rubber pad. The rubber pad in this process can be a solid or laminated part. The laminated pad is comprised of sheets of rubber, cemented and placed over each other. The advantage of the laminated pad is that different hardness can be used in different layers, where the hardest layer is placed close to the forming surface. In some cases the rubber cannot completely fill the corner of 90° between the plate and the form block. There will be a natural radius formed by rubber depending on its properties. Some typical cross sections of form blocks with auxiliary tools are shown in Figure 4.2[1, 2, 19]. These tools are increasing pressure required to form sharply contoured flanges. In order to take into account springing back in the flanges, the block is given an undercut as shown in the view A. To correctly direct the higher pressure level against the flange, a trap is usually used as shown in the view B. To eliminate the wrinkles in the sheet metal and increasing the pressure against the flange by using a roll, wedge or hinged wiping plate as shown in the views C, D and E, respectively. The function of the cover plate is to clamp the blanks on the form block. This prevents slipping and reduces undesired deformation of the web. The drawing ring, usually extends to more than 180° over the peripheral segment (view F) [1, 2, 3, 19].

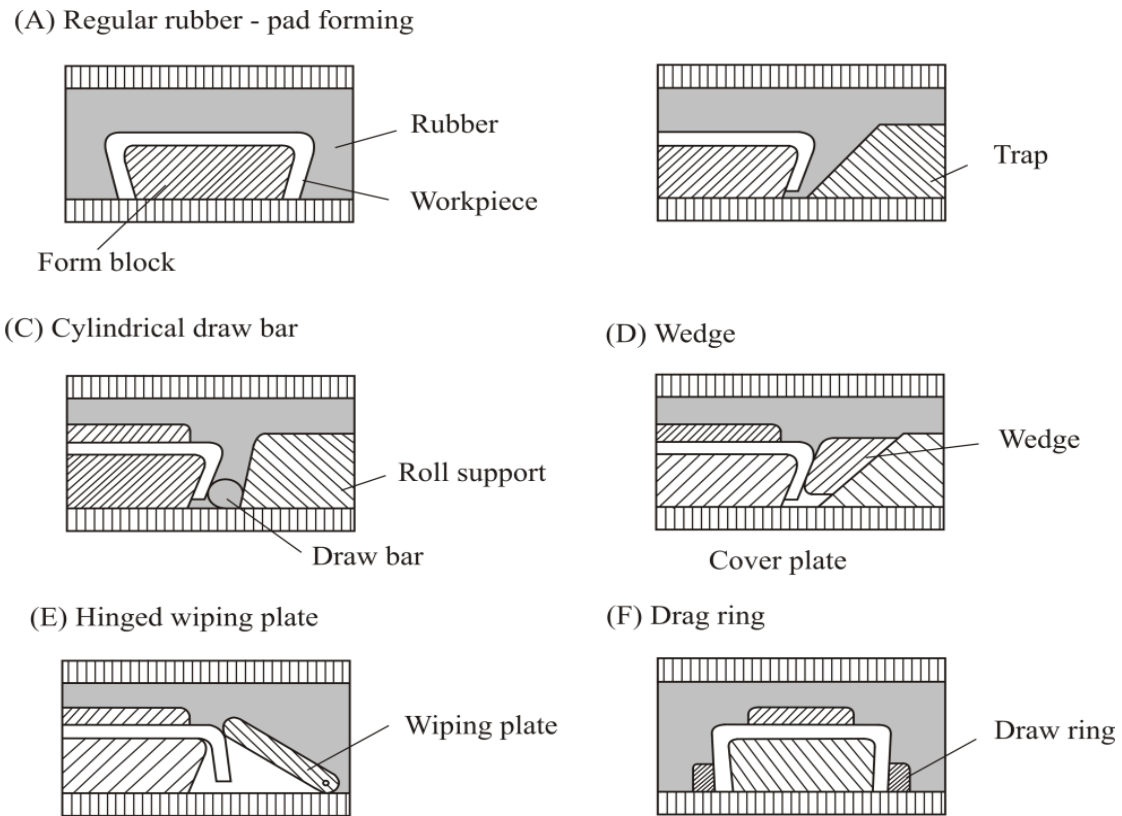


Figure 4.2 Typical cross sections of form blocks with auxiliary tools [19]

## 4.2 The Marform Process

The Guerin process is synonymous with the term rubber-pad forming. An improvement of the Guerin process is known as the Marform process, Figure 4.3, which features the addition of a blankholder and a die cushion to make the process suitable for deeper draws and to alleviate the wrinkling problems common to the Guerin process. Another variation of the Guerin process is the trapped-rubber process, in which the forming force is provided by a hammer instead of a hydraulic press. Like the Marform process, the trapped-rubber process can be used for deeper draws and results in less scrap due to wrinkling than it is the case with the basic Guerin process [1,2,3,]

A Marform unit comes as a package that can be installed in a hydraulic press having sufficient stroke length and shut height. However, a press that

incorporates a hydraulic cushion system into its bed has been designed specifically for Marforming. The rubber pressure used in this process ranges from 34 to 69 Mpa. It depends on the force capacity of the press and the surface area of the rubber pad. The rubber pad used in Marforming is similar to the one used in the Guerin process. It is normally 1.5 to 2 times thicker than the total depth of the part to be formed. The rubber pad can be protected from tear and wear by the use of a throw sheet, which is either cemented to the pad or thrown over the blank. Blankholder plates are usually made of low-carbon steel, where the formed block is made of cast light alloy. The contact surface is ground flat and polished to avoid scratching of the blank. The clearance between the form block and the mating hole in the blankholder is 0.76 to 1.52 mm per side to prevent rubber from squeezing out [1, 2, 3,19and 27].

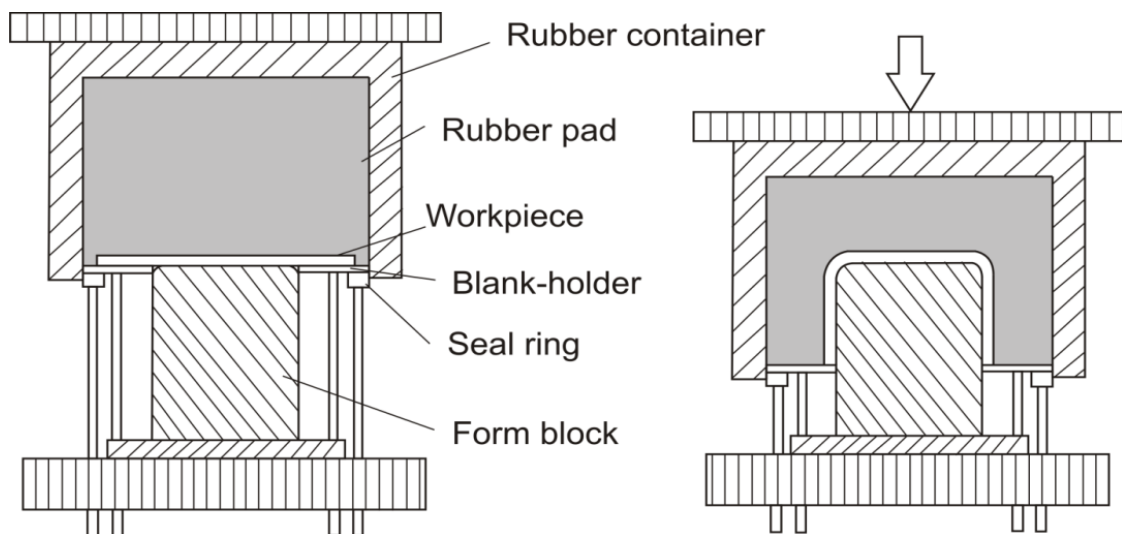


Figure4. 3 Tooling and setup for rubber-pad forming by the Marform process

### 4.3 The Verson-Wheelon Process

The Verson-Wheelon process was developed from the Guerin process and marketed by Verson Allsreel Press Company in the US. It uses higher pressure and is primarily designed for forming shallow parts, using a rubber pad as

either a die or a punch Figure 4. 4. A flexible hydraulic fluid cell forces the rubber pad to follow the contour of the form block and thus exerts a hydrostatic pressure on the workpiece. The distribution of pressure on the sides of the form block allows forming of wider flanges, narrower flanges, joggles, beads and ribs in flanges and web surfaces in a single operation. The form blocks in this process are made in the same way as in the Guerin process [1, 2, and 3].

This process can form deeper parts than the Guerin process. An important difference between the Guerin and the Wheelon process is in the way the forming pressure is generated. In the Wheelon process a rubber pad contained in the press body (above the rubber pad) is pressurized by hydraulic Wheelon presses (fluid cells), horizontal-type and much smaller than those needed for the Guerin process. Greater hydraulic pressure associated with the Wheelon presses makes it possible to form thick sheet metals, from 0.05 to 10 mm thickness. With uniform pressure developed in the rubber pad, the problems associated with stress concentration, such as crack and wrinkle forming can be avoided. As far as the depths of draw are concerned, this process is limited as much as the Guerin process. Verson-Wheelon presses are available with forming pressures ranging from 35 to 140 Mpa, which means that all the wrinkling is practically eliminated. The rubber pad used in this process is usually between 60-70 mm thick [1, 2, 3, and 19].

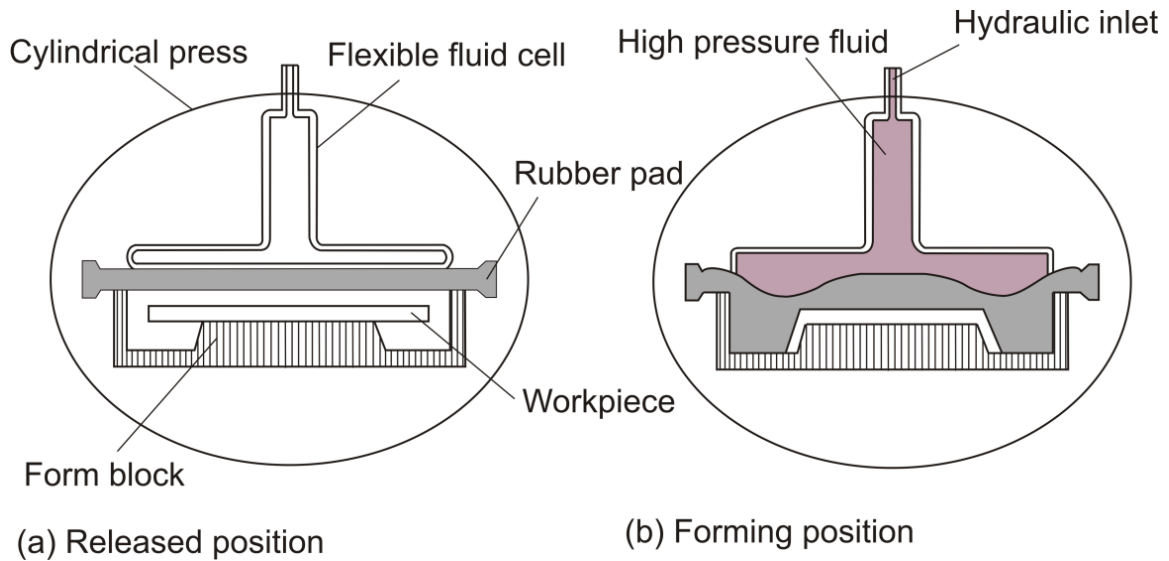


Figure 4.4 Verson-Wheelon processes

#### 4.4 The Demarest Process

The Demarest process was developed particularly to form axi-symatric shapes from cylindrical or conical semi-finished products figure 4.5. Cylindrical and conical parts can also be formed by a modified rubber bulging punch. The punch, equipped with a hydraulic cell, is placed inside the workpiece, which is in turn placed inside the die. Hydraulic pressure expands the punch and subsequently forms the workpiece, which in turn is placed inside the die. The rubber punch is lowered into the workpiece, and a steel cover is clamped over the whole assembly (Fig. c). The punch is expanded under 2.8 Mpa of hydraulic pressure, which forms the work metal into the curved shape of the die (Fig. d) [1, 2, 3, 19].

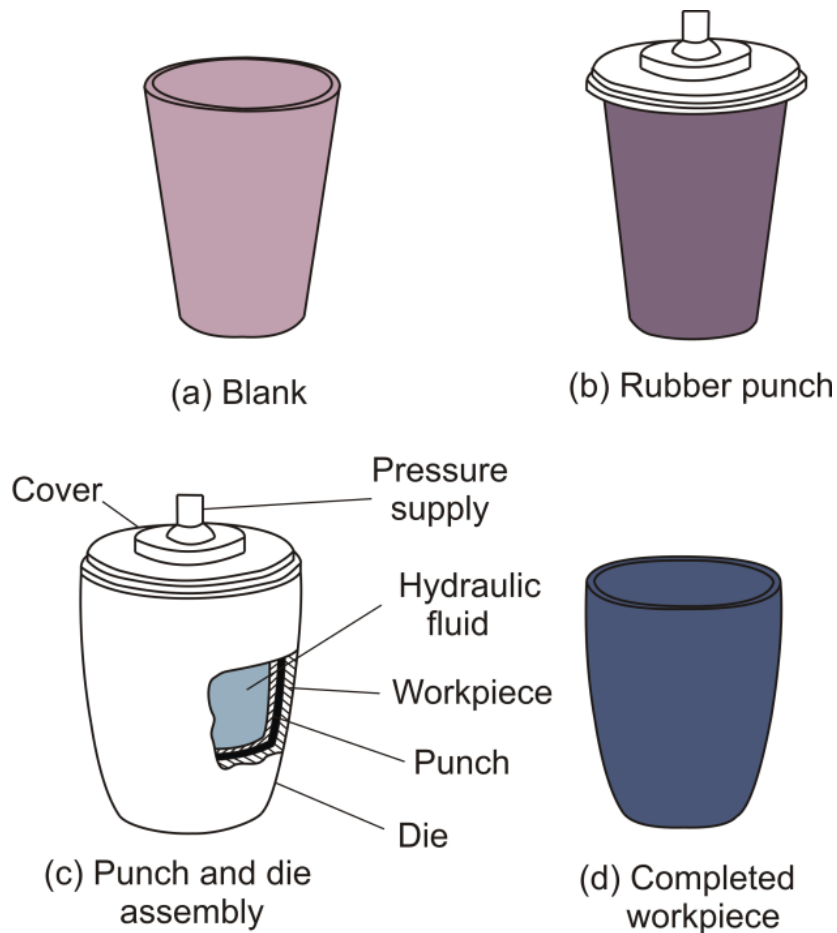


Figure 4.5 Demarest forming process

#### 4.5 The Verson Hydroform Process

The main difference between this process and the other rubber pad forming process is the fact that the die cavity is not completely filled with rubber but with hydraulic fluid. This cavity is termed the pressure dome, figure 4.6. A hydraulic pump delivers fluid under pressure to the pressure dome, the punch which can be made from tool steel, cold rolled steel, cast iron, zinc alloy, plastic, brass, aluminum, or hardwood - moves inside the cavity, opposed by the fluid pressure, which performs sheet metal forming. A 60-70 mm thick rubber diaphragm is put between the fluid and the sheet metal. The blankholder is supported by a solid bolster and does not move during the operation [1, 3]. A special press, called a Hydroform press, is used for this

process. A lower hydraulic ram drives the punch upward; the upper ram is basically a positioning device. A hydraulic pump delivers fluid under pressure to the pressure dome. The dome pressure ranges from 41 to 103 MPa depending on the material properties and geometry of the sheet. Similarly to the Marform process, the hydraulic action forming has a similar variable draw radius which prevents the formation of high local strains. As lower pressure is used in the initial part of the cycle, the curvature of the draw is shallow with a large radius which decreases with the increase in the forming pressure. Since no metal draw ring is used, no scratches or marks are produced on the outer surface of the sheet metal [1, 2, 3, 19,25and26].

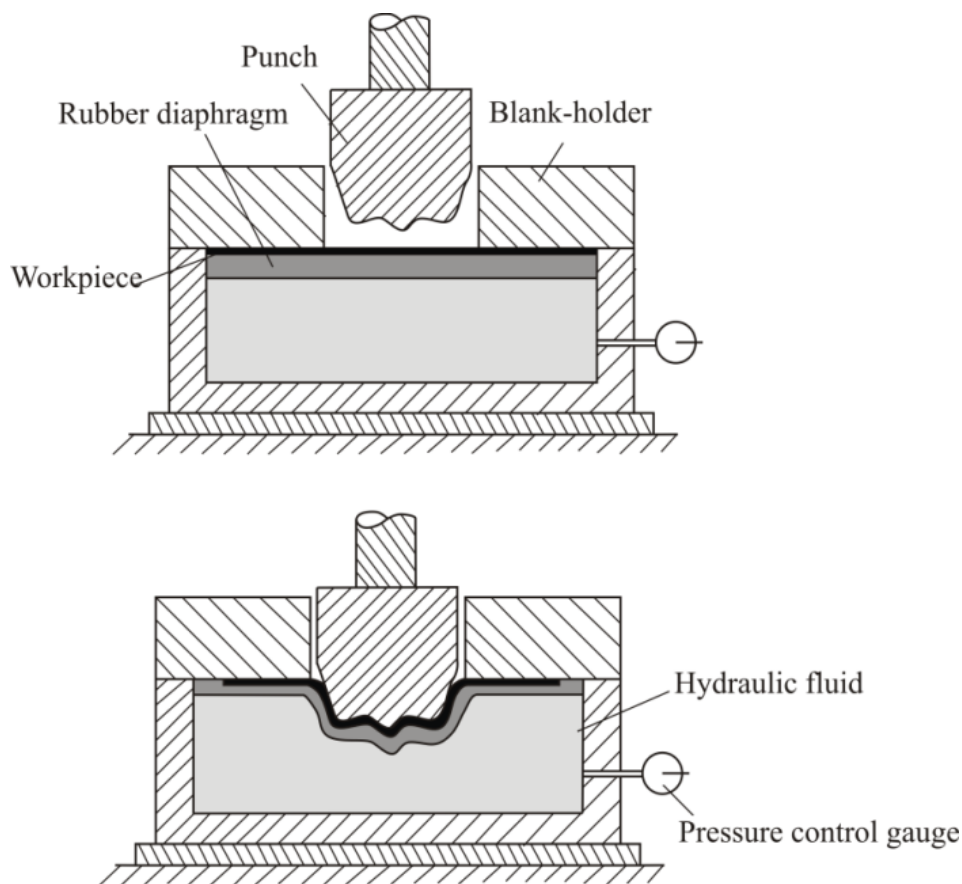


Figure4. 6 Verson hydroform process

The uniform pressure of the fluid against the rubber diaphragm causes the sheet metal to stick to the border of the punch; with a larger contact area than is

possible with metal dies allowing for more severe draws. Reduction in blank diameter for the first draw can be up to 70 % and subsequent draws can achieve 40 % reduction. A typical maximum diameter for this process is 630 mm with a maximum depth of 30 mm. Due to the large contact area and lower stress level, work-hardening is also reduced. Thinning is minimal and is expected to be less than 10 %. In this process, the draw depths range from 125 to 300 mm and the operation rate from 90 to 200 cycles per hour [ 1,2,3,19 and 27].

#### **4.6 SAAB Rubber-Diaphragm Process**

The SAAB fluid-form method was developed by the Swedish aerospace company, during the early 1950s. The process, illustrated in the Figure 4.7, uses a flexible diaphragm punch which assumes the shape of the die. The punch serves as a blankholder. The diaphragm is soft, and behaves quite like a fluid due to the high pressures used. In this process, the punch and blankholder of the conventional draw-die press are replaced by a steel cylinder which contains hydraulic fluid. The pressure is developed by the telescoping piston upon press closure.[1,2]

In the SAAB rubber-diaphragm method, hydraulic fluid is used, only pressurised by an actuator - no punch movement is provided. A hydraulic piston compresses the fluid against the rubber and forces the blank into the die cavity, as shown in the Figure 4.7, while the air vents are provided in the die to allow the air trapped between the workpiece and the die to escape. Otherwise the trapped air would prevent the workpiece to fill the cavity of the die. The figure 4.8 illustrates the steps of the SAAB process [ 1,2,19] .

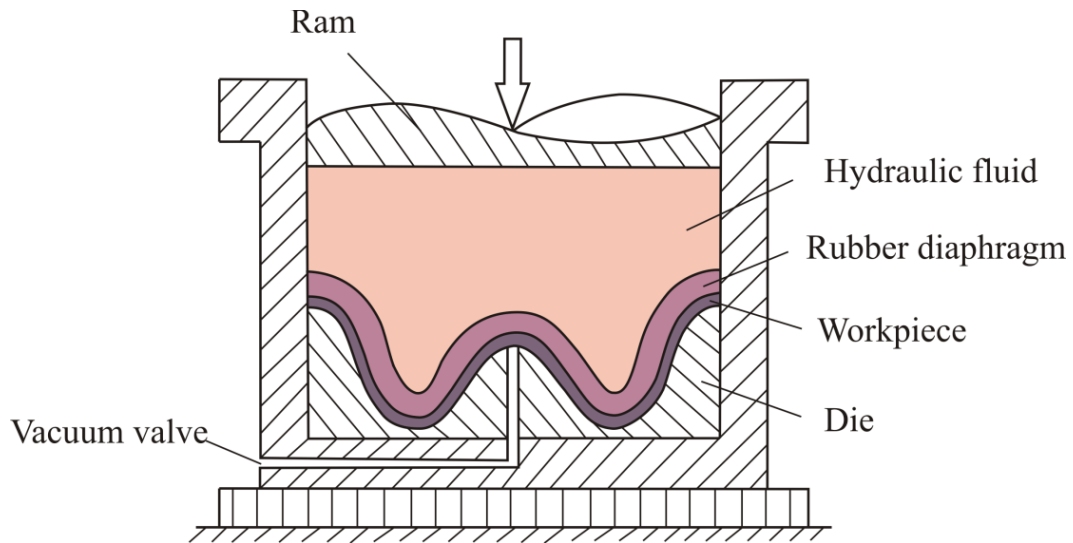


Figure4. 7 SAAB Rubber-Diaphragm process

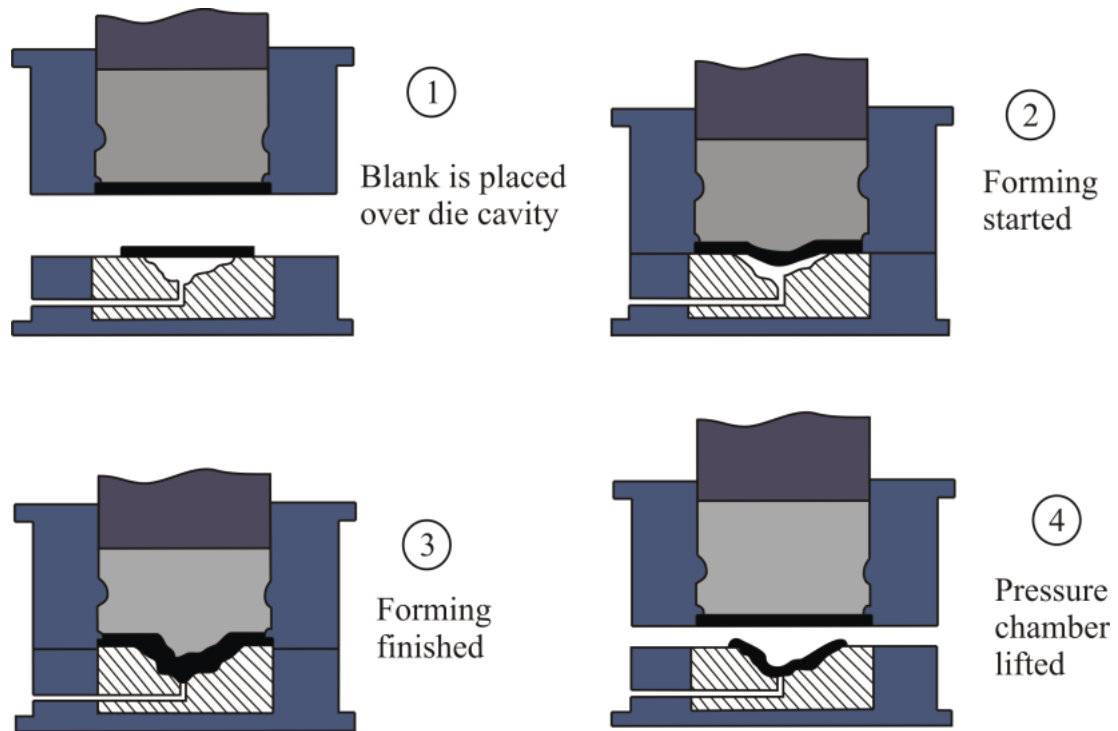


Figure4. 8 Stages of the SAAB fluid-form method of press working

### 4.7 Bulging Punches

Rubber punches can be used to make tubular parts that need to be expanded to a required form. The tooling for bulging one end of a tube using a

urethane rod is shown in the Figure 4.9. When load is applied on the urethane rod, it supplies the lateral pressure and the axial compression needed for the tube to be bulged. The friction between the urethane and the tube helps building the axial compressive stress and the axial feeding of the tube. The lateral pressure and the axial compression are not controlled independently, and thus the circumferential expansion possible with urethane bulging is limited when compared to hydraulic bulging. To avoid a possible fracture and a buckled tube in the process and to get successful bulging, proper length of the urethane rod should be chosen, or frictional conditions between the tube and the urethane should be changed. The amount of bulging is determined by the depth of the punch stroke. The bulged part can be easily removed after the forming operation as the rubber would resume its original shape when the press form is removed. This process is suitable for producing near-net-shape of tubular components such as T-branches, X-branches and angle branches. This provides an economical alternative to costly expanding using conventional metallic tools [1, 2, 3, and 19].

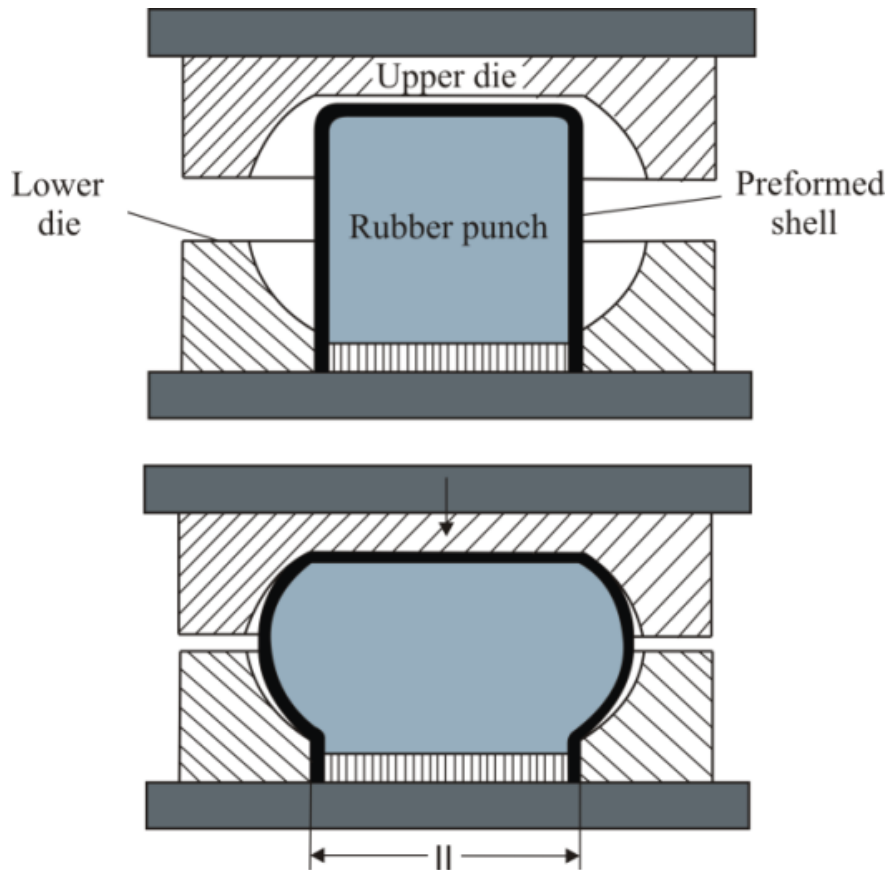


Figure4. 9Bulging Punches process

#### 4.8 Maslennikov's Process

This technique uses a rubber ring instead of the rigid punch and is used in the production of very deep cups Figure4.10. As the punch squeezes the urethane, the latter moves radially inwards, creating a radial friction force between the urethane and the sheet metal and forces the sheet onto die cavity. After squeezing the pad, the punch retracts and the pad retrains to its original shape [1, 2, 3, and 19]. Repeated squeezing of the rubber pad increases the depth of the cup up to the draw ratio of 6. This process is affected by the friction coefficient, hardness and dimension of the rubber. As the total drawing ratio increases, the tooling costs also increase since a punch and a die are required for each stage. However, the diameter and thickness variation of the cup need improvement by re-drawing and ironing.

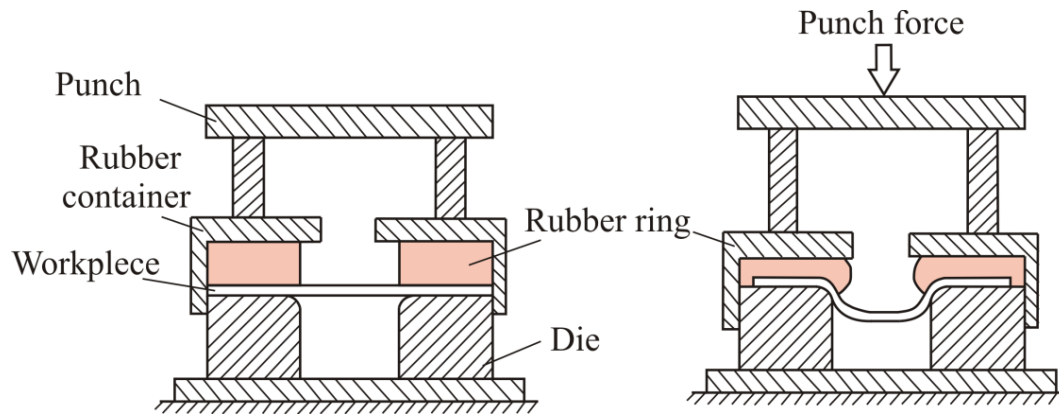


Figure4. 10 Maslennikov's deep drawing process

The number of cycles needed to obtain a particular draw ratio depends on various factors, including the pad thickness, the pad diameter and the diameter of the blank, the friction between the urethane and the sheet metal, lubrication of the die etc. The dimensional accuracy and thickness variation of the cup formed can be improved by modifying the Maslennikov technique using the metal punch [1,2,3,19].

#### 4.9 Tube Bulging

Bulge forming uses hydrostatic pressure to shape tubular components to the required form. This is an internal forming operation used to expand parts of a drawn shell or tube. The forming force is applied from inside the workpiece and is transmitted by a rubber pad. The tubular blank is subjected to very high hydrostatic pressure to stress the part beyond its elastic limit, thus yielding to the form of the surrounding die. This process is suitable for producing near-net-shape of tubular components such as T-branches, X-branches and angle branches. This provides an economical alternative to costly expanding using conventional metallic tools [1, 2]. The figure 4.11 shows how a certain section of the tube can be bulged. A punch which fits nicely to the internal diameter of the tube is used to squeeze the rubber contained in the tube as it descends. The compressed rubber rod exerts a lateral pressure on the tube to expand the tube circumferentially, while simultaneous axial feeding of the tube is secured by the

frictional traction on the tube as the rubber rod deforms relative to the tube. This lateral force forces the tube to expand and assume the shape of the die. The amount of bulging is determined by the depth of the punch stroke.

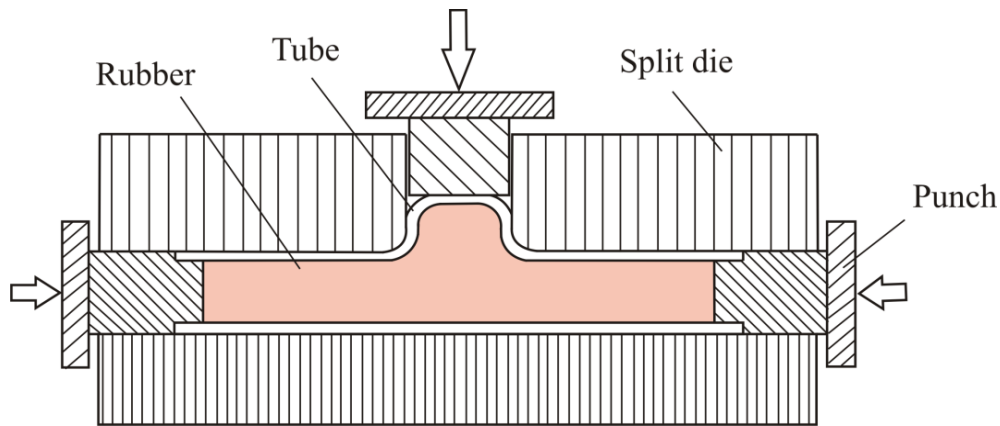


Figure4. 11Bulging T joint with rubber rod

The bulged part can be easily removed after the forming operation as the rubber would resume its original shape when the press form is removed. The figure4.12 shows the scheme of the free bulge forming technique. When the hydraulic ram compresses the rubber, the incompressible nature of the rubber will cause it to deform radially and push the sheet metal into the cavity of the die block. The removal of the finished part is achieved by dismantling the split dies. [ 1,2,3,19] .

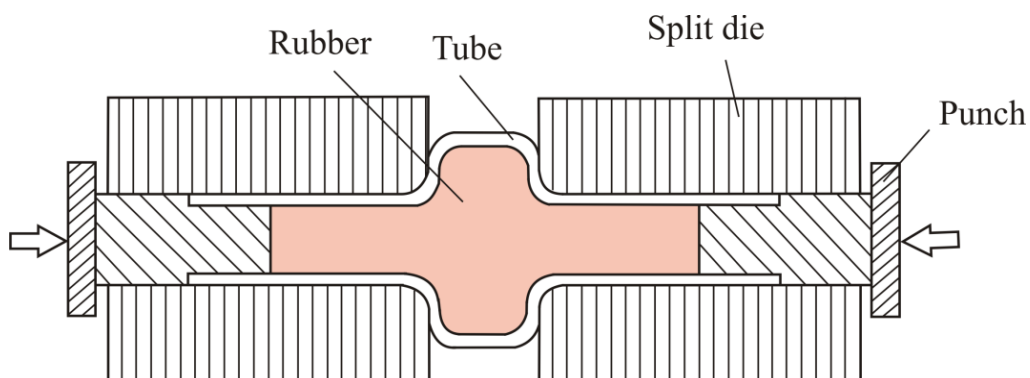


Figure4. 12 Free bulges forming of tube using rubber rod

#### 4.10 Flexible Tool Materials

Natural rubber, neoprene, urethane or other elastomers may be selected as a flexible-tool material in sheet metal forming. Compared to other materials, urethane has advantages such as good wear resistance, better thermal stability and greater load-bearing capacity [35, 36]. However, urethane has disadvantages such as short life cycle, due to various levels of hardness, then, a low working temperature leads to a limited number of strokes per minute to avoid the heat generated during the forming process, which, again, is a cause of failure in urethane [1, 2, 37,38and39].

#### 4.11 Industrial Application of Rubber Pad Forming

The rubber pad forming press technology is derived from the aircraft industry, where the forming process is complex and demands a metal surface without damages. Low tooling costs make this production technique highly appealing for products in small to medium sized series. With a pressing capacity up to 8.000 tons and sheet metal sizes up to 2200 x 1100 mm, it certainly gives more possibilities to create unique metal forms and designs as well as pressing several small parts at the same time. Phoenix 3D Metal further developed the technology, creating endless possibilities with the rubber pad forming press and making it applicable to different branches of the industry, such as exterior and interior building construction parts, Arts and design works,(Luxury) automotive parts ,Yacht building ,Industrial parts and smart constructions (medial sector, machinery and appliances, agriculture, etc.) [1, 2, 3, 19].

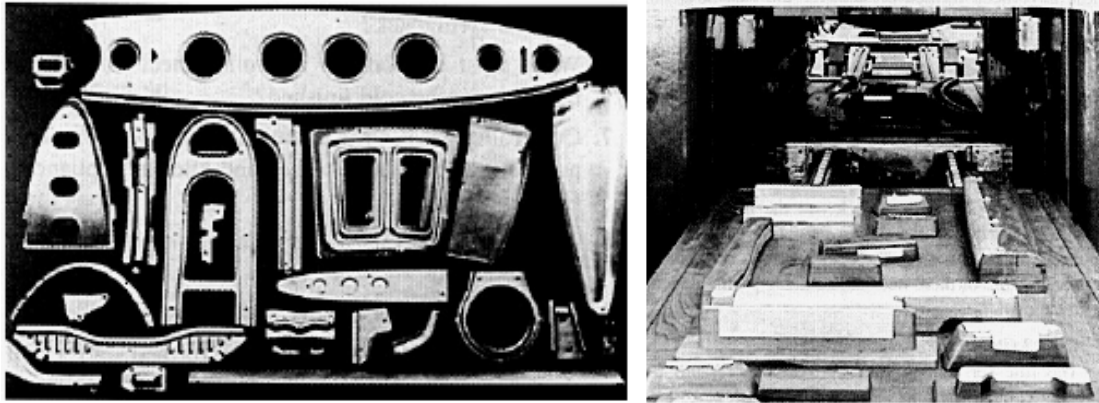


Figure4. 13 Examples formed ribs using rubber pad forming process

## **5. Die Design in CAD -CAM Environment in Sheet Metal Forming**

### **5.1 CATIA in Rubber Pad Forming Process**

CATIA is one of the leading product development solutions, used in many manufacturing organizations today. The range of CATIA capabilities allows it to be applied in a wide variety of industries, such as aerospace, automotive, industrial machinery, electrical, electronics, shipbuilding, plant design and consumer goods. [40]

Acronym CATIA stands for Computer Aided Three-dimensional Interactive Application and is used for a multi-platform CAD/CAM/CAE commercial software suite developed by the French company Dassault Systemes [41]. Written in the C++ programming language, CATIA is the cornerstone of the Dassault Systemes product lifecycle management (PLM) software suite. CATIA started as an in-house development in 1977 by French aircraft manufacturer Avions Marcel Dassault and its' primary use was the development of Dassault's Mirage fighter jet. Since then, software was improved on a regular basis and today many large companies (including Boeing, Airbus, Bombardier, BMW, Mercedes Benz, etc.) use CATIA for a complete product development process.

CATIA supports multiple stages of development, including conceptualization, design, manufacturing and engineering. It facilitates collaborative engineering across disciplines, including surfacing & shape design, mechanical engineering, equipment and systems engineering. CATIA also provides a suite of reverse engineering and visualization solutions to create modify and validate complex innovative shapes, from subdivision, styling, and Class A surfaces to mechanical functional surfaces. On the other hand, CATIA enables the creation of 3D parts from 3D sketches, sheet metal parts, and composites, molded, forged or tooling parts according to the definition of mechanical assemblies.

Much beyond pure CAD software packages, which provide geometry modeling features for design-centric users, CATIA delivers the keys to PLM for process-centric users. This means that the main purpose of CATIA is product creation: from the earliest product concept to production tooling. CATIA users can do that through integrated analysis, simulation, synthesis and optimization applications, which provide product engineering validation at each design step and ensure product quality.

Taking into account all the previously mentioned advantages, during the work on this thesis it was decided to use CATIA for creation of all the 3D models of light aircraft ribs used in FEM simulations, as well as tools for experimental set-up.

Since ribs and tools incorporate the airfoil shape of the wing, the starting point in the design of the rib is the airfoil selection, i.e. the selection of the suction surface (a.k.a. upper surface) generally associated with higher velocity and lower static pressure and the selection of the pressure surface (a.k.a. lower surface) which has a comparatively higher static pressure than the suction surface [42]. In general, these surfaces are not the same in shape, which means that they must be defined separately.

Over the years several families of airfoils were developed by the National Advisory Committee for Aeronautics (NACA). Many of these airfoil shapes have been successfully used as wing sections or tail sections for general aviation aircraft, as well as propellers and helicopter rotors [43]. The ordinates for numerous specific airfoils of these families at a coarse set of data points were published in a series of NACA reports. However, when performing parametric studies on effects of such variables as thickness, location of maximum thickness, leading-edge radius, etc., it is not always easy to rapidly and accurately obtain the ordinates of the desired shapes. To remedy this problem, the NASA Langley Research Center sponsored the development of computer programs for generation of ordinates of standard NACA airfoils.

Two separate programs were written. The first was documented in NASA TM X-3284 and produces ordinates for NACA 4-digit, 4-digit modified, 5-digit, and 16-series airfoils [44]. These thickness families are defined by algebraic equations. These thickness families are combined with appropriate mean lines to produce the final thick cambered airfoil. The second program was documented in NASA TM X-3069 and produces ordinates for NACA 6-series and 6A-series airfoils.

By using these programs it is possible to get exact x- and y- coordinates of points which define the upper and lower surface of airfoil. The coordinates of these points could be entered in CATIA's module Wireframe and Surface Design then and joined to form a curve using the option Spline (Figures 5.1 and 5.2). The Figures 5.1 and 5.2 show that 36 points were generated in order to define the shape of the curves for both surfaces (upper and lower) of the rib with the lightening hole, used in 3D FEM simulations in Ansys software. These curves can be "extruded" to form surfaces of the airfoil (shown in yellow in Figure 5.3) using the CATIA command Extrude. Obtained surfaces are "limiting" surfaces and they define geometric limits of the rib; in other words, geometry of the rib cannot exceed the upper and lower surface and must be defined within them. In Figure 3 the initial shape of the rib's wall is represented by black line.

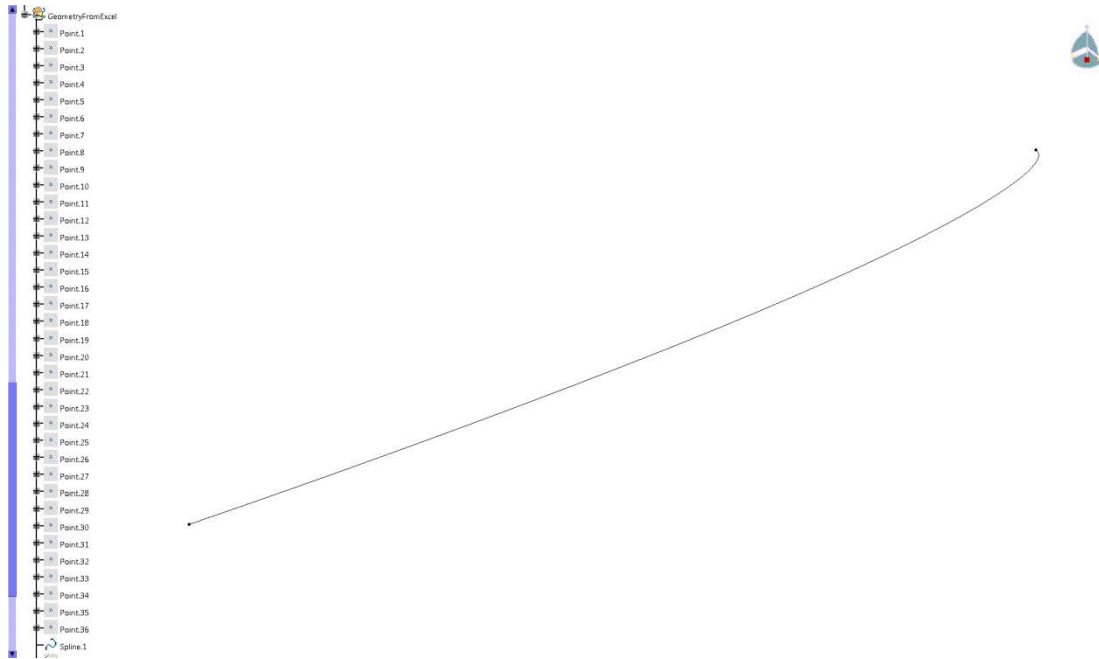


Figure5. 1 Creation of upper surface of airfoil using CATIA's option *Spline*

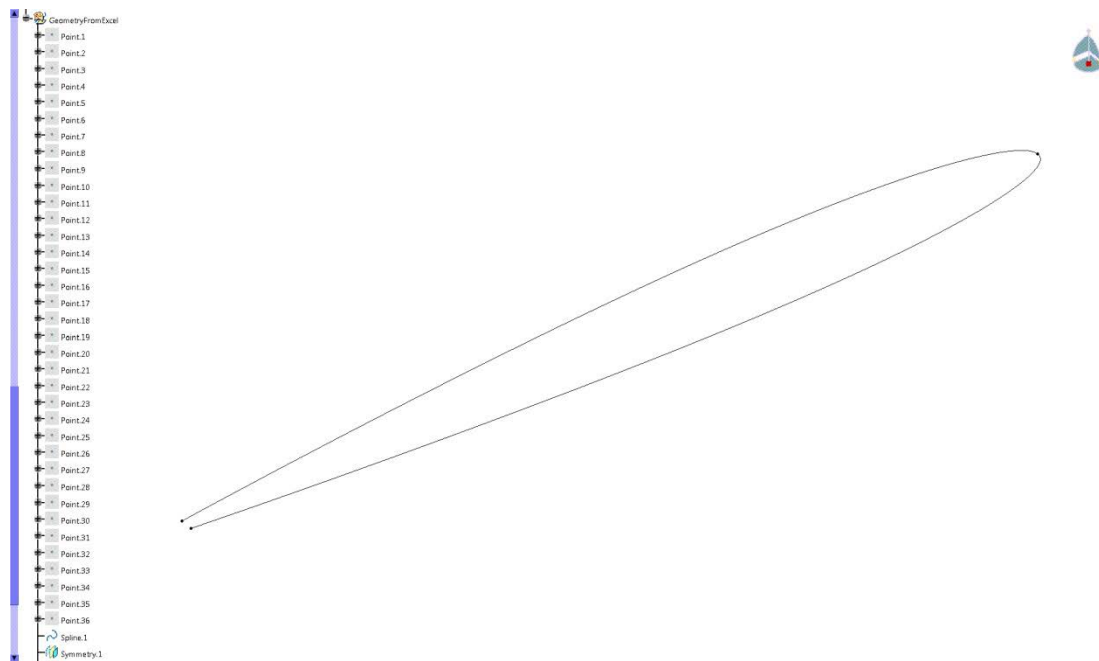


Figure5. 2 Creation of lower surface of airfoil using CATIA's option *Spline*

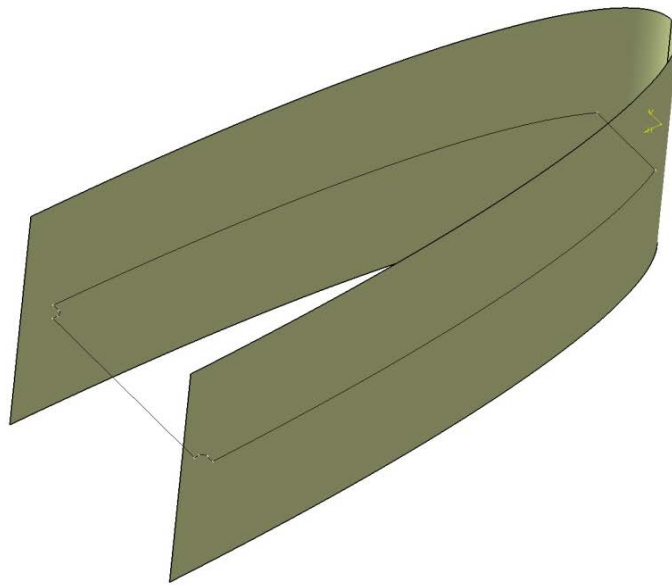


Figure5. 3 Design of surfaces of airfoil using command *Extrude*

To define 3D geometry of the rib using the obtained surfaces and drawn line, it is necessary to use another CATIA module Aerospace Sheet Metal Design. Firstly, sheet metal parameters (such as sheet thickness, default bend radius, bend allowance and joggle type) must be entered and then the command *Web* may be used to create the basic feature (wall) of the rib (Figure5.4).

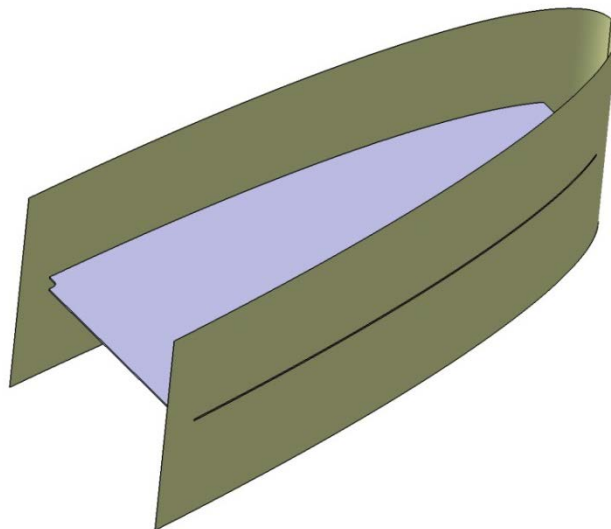


Figure5. 4 Basic wall of the rib created using command *Web*

Secondly, flanges have to be created which must follow the shape of the upper and lower surface. In order to ensure that, CATIA command Surfacic Flange is used. When creating a surfacic flange, the bend is propagated along the whole base feature with continuity in tangency. In certain cases this propagation prevents the surfacic flange from being re-limited: this happens when the selected edge allows propagation of the bend. [45]

To create a surfacic type of flange, a geometrical support must be chosen. It can either be a surface, a plane or a curve. In the case of the rib the with lightning hole, geometrical supports are the upper and lower surface of airfoil (Figures 5.5 and 5.6). In general, three types of support are available in CATIA:

- Exact: the selected support is to be used for the creation of the surfacic flange.
- Approximation: the support surface is approximated using a ruled surface. This ruled surface is defined from two curves: the OML, computed at the intersection between the support surface and the web plane, and a curve parallel to the OML, computed at a distance equal to the approximation length. This mode enables computation of the maximum deviation between the support geometry and the approximated surface.
- Angle: the support can also be defined by an angle with respect to the edge of a base feature.

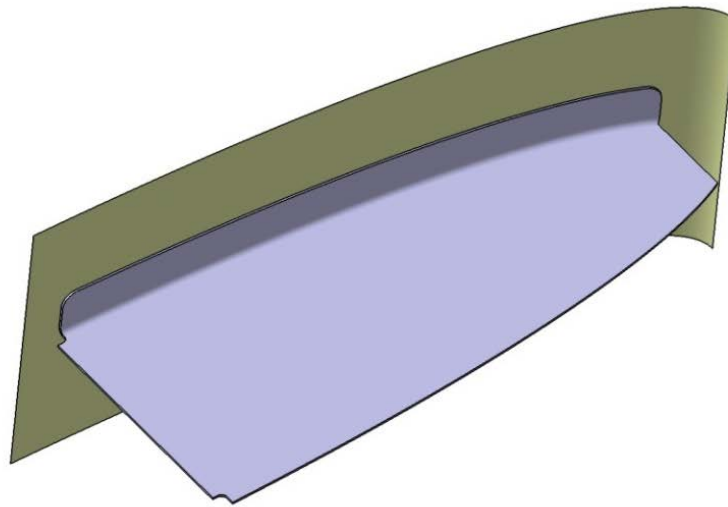


Figure5. 5 Surfacic flange defined by the lower surface of airfoil

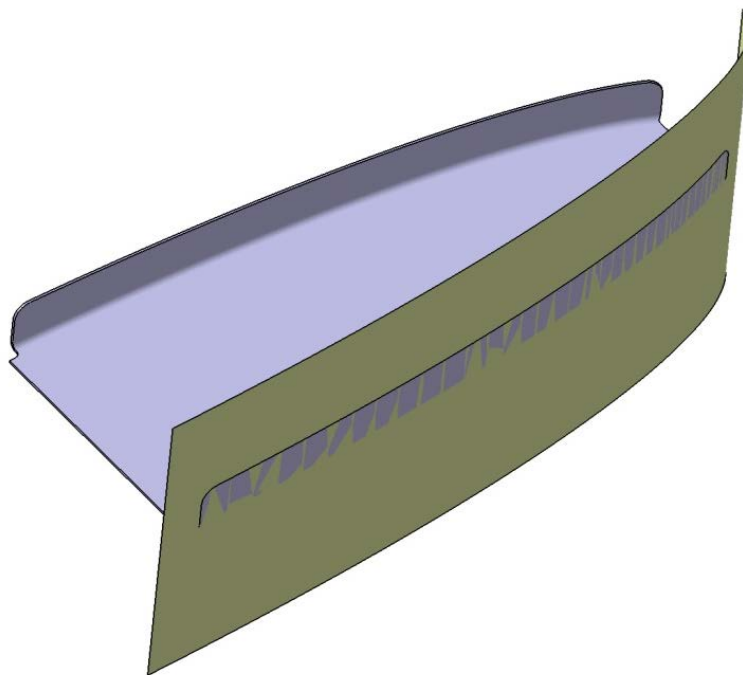


Figure5. 6 Surfacic flange defined by the upper surface of airfoil

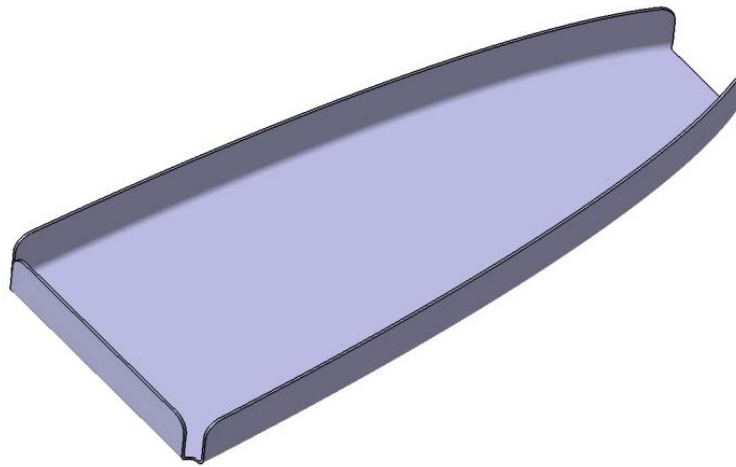


Figure5. 7 Flange obtained using command *Flange*

The last flange on the rib (shown in Figure5.7) may be created using the command *Flange*, because it is simple 3D geometry which doesn't follow any surface; the purpose of this flange is to provide connection between the rib and other elements in the tail assembly.

Thirdly, the joggles of the rib have to be defined in order to provide joggle joints. A joggle is a small offset near the edge of a piece of sheet metal, while a joggle joint is used where a strong joint and flat surface is needed to join two pieces of sheet metal or light plate. The joint allows one sheet of metal to overlap another, while maintaining a flush surface. In aircraft design, joggles are frequently used where compact connection between stringers and ribs are necessary.

In CATIA, a joggle is a feature which causes the main feature (i.e. a surfacic flange or a web) to be locally deformed and it cannot exist alone; it is always defined on a previously created flange or web. This means that the main feature and the joggle starting plane must be selected first, and then the following parameters of the joggle may be modified:

- Depth: offset from the support surface
- Runout: length of the offset, between the original surface of the surfacic flange or the web and the new surface (joggle)
- Clearance: length added to the offset at the joggle starting plane
- Start Radius: fillet between the runout and the surfacic flange or the web
- End Radius: fillet between the runout and the offset.

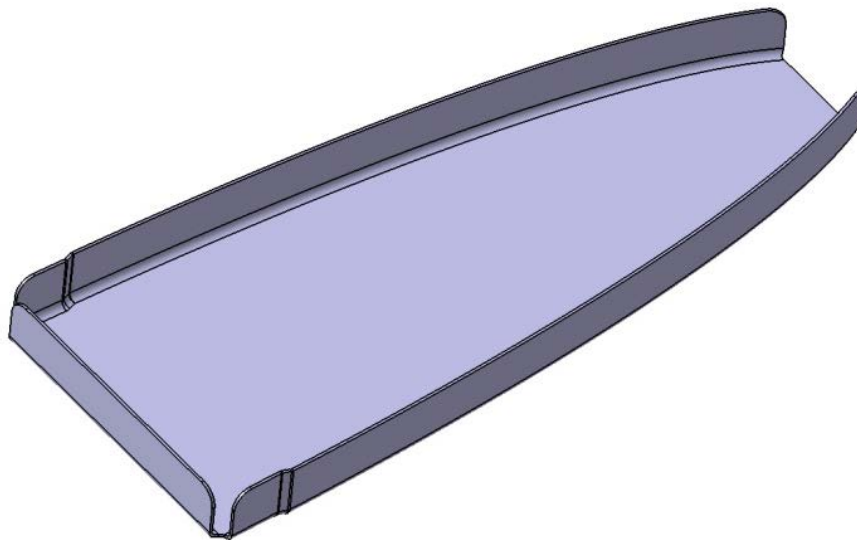


Figure5. 8 Two joggles defined on surfacic flanges using command *Joggle*

Finally, a flanged hole has to be defined. Most ribs used in aircraft design have this type of hole, also known as a lightening hole. The hole is cut in a rib to get rid of the weight, or lighten the structure, without losing any strength. A hole of several centimeters in diameter may be cut in at a point where the metal is not needed for strength; in most cases that is a web of a wingtail rib. The edges of the hole are flanged (bent outward) to give the metal rigidity. A Rib with flanged lightening holes is more rigid than a rib before the lightening holes were cut.

In CATIA, the center of the circle which defines the position of the lightening hole must be defined first (Figure5.9). Next, the radius of the hole must be entered, along with height, radius, angle and diameter of the flange (Figure 5.10). The final shape of the lightening hole is given in Figure 11.

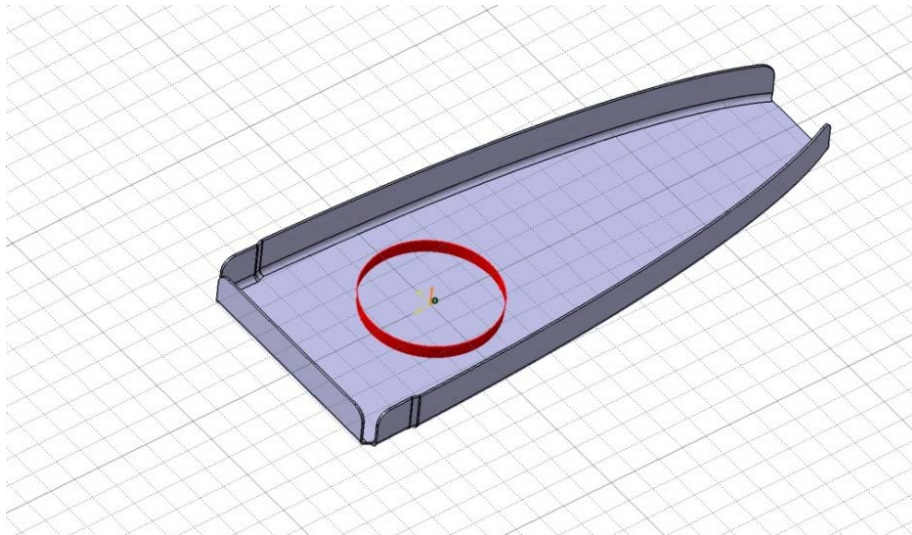


Figure5. 9 Exact position of the flanged hole must be defined first

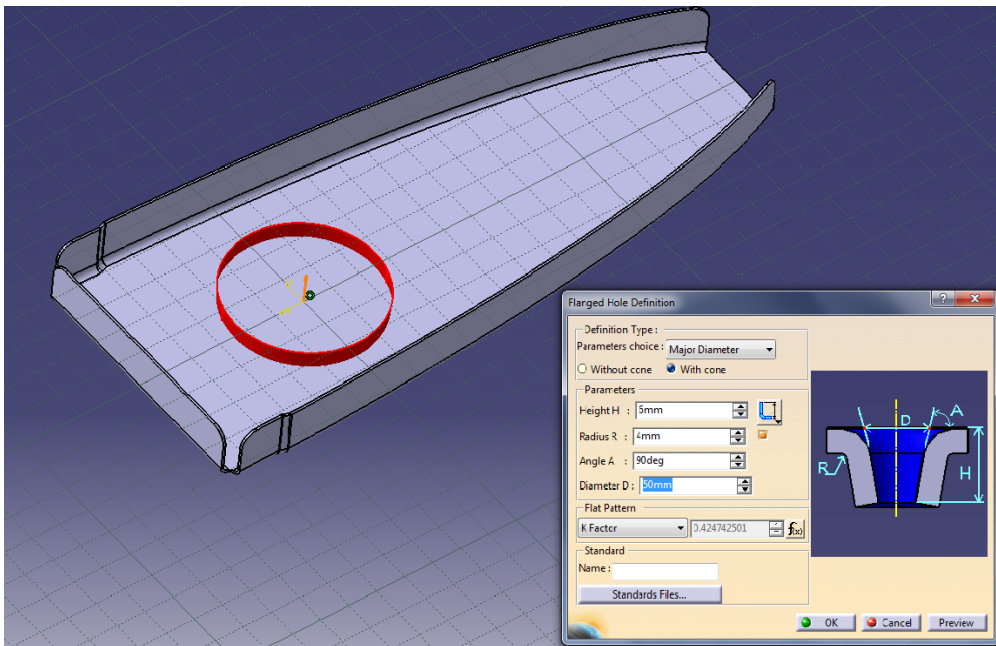


Figure5. 10 Parameters necessary to define flanged hole

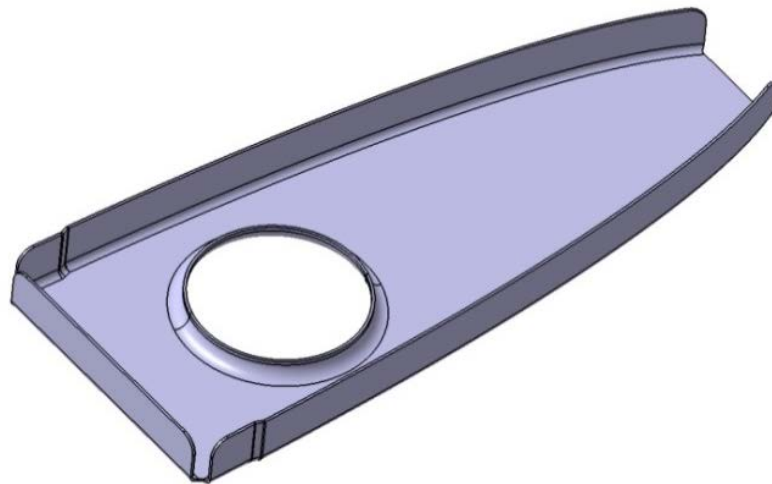


Figure5. 11 Final shape of the rib with lightening hole used in 3D FEM simulations as designed in CATIA v5

One of the main CATIA advantages is that after obtaining the final shape of the rib it is possible – in just a few steps – to define the shape of the blank and the geometry of the tool needed to produce the required rib. The shape of the blank may be obtained using the command *Unfold*, and after applying this command on the rib with the lightening hole it will be unfolded, as shown in Figure5.12. This operation, as well as all the previously described, must be performed in the Aerospace Sheet Metal Design module. Two small holes created on the blank (noticeable in Figure 5.12) will be used for fixing the blank on the tool during the rubber pad forming process.

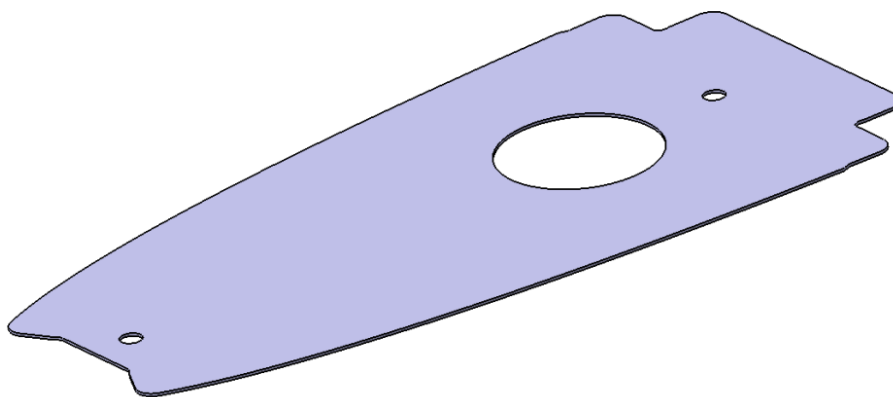


Figure5. 12 Shape of the blank obtained using command *Unfold*

To get the exact shape of the tool, several operations must be performed. Firstly, the shape of the rib must be used as a base for creation of the tool surfaces. The surfaces must be created in Wireframe and Surface Design module, using command Offset (Surface) and selecting – one by one – all the rib internal faces, keeping zero distance between them and newly created surfaces (shown in yellow in Figure 13). Secondly, the created surfaces must be closed and joined together to form a solid-like structure (shown in Figure 5.14). For that purpose the commands Fill (Surface) and Join (Surfaces) are used.

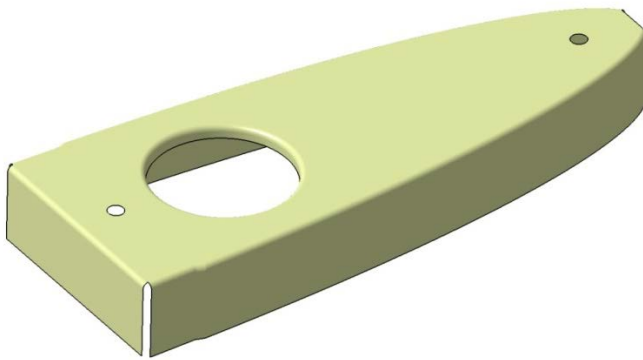


Figure5. 13 Creation of surfaces equivalent to internal faces of rib, using command Offset Surface

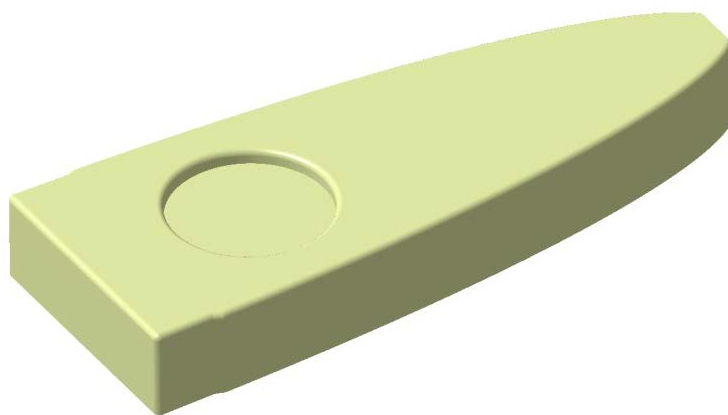


Figure5. 14 Shape of the surface after using commands *Fill* and *Join*

Finally, surface shown in Figure 5.14 can be used for tool creation. In the CATIA module Part Design there is a command Close Surface which creates a solid part within defined surface, filling the empty space with tool “material”. Final shape of the tool for the rib with the lightening hole is shown in Figure5.15.

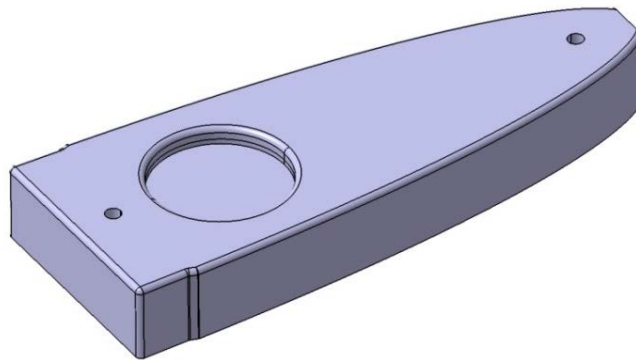


Figure5. 15 Final shape of the tool for rib with lightening hole

Figures 5.16 and 5.17 show the rib and the tool together, and it is obvious that they fit perfectly, confirming that all the operations necessary for the tool creation have been performed well. In Figure 5.18 the final shape of the rib with the lightening hole with all the dimensions is given.

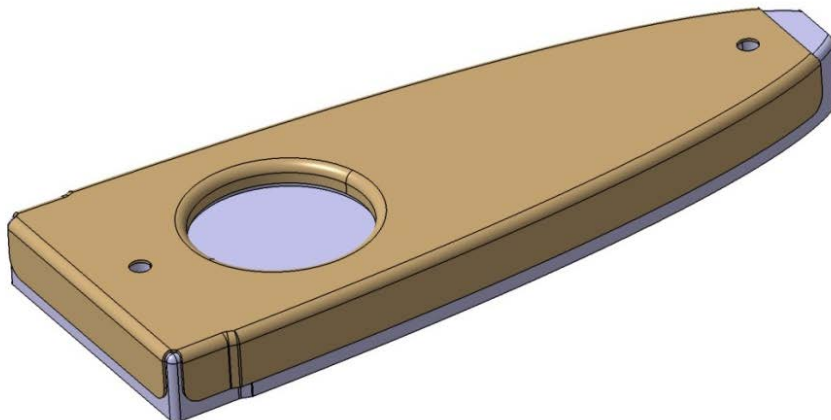


Figure5. 16 Rib with lightening hole and appropriate tool

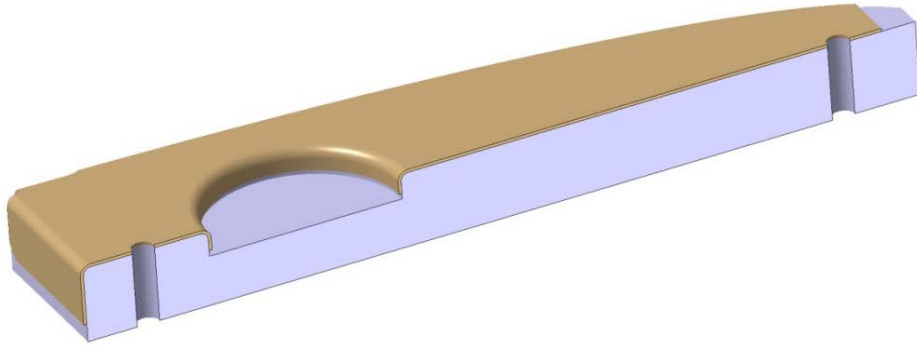


Figure5. 17 Cut view of the rib with lighteninghole and appropriate tool

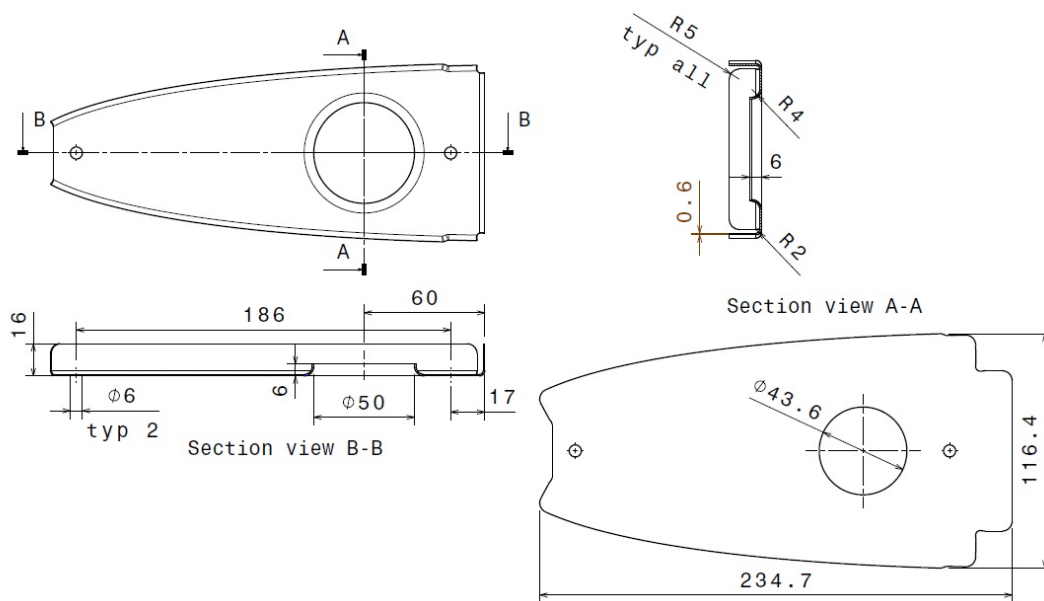


Figure5. 18 Dimensions of the rib with lightening hole

Once the virtual tool has been designed in CATIA, it is possible to completely simulate machining processes (that is, to choose appropriate tools and define their paths) necessary for rib tool manufacturing. For that purpose, the CATIA module Machining can be used.

This tool-path programming module was designed to optimize program operations. The CATIA Machining provides the user with efficient and easy-to-use NC programming and machining simulation options that significantly reduce overall manufacturing process time [46]. The interface uses contextual menus and selection boxes with sensitive zones and the work environment adapts to each context and work phase. Rapid tool-path computing time enables any choice of machining strategy to be factored in immediately. This helps optimize the fine-tuning and modification stages, thus significantly reducing NC programming time.

CATIA Machining offers completely integrated environment for machining simulation ranging from the simulation of material removal, analysis of remaining material to realistic machine simulation based on ISO-code. This realistic virtual simulation enables user to validate, early on in the process, that the part will be correctly machined the first time and without any collisions. Manufacturing documentation is generated automatically and includes the machining phases, tools, machine and the cutting parameters.

By using CATIA machining domain it allows the user to have access to the design intent without having to do lengthy or error prone translations into another CAM packages. Because of this, any design changes can easily be updated and the effects on the manufacturing process can be assessed, in terms of effects on tooling, holding jigs & fixtures, even the size of the stock.

CATIA machining provides an efficient, yet easy to use system to create NC part programs to significantly reduce the overall time to final product. Through the use of knowledge based information, a user can re-use manufacturing strategies on similar components to speed up the process of writing NC programs, as well as applying “best practice methods” defined by other, more experienced users.

CATIA machining covers the complete spectrum of NC programming, including:

- 2.5 axis Prismatic machining
- 3 axis Surface machining.
- Lathe/ Turning.
- Multi-axis Surface machining.
- Multi-axis multi pocketing, and
- Mill/Turn machining.

In Figure 5.19, machining operations necessary for manufacturing of the previously designed rib tool are shown. As it can be seen, eight steps are required in order to get the final shape of the tool, including facing, prismatic machining, profile contour roughing, profile contour finishing, pocketing, isoperimetric machining and drilling.

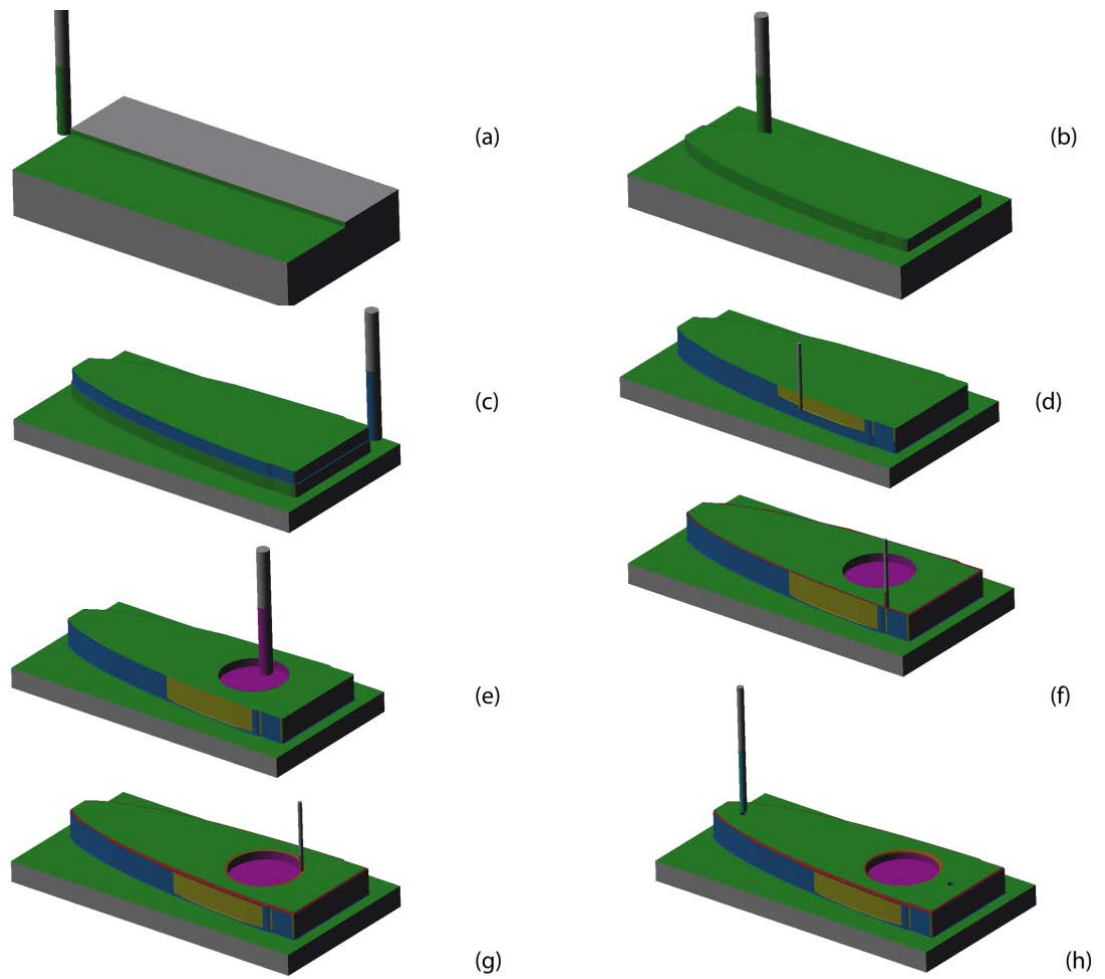


Figure 5.19 Machining operations used in simulation of rib tool manufacturing:  
(a) Facing, (b) Prismatic roughing, (c) Profile contour roughing, (d) Profile contour finishing, (e) Pocketing, (f) and (g) Isoperimetric machining, (h) Drilling

## **6. Finite Element Analyses of Sheet Metal Rubber Pad Forming Process**

The finite element method (FEM) has become a staple for predicting and simulating the physical behavior of complex engineering systems. The commercial finite element analysis (FEA) programs have gained common acceptance among engineers in industry and researchers at universities and government laboratories.

The FEA method, originally introduced by Turner et al. (1956), is a powerful computational technique for approximate solutions to a variety of "real-world" engineering problems having complex domains subjected to general boundary conditions. FEA has become an essential step in the design or modeling of a physical phenomenon in various engineering disciplines. A physical phenomenon usually occurs in a continuum of matter (solid, liquid, or gas) involving several field variables. The field variables vary from point to point, thus possessing an infinite number of solutions in the domain.

The basis of FEA relies on the decomposition of the domain into a finite number of subdomains (elements) for which the systematic approximate solution is constructed by applying the variational or weighted residual methods [47]. In effect, FEA reduces the problem to that of a finite number of unknowns by dividing the domain into elements and by expressing the unknown field variable in terms of the assumed approximating functions within each element. These functions (also called interpolation functions) are defined in terms of the values of the field variables at specific points, referred to as nodes. Depending on the geometry and the physical nature of the problem, the domain of interest can be discretized by employing line, area, or volume elements. Each element, identified by an element number, is defined by a specific sequence of global node numbers. These nodes make a grid called a mesh (Figure 6.1).

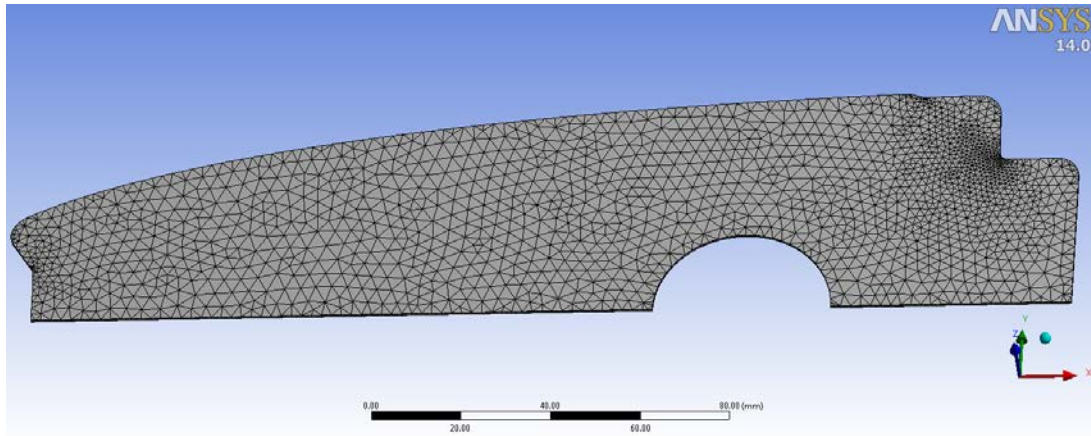


Figure6. 1 Three-dimensional finite element mesh of the blank for rib with a lightening hole

This mesh must be programmed to contain the material and structural properties which define how the structure will react to certain loading conditions.

The ability to discretize the irregular domains with finite elements makes the method a valuable and practical analysis tool for the solution of boundary, initial, and eigenvalue problems arising in various engineering disciplines.

### 6.1. Major Steps in FEA

The finite element analysis method requires the following major steps:

- Discretization of the domain into a finite number of subdomains (elements).
- Selection of interpolation functions.
- Development of the element matrix for the subdomain (element).
- Assembly of the element matrices for each subdomain to obtain the global matrix for the entire domain.
- Imposition of the boundary conditions.
- Solution of equations.
- Additional computations (if desired).

The construction of solutions to engineering problems using FEA requires either the development of a computer program based on the FEA formulation or the use of a commercially available general-purpose FEA program such as ANSYS [48] or ABAQUS [49]. Before using any software to generate an FEA model of a physical system, the following questions should be answered based on engineering judgment and observations:

- What are the objectives of the analysis?
- Should the entire physical system be modeled, or just a portion?
- How much detail should be included in the model?
- How refined should the finite element mesh be?

In answering such questions, the computational expense should be balanced against the accuracy of the results. Therefore, any finite element program can be employed in a correct and efficient way after considering the following:

- Type of problem.
- Time dependence.
- Nonlinearity.
- Modeling idealizations/simplifications.

## **6.2. Types of Structural Problems That Can Be Analyzed by FEM**

The FEM programs are capable of simulating problems in a wide range of engineering disciplines [50]. However; this thesis focuses on the structural analysis, which is based on calculation of deformations, stress and strain fields, as well as reaction forces in a solid body. Structural analysis addresses several different structural problems, for example:

- Static Analysis (where the applied loads and support conditions of the solid body do not change with time; nonlinear material and geometrical properties such as plasticity, contact, creep, etc., are available).

- Modal Analysis (this option concerns natural frequencies and modal shapes of a structure).
- Harmonic Analysis (the response of a structure subjected to loads only exhibiting sinusoidal behavior in time).
- Transient dynamic (the response of a structure subjected to loads with arbitrary behavior in time).
- Eigenvalue Buckling: This option concerns the buckling loads and buckling modes of a structure).

The solution for each of these analysis disciplines provides nodal values of the field variable. This primary unknown is called a degree of freedom (DOF). The analysis discipline should be chosen based on the quantities of interest.

### 6.3. Nonlinearity

Most real-world physical phenomena exhibit nonlinear behavior. There are many situations in which assuming a linear behavior for the physical system might provide satisfactory results. On the other hand, there are circumstances or phenomena that might require a nonlinear solution. A nonlinear structural behavior may arise because of geometric and material nonlinearities, as well as a change in the boundary conditions and structural integrity. These nonlinearities are discussed briefly here.

#### 6.3.1. Geometric Nonlinearity

There are two main types of geometric nonlinearity:

- *Large deflection and rotation*: If the structure undergoes large displacements compared to its smallest dimension and rotations to such an extent that its original dimensions and position, as well as the loading direction, change significantly, the large deflection and rotation analysis becomes necessary. For example, a fishing rod with a low lateral stiffness under a lateral load experiences large deflections and rotations.

- *Stress stiffening*: When the stress in one direction affects the stiffness in another direction, stress stiffening occurs. Typically, a structure that has little or no stiffness in compression while having considerable stiffness in tension exhibits this behavior. Cables, membranes, or spinning structures exhibit stress stiffening.

### 6.3.2. Material Nonlinearity

Typical nonlinear stress-strain curves are given in Figure 6.2. A linear material response is a good approximation if the material exhibits a nearly linear stress-strain curve up to a proportional limit and the loading is in a manner that does not create stresses higher than the yield stress anywhere in the body.

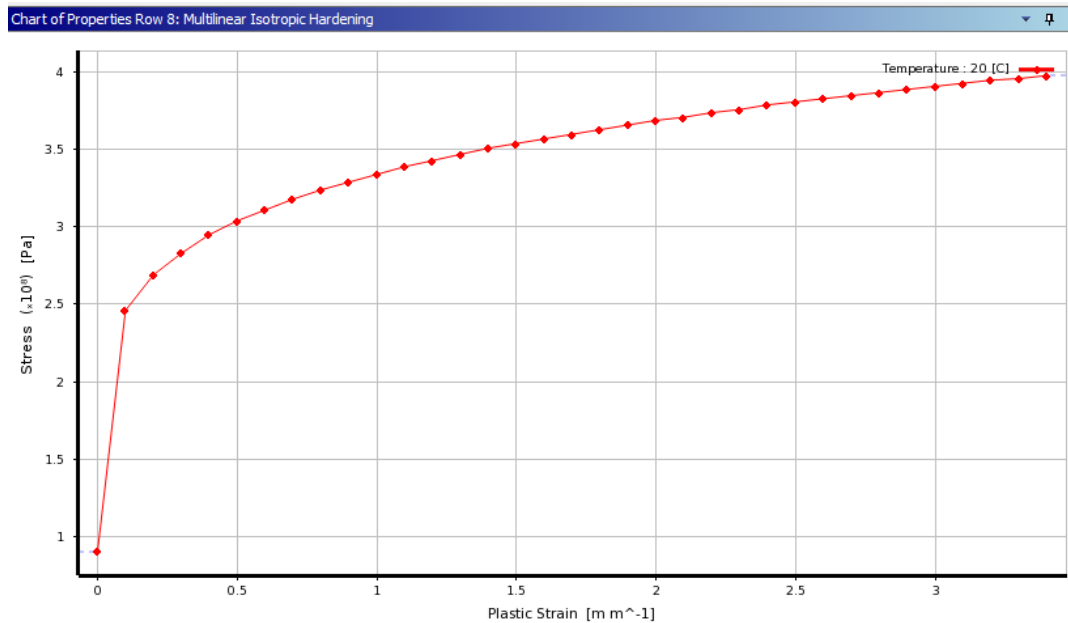


Figure 6.2 stress strain curves presented in ansys in engineering data

Nonlinear material behavior is characterized as:

- Plasticity: Permanent, time-independent deformation.
- Creep: Permanent, time-dependent deformation.
- Nonlinear Elastic: Nonlinear stress-strain curve; upon unloading, the structure returns back to its original state—no permanent deformations.
- Viscoelasticity: Time-dependent deformation under constant load.
- Full recovery upon unloading.
- Hyperelasticity: Rubber-like materials.

### **6.3.3. Changing-Status Nonlinearity**

Many common structural features exhibit nonlinear behavior that is status dependent. When the status of the physical system changes, its stiffness shifts abruptly. The most FEM programs offer solutions to such phenomena through the use of nonlinear contact elements and/or birth and death options. This type of behavior is common in modeling manufacturing processes such as that of a shrink-fit.

The possibility to perform simulations of sheet forming processes was for a long time an unattainable desire in the sheet forming industry. Engineers like to be able to reveal any possible forming defects at an early stage, and to minimize the need for expensive modifications of the tools in a trial-and-error process. From a theoretical perspective the forming problem was, however, considered to be a very complicated problem in the early days of FEM. Modeling sheet metal forming problems require accurate characterization of effects like nonlinear material behavior, large deformations, and complicated contact conditions between the tools and the blank. Because of all the difficulties previously mentioned, an industrial forming operation was considered to be an extremely computationally demanding task.

But, from the beginning of the 1990s there was an explosive increase of the practical utilization of sheet forming simulations within the industry, and from the middle of this decade most companies within the automotive and the aircraft industry were performing sheet forming simulations on a regular basis. Dynamic, explicit codes were dominating the software market [51]. General purpose codes like LS-DYNA and ABAQUS/Explicit, and specialized codes such as PAM-STAMP and OPTRIS are examples of codes that were in use those days.

Today (2013), AutoForm is probably the most commonly used code in the industry for sheet stamping simulations. Beside this code the software market is still dominated by various dynamic, explicit codes like ANSYS-DYNA, ABAQUS/Explicit and STAMPAK. The use of other types of codes is now only marginal. For all FEA of sheet metal rubber forming processes in this thesis ANSYS and ABAQUS codes will be used.

#### **6.4. Mesh Density**

In general, a large number of elements provide a better approximation of the solution. However, in some cases, an excessive number of elements may increase the round-off error. Therefore, it is important that the mesh is adequately fine or coarse in the appropriate regions. How fine or coarse the mesh should be in such regions is another important question. Unfortunately, definitive answers to the questions about mesh refinement are not available since it is completely dependent on the specific physical system considered. However, there are some techniques that might be helpful in answering these questions [50]:

- Adaptive Meshing: The generated mesh is required to meet acceptable energy error estimate criteria. The user provides the "acceptable" error level information. This type of meshing is available only for linear static structural analysis.

- **Mesh Refinement:** An analysis with an initial mesh is performed first and then reanalyzed by using twice as many elements. The two solutions are compared. If the results are close to each other, the initial mesh configuration is considered to be adequate. If there are substantial differences between the two, the analysis should continue with a more-refined mesh and a subsequent comparison until convergence is established.
- **Submodeling:** If the mesh refinement test yields nearly identical results for most regions and substantial differences in only a portion of the model, the "submodeling" should be employed for localized mesh refinement.

Since structures may exhibit symmetry in one or more categories (axisymmetry, rotational symmetry, planar or reflective symmetry, symmetry in material properties, loading, displacements, etc.) it is recommendable to try to find the smallest possible segment of the structure that would represent the entire structure. If the physical system exhibits symmetry in geometry, material properties, loading and displacement constraints, it is computationally advantageous to use symmetry in the analysis. Typically, the use of symmetry produces better results as it leads to a finer, more detailed model than would otherwise be possible.

A three-dimensional finite element mesh of the rib shown in Figure 6.1 contains 394828 tetrahedral elements with 100282 nodes. However, the two-dimensional mesh of the cross section (Figure 6.3) necessary for the rubber-pad forming analysis has 8427 quadrilateral elements and 8972 nodes. The use of 2D elements in this case reduces the CPU time required for the solution while delivering the same level of accuracy in the results.

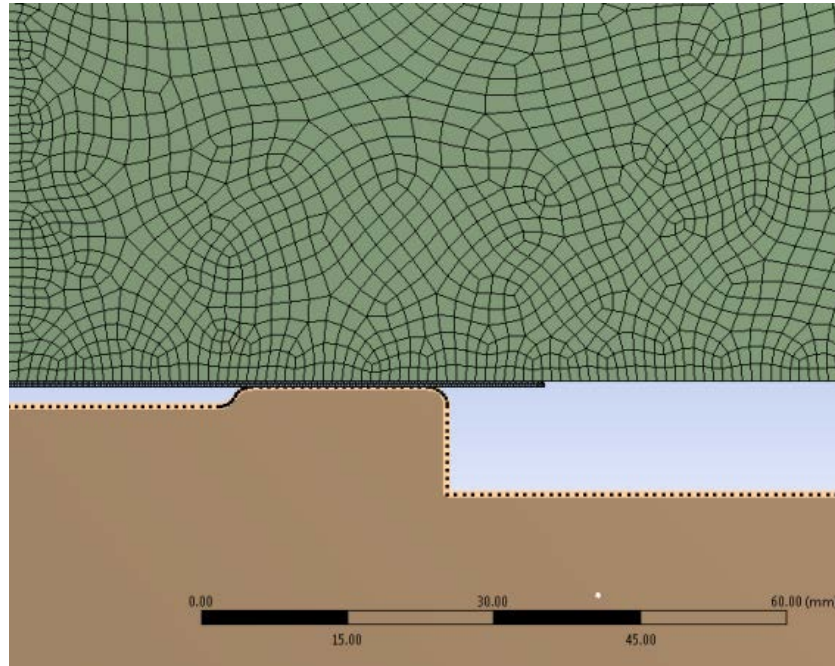


Figure6. 3 2D symmetrical mesh of rib with a lightening hole using rubber pad forming process

## 6.5. Computer Aided Engineering With ANSYS

### 6.5.1. Organization of ANSYS Software

There are two primary levels in the ANSYS program: Begin Level (which is gateway into and out of ANSYS and platform to utilize some global controls) and Processor Level (which contains the Preprocessor, Solution and Postprocessor that are used to conduct finite element analyses).

#### 6.5.1.1 ANSYS Analysis Approach

There are three main steps in a typical ANSYS analysis [47]:

- Model generation (building model by using CAD software like CATIA or within ANSYS, simplifications, idealizations, definition of material properties and generation of finite element model – mesh).
- Obtaining the solution (definition of boundary conditions, starting the simulation).
- Review of results (plot/list results, check for validity).

Each of these steps corresponds to a specific processor or processors within the Processor Level in ANSYS. In particular, model generation is done in the Preprocessor and application of loads and the solution is performed in the Solution Processor. Finally, the results are viewed in the General Postprocessor and Time History Postprocessor for steady-state (static) and transient (time-dependent) problems, respectively. There are several other processors within the ANSYS program. These mostly concern optimization and probabilistic-type problems. The most commonly used processors will be described here briefly.

#### **6.5.1.2. ANSYS Preprocessor**

Model generation is conducted in this processor, which involves material definition, creation of a solid model, and, finally, meshing. Important tasks within this processor are:

- Specification of element type.
- Definition of real constants (if required by the element type).
- Definition of material properties,
- Creation of the model geometry.
- Generation of mesh.

Although the boundary conditions can also be specified in this processor, it is usually done in the Solution Processor.

#### **6.5.1.3. ANSYS Solution Processor**

This processor is used for obtaining the solution for the finite element model that is generated within the Preprocessor. Important tasks within this processor are:

- Definition of analysis type and analysis options,
- Specification of boundary conditions.
- Obtaining solution.

#### 6.5.1.4. ANSYS General Postprocessor

In this processor, the results at a specific time (if the analysis type is transient) over the entire or a portion of the model are reviewed. This includes the plotting of contours, vector displays, deformed shapes, and listings of the results in tabular format.

#### 6.5.1.5 ANSYS Time History Postprocessor

This processor is used to review results at specific points in time (if the analysis type is transient). Similar to the General Postprocessor, it provides graphical variations and tabular listings of results data as functions of time.

### 6.6. ANSYS Workbench interface

There are three methods to use ANSYS. The first is by means of the classic graphical user interface (GUI) based on popular Windows and X-Windows platforms (Figure6.4).

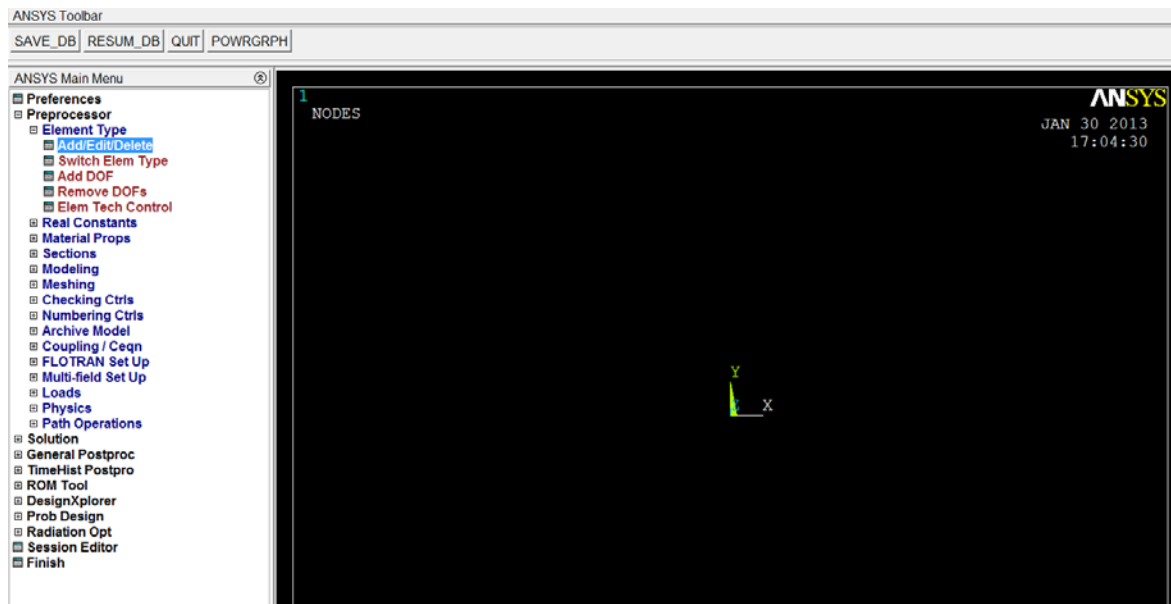


Figure6. 4 Classic ANSYS interface

The second is by means of command files (Figure6.5). The command file approach has a steeper learning curve for many, but it has the advantage that

the entire analysis can be described in a small text file, typically in less than 50 lines of commands. This approach enables easy model modifications and minimal file space requirements.

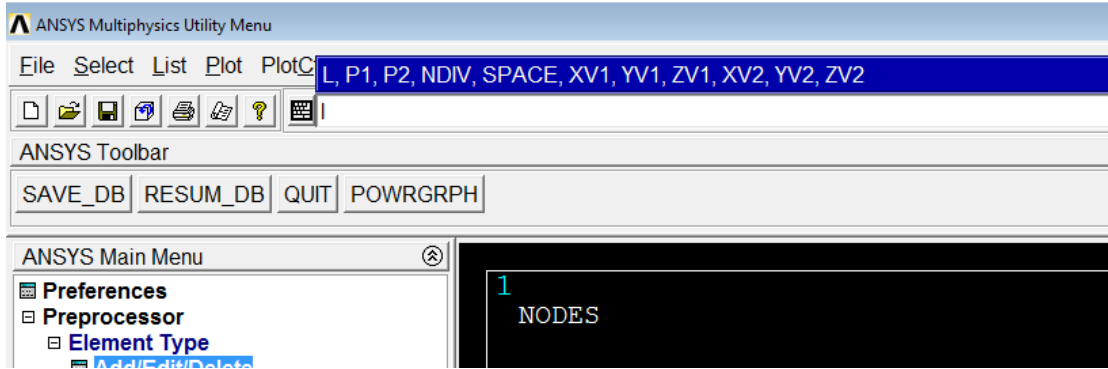


Figure6. 5 Command File

The third method is by means of completely new GUI known as ANSYS Workbench (Figure6.6).

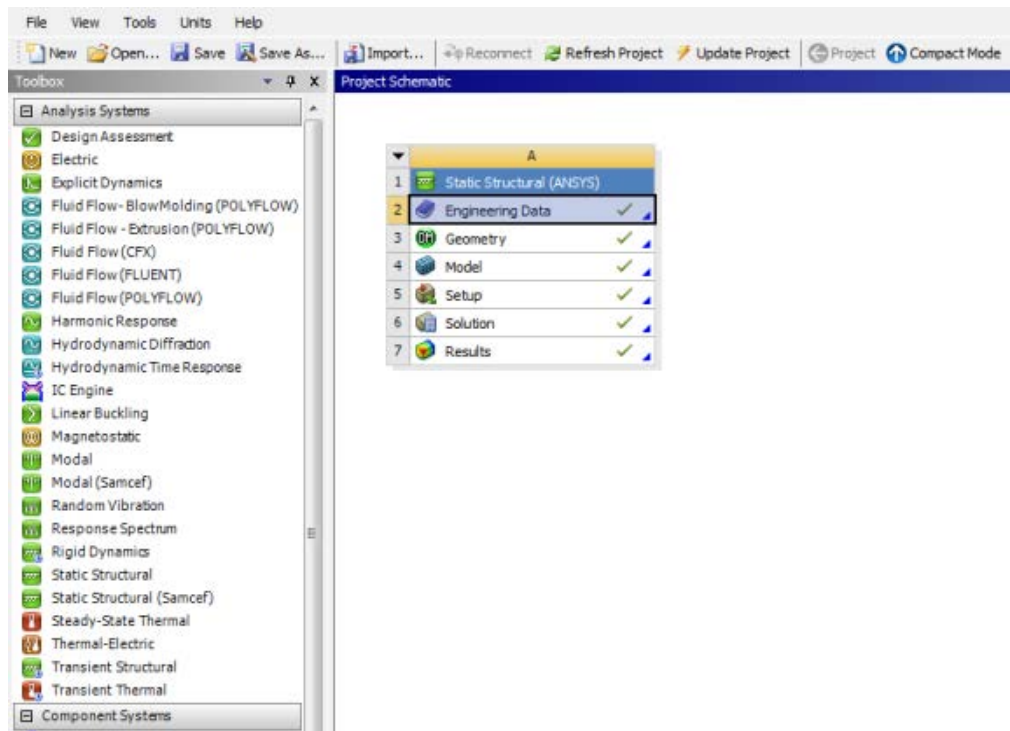


Figure6. 6 ANSYS Workbench

The Workbench has evolved for years but matured more in recent days, and the version 14.5 has been an important step forward. Before the Workbench gets mature enough, most engineers used the classic GUI (now it is dubbed ANSYS APDL). The classic GUI is still driven by text commands, and the user-unfriendly language imposes unnecessary constraints that make the use of the software extremely difficult and painful. The difficulties come from many aspects, for example, modeling geometries, setting up contacts or joints, setting up nonlinear material properties, transferring data between two analytical systems, etc. As a result, engineers often restricted themselves within limited types of problems, for example, working on mechanical component simulations rather than mechanical system simulations. Comparing with the APDL, the real power of the Workbench is its user-friendliness. It releases many unnecessary constraints.

The Workbench GUI is the gateway to all of the ANSYS applications. It can be thought of as the "main program" of the Workbench. It supports two types of applications: native applications and data integrated applications. Native applications are those directly supported in the Workbench GUI, i.e., their program codes and database bind together with the Workbench GUI. The native applications currently supported are Project Schematic, Engineering Data and Design Exploration. Data integrated applications are independent programs: they have their own GUI's and databases. They communicate with the Workbench GUI or other applications through out-of-core database files. Data integrated applications currently supported include Design Modeler, Mechanical, Mechanical APDL, Fluent, CFX, etc.

The Workbench GUI is divided into two sections: on the left there is a Toolbox, and on the right there is the Project Schematic (Figure 6.6). Many predefined templates of Analysis Systems can be seen in the Toolbox (in Workbench, the "analysis" and "simulation" are often interchangeable, for example, "static structural analysis" is synonymous to "static structural

simulation.") A double-click places required template in the Project Schematic. The Static Structural system contains six "cells" (Figure 6.7) implying that it consists of six steps: (a) preparing engineering data, (b) creating a geometric model, (c) dividing the geometric model into a finite element mesh, (d) setup loads and supports, (e) solving the model, and (f) viewing the results. Double-clicking each cell will bring up a fresh application to process that step.

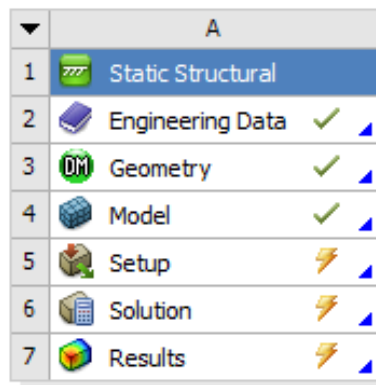


Figure 6.7 Static structural components

By double-clicking the Engineering Data cell in the Static Structural analysis system the Engineering Data application will show up on the top of the Workbench GUI. If the material of the model is an isotropic elastic (so-called *linear material*), option Isotropic Elasticity must be selected and the values of Young's modulus and Poisson's ratio must be entered. On the other hand, if the stress-strain relation is not linear, material is considered as *nonlinear*. In reality, most of materials exhibit more or less nonlinearity. In many cases, the nonlinearities are negligible, and we use Hooke's law to describe the stress-strain relation. In other cases, when the material nonlinearities are not negligible (for example, rubber used in sheet metal forming process) *nonlinear material models* must be used to define stress-strain relations.

A material model is usually a mathematical formulation with some parameters, called *material parameters*. To fully define a material, an engineer must select a material model and provide the material parameters. The material

parameters are usually obtained by data-fitting the results of a series of material testing. The Workbench provides a non-elastic material model, called - *plastic material model*. The current version of Workbench does not provide time-dependent models (also called creep models) or rate dependent models. It is available only through the use of APDL.

### 6.6.1. Elastic versus Plastic Materials

If the strain is not totally recovered after a complete release of the stress, that behavior is called plasticity and the residual strain is called a plastic strain. If the strain is totally recoverable, that is, there is no residual strain after complete release of stress, the behavior is called elasticity and the material is said to be elastic(Figure6.2) .

Following this definition of elasticity, we may classify the elastic materials into three categories: (1) linear elastic, (2) nonlinear hysteresis elastic, and (3) nonlinear non-hysteresis elastic, or simply nonlinear elastic [50]. The current version of ANSYS (including APDL) doesn't provide a material model to include the hysteresis behavior. The hysteresis behavior must be included in terms of material damping. Most of materials have more-or-less a hysteresis behavior; however, as long as it is small enough, we may neglect the hysteresis behavior.

Nonlinear non-hysteresis elastic materials are characterized by the fact that the stressing curve and the unstressing curve are coincident: the energy is conserved in stressing-unstressing cycles. The challenge of implementing nonlinear elastic material models comes from the fact that the strain may be as large as 100% or even 200%, such as rubber under stretching or compression. This kind of superlarge deformation elasticity is given a special name: *hyperelasticity*.

*Plastic* materials are characterized by the presence of the residual strain, or plastic strain. Note that the hysteresis is always present in plastic materials: there is always energy loss in stressing-unstressing cycles.

### 6.6.2. Test Data Needed for Hyperelasticity:

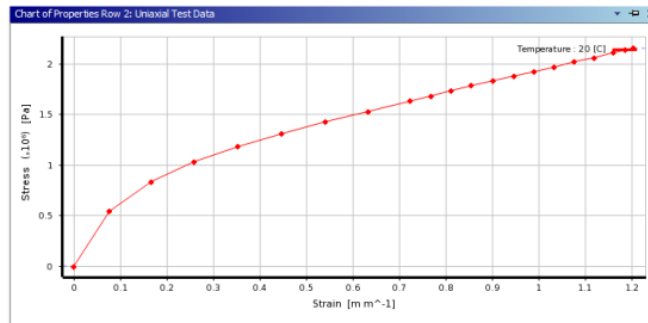
In plasticity or linear elasticity, a stress-strain curve is used to describe the behavior of material, and the stress-strain curve is usually obtained by a tensile test. Since only tension behavior is investigated, other behaviors (compression, shearing) must be drawn from the tensile test data. In plasticity or linear elasticity, we implicitly made some assumptions: (a) the compressive behavior is symmetric to the tension behavior in the sense that they have the same Young's modulus, and the same Poisson's ratio. The symmetry may not be true when the strain is large. We may need to conduct a compressive test to assess the Young's modulus and Poisson's ratio for the compressive behavior. (b) The shear modulus  $G$  is related to Young's modulus and Poisson's ratio. Again, this assumption may not be true when the strain is large. We may need to conduct a shear test to assess the shear modulus for describing the shearing behavior. (c) We also assume that the bulk modulus  $B$  is related to Young's modulus and Poisson's ratio by

$$B = \frac{E}{3(1-2\nu)} \quad (\text{Eq.6. 1})$$

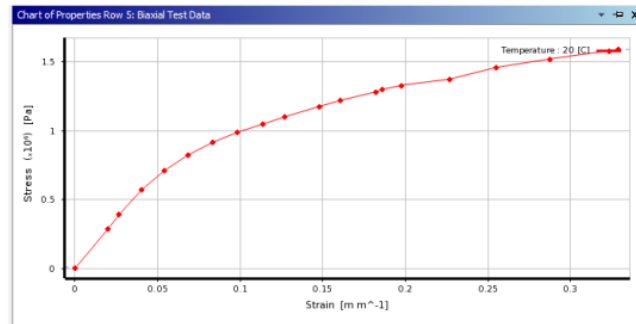
Again, this assumption may not be true when the strain is large. We may need to conduct a volumetric test to assess the bulk modulus for describing the volumetric behavior. It must be noted that, in many cases, the bulk modulus is almost infinitely large (i.e., the material is incompressible). For these cases, we usually assume incompressibility without conducting a volumetric test. Further, when the strain is large, all the moduli (tensile, compressive, shear and bulk) are no longer constant; they change along stress-strain curves. Nonlinear elasticity with large strain is also called hyperelasticity (Figure 6.8) [50].

In brief, to describe hyperelasticity behavior, we need the following test data: (a) a set of uniaxial tensile test data, (b) a set of uniaxial compressive test data, (c) a set of shear test data, and (d) a set of volumetric test data if the material is compressible. It is possible that a set of test data is obtained by

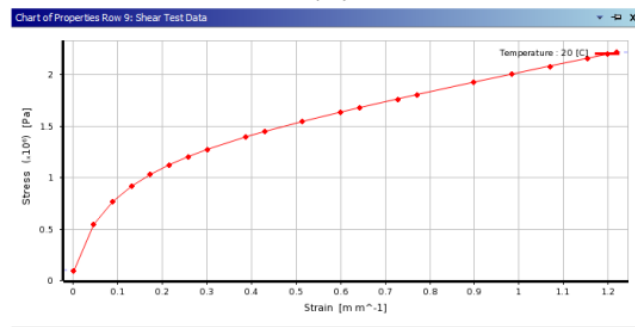
superposing two sets of other test data. For example, the set of uniaxial compressive test data can be obtained by adding a set of hydrostatic compressive test data to a set of equibiaxial tensile test data. Reasons for doing this are as follows: (a) A biaxial tensile test may be easier to conduct than a compressive test in some testing devices; (b) For incompressible materials, hydrostatic compressive test data are trivial: all strains have zero values.



(a)



(b)



(c)

Figure6. 8 The tests data for dicribe hyperleastic model ,a) uniaxial tensile test ,b) uniaxial compressive test c) shear test

## 7. Numerical Modeling of Rubber Pad Forming Process

The conventional way to develop press-formed metallic components requires a burdensome trial-and-error process for setting-up the technology, whose success depends largely on the operator's skill and experience. The finite element simulations of a sheet metal forming process help the manufacturing engineer to design the forming process by shifting the costly press shop try-outs to the computer-aided design environment.

Numerical simulations of the manufacturing process, such as rubber-pad forming, have been introduced in order to avoid the trial-and-error procedure and shorten development phases when tight times-to-market were compulsory. But, development of a numerical model which would be able to successfully simulate the rubber pad forming process is not an easy task. On the other hand, a well defined finite element model can be used for blank and rubber behavior analyses during many different processes. This chapter will address the simulation and investigation of the significant parameters (such as forming force and stress and strain distribution in a blank) associated with the rubber-pad forming process and capabilities of this process regarding the manufacturing of aircraft wing ribs. The simulation and investigation carried out (and presented in this chapter) identified the stress and strain distribution in a blank as well as a forming force. Experimental analyses of the rib with the lightening hole (presented in next chapter) showed a good correlation between FE simulations and experimental results.

### 7.1. Finite Element Modelling of Three Different Sheet Metal Elements

Numerical simulations of the rubber-pad forming processes are complicated mainly because of the large deformation of the rubber-pad. As a consequence, a mesh distortion may occur in a simulation, which could lead to inaccurate and incomplete results. This is why FE analyses must be carried out

carefully and with understanding of physical phenomena of the rubber pad forming process.

The commercial finite element software Ansys was used for FE simulations presented in this chapter. In order to reduce the processing time and improve the precision of calculations, 2D FE models were created for three different sheet metal elements (a straight rib, a stringer and a rib with the lightening hole) and analyses were carried out for each model. Figure 7.1 illustrates these three geometrical models respectively.

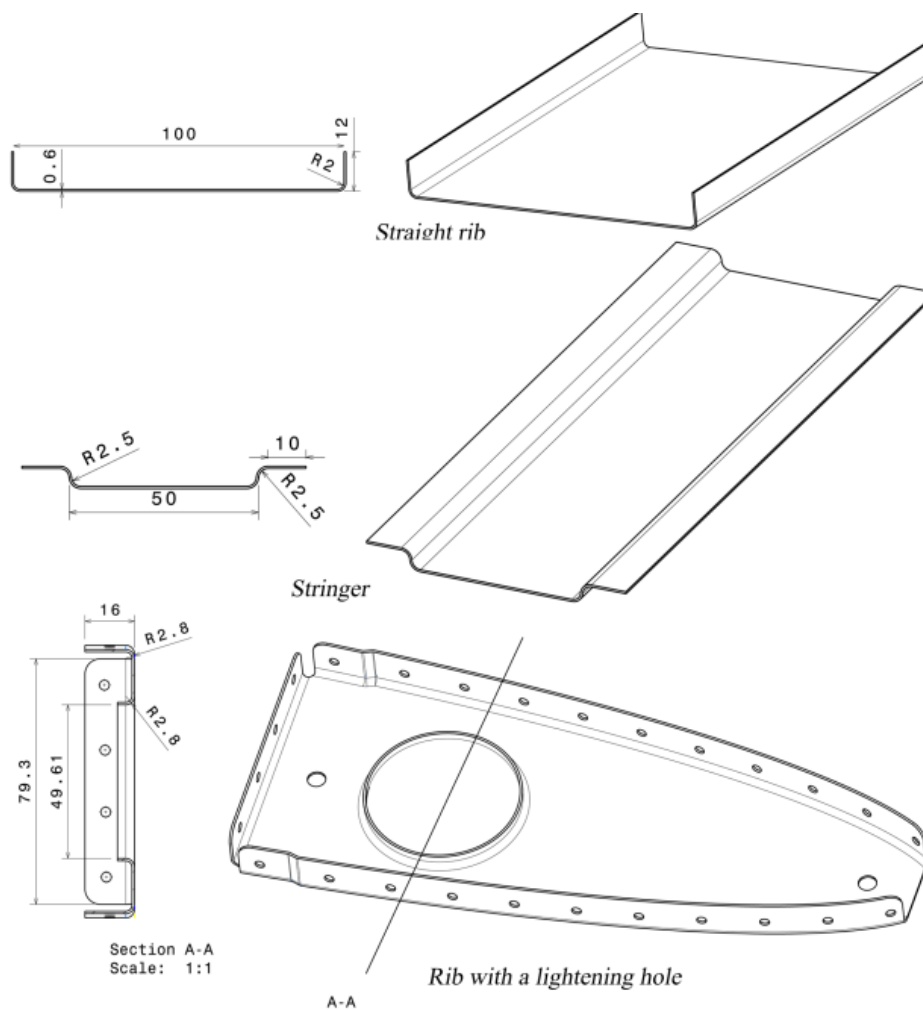


Figure 7.1 Geometrical models used in investigation from top: (a) straight rib, (b) stringer and (c) rib with a lightening hole

The models in FE analyses included three elements only: a rigid die, a blank and a rubber-pad (a flexible punch). In order to simplify the numerical model, the container of the rubber-pad was not modeled. To eliminate the influence of the container, the frictionless support constraints were applied on opposite sides of the rubber, while a displacement constraint was applied on the upper edge of a 2D rubber model (Figure 7.2).

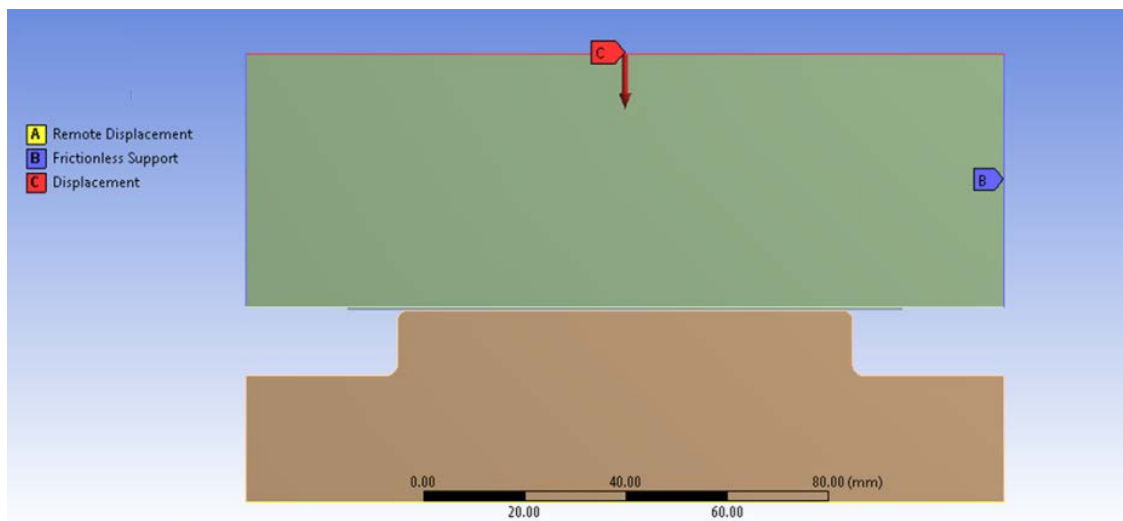


Figure7. 2: Constraints used in FE simulation

The die was modeled as a rigid body, because the stress and strain of the die were not analyzed and the die material (steel) is much less deformable than the blank material (aluminum). So, the material properties attached to the die were not important, and a mesh was not generated either. This eliminated unnecessary calculations causing a decrease in both the run time and errors in the numerical solution.

Because the blank undergoes a large plastic-strain deformation during the forming process, the stress-strain test data up to the failure were required to define the blank material in simulation (Figure 7.3). The blank was considered as a multilinear isotropic hardening material. In FE simulations of the blank

behavior, von Mises yield criterion coupled with isotropic work hardening assumption was used [18].

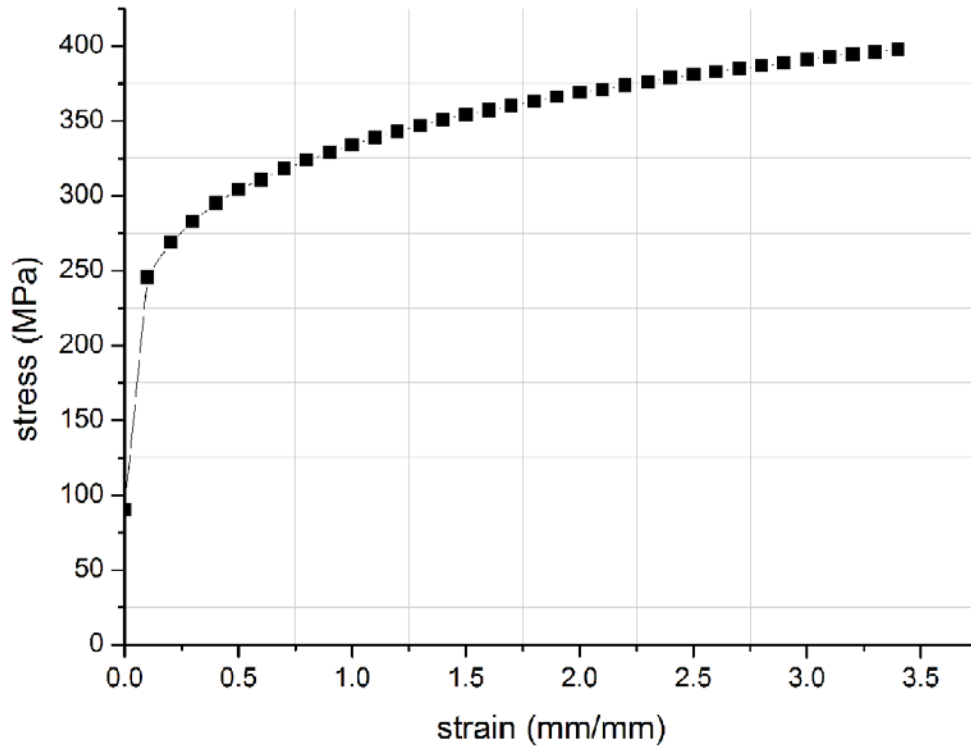


Figure7. 3: Experimental tensile stress- strain curve for aluminum blank sheet

The rubber-pad undergoes nonlinear hyperelastic deformation. The behavior of the nonlinear hyper-elastic and incompressible rubber-like material is usually described by the Mooney-Rivlin model that uses a strain energy function  $W$ . The derivative of  $W$ , with respect to a strain component, determines the corresponding stress component:

$$\sigma_y = \frac{\partial w}{\partial \sigma_y} \quad (\text{Eq.7. 1})$$

$$W = \sum_{k+m=1}^n C_{km} (I - 3)^m + \frac{1}{2} k (I_3 - 1)^2 \quad (\text{Eq.7. 2})$$

where  $I_1$ ,  $I_2$  and  $I_3$  ( $I_3 = 1$ ) are the strain invariants,  $k$  is the bulk modulus

and  $C_{km}$  is the constant of the Mooney-Rivlin material model for incompressible material.

Usually, two Mooney-Rivlin parameters  $C_{10}$  and  $C_{01}$  are used to describe hyperelastic rubber deformation<sup>7</sup>. In FE models, the Polyurethane rubber with Shore A hardness of 70 (HD70) was used for a rubber-pad. The values of  $C_{10}$  and  $C_{01}$  were 0.736MPa and 0.184MPa, respectively [3, 8, 16 and17].

An aluminum plate with 0.6mm thickness was used as a blank. The aluminum properties were determined via stress-stain curve obtained from the tensile tests [8,9], as shown in Figure 11. For this alloy the elastic module  $E$  is 71GPa and Poisson ratio  $\nu$  is 0.334.

During the rubber-pad forming process, the materials exhibit large deformations and rotations. There is a friction contact at the blank interfaces, too. At the same time, geometry nonlinearities are arising from a nonlinear strain-displacement relationship, as well as nonlinearities associated with material properties. According to that, the geometric nonlinearity option was activated in the nonlinear solution procedure.

The friction behavior between the two different pairs of contact (rubber-pad - blank and blank-die) was all assumed to follow Coulomb's model [3,8]. The friction coefficient at the former and latter contact pair were considered to be 0.2 and 0.1 respectively [3, 8, 16]. Table 7.1 shows the specifications of the contact regions.

| <b>Parts in contact</b>   | <b>Contact type</b>                                |
|---------------------------|--|
| <b>Die &amp; Blank</b>    | <b>Frictional contact (0.1) node to surface</b>    |
| <b>Blank &amp; Rubber</b> | <b>Frictional contact (0.2) surface to surface</b> |
| <b>Die &amp; Rubber</b>   | <b>Frictional contact (0.1) node to surface</b>    |

Table7. 1 Interface contact

The interface contact between the blank–rubber-pad, blank–die and die–rubber were modeled as deformable and ANSYS solves these tasks on the basis of the contact-target surface approach with adjustable impenetrability constraint that assures contact compatibility. The CONTA 175 (node to surface contact) finite element was used on the blank’s surfaces at the interface between blank-die and on the rubber surface at the interface between rubber-die. The CONTA171 (surface to surface contact) was used on the surface of a rubber-pad at the interface between blank and rubber-pad. The other surfaces at each interface were modeled with the TARGE169 element. It can be summarized that, in all interface contacts, the upper surfaces of the die and the blank were considered as a target, while the lower surface of the blank and the upper surface of the rubber-pad were considered as a contact.

As mentioned above, the container was not modeled, so – in order to fix the rubber-pad correctly – frictionless supports had to be applied on the side edges of the rubber. Remote displacement was applied on the lower edge of the die. The displacement was applied on the top edge of the rubber in order to simulate the forming load on the blank (Figure 7.2). All deformable materials have been modeled with Plane183 finite element (2-D element with 8 or 6 nodes). Plane183 has quadratic displacement, plasticity, hyper-elasticity, creep, stress stiffening, large deflection and large strain simulation capabilities. The number of nodes and elements used for blank and rubber-pad are presented in the Table 7.2.

| Modes                          | Blank |          | Rubber pad |          | Rigid Die |          |
|--------------------------------|-------|----------|------------|----------|-----------|----------|
|                                | Nodes | Elements | Nodes      | Elements | Nodes     | Elements |
| <b>Straight rib</b>            | 2161  | 1680     | 4253       | 3958     | 205       | 204      |
| <b>Stringer</b>                | 768   | 157      | 7254       | 2299     | 304       | 152      |
| <b>Rib with lightning hole</b> | 863   | 615      | 5490       | 5181     | 208       | 207      |

Table7. 2 Number of nodes and elements for three models

### 7.1.1. Results obtained in FEM Simulations and Discussion:

As mentioned above, the forming force was presented as displacement applied on the upper edge of the rubber-pad. Figure 7.4 illustrates the step-by-step forming process using the rubber-pad. It is clear that the process can be divided into three stages (or steps). The first stage is the flexible die (rubber-pad) self-deformation; the second starts with blank deformation (under the pressure of a rubber-pad when it reaches the bottom of a rigid die); and, finally, during the third stage the blank fills the die cavities until they are completely filled.

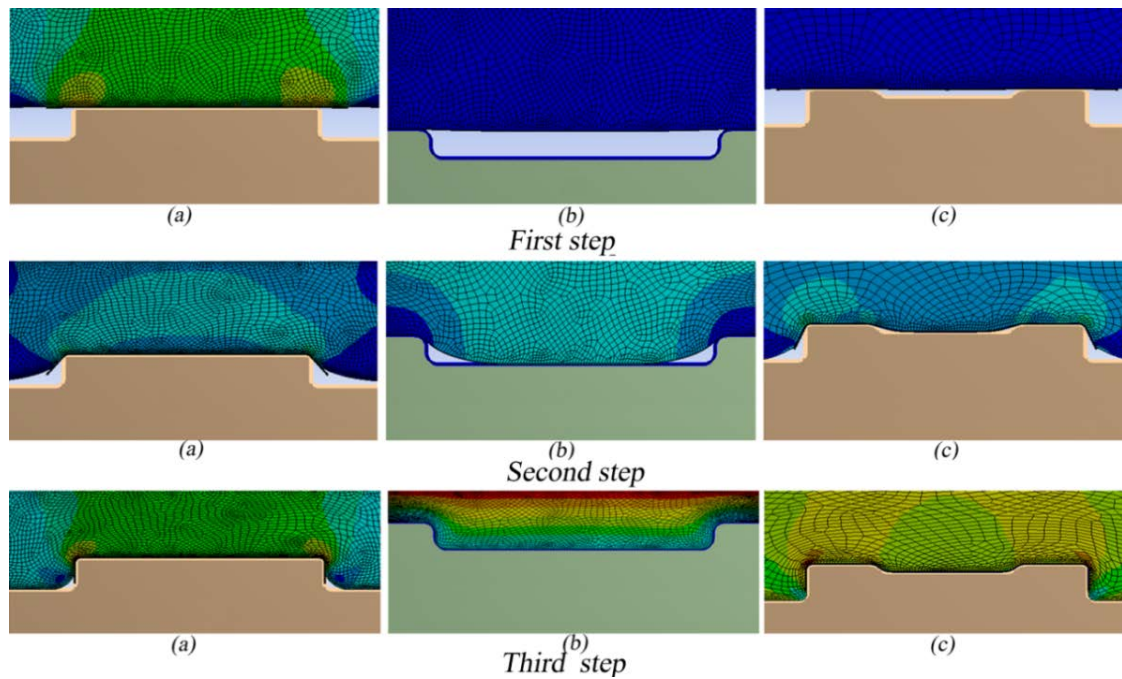


Figure 7.4 Forming steps during the rubber-pad forming: a) straight rib,  
b) Stringer and c) rib with a lightening hole

The convergences of the forming forces for each model, obtained through FE simulations, are shown in Figure 7.5.

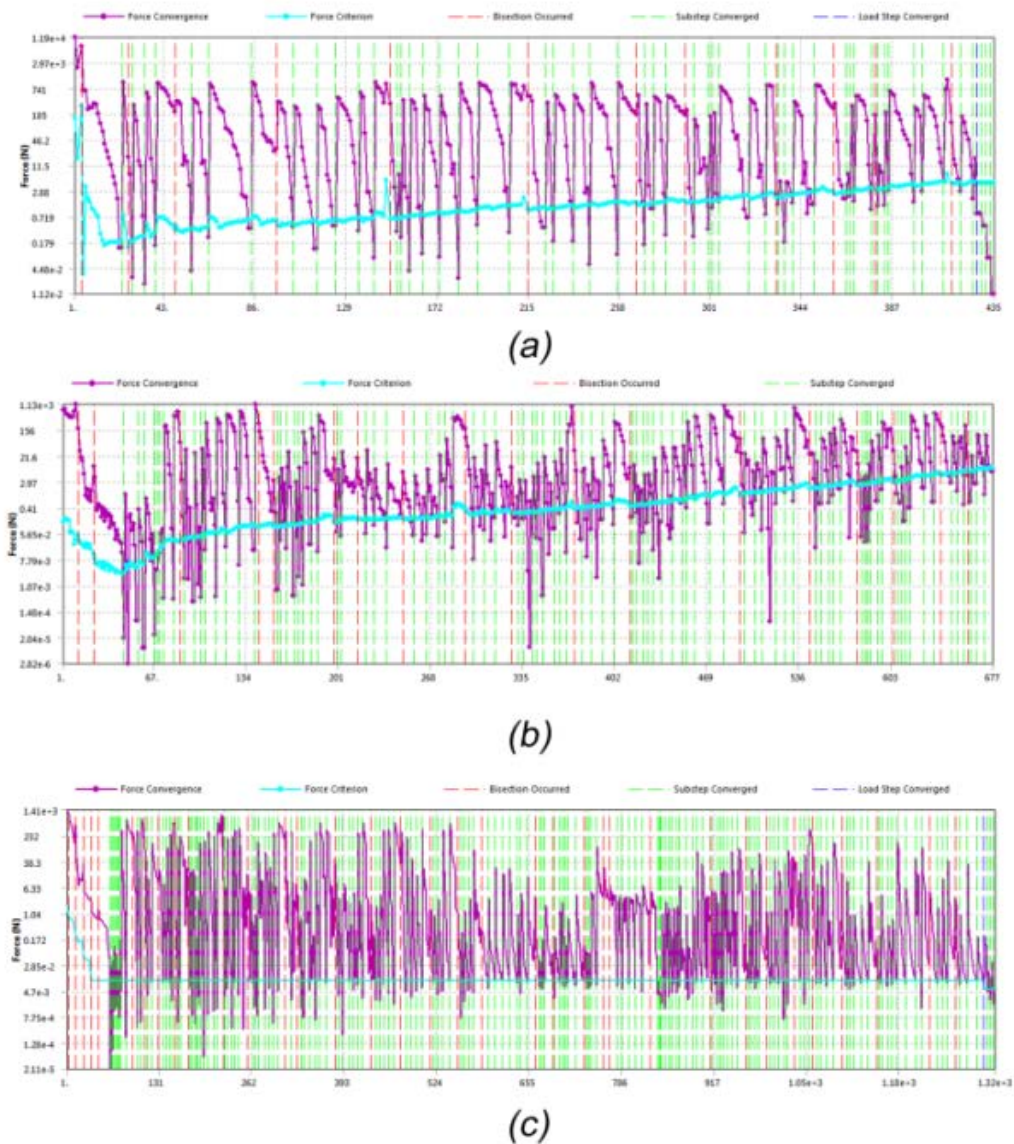


Figure 7.5: Convergence of forming force for a) straight rib, b) Stringer and c) rib with a lightening hole

Figure 7.6 shows that the highest value of forming force is present in the rib with lightening hole (6735 N), while the lowest is achieved in the straight rib (867N). It can be seen that the magnitude of forming force increases as the geometry of the rib becomes more complex, that is as more bending regions have to be obtained (see Table 7.3).

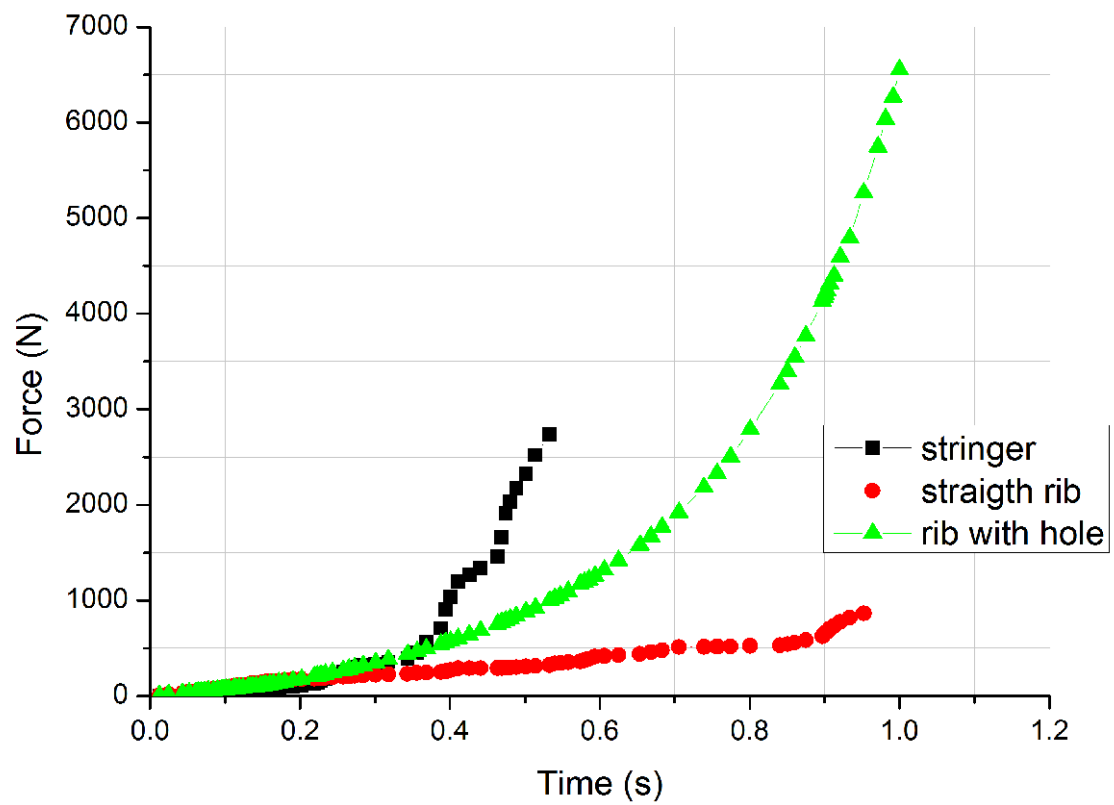


Figure7. 6: Forming forces in three models

| MODEL                    |     | Equivalent stress [MPa]     | Equivalent plastic strain [mm/mm] | Reaction force [N] |
|--------------------------|-----|-----------------------------|-----------------------------------|--------------------|
| Straight rib             | max | 224.74<br>(occurs on blank) | 0.115<br>(occurs on blank)        | 866.43             |
|                          | min | 1.2e-4                      | 0.0                               |                    |
| Stringer                 | max | 221.29<br>(occurs on blank) | 0.1268<br>(occurs on blank)       | 2734.7             |
|                          | min | 7.032                       | 0.0                               |                    |
| Rib with lightening hole | max | 241.45<br>(occurs on blank) | 0.206<br>(occurs on blank)        | 6553.8             |
|                          | min | 0.101                       | 0.0                               |                    |

Table 7.3 Summarization of results obtained in the rubber-pad sheet metal forming simulations

FE simulation of the forming process for the stringer and the rib with the lightening hole goes through three stages/steps (corresponding to the forming process), while the straight rib forming can be performed in the first two steps (because there is no cavity to fill). During the first step – self-forming of the rubber – rubber deforms elastically and offers a counter pressure, so the forming load is very small (Figure7.6). The time needed for this step is short (between 20% and 35% of the total simulation time). After 20% of the simulation time for the straight rib and 35% for other models, the second step starts, and the forming load increases slightly to produce outer bending. During the last

step, after approximately 65% of the simulation time, the blank starts to fill the cavity of the rigid die, and forming force increases sharply (Figures 7.6 and 7.7).

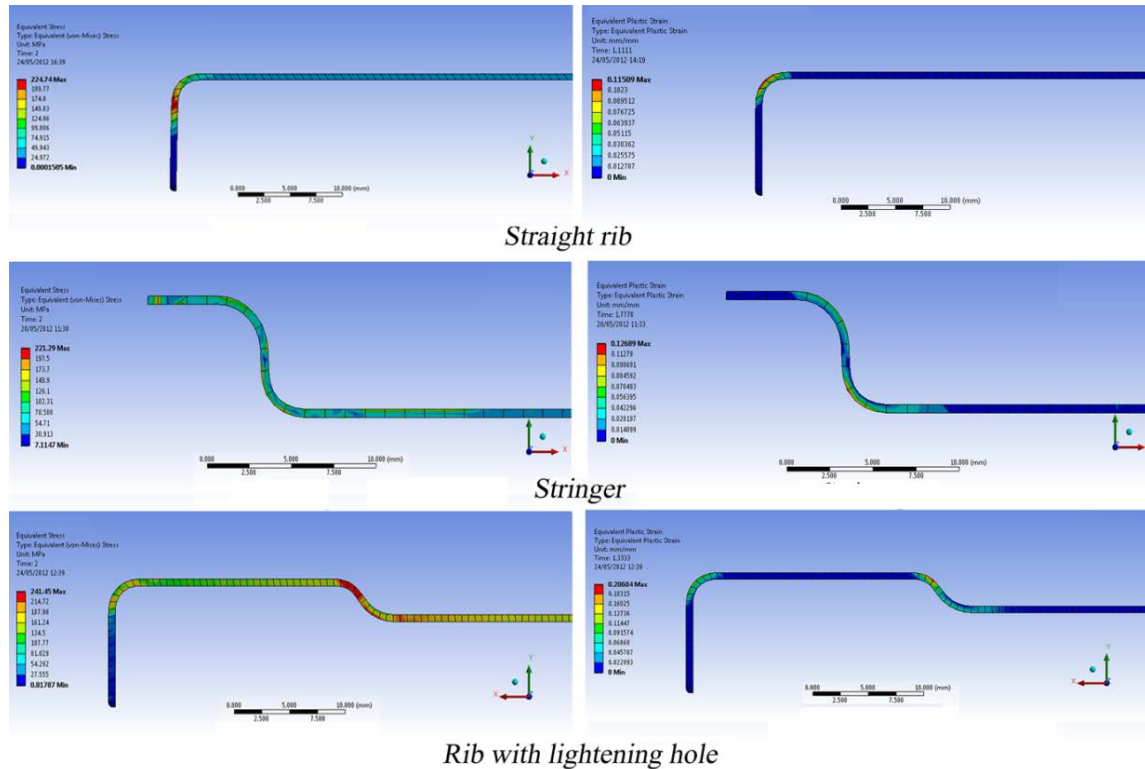


Figure 7.7: Equivalent stress (left column) and plastic strain (right column) in straight rib, stringer and rib with a lightening hole (from the top).

According to the results of FE simulations, it's obvious that the highest value of forming force will be obtained in case of the most complex sheet metal geometry (rib with lightening hole), where several bends with different radii must be produced. This is in correlation with empirical data [5, 8, 16 and 17] which means that used FE models have been defined well.

Along with calculation of forming force, stress and strain analyses were performed. As it was expected, the stress and strain concentrations in a blank accumulate in the last two stages.

Figure 7.7 shows the equivalent stresses (in MPa, left column) and plastic strains (in mm/mm, right column) in blanks at the end of forming processes for

all FE models. The summarization of the maximum and minimum stress and strain values, presented in Figure 7.7, is also given in Table 7.3. Table 7.3 shows that maximum equivalent stress and plastic strain appear in the rib with lightening hole (241.45 MPa and 0.206 mm/mm, respectively), while the minimum values of equivalent stress and plastic strain are in straight rib (224.74 MPa and 0.115 mm/mm respectively).

As we said before, the stress and plastic strain increase with increasing complexity of rib geometry, as well as the number of bend radii. The reason for that, according to [3,5], is that the blank is suffering not only from tensile and tangential stresses, but also from stress coming due to bending pressure imposed by the tool. Then, thinning phenomenon starts homogeneously and, eventually, the necking appears. Necking can induce the crack, which is not unusual in this forming process [3]. The crack starts when the blank undergoes stretching forces and when ultimate stress is reached during the second or third stage of the forming process.

According to Sala [3] and Takuda [51], the maximum plastic strain which can be considered for forming of this type of aluminum alloy **is approximately 0.186 mm/mm**. This value of plastic strain was used as a reference for crack appearance predictions in FE simulations presented in this chapter. The value of plastic strain obtained in a forming simulation of the rib with lightening hole (0.206 mm/mm) indicated the possibility of crack appearance in outer radius of lightening hole, while plastic strain values for other two models were less than 0.186 mm/mm. Experiments with rubber-pad (see next chapter) showed that FE predictions were good.

Taking into account all facts mentioned above, the following conclusions may be drawn:

- Finite element simulation of the rubber-pad forming process could be very useful tool for understanding and improving forming operations, because it provides important data for determination of

the forming parameters and operation time. Developed FE models and method proposed in this chapter have proved to be sufficiently effective in the predictions of the final shape of the component, and regions of possible crack appearance (see also next chapter).

- The FE simulations showed that the maximum stresses and strains in all cases were at the flanges and the corners. The minimum stress and plastic strain were achieved in straight rib (rib with the simplest geometry), while the maximum stress and plastic strain were presented in the rib with lightening hole (the most complex geometry). These results have been validated in experiments (next chapter), as well as the fracture criterion used for crack predictions. The FE simulations proved that the simpler tools would reduce lead times and enable rapid production of small parts, without possibility of crack appearance during forming. On the other hand, geometry of more complicated – but necessary – tools must be defined very carefully, with determination of fillets' radii which will minimize the chance of fracture. FEM can help this determination (see section below), while additional potential applications – such as 3D model simulations and tools optimization – are also possible.
- However, it must be noticed that the optimization procedure of the press-forming processes – owing to the presence of hardly reproducible phenomena like friction and lubrication – should never be limited to simple numerical simulations; rather, these latter phenomena could contribute to saving costs and reducing time-to-market, currently held up by empirical trial-and-error processes.

## **7.2. Optimization of The Sheet Metal Forming Tool Geometry in a rubber pad forming process with flexible punch- Numerical Approach.**

In the previous section, the results of FE analysis of a rubber-pad sheet metal forming process for 3 different cases were presented, which showed that

the value of plastic strain obtained in a simulation of the rib with the lightening hole (0.206 mm/mm) might indicate the possibility of crack appearance in outer radius of the lightening hole during forming. In experiments with rubber pad forming of aircraft tail ribs (presented and discussed in next chapter), cracks actually occurred in outer radii, which led to a conclusion that geometry of the tool would have to be fixed (in other words, value of outer radii had to be changed). But, the following questions appeared: how to select the right value of outer radius (or radii) and whether the crack appearance is connected to these radii only or to the other geometrical parameters as well?

To come to a satisfying answer(s), it was decided to perform several FE simulations with different combinations of geometry values shown in Figure 7.8.

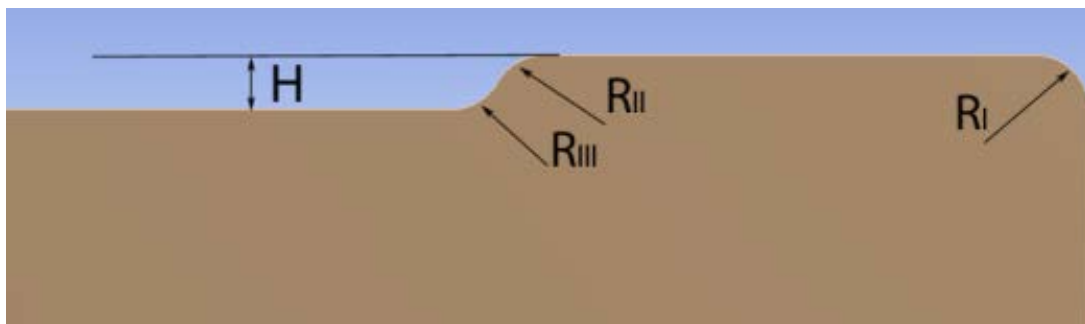


Figure 7.8: Geometry parameters varied in FE simulations of rubber pad forming

In defining the FE model in ANSYS, the same approach as described in the previous section was used. For the purpose of processing time reduction and calculation precision improvement, it was decided to model only a half of the geometry (2D axisymmetric case) and then to perform simulations with different combinations of RI, RII, RIII and H. Comparison of obtained results should lead us to the optimized tool geometry, with the smallest possible values of predicted stresses and strains during the metal forming process.

According to this decision, FE models were created for different die dimensions (parameters). Figure 7.9 illustrates a geometry model used in

simulations. This model included three parts only (i.e. their halves): a rigid die, a blank and a rubber pad (a flexible punch). For the purpose of simulation simplification, the rubber pad container was not considered and constraints were applied on the rubber pad instead of the container (as shown in Figure7.9).

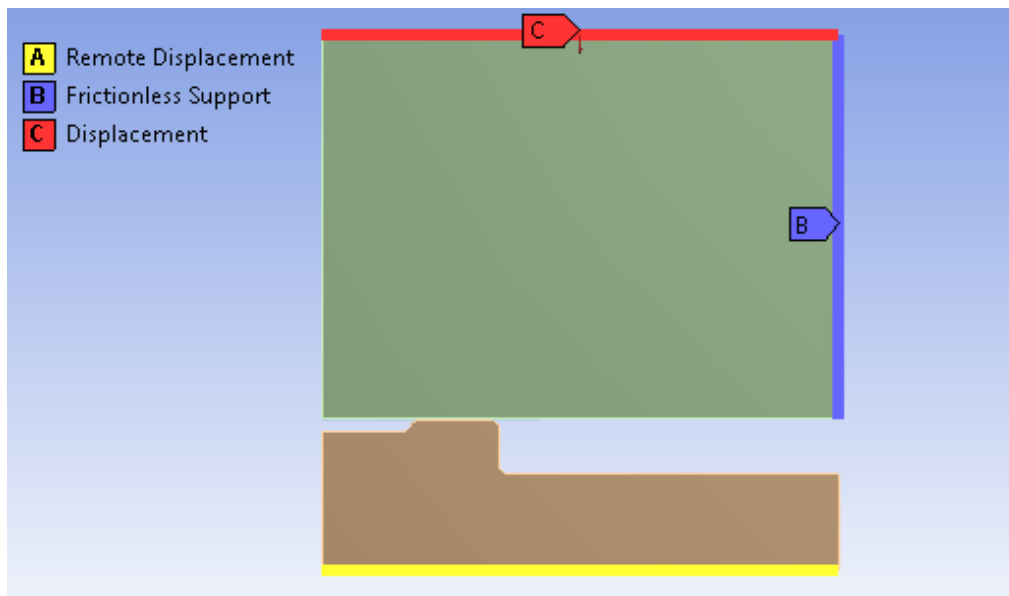


Figure7. 9: Constraints as applied in symmetry FE model of rib with lighten hole

Again, the die was modeled as rigid body, so a mesh for this element was not generated (Figure 7.10). Multilinear isotropic hardening properties of 2024-T3 aluminum alloy were assigned to the blank in order to successfully simulate large plastic strain of the blank. These properties were determined from stress-strain curve obtained in the tensile test (Figure 11). For this material the elastic module (E) is 71GPa and Poisson ratio ( $\nu$ ) is 0.334.

Von Mises yield criterion coupled with isotropic work hardening assumption was also applied. The behavior of the nonlinear hyperelastic and incompressible rubber-like material was again described by Mooney-Rivlin model. HD70 was used as a material of a rubber pad, with the values of C10 and C01 equal to 0.736 MPa and 0.184 MPa, respectively.

The frictional behavior between the rubber pad and the blank, as well as the die and the blank, were assumed to follow Coulombs model. The friction coefficient at the former and later contact pair were considered to be 0.2 and 0.1 respectively. Thickness of the blank used in the simulation was 0.6mm.

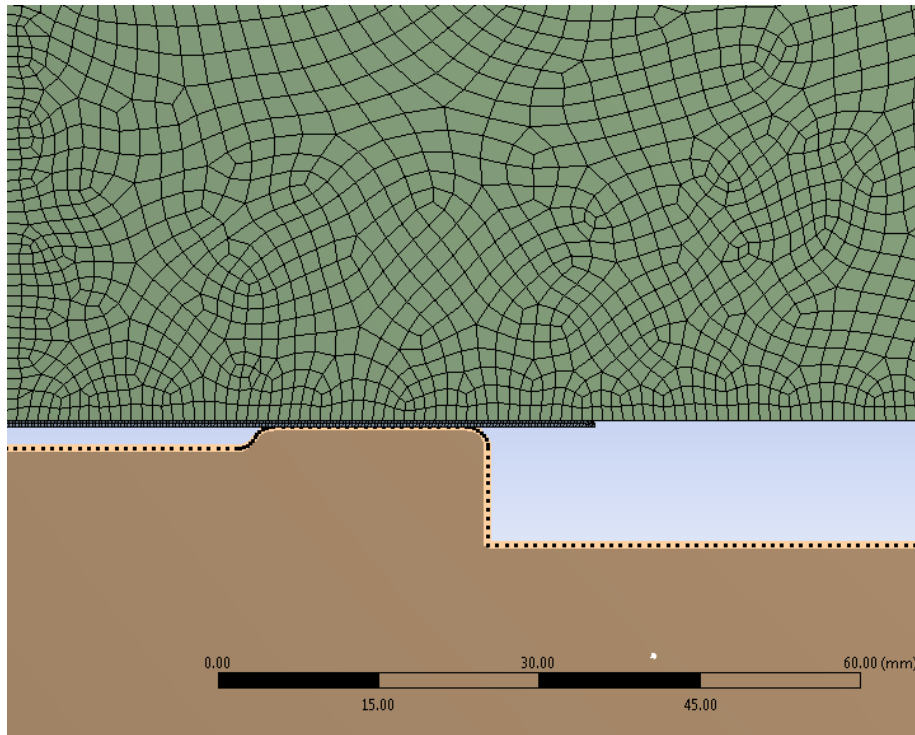


Figure7. 10: Rigid punch, sheet metal and rubber pad models

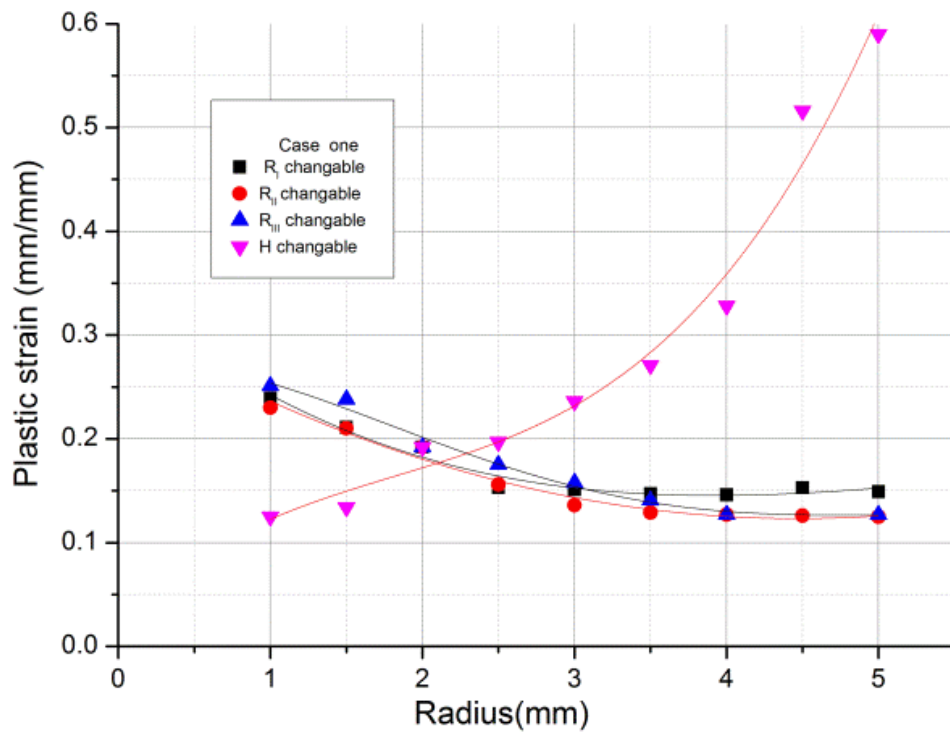
As already mentioned, the container was not modeled in order to fix the rubber pad correctly. The frictionless support was applied on the side surfaces of the rubber. In order to simulate the forming load on the blank, the displacement was applied on top surface of the rubber. Remote displacement (with zero values in all directions) was applied on the lower surface of the die (Figure7.9). It should be mentioned that the number of nodes in FE models of blank, rubber pad and die was 200, 4450 and 200 respectively, while the number of FE elements was 102, 4220 and 172, respectively.

### 7.2.1 Results and Discussion:

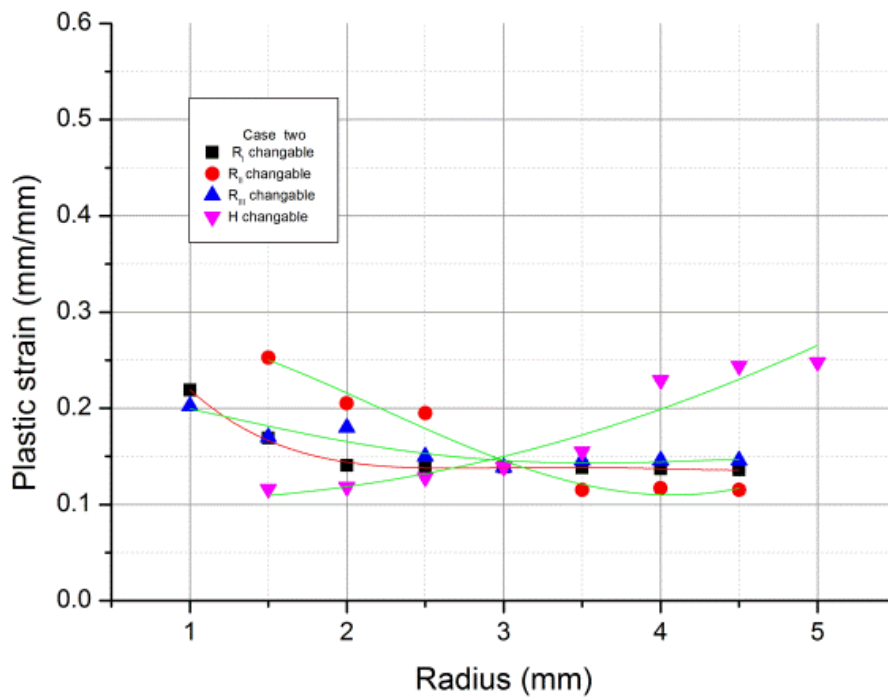
As it is mentioned above, the rubber pad forming process can be divided into three stages: the first is the self-deformation of a rubber pad, the second is the outer bending forming and, finally, the blank flows in to the cavity of the die. Again, according to Sala [3] and Takuda [51], the acceptable value of plastic strain for 2024-T3 aluminum is 0.186 mm/mm and this value was used as a boundary in FE simulations. This means when the value of plastic strain in the simulation reached 0.186 mm/mm the model was considered as unacceptable. Generally speaking, some parameters have higher influence on the value of plastic strain during the rubber pad forming process (tool geometry, hardness of the rubber, used lubricants), and here tool geometry parameters ( $R_I$ ,  $R_{II}$ ,  $R_{III}$  and  $H$  shown in Figure 7.8) have been studied.

In order to study the effect of the values of these parameters on the rubber pad forming process,  $R_I$ ,  $R_{II}$ ,  $R_{III}$  and  $H$  have been varied. Firstly, values of  $R_I$ ,  $R_{II}$  and  $R_{III}$  were fixed (2mm in the first case and 3mm in the second), while the fourth parameter  $H$  has been varied. The same procedure was repeated with other combinations of parameters (3 values were fixed, the fourth was changeable) in order to analyze the effect of each of them on strain concentration and to find combination that will minimize plastic strain. On the basis of the obtained results, more FE models of tools (with different values of geometry parameters) have been developed and analyzed. These simulations showed that the values of stress and strain strongly depend on the tool rib geometry ( $R_I$ ,  $R_{II}$ ,  $R_{III}$  and  $H$ ).

Different FE models based on different tool dimensions for both cases (fixed values 2mm & 3mm) were used in simulations. The geometry parameters that were not fixed were varied from 1 mm to 5 mm. Figure 7.11 illustrates the relationships between the plastic strain and the geometry parameters for each model in the case one and the case two.



(a)



(b)

Figure7. 11: Influence of geometry parameters on plastic strain during rubber pad forming process: a) case one, b) case two

As it can be seen in Figure 11, plastic strain strongly depends on the geometry parameters  $R_I$ ,  $R_{II}$ ,  $R_{III}$  and  $H$  and these dependencies may be expressed in mathematical terms. It is also clear that increasing the values of  $R_I$ ,  $R_{II}$  and  $R_{III}$  or decreasing the value of  $H$  (while other parameters are fixed), the plastic strain decreases. At the same time, the capability of forming the blank increases, too. However, when  $R_{II} \geq 2$ ,  $R_I \geq 2$  and  $H < R_{II}$ , for example, the plastic strain is less than 0.186 mm/mm (as can be seen in Tables 7.4, 7.5, 7.6 and 7.7).

| Tool radius<br>$R_I$<br>[mm] | Stress<br>[MPa] |          | Strain<br>[mm/mm] |          | Reaction Force [N] |          | Filling cavity |          |
|------------------------------|-----------------|----------|-------------------|----------|--------------------|----------|----------------|----------|
|                              | Case one        | Case two | Case one          | Case two | Case one           | Case two | Case one       | Case two |
| 1                            | 300             | 300.63   | 0.219             | 0.211    | 3665               | 6621     | No             | No       |
| 1.5                          | 295             | 300.92   | 0.218             | 0.1689   | 7066               | 5676     | No             | No       |
| 2                            | 300.47          | 302.44   | 0.192             | 0.1406   | 9490               | 5773     | No             | No       |
| 2.5                          | 300             | 301.24   | 0.153             | 0.1393   | 7391               | 5773.8   | No             | No       |
| 3                            | 298             | 301.41   | 0.151             | 0.139    | 7092               | 6556.5   | No             | No       |
| 3.5                          | 298             | 301.35   | 0.147             | 0.138    | 6799               | 6915.3   | No             | No       |
| 4                            | 301             | 303.71   | 0.146             | 0.137    | 6790               | 6904.9   | No             | No       |
| 4.5                          | 301             | 302.61   | 0.146             | 0.136    | 6646               | 6993.8   | No             | No       |
| 5                            | 301             | 304      | 0.14              | 0.130    | 6637               | 6879     | No             | No       |

Table 7. 4 Values of equivalent stress, plastic strain and reaction force obtained in FE simulations with fixed values of  $R_{II}$ ,  $R_{III}$  and  $H$  (first case 2 mm, second case 3 mm) and changeable value of  $R_I$

| Tool radius<br>$R_{II}$<br>[mm] | Stress<br>[MPa] |             | Strain<br>[mm/mm] |             | Reaction<br>Force [N] |             | Filling<br>cavity |              |
|---------------------------------|-----------------|-------------|-------------------|-------------|-----------------------|-------------|-------------------|--------------|
|                                 | Case<br>one     | Case<br>two | Case<br>one       | Case<br>two | Case<br>one           | Case<br>two | Case<br>one       | Case<br>two  |
| 1                               | 299             | 303.76      | 0.234             | 0.348       | 9384                  | 5710        | Yes<br>crack      | Yes<br>crack |
| 1.5                             | 297             | 297.45      | 0.21              | 0.2526      | 9999                  | 5714.9      | Yes<br>crack      | Yes<br>crack |
| 2                               | 300.47          | 305.75      | 0.192             | 0.205       | 9490                  | 6917.7      | No                | Yes          |
| 2.5                             | 297             | 304.15      | 0.156             | 0.195       | 6418                  | 6921.4      | No                | Yes          |
| 3                               | 300             | 301.41      | 0.15              | 0.139       | 4206                  | 6556.5      | No                | Yes          |
| 3.5                             | 302             | 301.44      | 0.129             | 0.127       | 5374                  | 6556.5      | No                | No           |
| 4                               | 299             | 303.22      | 0.138             | 0.117       | 5121                  | 6932.4      | No                | No           |
| 4.5                             | 302             | 301.44      | 0.129             | 0.115       | 5125                  | 6556.5      | No                | No           |
| 5                               | 298             | 301         | 0.125             | 0.124       | 6411                  | 6508.8      | No                | No           |

Table 7. 5 Values of equivalent stress, plastic strain and reaction force obtained in FE simulations with fixed values of RI, RIII and H (first case 2 mm, second case 3 mm) and changeable value of RII

| Tool<br>radius<br>$R_{III}$<br>[mm] | Stress<br>[MPa] |             | Strain<br>[mm/mm] |             | Reaction<br>Force [N] |             | Filling<br>cavity |             |
|-------------------------------------|-----------------|-------------|-------------------|-------------|-----------------------|-------------|-------------------|-------------|
|                                     | Case<br>one     | Case<br>two | Case<br>one       | Case<br>two | Case<br>one           | Case<br>two | Case<br>one       | Case<br>two |
| 1                                   | 299             | 279.2       | 0.191             | 0.2024      | 9490                  | 8150        | No                | No          |
| 1.5                                 | 300             | 304         | 0.159             | 0.17        | 8567                  | 6559.6      | No                | No          |
| 2                                   | 300             | 301         | 0.192             | 0.18        | 9490                  | 6924        | No                | No          |
| 2.5                                 | 300             | 301         | 0.168             | 0.15        | 7766                  | 6924        | Yes               | No          |
| 3                                   | 300             | 301.41      | 0.157             | 0.139       | 4206                  | 6556.5      | Yes               | Yes         |
| 3.5                                 | 301             | 301.4       | 0.142             | 0.146       | 5376                  | 6557        | Yes               | Yes         |
| 4                                   | 300             | 303         | 0.137             | 0.146       | 5873                  | 5985        | Yes               | Yes         |
| 4.5                                 | 300             | 304         | -                 | 0.13        | 5873                  | 5985        | yes               | Yes         |
| 5                                   | 300             | 301.4       | 0.127             | 0.145       | 3062                  | 5986.5      | yes               | Yes         |

Table 7. 6 Values of equivalent stress, plastic strain and reaction force obtained in FE simulations with fixed values of  $R_I$ ,  $R_{II}$  and  $H$  (first case 2 mm, second case 3 mm) and changeable value of  $R_{III}$

| Tool height<br>H<br>[mm] | Stress<br>[MPa] |             | Strain<br>[mm/mm] |             | Reaction<br>Force [N] |             | Filling<br>cavity |             |
|--------------------------|-----------------|-------------|-------------------|-------------|-----------------------|-------------|-------------------|-------------|
|                          | Case<br>one     | Case<br>two | Case<br>one       | Case<br>two | Case<br>one           | Case<br>two | Case<br>one       | Case<br>two |
| 1                        | 299             | 302         | 0.143             | 0.098       | 7191                  | 5963        | yes               | Yes         |
| 1.5                      | 300             | 300         | 0.143             | 0.116       | 7191                  | 5913        | yes               | Yes         |
| 2                        | 300.4           | 300.35      | 0.192             | 0.118       | 9490                  | 5860        | No                | Yes         |
| 2.5                      | 300.7           | 304.78      | 0.197             | 0.1278      | 9393                  | 5812.5      | No                | Yes         |
| 3                        | 300             | 301.41      | 0.236             | 0.139       | 9301                  | 6556.5      | No                | Yes         |
| 3.5                      | 295             | 303.9       | 0.271             | 0.155       | 9228                  | 6502.7      | No                | yes         |
| 4                        | 298             | 301.79      | 0.328             | 0.229       | 8469                  | 68123       | No                | No          |
| 4.5                      | 300             | 300.93      | 0.438             | 0.244       | 8138                  | 6738        | No                | No          |
| 5                        | 300             | 301.44      | 0.59              | 0.248       | 7500                  | 6706.8      | No                | No          |

Table 7.7 Values of equivalent stress, plastic strain and reaction force obtained in FE simulations with fixed values of  $R_I$ ,  $R_{II}$  and  $R_{III}$  (first case 2 mm, second case 3 mm) and changeable value of H

On the other hand, when  $R_I$  equals 1 mm and 1.5 mm, respectively, the plastic strain is greater than acceptable plastic strain 0.186 mm/mm (in both cases - one and two). Magnitudes of the plastic strain in case one are 0.219 mm/mm (when  $R_I=1$  mm, Figure 7.12) and 0.211 mm/mm (when  $R_I=1.5$  mm, Figure 7.13), while magnitudes of the plastic strain in case two are 0.218 mm/mm (when  $R_I=1$  mm, Figure 7.12) and 0.167 mm/mm (when  $R_I=1.5$  mm, Figure 7.13). Figure 7.12 and Figure 7.13 show that stress concentration appears in  $R_I$  region in both cases. However, if H is greater than  $R_{II}$  ( $H=4.5$  mm, Figure 7.14), the maximum plastic strain is 0.438 mm/mm in the first case and 0.244 mm/mm in the second case (which is greater than 0.186 mm/mm) and stress concentration takes place at  $R_{II}$  region. But, when H is less than  $R_{II}$ , the value of plastic strain is always less than 0.186 mm/mm (Table 7.7 and Figure 7.17). The

plastic stain is less than 0.186 mm/mm when  $R_I > 2$  mm, and similar can be said about radius  $R_{II}$ , which must be greater than 2.5mm (as shown in Tables 7.4 and 7.5 and Figures 7.15 and 7.16).

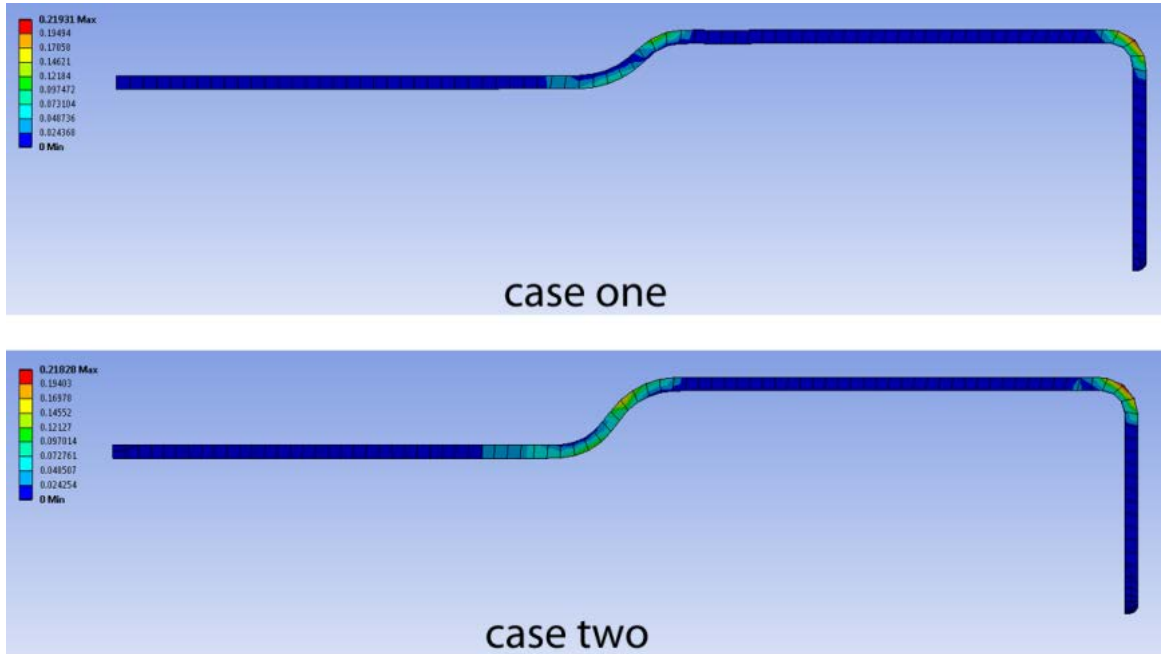


Figure7. 12:  $R_I=1$  mm a) first case ( $R_{II}$ ,  $R_{III}$ , and H equal 2 mm) b) second case ( $R_{II}$ ,  $R_{III}$ , and H equal 3 mm)

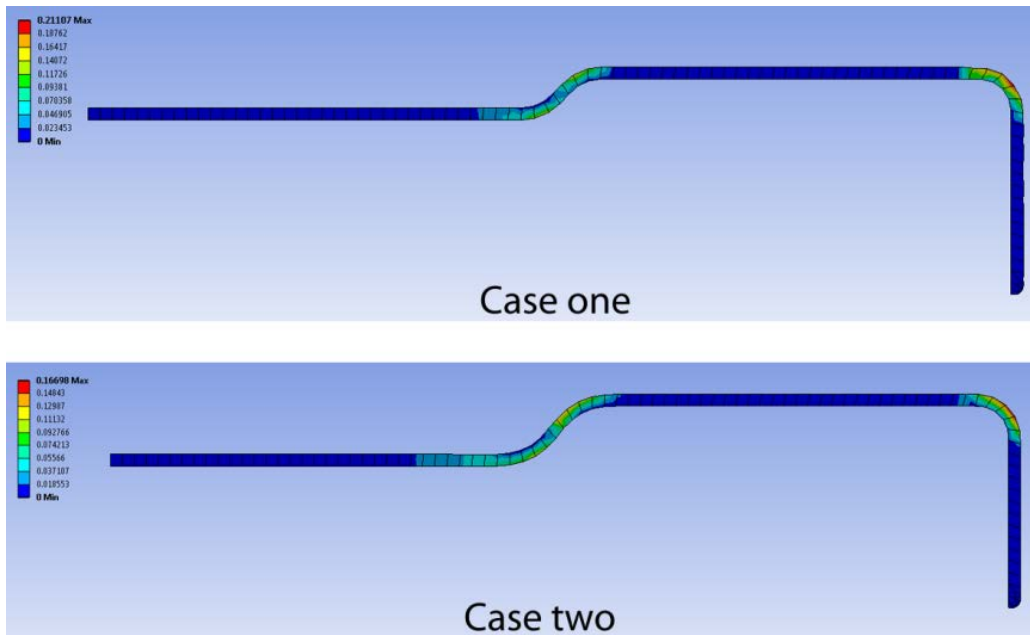


Figure7. 13 : $R_I=1.5$  mm a) first case ( $R_{II}$ ,  $R_{III}$ , and H equal 2mm) b) second case ( $R_{II}$ ,  $R_{III}$ , and H equal 3mm)

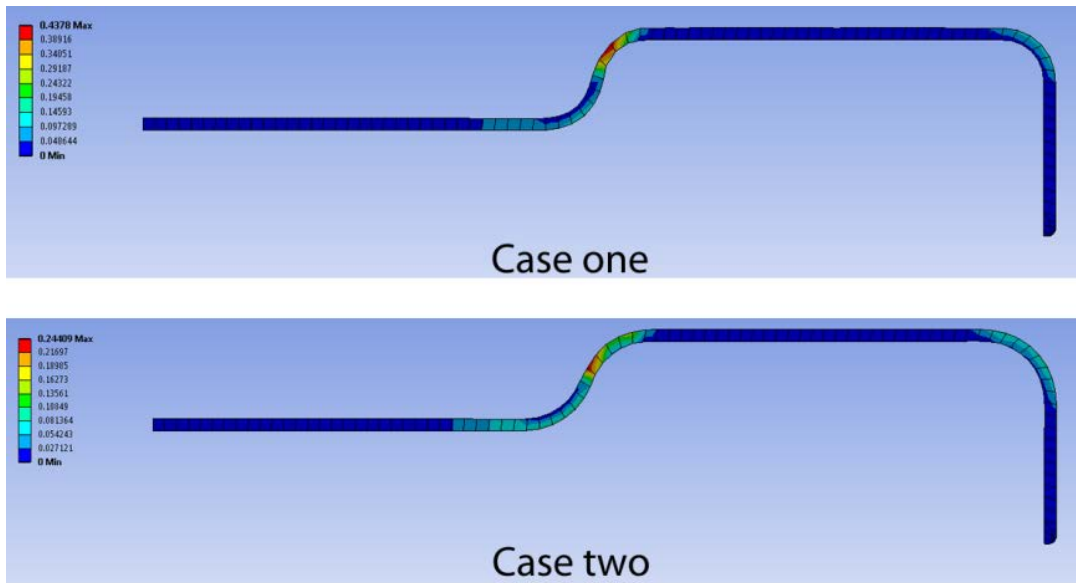


Figure7. 14: H=4.5 mm a) first case ( $R_I$ ,  $R_{II}$  and  $R_{III}$  equal 2 mm) b) second case ( $R_I$ ,  $R_{II}$  and  $R_{III}$  equal 3 mm)

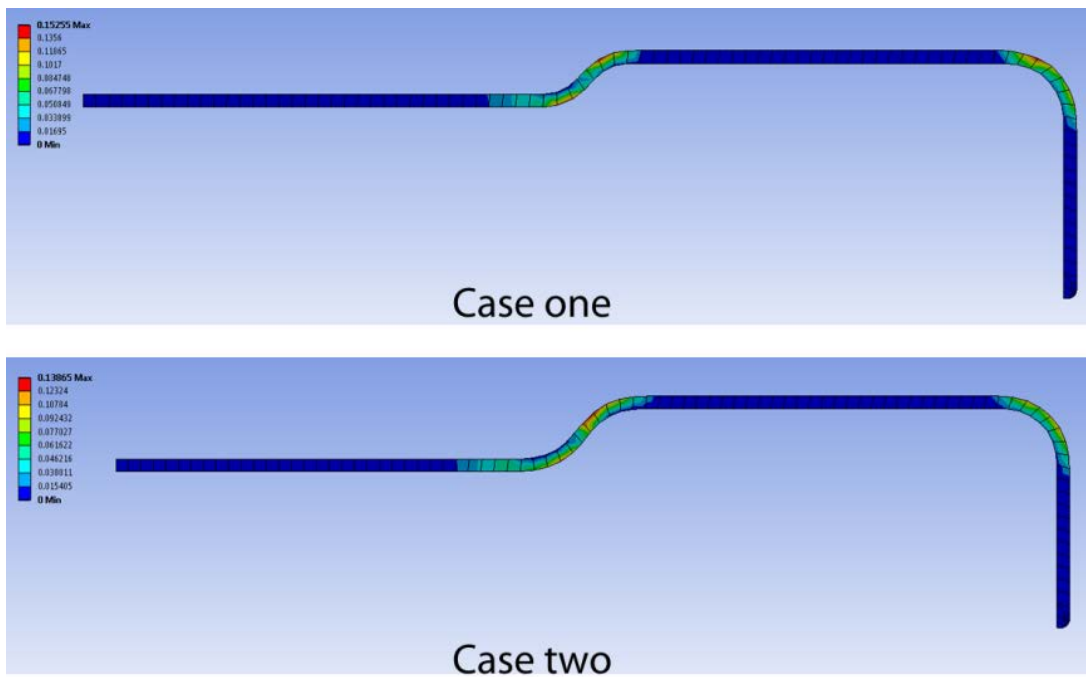


Figure7. 15:  $R_I=2.5$  mm a) first case ( $R_{II}$ ,  $R_{III}$  and H equal 2 mm) b) second case ( $R_{II}$ ,  $R_{III}$  and H equal 3 mm)

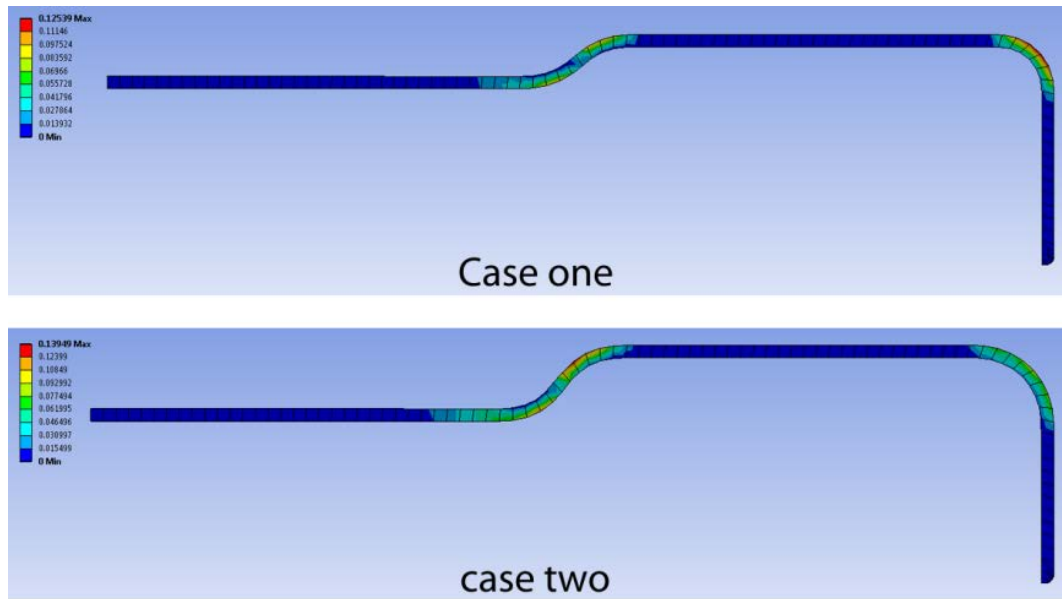


Figure7. 16:  $R_{II}=3$  mm a) first case ( $R_I$ ,  $R_{III}$ , and  $H$  equal 2 mm) b) second case ( $R_I$ ,  $R_{III}$ , and  $H$  equal 3 mm)

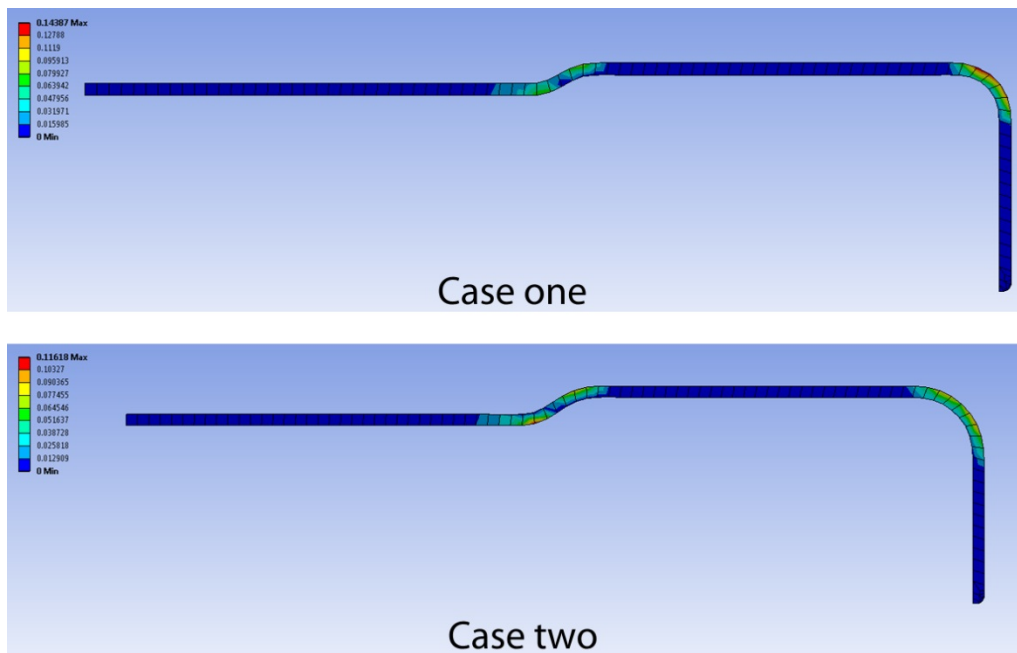


Figure7. 17:  $H=1.5$  mm a) first case ( $R_I$ ,  $R_{II}$ , and  $R_{III}$  equal 2 mm) b) second case ( $R_I$ ,  $R_{II}$ , and  $R_{III}$  equal 3 mm)

The reason might be referring to the reference [3] which mentioned that the blank could be affected not only by tensile stress and tangential stress but also from stress coming due to the bending pressure imposed by the tool.

Simulations showed that the values of  $R_{III}$  in all the models and both cases should be greater than or equal to  $R_{II}$  in order to make an easy forming and to avoid uncompleted cavity tool forming (Table 7.6 and Figure 7.18). In Figure 7.18 it is obvious that when  $R_{III}=1.5$  mm, and  $R_{II}$  is 2 mm (the first case) and 3 mm (the second case), cavity of the tool is not completely filled (there is a gap between the sheet and tool surface). When  $R_{III}=3.5$  mm and  $R_{III}=4.5$  mm (which is greater than the value of  $R_{II}$  in both cases) the cavity is completely filled and the value of plastic strain is within acceptable range (Table 7.6).

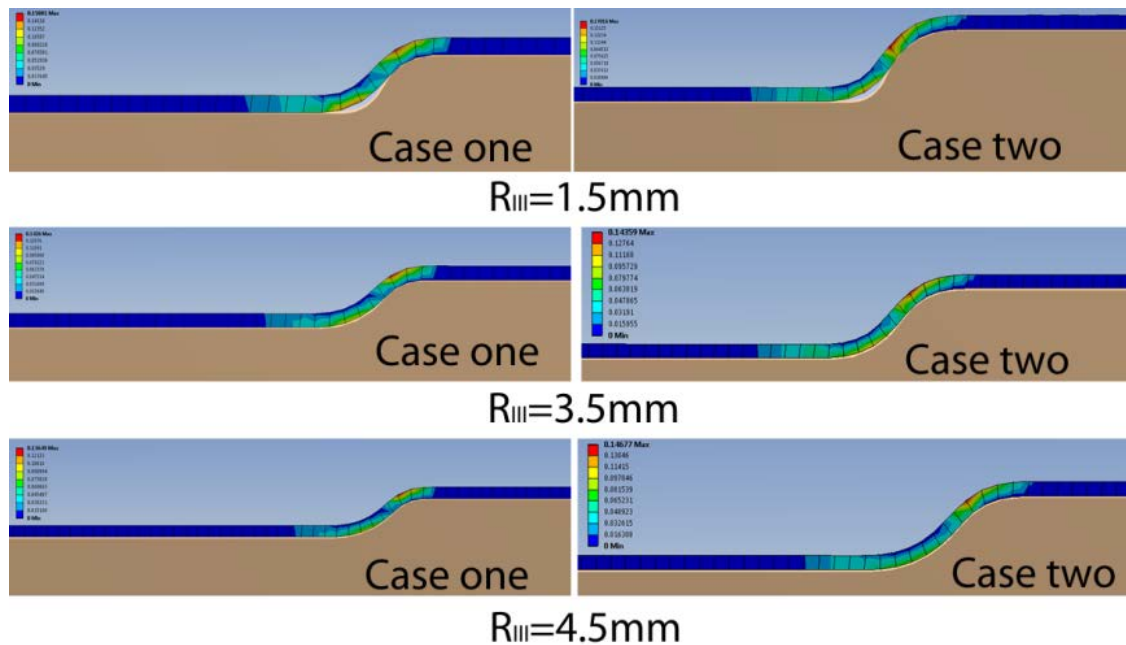


Figure 7.18: The influence of  $R_{III}$  on the filling the cavity of the tool rib a) Case one ( $R_I$ ,  $R_{II}$  and  $R_{III}$  equal 2mm) b) Case two ( $R_I$ ,  $R_{II}$  and  $R_{III}$  equal 3mm)

Furthermore, even if we select parameters ( $R_I$ ,  $R_{II}$ ,  $R_{III}$  and  $H$ ) randomly, we come to the same conclusions as previously described. For example, Figure 7.19 shows four different combinations of these parameters. In the case when  $R_{II}=H=3$  mm and  $R_{III}$  is equal to 2mm, the plastic strain is less than limit strain (magnitude is 0.182 mm/mm), but the tool cavity is not completely filled, because  $R_{III}$  is less than  $R_{II}$  (Figure 7.19 (a)). However, when  $H=4$ mm and at the same time greater than  $R_{II}$  (which is 3 mm and is equal to  $R_{III}$ ), the plastic strain

(0.215 mm/mm) is higher than acceptable plastic strain, but the tool cavity is completely filled by sheet (value of  $R_I$  is 2,5mm Figure 7.19(b)). The Figure 7.19(c) shows that plastic strain is equal to 0.128 mm/mm and that tool cavity is not completely filled when  $R_{II}$  is equal to 4 mm and greater than both,  $H$  and  $R_{III}$  (3mm). When  $R_{II}$  is equal to  $H$  (4 mm) and  $R_{III}$  is equal to 5 mm, the plastic strain is 0.138 mm/mm and the tool cavity is completely filled (as shown in Figure 7.19(d)).

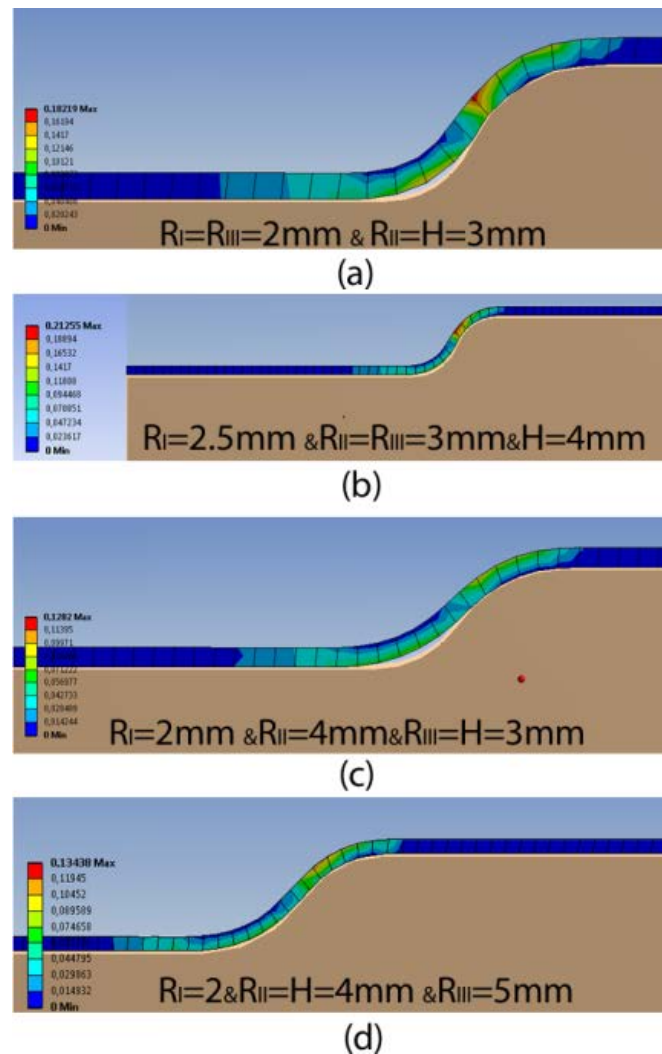


Figure7. 19: Randomly selected geometry parameters

Similar conclusions may be drawn for more randomly selected parameters (shown in Figure 7.20) after performing FE simulations.

For example, in Figure 7.20(a) the plastic strain value is 0.212 mm/mm and it is higher than acceptable plastic strain (0.186 mm/mm). This high value of plastic strain is because  $H=4$  mm which is greater than  $R_{II}$  (3mm). Furthermore, the value of  $R_I$  is equal to 1.5 mm and less than 2 mm. However, the tool cavity is completely filled by sheet when  $R_{II}=R_{III}= 3$  mm. When the value of  $R_I$  is equal to 1 mm and the other parameters ( $R_{II}$ ,  $R_{III}$  and  $H$ ) are equal to 3 mm, the plastic strain value is 0.218 mm/mm and it is concentrated at  $R_I$  region, but the tool cavity is completely filled because  $R_{III}$  is equal to  $R_{II}=3$ mm (Figure 7.20(b)). The plastic strain is equal to 0.129 mm/mm when the value of  $R_I$  is equal to 2 mm and the value of  $H$  is equal to 3mm, which is less than  $R_{II}$  (4mm). But, the tool cavity is not filled because  $R_{III}$  is equal to 2 mm and less than  $R_{II}$  (Figure 7.20(c)).

When  $R_I=1.5$  mm,  $R_{II}=2$  mm and  $R_{III}=H= 3$ mm, the plastic strain value is 0.217 mm/mm and the tool cavity is completely filled ( $R_I$  is less than 2mm and  $H$  and  $R_{III}$  greater than  $R_{II}$ , Figure 7.20(d)). The tool cavity is completely filled with low plastic strain value (0.142 mm/mm) in the case when  $R_I$  is equal to 2 mm and  $R_{II}=R_{III}=H=3$  mm (Figure 7.20(e)).

The same tool cavity situation happens as previously, when  $R_I=2$  mm,  $R_{II}=R_{III}=3$  mm and  $H$  is equal to 2 mm (which less than  $R_{II}$ ) and the plastic strain is 0.118 mm/mm (Figure 7.20(f)). On the other hand, when  $H$  is equal to 3mm and  $R_I=R_{II}=R_{III}=2$  mm (that is  $H>R_{II}$  and  $R_{III}<R_{II}$ ), the value of plastic strain is 0.198 mm/mm and is higher than 0.186 mm/mm and the tool cavity is not completely filled (Figure 20(g)). The figure 20(h) shows that the sheet completely fills the tool cavity with the low value of plastic strain (0.129 mm/mm). As it can be seen, this happens when  $R_{III}=3$  mm and  $R_{II}=4$ mm, while  $H=3$  mm is less than  $R_{II}$  and  $R_I$  is equal to 2mm.

Figures 7.20(j) and 7.20(k) show that when the first three geometry parameters ( $R_I$ ,  $R_{II}$ ,  $R_{III}$ ) are equal to 2 mm, 4 mm and 5 mm respectively, and  $H$  is less than or equal to  $R_{II}$  (4 mm in Figure 7.20(j) and 3 mm in Figure 7. 20(k)),

the plastic strain is less than 0.186 mm/mm (0.175 mm/mm in Figure 7.20(j) and 0.134 mm/mm in Figure 7.20(k)). In the case when  $H=3$  mm and is equal to  $R_{III}$  (which is less than  $R_{II}=4$  mm, Figure 7.20(h)), while  $R_I$  equal to 2 mm, the tool cavity is completely filled with sheet metal, and value of the plastic strain is low (0.129 mm/mm).

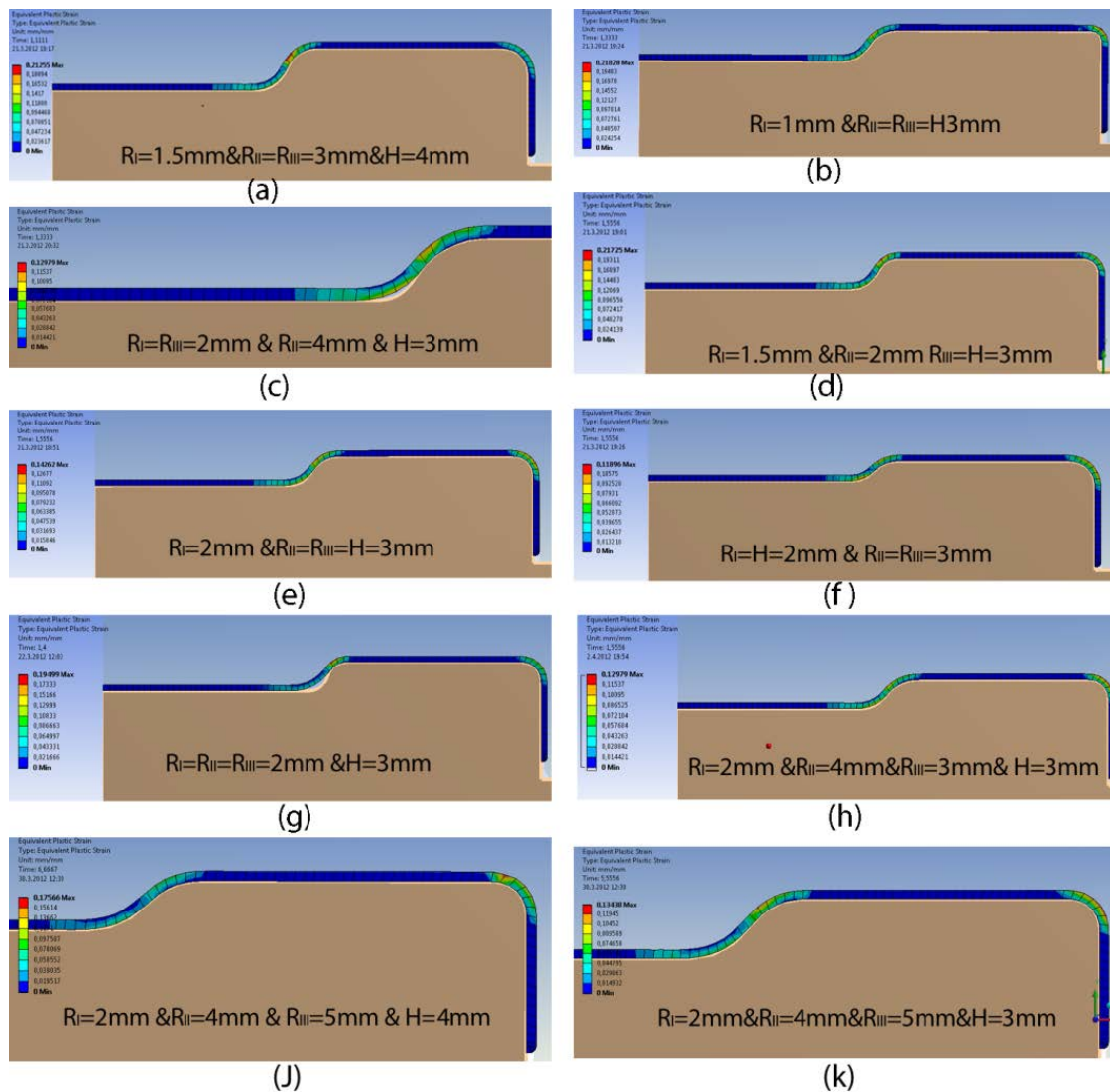


Figure 7. 20: More randomly selected geometry parameters

To get plastic strain in the blank less than 0.186 mm/mm and completely fill the cavity of the tool, the values of  $R_{II}$  &  $R_{III}$  should be increased with decreasing the value of  $H$ . On the other hand, it is known that an increase of the

bending radius may cause increase in the springback phenomenon, which is not preferable. Therefore, to get an acceptable tool design we have to make a kind of a compromise of the values of these parameters.

This is why a connection between the values of  $R_I$  and  $R_{II}$  and the springback phenomenon will be analyzed in next section using the FE method. As we saw in the presented results of simulations, the influence of  $R_{III}$  and  $H$  on filling of the tool cavity is significant, but  $R_{III}$  and  $H$  are not influencing the springback, while the influence of  $R_I$  and  $R_{II}$  on both phenomena is very important.

In this study two different cases were analyzed using FE simulations and several different FE models of rib tools have been developed for the purpose of investigating the geometry of tool used in rubber pad forming process. These models were analyzed in details numerically, and the most important conclusions of this study could be:

- The values of  $R_I$  and  $R_{II}$  should be greater or equal to 2 mm in order to avoid stress concentration in their regions. However, the plastic strain will not reach unacceptable plastic strain.
- To avoid the thinning phenomenon and to make an easy forming with complete rib tool cavity filling, the value of  $H$  should be less than  $R_{II}$  and the value of  $R_{III}$  should be greater than or equal to  $R_{II}$ .

### 7.3. Using FEA in Springback Simulations

As a fundamental process in metallic forming technologies, sheet metal forming is widely being employed in aerospace fields. It is because a final sheet product of desired shape and appearance can be quickly and easily produced with a relatively simple tool set. As we emphasized before, sheet metal forming may frequently produce unacceptable products with wrinkles, tear or poor

dimension precision, unless tool and process parameters are appropriately chosen.

In particular, the dimension precision becomes a major concern in the sheet metal bending process owing to the considerable elastic recovery during unloading which leads to the *springback* and sidewall curl. Hence, the tool design, for given specific sheet material and final product dimension, should be based upon the accurate prediction of elastic recovery amount. Due to the effects of elastic springback, die designs are usually finalized only after the fabrication and testing of multiple prototypes. The main reasons for this are: firstly, the elastic recovery phenomenon is influenced by a combination of various process parameters, such as the tool shape and dimension, the temperature change and frictional contact condition, the material properties, and so on [52]. Thus, springback and sidewall curling are case-dependent. Secondly, the prediction accuracy by analytical approach is quite low because of the limitation in mathematical modeling of process and solving methods. Of course, such a limitation resulted from the problem nonlinearity and other process complexities.

Commonly, the cross section of the sheet does not become fully plasticized in sheet-metal forming processes. In bending, the mid-layer of the sheet will deform elastically only, and will therefore cause elastic springback in the material when the forming load is removed. This elastic recovery occurs because of the release of elastic stresses. An approximate formula for springback is given in the terms of a relation between the initial bending radius  $R_1$  and the final bending radius (after springback)  $R$  [53].

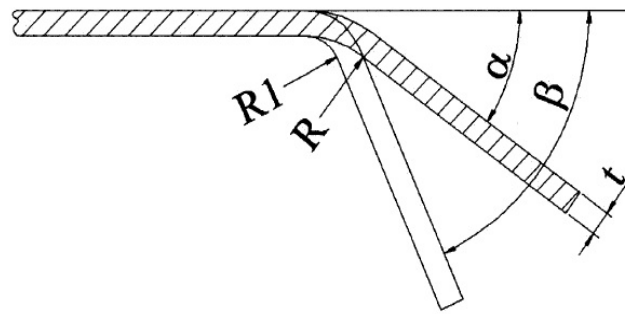


Figure 7. 21: Springback parameters

The amount of elastic recovery after unloading mainly depends on the ratio of the angles and the mechanical properties of the metal. Springback increases with increasing strength and decreasing elastic modulus. Angles and radii related to springback in order to define so called *the springback factor K* are illustrated in Figure 7.21[54].

In the bent-up region of the sheet, it is assumed that the arc length on the neutral axis,  $W$ , remains unchanged during the process. The relationship between the arc length,  $W$ , and the angles, radii and thickness  $t$  of sheet metal related to springback is:

$$W = \beta \left( R_1 + \frac{t}{2} \right) = \alpha \left( R + \frac{t}{2} \right) \quad (\text{Eq.7. 3})$$

Where  $\alpha$  and  $\beta$  are in radians. Using this relationship, the springback factor  $K$  is defined as [53]:

$$K = \frac{\alpha}{\beta} = \frac{R_1 + \frac{t}{2}}{R + \frac{t}{2}} \quad (\text{Eq.7. 4})$$

According to [55], for any metal, the springback factors lie between 0.9 and 1.0 for very small bend radii, e.g.  $1t$ ,  $2t$ ,  $3t$ . It then decreases at a progressively faster rate as the bend radius becomes larger. At a critical radius, the springback factor would become zero. If the metal is bent to a radius larger than this critical

value, the deformation would be entirely elastic. This critical radius is dependent on the type of metal (using the springback factor equation, the part radii may be calculated and the graph of springback factor against part radius can be plotted).

There are several methods to counter the effect of springback, but the next three ones are the most commonly used in the industries today:

(a) Overbending: The commonest method to combat springback is to bend the part to a smaller radius of curvature than is desired, so that when springback occurs the part has the proper radius. This method of combating the springback will be analyzed in this section in both the straight rib and the rib with the lightening hole.

(b) Coining the bend. In this method, bending is achieved by pushing with a punch, and letting the metal bend into a die; at the end of the cycle, a relatively large squeezing force is exerted, which creates a permanent bend angle. The design of a die for a given part may undergo many rounds of iterations in the debugging stage before a satisfactory geometry is obtained.

(c) Bottoming: It consists of striking the metal severely at the bend area so that the compressive strains are above the yield point.

In order to reduce the time spent on such manual corrections of the die, a parametric study may be conducted on how the inclusion of a step in the die or die radius may reduce springback. The results of parametric studies provide a better understanding of how basic die parameters (die clearance, die radius, step height and step distance) affect springback.

### **7.3.1. Finite Element Analysis of Springback**

In recent years, finite element analyses (FEA) have been used for predicting springback deformations in sheet metal forming processes. Using this solution technique on actual components in the right manner, numerically predicted springback deformations can be within 1% of production values. The

results of the numerical investigation [54, 56 and 57] indicate that the coupled finite element procedure can be utilized to significantly reduce the number of die prototype designs that are currently required in sheet metal stamping operations.

FEA provides numerical trial-and-error procedures, which lead to a less-time-consuming and more economical way of designing and producing dies. We saw in the previous chapters of this thesis that commercially available FEA programs (like Ansys) provide effective and powerful tools and environments to model and simulate various operations, such as metal-forming applications. These programs include useful and user-friendly graphical user interfaces, which facilitate pre- and post-processing stages. Also, as aluminium (widely used in aerospace industry) is a relatively expensive material, FEA may be employed in the design stages in order to reduce material and production costs.

Many researches used FEA to study springback in sheet metal forming. Nagtegaal and Taylor [58] found that the implicit method is able to handle springback calculations very effectively. In 1992, Karafilis and Boyce [59] introduced the finite element method for designing dies in sheet metal forming using springback calculations. Sim and Boyce [60] later provided a real-time control scheme based on models of “averaging” in processing stresses and strains that provided repeatability of end product quality in terms of final shape, failure modes, and material state. Finn et al. [61] predicted springback in automotive body panels by combining the commercial codes LS-DYNA3D and NIKE3D. In 1995, Wu et al. [62] developed an iterative FEM algorithm to systematically generate a complete geometrical description of the tooling surface with springback compensation taken into consideration. In a similar work, Karafilis and Boyce [63] developed an FEM tooling design algorithm which compensated for springback by modifying the tooling shape. Narasimhan and Lovell [64] even coupled the implicit and explicit finite

element methods to predict springback in sheet metal stamping so as to minimize die prototype design time.

Previously mentioned investigations showed that die radius, clearance, step height and step distance (Figure7.22) must be optimized in order to reduce springback.

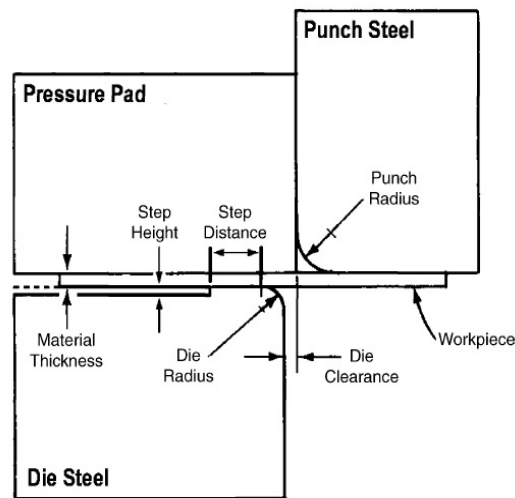


Figure7. 22: Definition of die parameters[56]

Of the four parameters, the die radius and clearance have the more significant effects on springback compared to the step height and step distance and may therefore be used more often to control springback [56]. The step height and step distance may be better used to fine-tune the die. If the die design allows for small radius, the recommendation is to use as small a die radius as possible to reduce springback. However, care must be taken to avoid using a die radius smaller than the minimum bend radius of the metal, so as to prevent the bend area from cracking [65].

The rib blanks are cut from sheets aluminum and the rib flanges are then formed by bending them over the edge of the form block using the rubber pad forming process. The finished flanges of the ribs should end up at a 90 degree angle to the rib web, but if we try to form the edges of the rib at a 90 degree

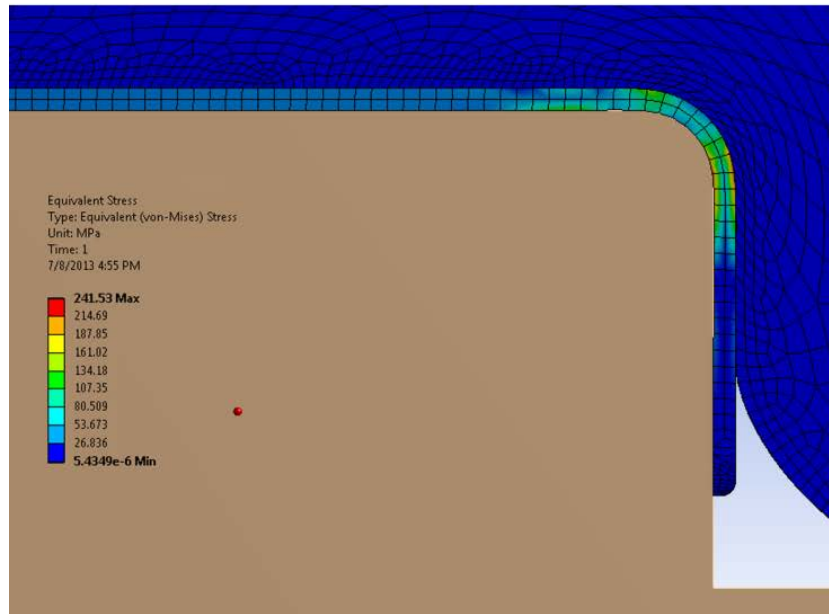
angle and bend the aluminum over this value, no matter how much we press it, the aluminum will springback a small amount and the bend will result in a less than 90 degree angle. To account for springback while forming the ribs, the tool must be set up to have a correction angle for springback. This resulted in the edges of the tool blocks having more than 90 degree angle edge instead of a true 90 degrees, and this angle depends on the value of the bend radius. This results in a net effect of closer to the required 90 degree angles when the flanges are formed.

In the finite element model presented in this thesis, the workpiece, the male die steel and the pressure rubber pad form the main components. In the 2D model definition in Ansys, the die is defined by rigid surfaces, while rubber pad and the workpiece are represented by a deformable mesh. The simulation begins with the rubber pad in contact with the workpiece. The rubber pad then moves down to pressure the workpiece, bending it around the steel die. Constrains and friction coefficient used in springback simulation are illustrated above in the rubber pad forming simulation. See Figure (10) for the straight rib and Figure 17 for the rib with the lightening hole.

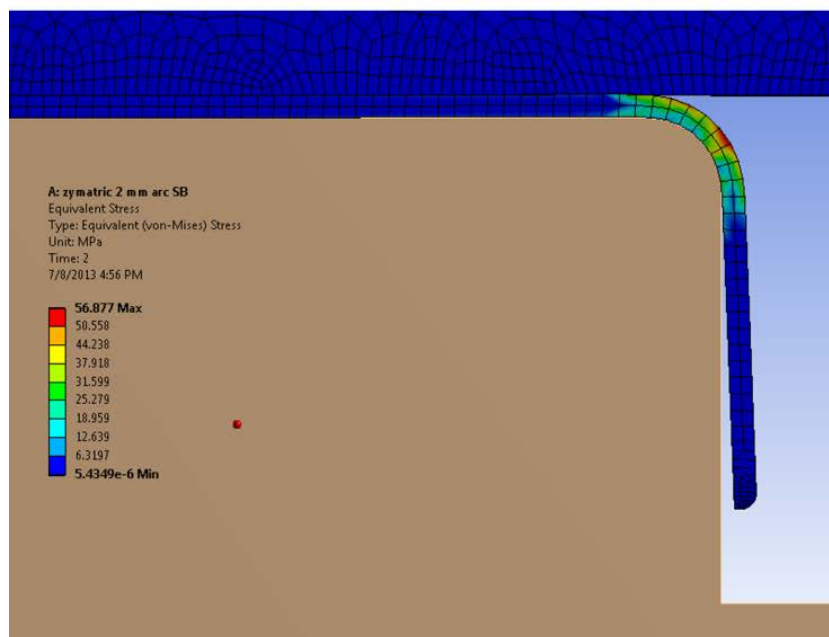
The material used in all the simulations is aluminum 2024-T3. Properties of this material are taken from [66], and are shown in Table 7.1. The assumed plastic region of the flow curve of 2024-T3 is shown in Figure 7. 3.

The springback predictions were obtained for two different geometries of the rib (the straight rib and the rib with the lightening hole) and simulations have been performed for different bend radii. In the case of the straight rib the bend radius has changed from 1mm to 5mm, with the step of 0.5mm. Figure 7.23 illustrates Von Misses stress in the loading-unloading forming process for the straight rib, when the bend radius is 2 mm. Figure 7.24 shows the influence of the variations of bend radius value of the straight rib on the calculated springback factor, and it shows how the springback factor depends strongly on the bend radius. As it can be seen in the graph in Figure 7.24, *as the bend radius*

increases the springback factor decreases. On the other hand, as the bend radius decreases the springback factor increases.



(a)



(b)

Figure7. 23: Von Misses stress in rubber forming process for straight rib during a) loading forming process and b) unloading forming process

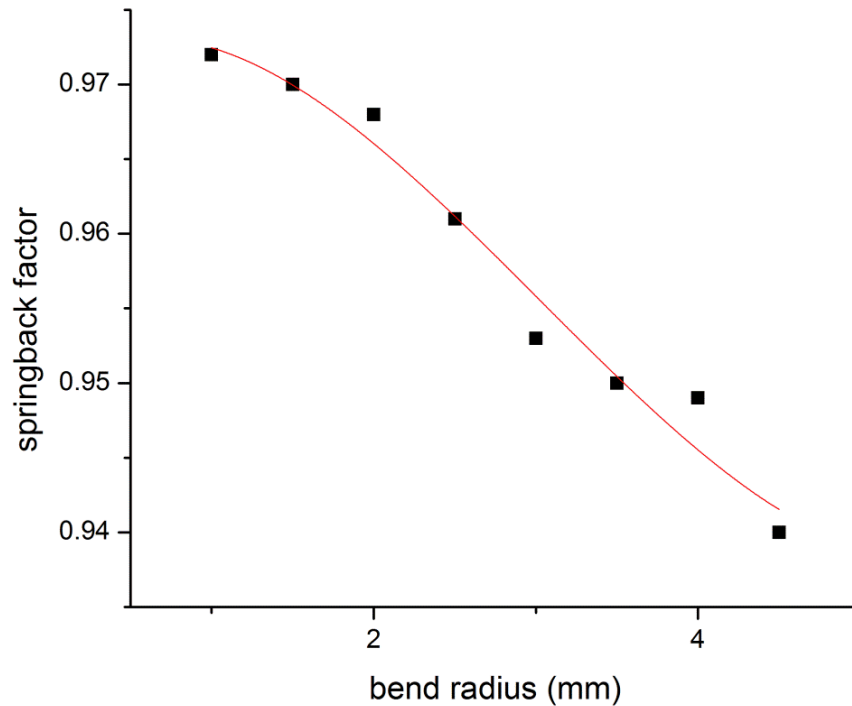


Figure7. 24: Influence of the bend radius in straight rib on the springback factor

In general, there is a certain bend radius of the tool which will minimize springback, because – as it has been mentioned before – the bend radii have high influence on the springback phenomenon. On the other hand, the widely used method for overcoming springback in production is to overbend the sheet to get an exact angle on the part. The main aim of FE simulations of rubber pad forming processes used in this research was to accredit the angle for overbending which will provide the right angle in bend flange after springback takes place. For that purpose, many different FE models were developed (that is, tools with different drifted angles have been modelled) and in Figure 7.25 the most successful model is shown. It was found that the value of the overbending angle should be around 2 degrees to get almost the right angle of the flange after springback. The same figure also shows the last step of the loading process (Figure7.25 (a)) as well as unloading (Figure 7.25(b)) and it is clear that the final flange angle is very close to 90 degrees

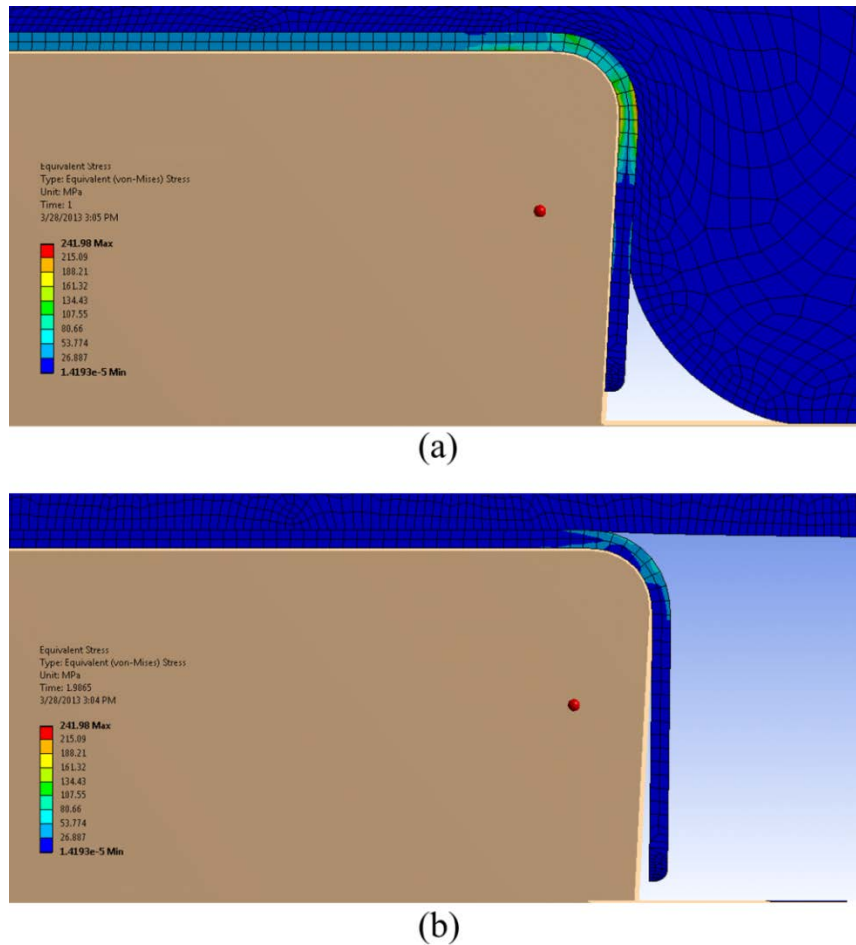


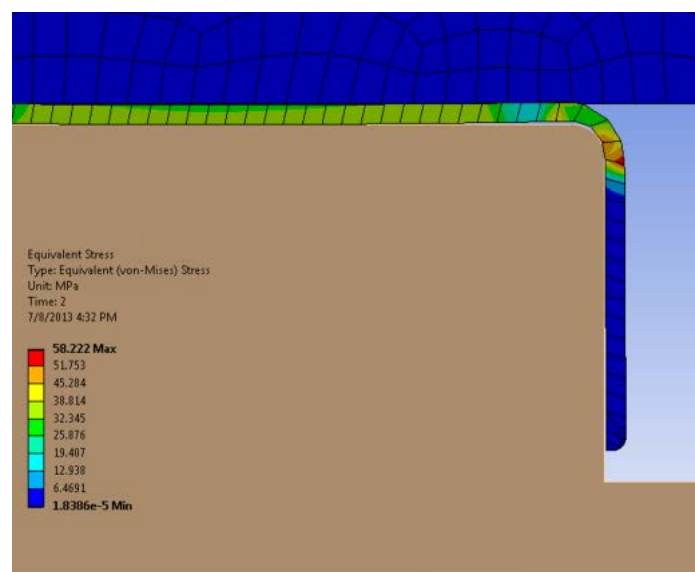
Figure7. 25: Overbending in rubber pad forming process for straight rib

a) last load step, b) unload step

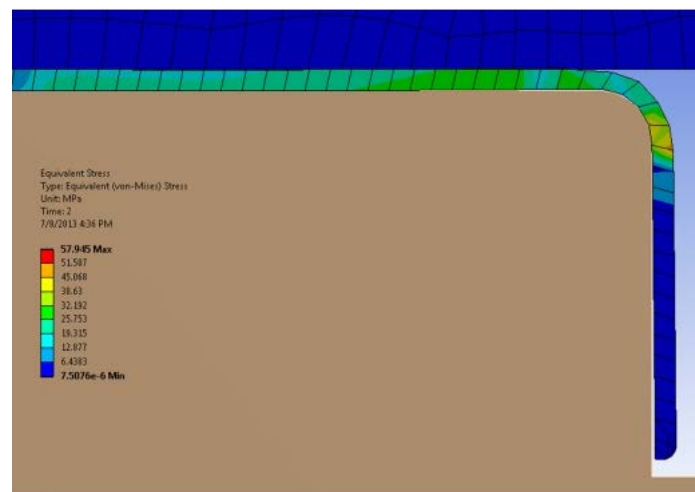
In order to find connections between geometry parameters  $R_I$  and  $R_{II}$  in the rib with the lightening hole (shown in Figure 7.8) and the springback factor  $K$ , radii  $R_I$  and  $R_{II}$  have been varied separately from 1 mm to 5mm (with the step 0.5 mm), while the other parameters ( $R_{III}$  and  $H$ ) remained constant and had a fixed value of 2 mm. The simulations have been carried out in a similar way like previously described: one parameter ( $R_I$ ) was fixed and the other one ( $R_{II}$ ) was changeable, and then procedure was repeated the other way round ( $R_{II}$  fixed,  $R_I$  changeable). After performing tens of FE simulations, some conclusions could be drawn.

Figure 7.26, for example, shows that there is no amount of springback at  $R_I$  when it has values of 1 mm and 1.5 mm, which means that these values of the

radius are under critical value, but this is also an indicator of crack appearance in the region of  $R_I$ . Moreover, the plastic strain has a value higher than the reference plastic strain used in the previous section for crack appearance predictions, and it was found that  $R_I$  should be greater or equal to 2 mm. So, this approach can be used for verification of the rubber pad forming simulations previously performed, too. The amount of springback as a function of  $R_I$  is shown in Figure 7.27 and it is clear that the springback factor decreases with an increase of the value of bend radius.



(a)



(b)

Figure 7. 26: Springback is not presented in rib with lighten hole when a)  $R_I= 1\text{mm}$  and b)  $R_I=1.5\text{mm}$

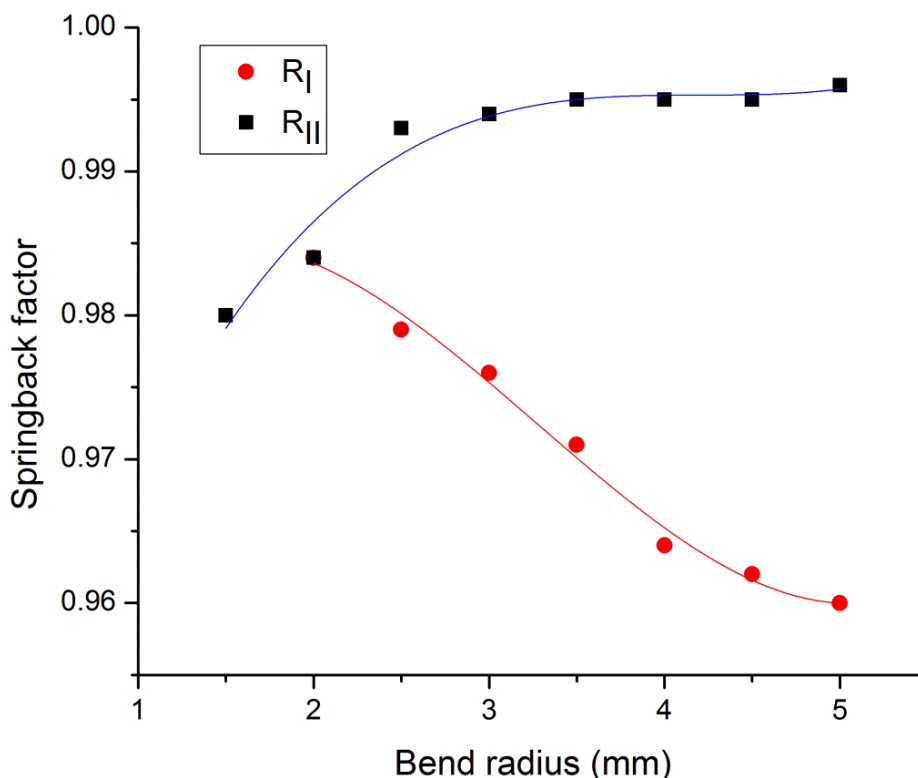


Figure 7.27 Influence of the bend radii  $R_I$  and  $R_{II}$  in rib with lighten hole on the springback factor  $K$

On other hand, Figure 7.27 illustrates that springback factor is increasing when the other radius ( $R_{II}$ ) is increasing, and the reason for that might be that the lightening hole makes the rib stiffer in that area and as a result a smaller amount of springback appears. The value of the springback factor  $K$  increases sharply when the bend radius  $R_{II}$  moves from 2 mm to 2.5 mm and after that there is no significant change in  $K$  when  $R_{II}$  is changing from 2.5 mm to 5 mm. However, when  $R_{II}$  is equal to 1mm there is no springback in  $R_{II}$  region (Figure 7.28) and, as expected, the plastic strain at  $R_{II}$  is higher than the reference plastic strain used as a reference for crack appearance predictions. This is almost the same situation as those previously discussed (when  $R_I$  was 1 mm and 1.5mm) and, consequently, the same conclusions may be drawn.

Results of all two-dimensional FE simulations performed for the straight rib and the rib with the lightening hole are summarized and given in Table 7. 8, Table 7.9 and Table 7.10. Figure 7.29 shows the last loading step and unloading step in FE simulation of the stringer.

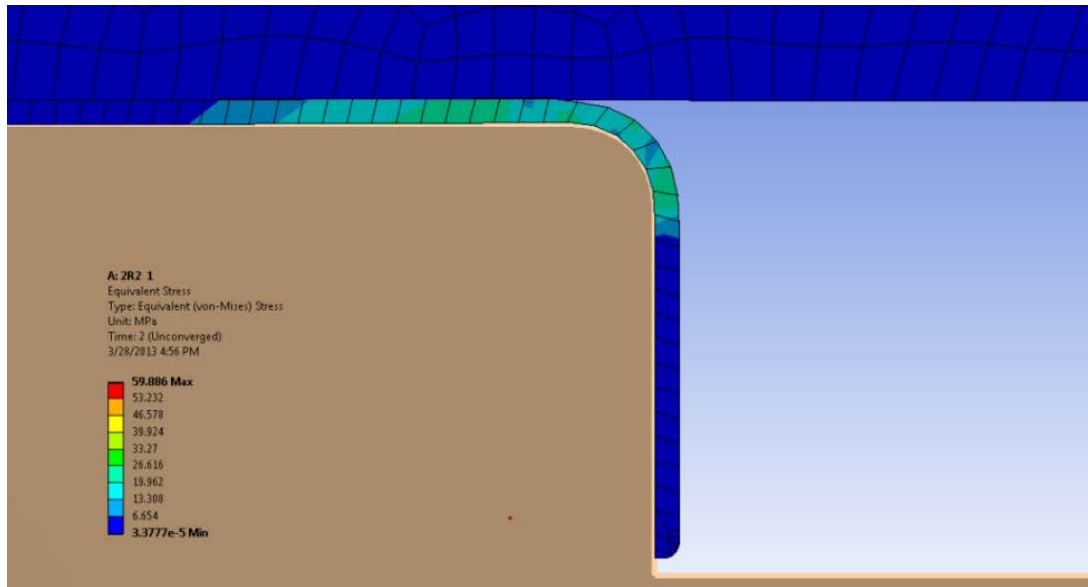


Figure7. 28: Springback is not presented when  $R_{II}= 1\text{mm}$  in rib with lighten hole

| <b>R [mm]</b>                  | <b>1</b> | <b>1.5</b> | <b>2</b> | <b>2.5</b> | <b>3</b> | <b>3.5</b> | <b>4</b> | <b>4.5</b> | <b>5</b> |
|--------------------------------|----------|------------|----------|------------|----------|------------|----------|------------|----------|
| <b><math>\alpha</math> [°]</b> | 87.44    | 87.33      | 87.2     | 86.5       | 85.77    | 85.55      | 85.4     | 85         | 79.25    |
| <b><math>\beta</math> [°]</b>  | 90       | 90         | 90       | 90         | 90       | 90         | 90       | 90         | 90       |
| <b>K</b>                       | 0.972    | 0.970      | 0.968    | 0.961      | 0.953    | 0.95       | 0.949    | 0.94       | 0.88     |
| <b>Overbend angle[°]</b>       | 2.56     | 2.67       | 2.8      | 3.5        | 4.23     | 4.33       | 4.5      | 5          | 10.25    |

Table7. 8 Values of springback factor K and overbend angle for straight rib when bend radius R is changeable where the other geometry parameters are fixed

| $R_I$ [mm]         | 1     | 1.5   | 2     | 2.5   | 3     | 3.5   | 4     | 4.5   | 5     |
|--------------------|-------|-------|-------|-------|-------|-------|-------|-------|-------|
| $\alpha$ [°]       | 0     | 0     | 88    | 87.84 | 87.55 | 87.4  | 86.8  | 87.58 | 86.46 |
| $\beta$ [°]        | 90    | 90    | 90    | 90    | 90    | 90    | 90    | 90    | 90    |
| K                  | crack | crack | 0.981 | 0.976 | 0.973 | 0.971 | 0.964 | 0.962 | 0.96  |
| Overbend angle [°] | -     | -     | 2.0   | 2.16  | 2.45  | 2.6   | 3.2   | 2.42  | 3.54  |

Table 7. 9: Values of springback factor K and overbend angle for rib with lightening hole when bend radius  $R_I$  is changeable where the other geometry parameters are fixed

| $R_{II}$ [mm]      | 1     | 1.5  | 2     | 2.5   | 3     | 3.5   | 4     | 4.5   | 5     |
|--------------------|-------|------|-------|-------|-------|-------|-------|-------|-------|
| $\alpha$ [°]       | crack | 88.2 | 88.56 | 89.37 | 89.46 | 89.55 | 89.55 | 89.55 | 89.64 |
| $\beta$ [°]        | 90    | 90   | 90    | 90    | 90    | 90    | 90    | 90    | 90    |
| K                  | -     | 0.98 | 0.984 | 0.993 | 0.994 | 0.995 | 0.995 | 0.995 | 0.996 |
| Overbend angle [°] | -     | 1.8  | 1.44  | 0.63  | 0.54  | 0.45  | 0.45  | 0.45  | 0.36  |

Table 7. 10 Values of springback factor K and overbend angle for rib with lightening hole when bend radius  $R_{II}$  is changeable where the other geometry parameters are fixed

In addition, after obtaining satisfactory results in 2D simulation of springback phenomenon, it was decided to perform more complex and challenging 3D simulations of the same process. In the 3D model definition in Ansys (which is almost the same as the model used for the 2D springback analysis), the die has been defined as a rigid body, while the rubber pad and workpiece were represented by a deformable mesh. The friction coefficient and

material properties used in 3D springback simulation were taken from the above mentioned 2D rubber pad forming simulation. Constrains used in the 3D simulations of bending of blank for the straight rib are shown in Figure 7.29. The frictionless support was applied on the rubber pad side surfaces, simulating the influence of the container on the rubber pad (Figure 7.29). Figure 7.30 shows a complete 3D FE model as used in the simulation. It can be seen that one half of the real set-up was modeled, and then symmetry conditions were applied.

The rubber pad is in contact when a sheet metal forming simulation starts. While the rubber moves and pressurizes the sheet, the sheet bends around the rigid die to get the final shape of the rib.

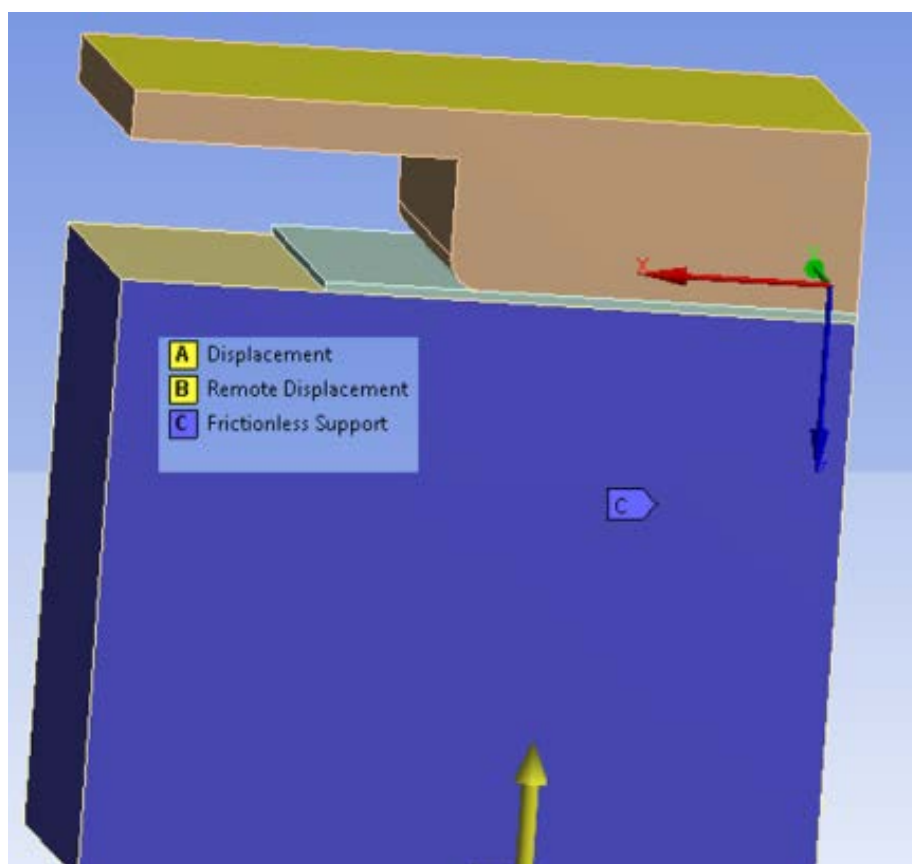


Figure7. 29: Constrains applied in symmetrical 3D model for the simulation of the forming of straight rib using rubber pad technique

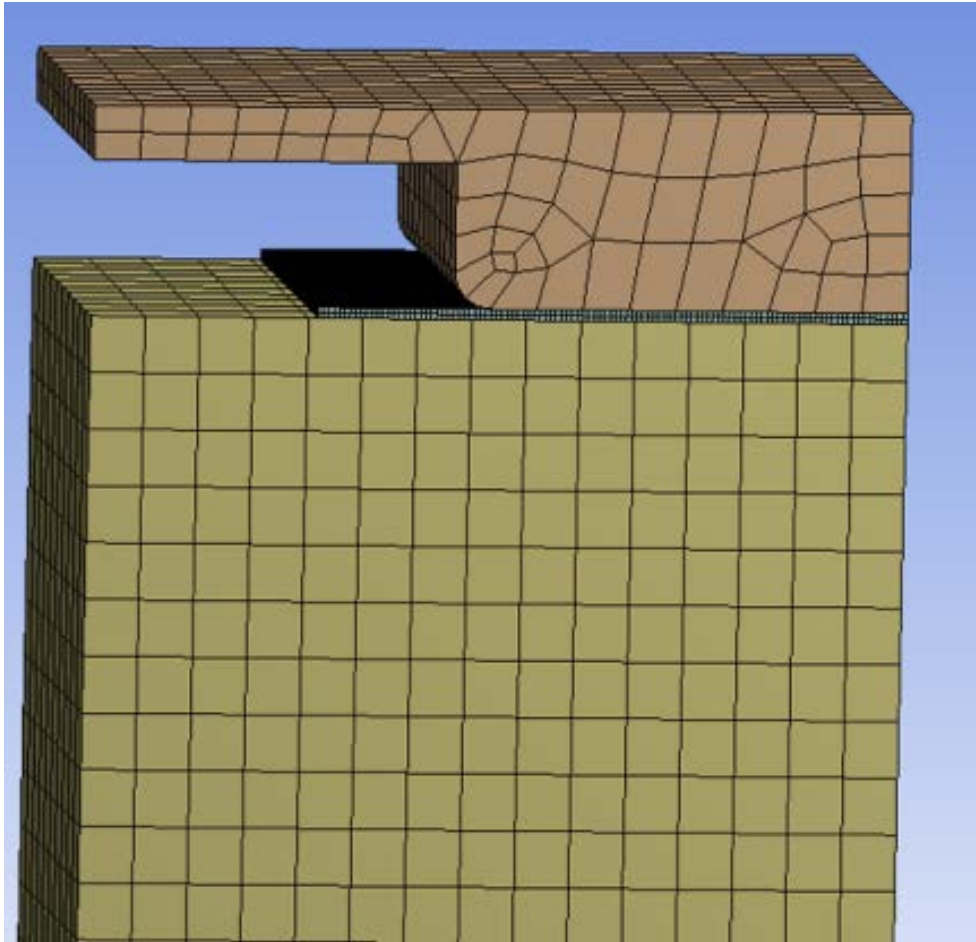


Figure7. 30: 3D FE mesh of symmetrical model used in simulation of the forming of straight rib using rubber pad technique

Figure 7.31 shows equivalent Von Mises stresses obtained at the last load step and unload step in the 3D simulation of rubber pad forming of the straight rib. Figure 38 shows that the value of stress in the last load step is 250.96MPa, while the value of stress in the unload step is much lower (91.45MPa) which is expectable and it is clear in Figure 7.31 (b) that springback occurs in simulation. This model proved that it is possible to simulate springback during a rubber pad forming process even in 3D environment, but because springback was already analyzed in details in 2D simulations, it was decided to use 3D simulations only for the purpose of comparing the geometry of ribs obtained in the simulations against the geometry of ribs obtained in the experiment. Aims of this approach

(using 3D models in the rubber pad forming process) were the development of reliable three-dimensional FE models that can be successfully used in such simulations and the verification of the final shapes of the ribs after forming, with all the expectable phenomena such as springback and wrinkling.

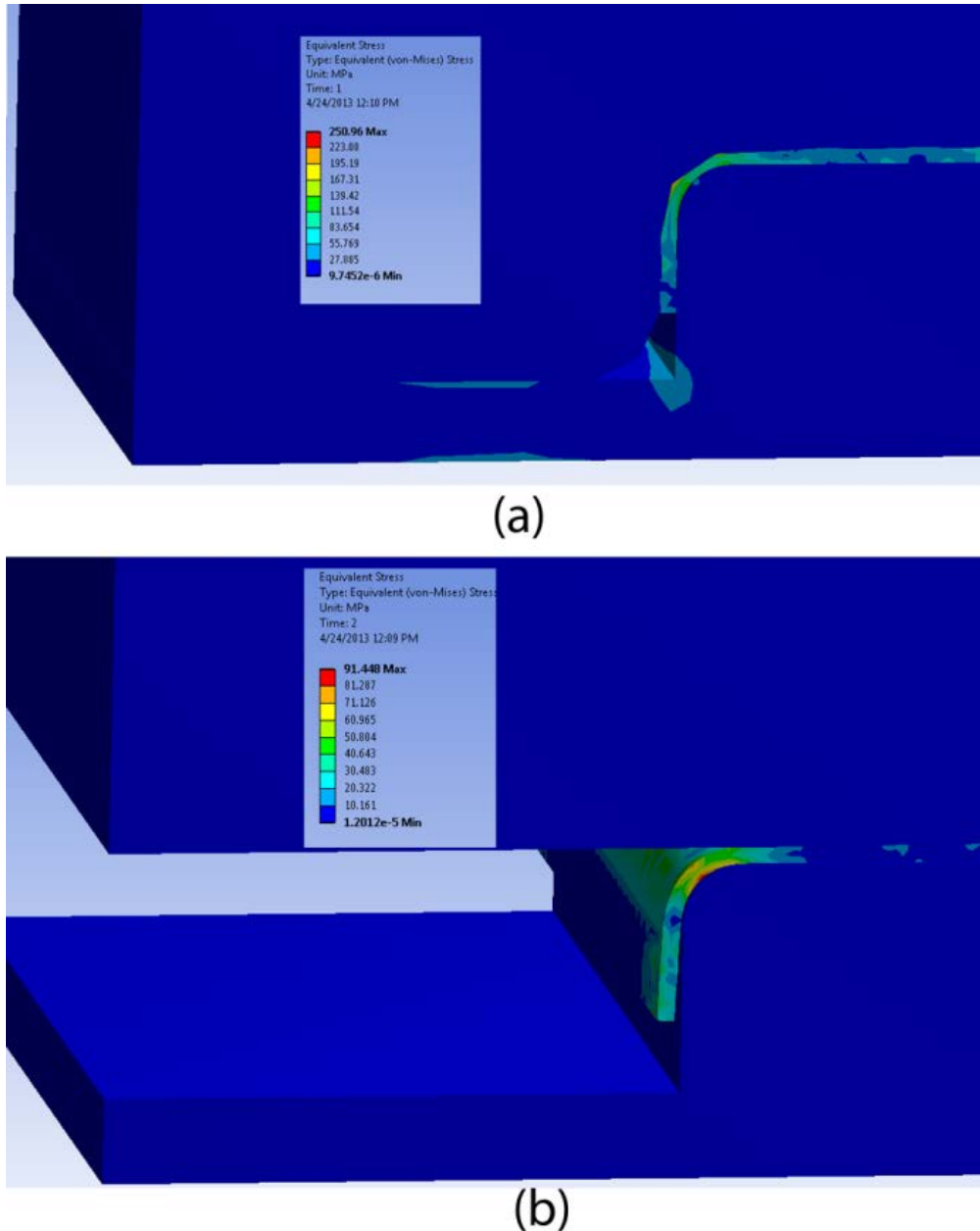


Figure 7.31: 3D FEM simulation of rubber pad forming process of symmetrical model of straight rib: a) load step b) unload step

In Figure 7.32 the shape of one rib of the light aircraft horizontal tail obtained in 3D simulation of the rubber pad forming process can be seen.

Figure 7.32(a) shows the last load step of the forming process, where the rigid die is transparent and the rubber pad surrounds the outer surface of the rib (the rigid die was assigned transparency so the complete model of the bended rib could be seen). Figure 7.32(b) shows unload step and it is clear that rubber is not surrounding the rib anymore (one half of the set-up was modelled and symmetry conditions were used). Furthermore, springback phenomenon is presented in this model as well as wrinkling, which will be described in the next section.

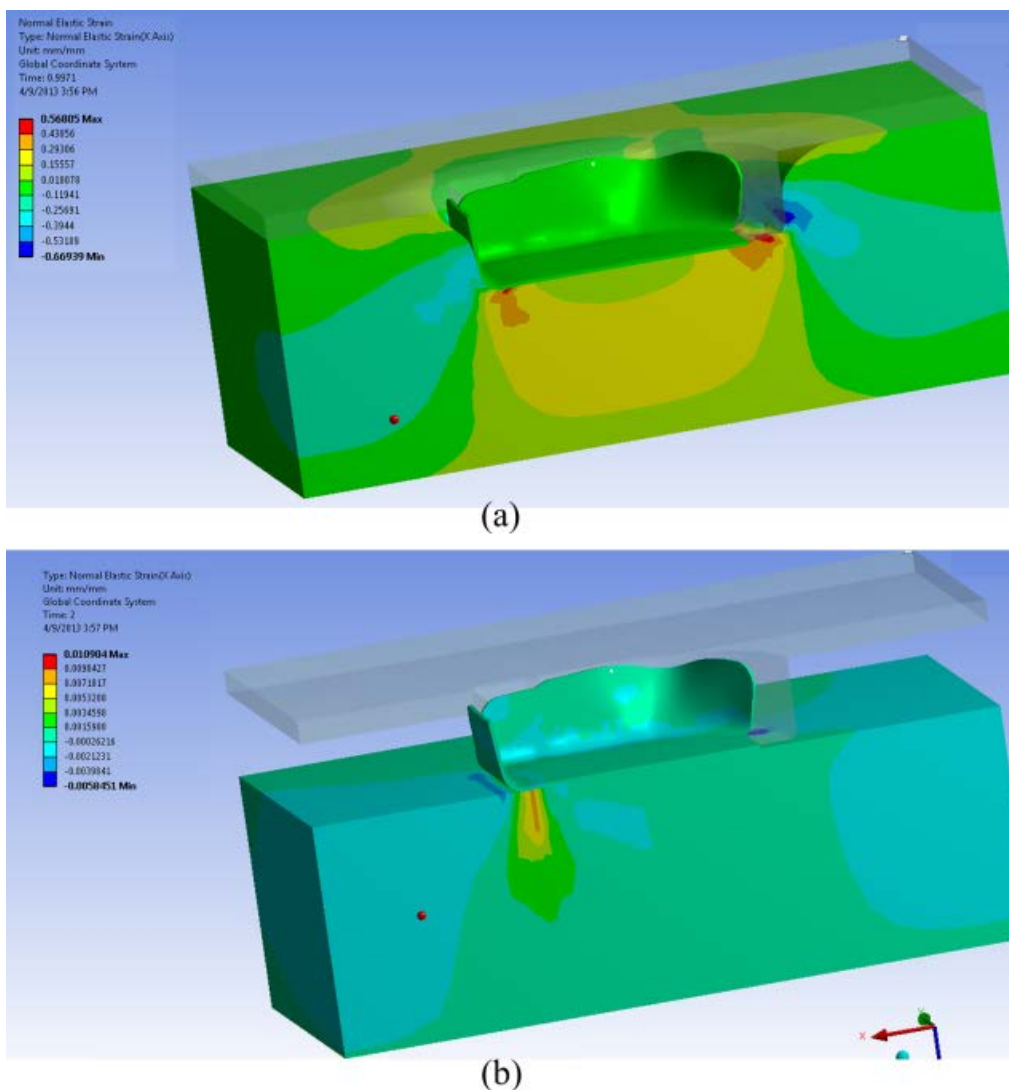


Figure 7. 32: FEM simulation of one half of the rib of light aircraft horizontal tail using rubber pad forming process: a) load step, b) unload step

#### 7.4. Wrinkling in Formed Ribs Using Rubber Pad Forming Process

Wrinkling is an undesirable result in sheet metal forming, especially when it occurs on outer skin panels where final part appearance is critical. Additionally, large wrinkles may damage dies and interfere with part assembling and function. The prediction and prevention of wrinkling are therefore extremely significant in sheet metal operations. This instability problem can be partially alleviated by the use of a blank holder with an adequate force and/or appropriate drawbeads [67].

Wrinkling is increasingly becoming one of the most common and trouble-some modes of unacceptable deformation in sheet metal forming. Wrinkling can be viewed as a plastic buckling process in which the wavelength of the mode in one direction is extremely short. The mode is a local one which depends on the local curvatures and thickness of the sheet, on its material properties, and on the stress state. Conditions for the onset of wrinkling in doubly-curved sheet metal undergoing forming are obtained from a plastic buckling analysis for short wave length, shallow modes. The region of the sheet susceptible to wrinkling is assumed to be unconstrained by the die. When the principal axes of the membrane stress state coincide with the principal axes of the curvatures, simple formulas for the stresses or strains at wrinkling are obtained [68].

During press-forming operations (mainly in case of axi-symmetric and double curvatures shapes), the sheet metal edges are drawn towards a region of smaller perimeter, inducing compressive hoop stresses. If these stresses reach critical values, buckling occurs, leading to corrugations, which become sharp and protruding wrinkles. The main causes of these defects reside in the abrupt changes of cross-section, as well as in the blankholders poor efficiency [3, 68]. According to [67], during the viscous pressure deep drawing process, the flange wrinkling occurs under the combination of the radial of tension stress and the circumferential compression stress. With increase of the interface force, the

radial stress of flange sheet metal increases and the circumferential stress decreases correspondingly and the yield stress is constant. The onset of flange wrinkling is thus restrained [69, 70].

In the FEM simulations, the wrinkling in sheet metal cannot appear in 2D simulation of sheet metal bending. So, this is why 3D simulations have been used to illustrate the wrinkling region in a rib during rubber pad forming process. As described earlier in this chapter, the specifications of 3D FEM simulations (such as contacts, material properties and constraints) were the same. Figures 7.33 and 7.34 show these constraints, as well as FE mesh of the symmetrical model of the blank of the rib with lightening hole, (respectively).

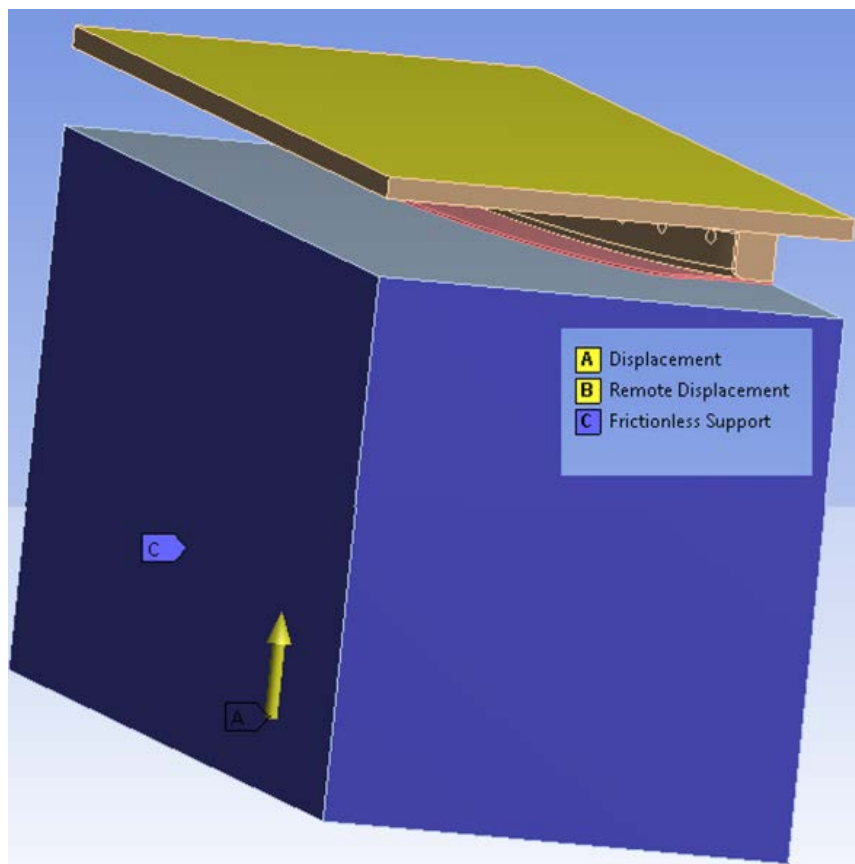


Figure 7.33 Constraints applied in 3D model for the simulation of the forming of rib with lightening hole using rubber pad technique

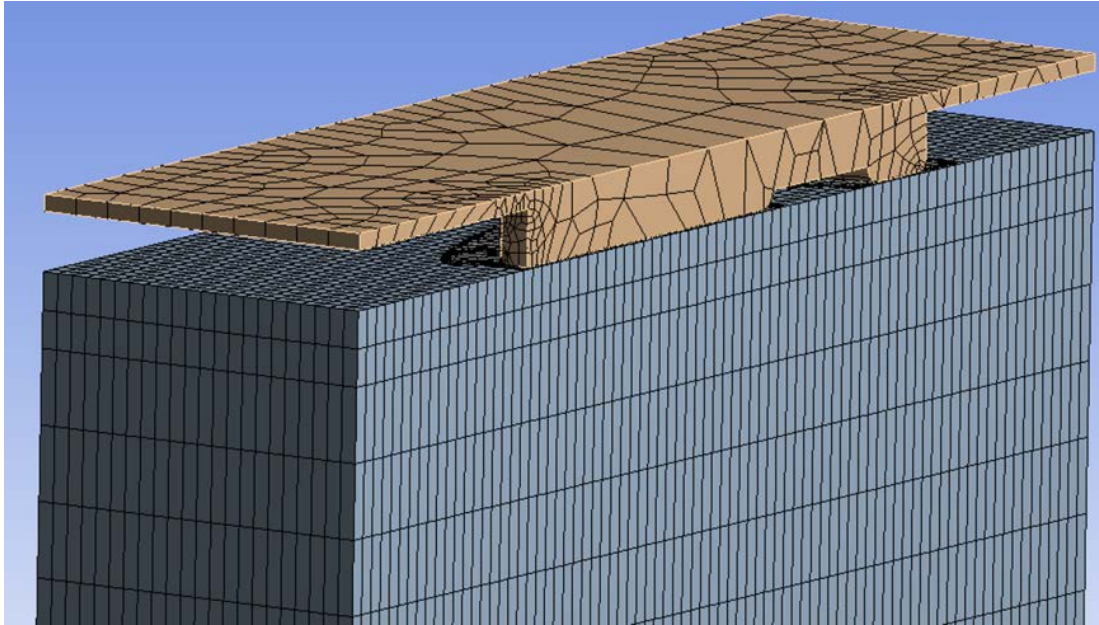


Figure 7.34: FE mesh used in analysis of symmetrical model of the rib forming using rubber pad

The Figure 7.35 shows the first and the last step of 3D symmetrical simulation of forming in a case of the rib with the lightening hole. The first step (Figure 7.35(a)) is self-compression of the rubber pad (as mentioned before), while the last forming step (Figure 7.35(b)) leads to the final shape of the rib. For better observing, Figure 7.35 was rearranged (everything except the blank was hidden) and Figure 7.36 was obtained.

Figure 7.37 shows the 3D symmetry model of a formed rib with a lightening hole as obtained in simulation. As it can be seen in Figure 7.37, there is no wrinkling in the straight flange, but the wrinkling occurs in the curved flange and it increases as the curvature of the flange increases. This is in agreement with the previously mentioned reference [3], which leads us to the conclusion that FE simulation was performed well. The next chapter offers experimental evidence for these findings and everything will be discussed in detail later.

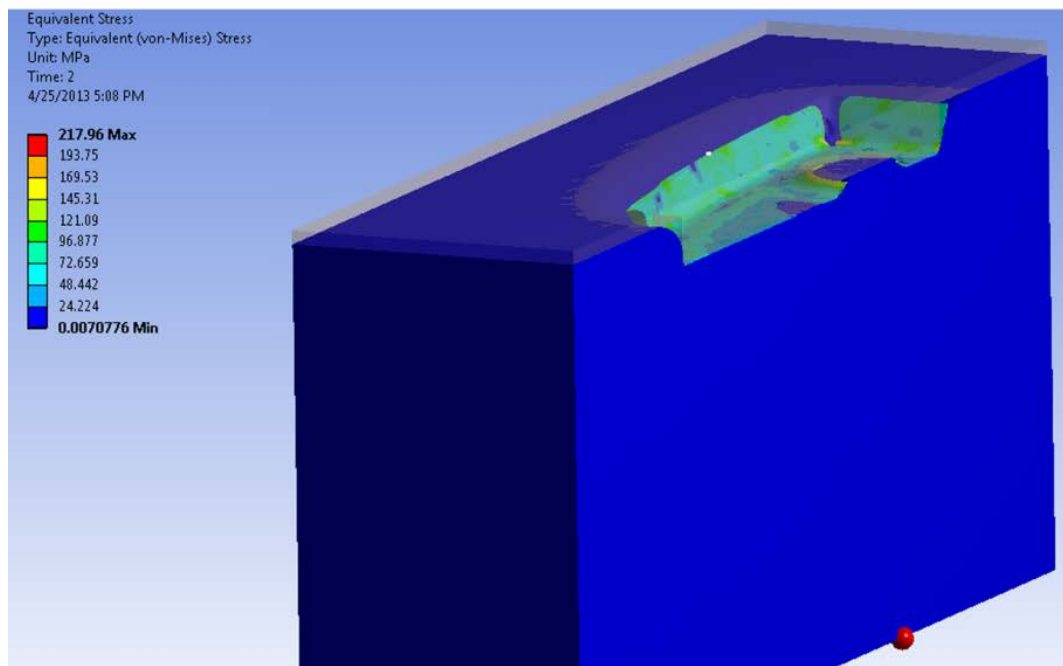
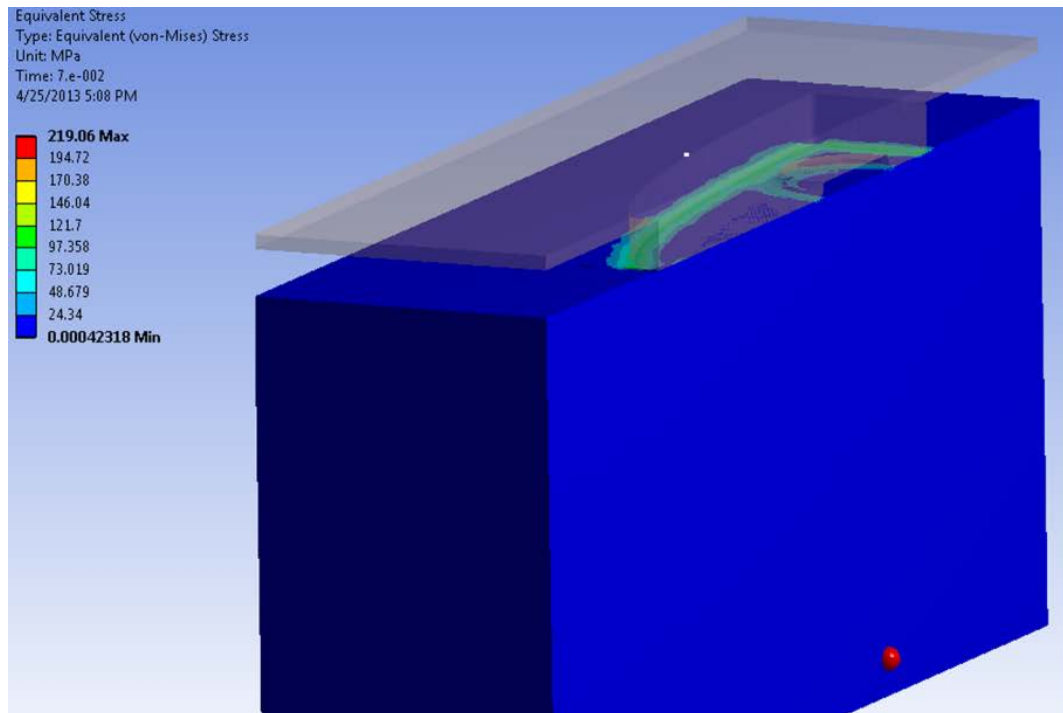
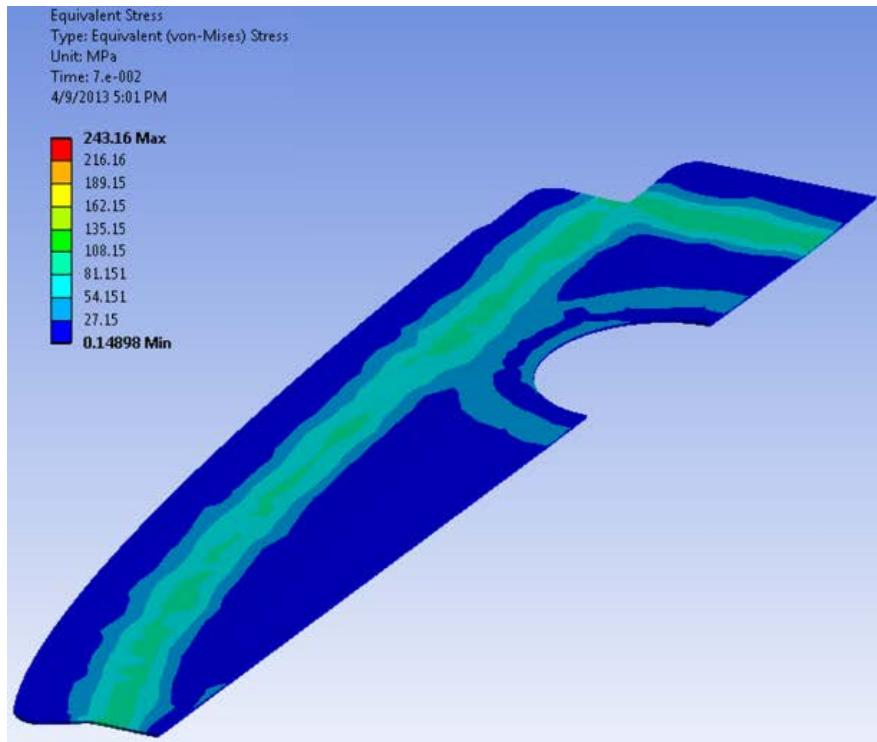
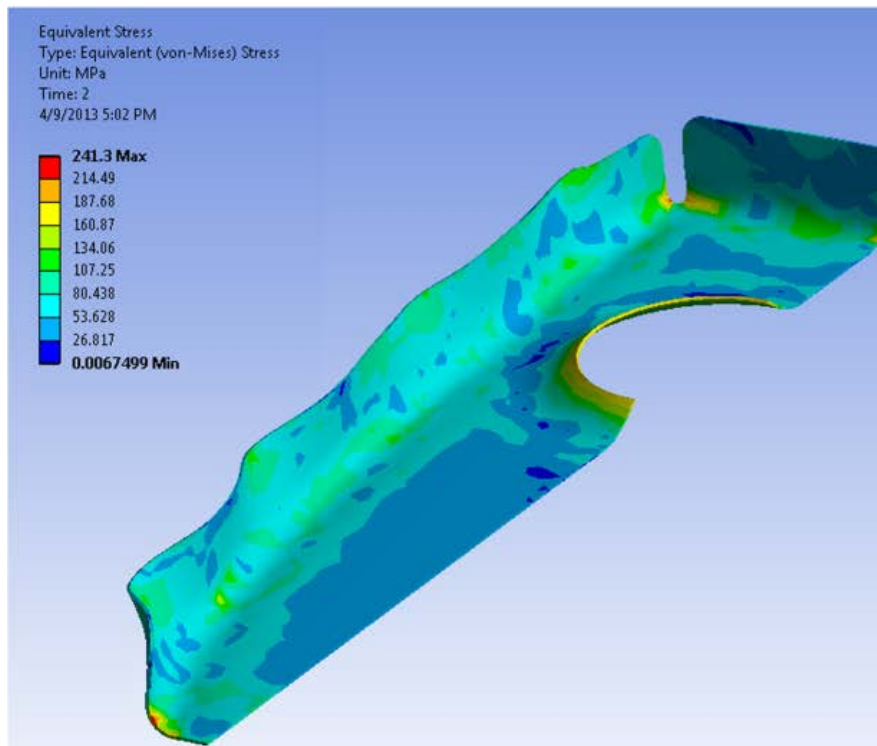


Figure 7. 35: FE simulation of forming the rib with lightning hole using rubber pad forming process: a) first step, b) final step



(a)



(b)

Figure7. 36: FE simulation of forming a blank of rib with lightening hole

a) first step, b) last step

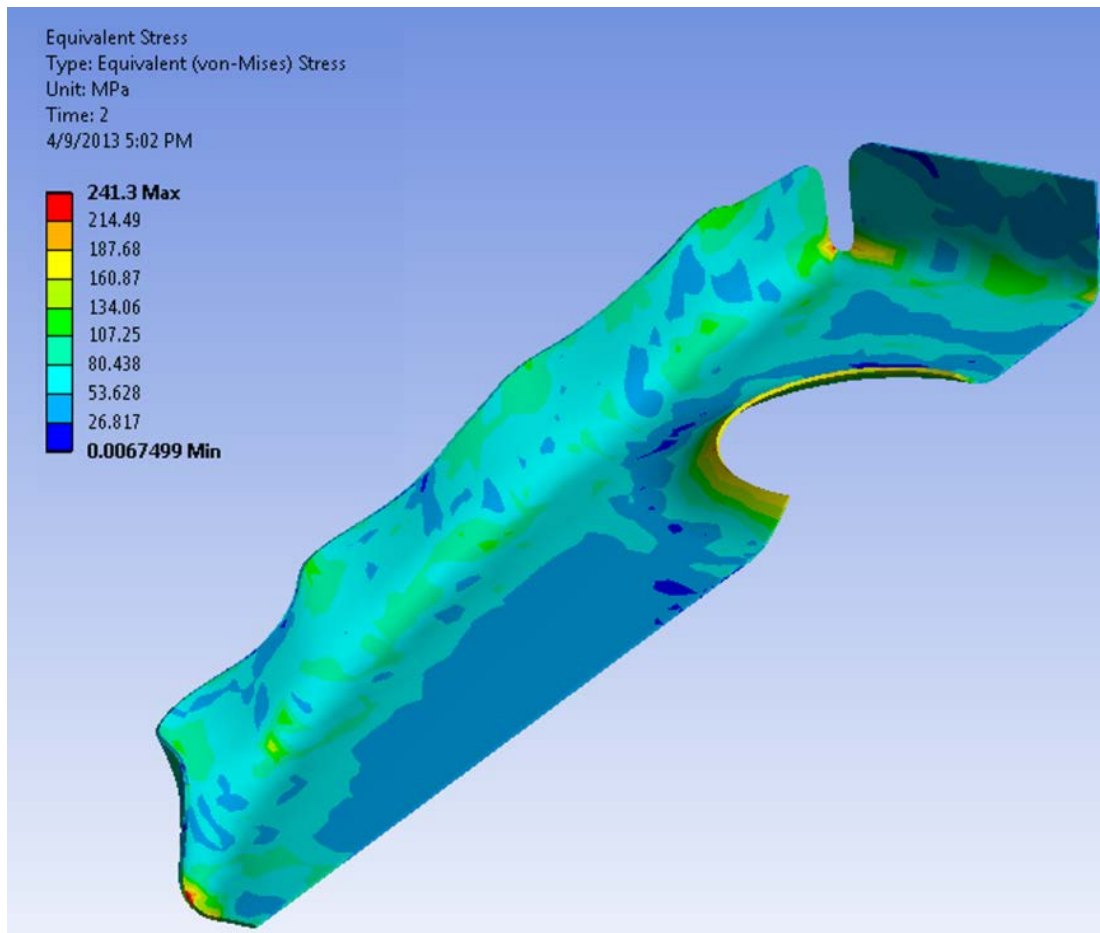


Figure 7.37: Wrinkling in FEM model of formed rib with lightening hole

As it is mentioned above, the wrinkling may damage the part or assembly and jeopardize its' function. In the past, the trial and error procedure and the operator experience optimized part and die design. Today, as shown in this thesis, finite element modeling can be used to design part, and die and simulate sheet metal forming process, thus significantly reducing the costs of tooling and labour. Designing the blank geometry, keeping in mind that good design minimizes excess of material, can reduce the potential for wrinkling. Also, one must be aware that reduced part complexity and advantages of symmetry asymmetry can also help.

The Figure 7.38 shows bad design of other rib of light aircraft horizontal tail which experiences overlapping and high amount of wrinkling in curved

flange during rubber pad forming process. This is not allowed in production, because this amount of wrinkling is not easy to correct after manufacturing. 3D FE simulations can help identify this high wrinkling in an early phase of design where model corrections are easy to implement. For example, after performing simulations with old design (Figure 7.39(a)) and obtaining high wrinkling, this rib was redesigned in CATIA v5 software, as shown in Figure 7.39(b). Simulations with the new shape of the blank were performed and acceptable wrinkling was obtained, as can be seen in Figure 7.40. Redesigned shape gives each side of curved flange possibility to move separately during the forming process and this produces lower wrinkling in curved flange, compared to wrinkling of the original blank. This wrinkling can be corrected by operator allowing the use of this rib in aircraft tail assembly.

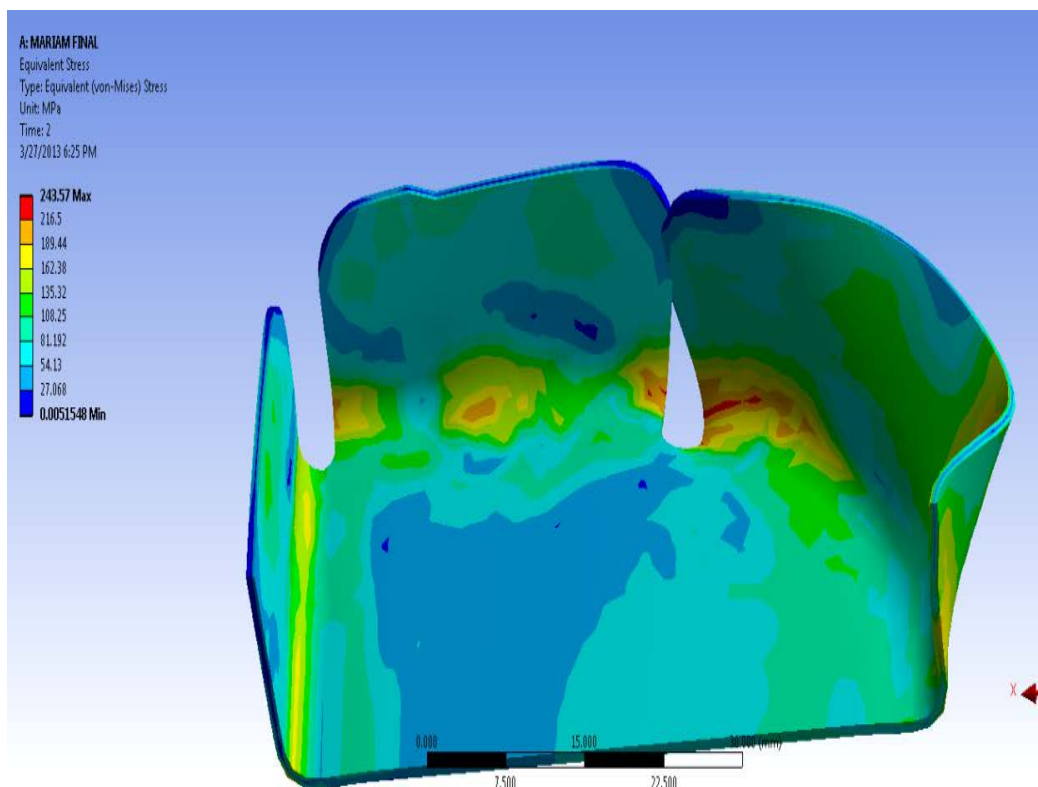


Figure 7.38: Undesirable 3D model result rib

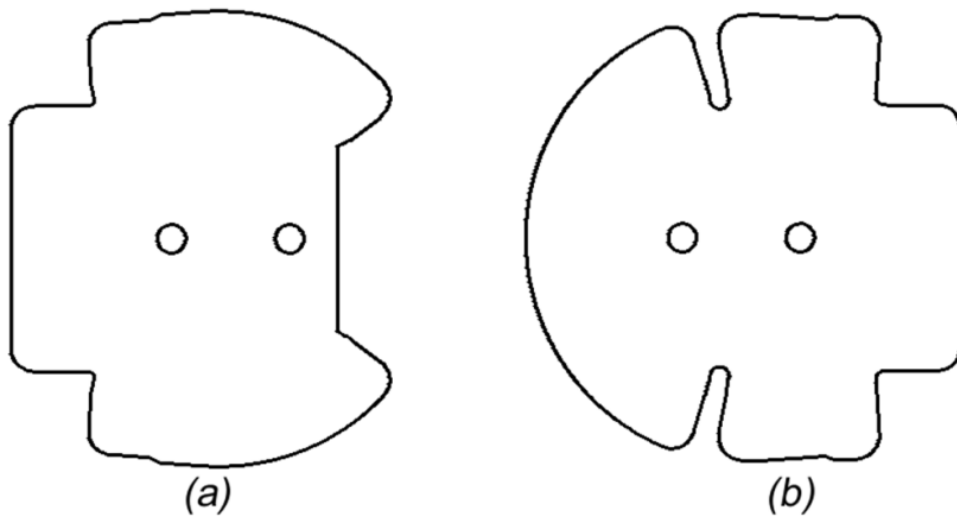


Figure7. 39: Optimization of the blank shape: a) original blank, b) redesigned blank

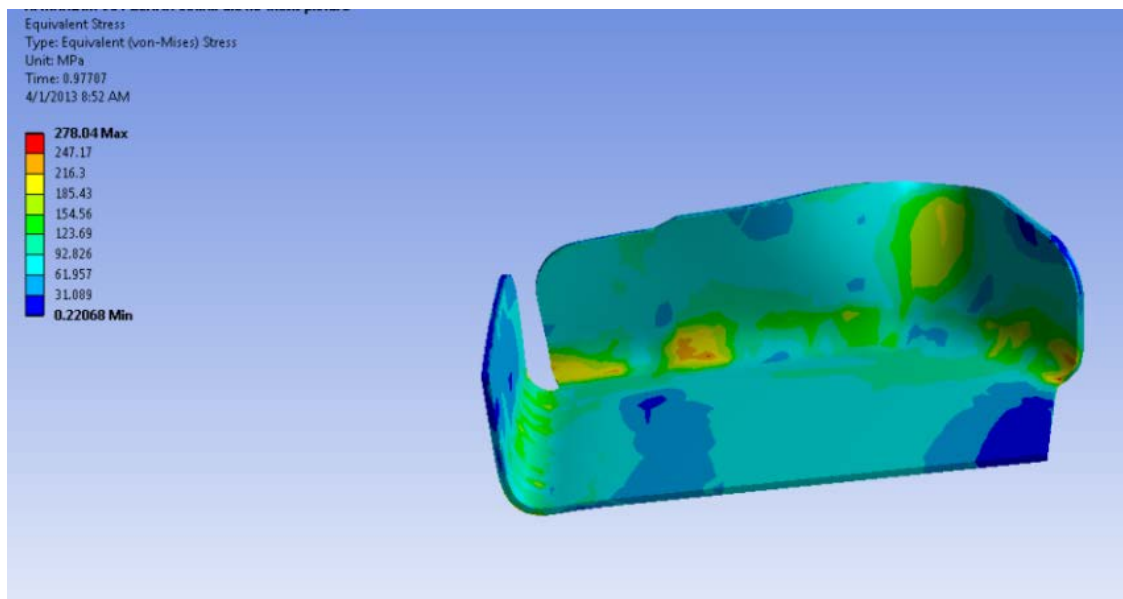


Figure7. 40: 3D model of the rib after redesign

In the next chapter, shapes of the ribs obtained in 3D simulation (before and after redesign) and presented here will be compared to shapes of the real ribs obtained in the rubber pad forming process.

The springback and wrinkling phenomena must be taken into account during sheet metal forming using rubber pad forming process in order to get right the final product. According to that FEM simulation in 2D and 3D have been running to analyze both the springback and wrinkling phenomena in order to reduce the influence these phenomena have on the final shape of the horizontal tail ribs. The most important conclusion can be summarized as:

- Finite element simulation of the rubber-pad forming process in 2D and 3D could be very useful tool for understanding and improving forming operations. Developed FE models of rubber pad forming process allowed us to predict the final shape of the ribs to avoiding any defects which can appear in the product during the forming process.
- The springback factor increasing as the bend radius of straight rib increases
- The correction angle of a springback in straight rib is  $2[^\circ]$  to get almost right angle
- The springback increase also as the  $R_I$  increases in rib with lighting hole where there is no any amount of springback when the value of this radius equal to 1mm and 1.5 mm, it means these value are under critical value ,which indicates the crack in  $R_I$  region is expected.
- The springback decreases also as the  $R_{II}$  increases in rib with lighting hole, which means the lighting hole in the rib works as stiffener in the rib ,the value of  $R_{II}$  should be greater than 1 mm to avoiding critical radius ,which the leads to eliminate the possibility of crack appearances in  $R_{II}$  region .
- The wrinkling phenomena is taken place in 3D FEM in curvature flange, and the amount of wrinkling increase as the curvature arc

decreases while in all 3D models which developed in the section ,there is no and amount of wrinkling in straight flange region .

- In some cases it is useless to make correction on the rib after production, and it is easy to make redesign the blank shape in early design phase to at least reduce the amount of wrinkling. On the other hand we should keep the functionality of the product in its purpose after redesign the blank.

## 8. Experimental Validation of Numerical Results

In order to confirm previously presented conclusions drawn on the basis of 2D and 3D FEM simulations performed in Ansys, it was decided to organize experimental investigations of rubber pad forming process with real sheet metal parts and, at the end of the day, to compare experimental and numerical findings.

The apparatus used in these experiments was built around a hydraulic press machine (produced by REXROTH, Germany), with the maximum capacity of  $F=160$  t (Figure8.1). An experimental set-up (shown in Figure8.2b) was used, along with the assembly of a die set (schematically shown in Figure8.2a).



Figure8. 1: Hydraulic press machine and experimental rubber pad forming set-up

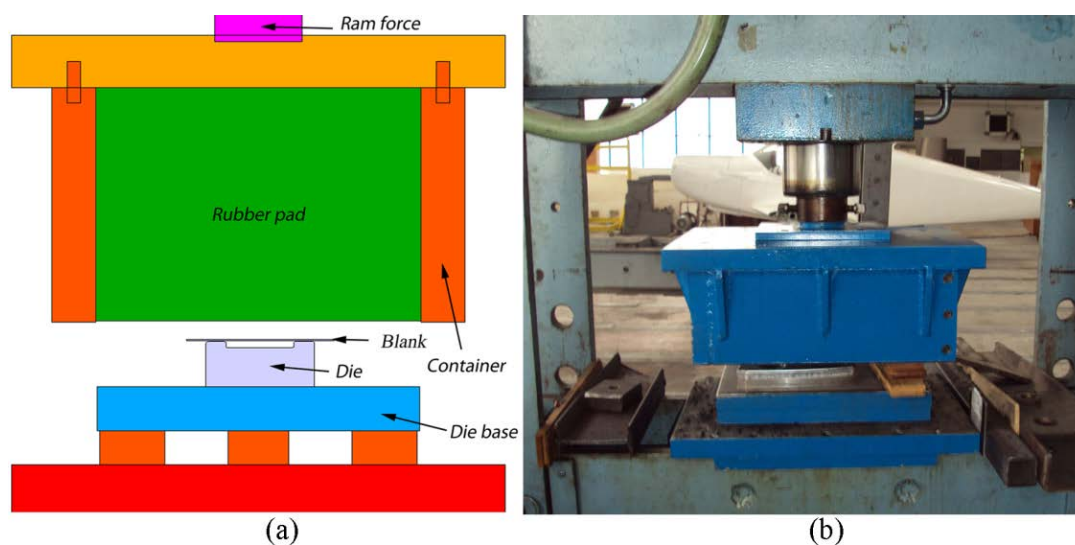


Figure8. 2: a) Schematic representation of the assembly of a die set b) Experimental set-up

The rubber-pad container was made of steel, while dies were made of wood. The main reasons why steel was not used as a die material were very high costs of producing such tools and the purpose of experiments – to measure stresses and strains on contact areas between blank and punch, not on the tools. Polyurethane rubber with a Shore A hardness of 70 (HD70) was used as a rubber pad. The experiment begins with the die placed on the base of the hydraulic press machine and then the aluminum blank is introduced between the die and the flexible punch. After this, the flexible punch pushed by hydraulic cylinder moves down to stamp the blank.

During the experiment, the force on the die produced by flexible punch was measured by force transducer of type U10M 125kN, manufactured by Hettinger Baldwin Messtechnik, Germany (Figure8.3). Displacement of the flexible punch was measured by potentiometer displacement transducer PM2S 150mm, manufactured by ELAP Spa, Italy (Figure 4). Stresses and strains were measured in different areas of blanks (Figure8.5 shows aluminum blank for rib with lightening hole, where stresses were measured at 6 points around the

hole), using aluminum strain gauges of the type 1-LY13-10/120, produced by Hettinger Baldwin Messtechnik. Each strain gauge was connected to one dummy strain gauge into one half of Wheatstone bridge circuit, and then with the acquisition system (Figure8.6). Data acquisition and analysis were performed using SPIDER8 measurement acquisition system and software package Catman Express produced by Hettinger Baldwin Messtechnik (Figure8.7). *It is important to mention that data collected from strain gauges, reaction force instruments and displacements transducer are not discussed in this thesis because they were not the aims of investigations within this thesis, but they will be used in further researches.*

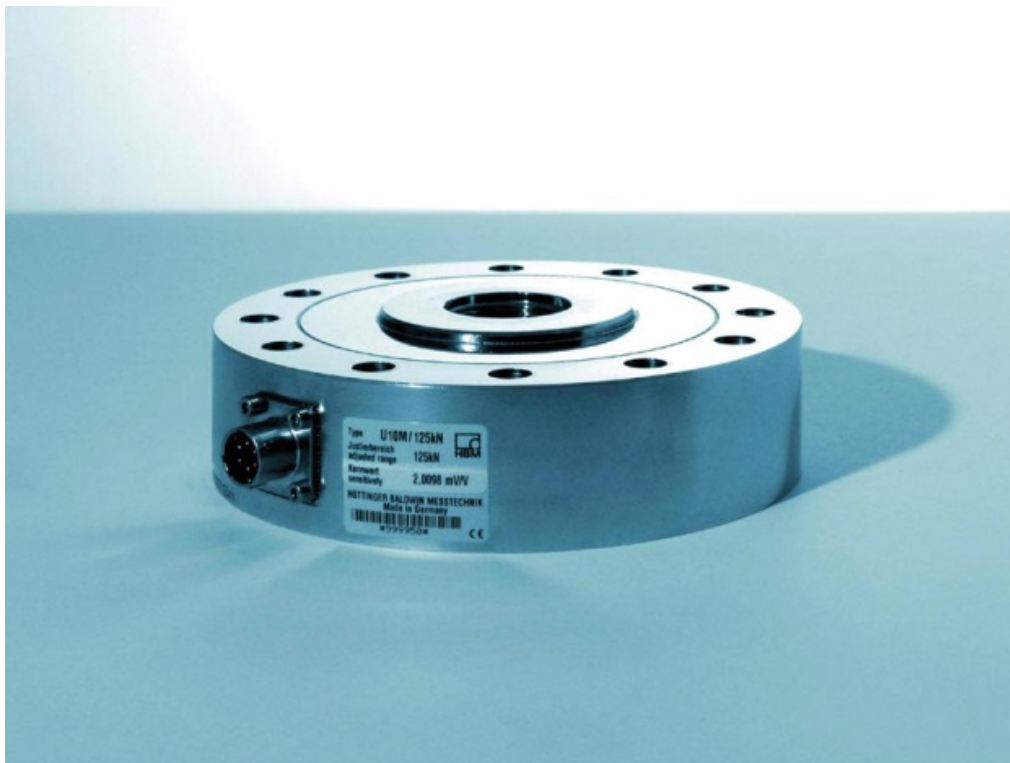


Figure8. 3: Force transducer of type U10M 125kN

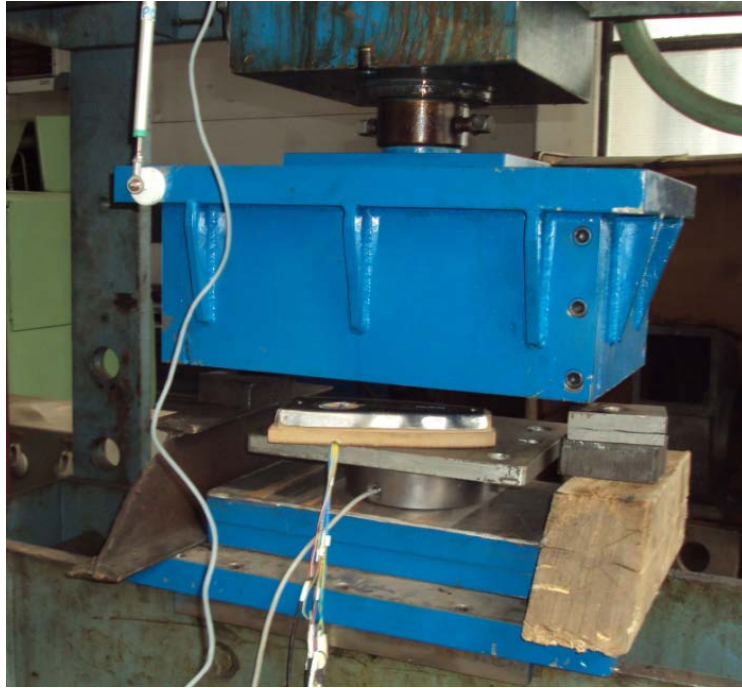


Figure8. 4: Position of the displacement transducer PM2S 150mm used in experiments

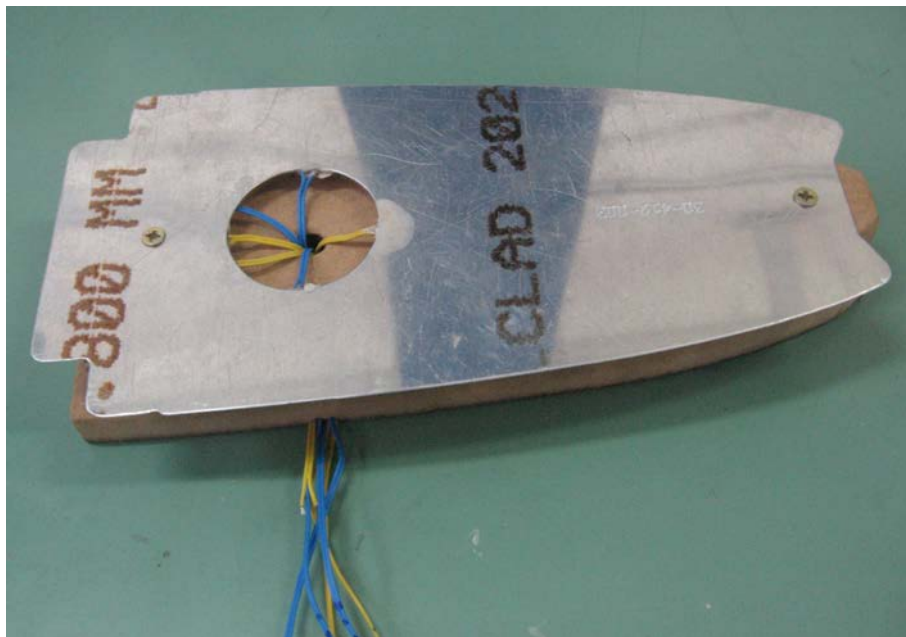


Figure8. 5 :Position of strain gauges used on the blank for rib with lightening hole

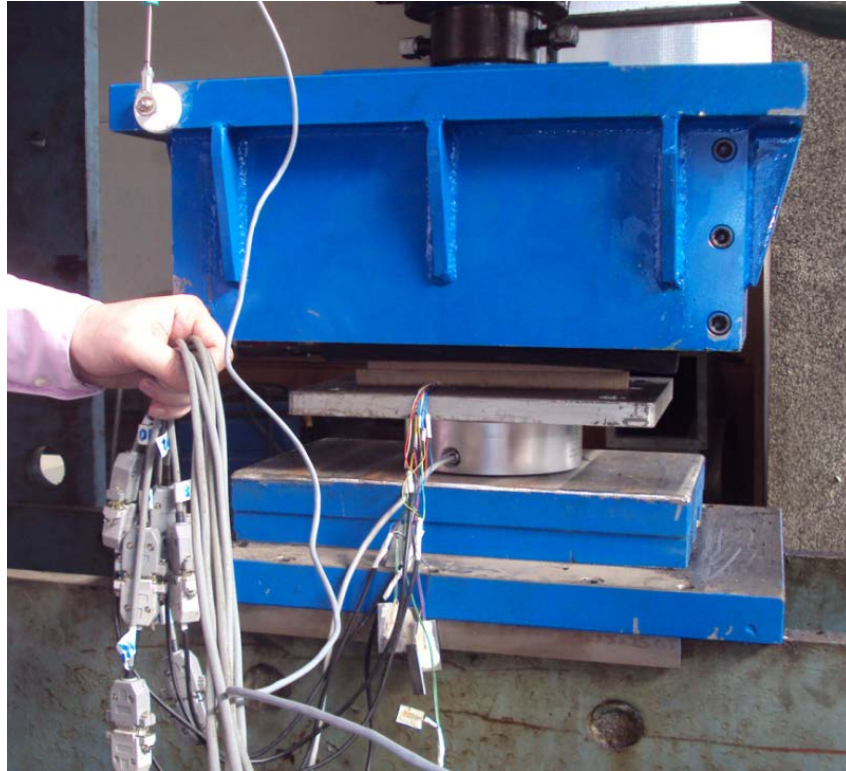


Figure8. 6 Cables and connectors used to transmit measured values to the acquisition system

Before performing the experiments, several actions should have been taken. Firstly, dies had to be produced. In previous chapters, description of machining operations necessary for one rib tool manufacturing was given. All machining steps required to define the shape of the tool for the rib with lightening hole (facing, prismatic machining, profile contour roughing, profile contour finishing, pocketing, isoperimetric machining and drilling) were simulated in CATIA and then appropriate G-code was generated. File with G-code was main input file for MACH3 software (Figure8.8) which controls CNC machine EMAX (Figure 9) used for wooden tools manufacturing.



Figure8. 7:Spider8 acquisition system

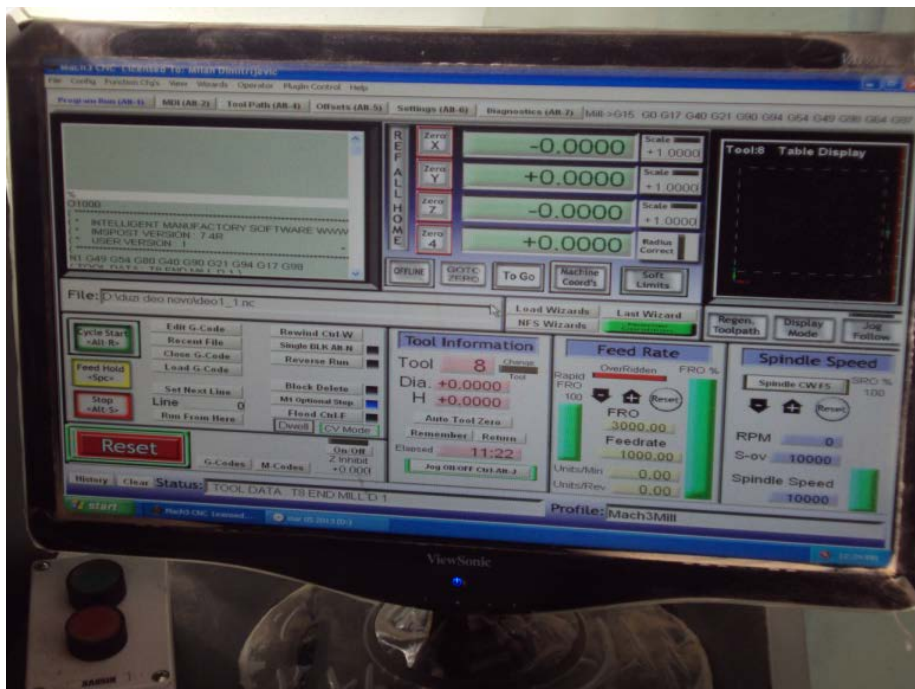


Figure8. 8: Screenshot of MACH3 software windows



Figure8. 9: CNC machine used for wooden tools manufacturing

Figure8.10 shows machining operations performed on CNC machine EMAX during rib tool manufacturing. All eight operations were identical to those simulated in CATIA and dimensions of produced wooden tool were within required tolerances, confirming that process of transforming virtual tool for the rib with lightening hole into real one was performed well. Wooden tools for other ribs used in experiments have been made in similar way and can be seen in Figure 11.

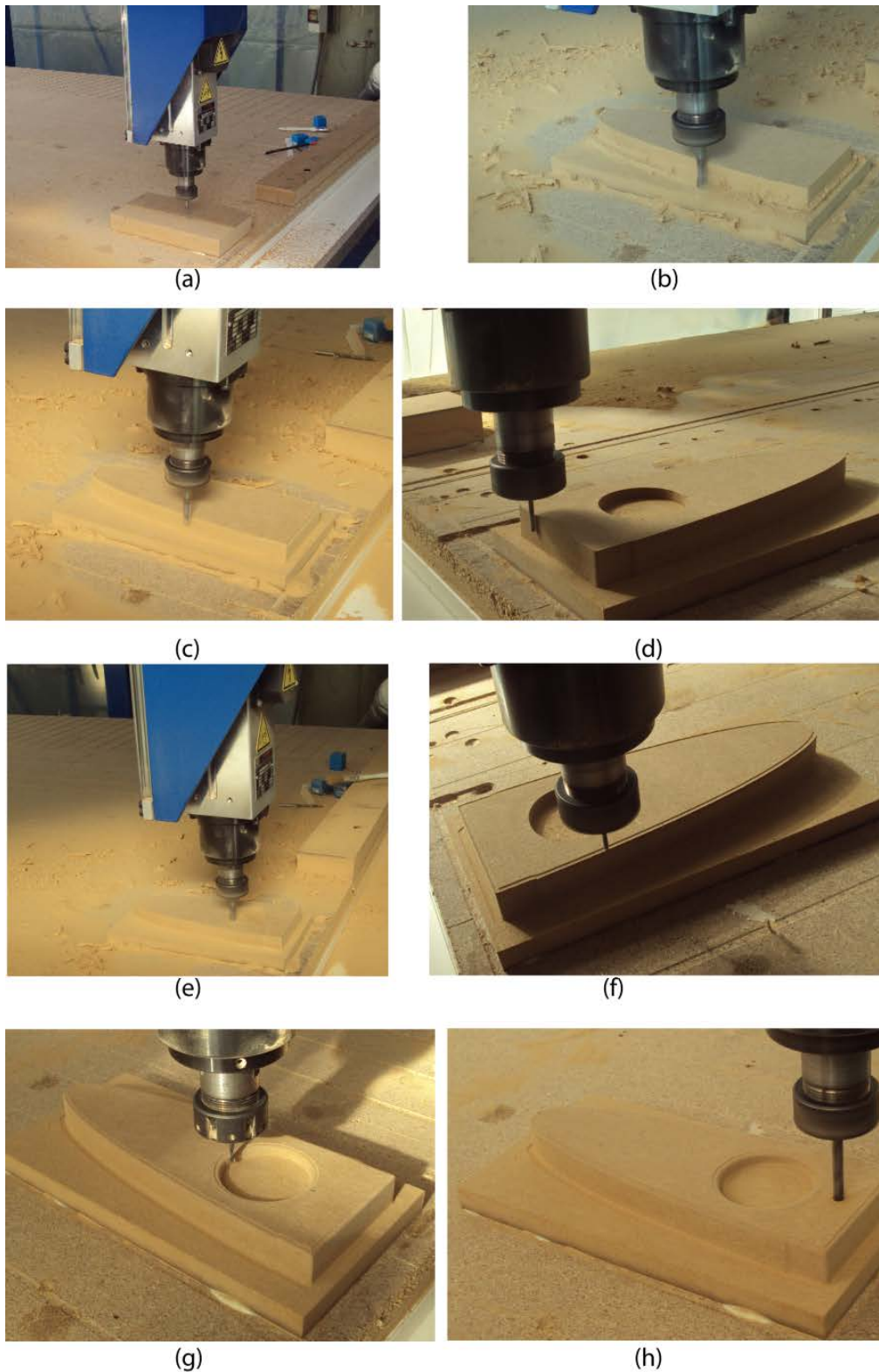


Figure 8.10: Machining operations used in rib tool manufacturing: (a) Facing, (b) Prismatic roughing, (c) Profile contouring roughing, (d) Profile contouring finishing, (e) Pocketing, (f) Isoperimetric marching, (g) Isoperimetric marching, (h) Drilling

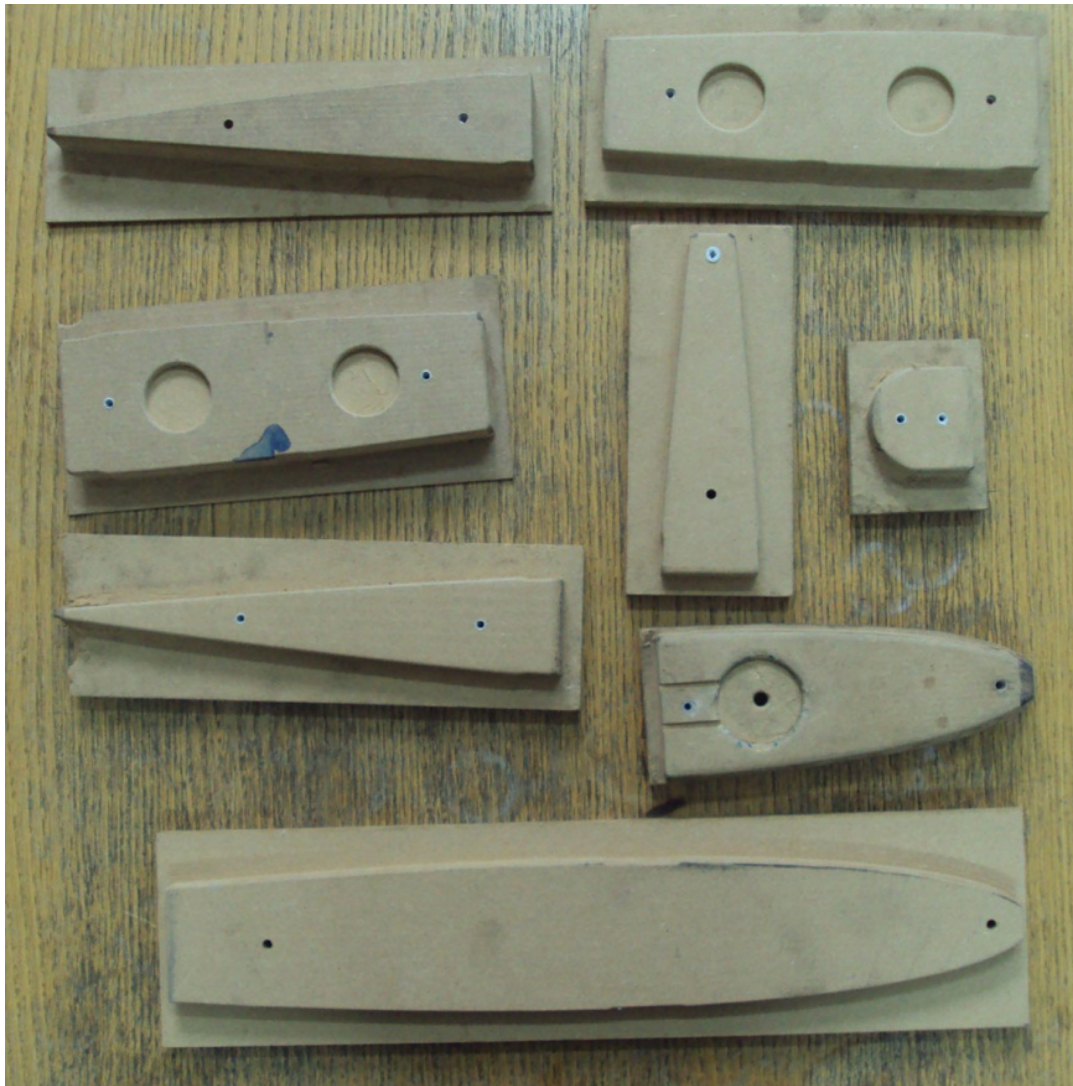


Figure8. 11: Wooden tools for ribs of horizontal tail

Secondly, aluminum blanks had to be cut. After unfolding the designed ribs in CATIA, they had to be organized and prepared in appropriate way for cutting, i.e. they had to be put on single piece of sheet metal in a fashion which would minimize the waste of material (Figure8.12). Again, G-code was generated, but another type of NC machine (FlexiCam) was used for blanks cutting (Figure8.13). Obtained aluminum blanks are shown in Figure8.14, while Figure8.15 shows blanks fixed in tools and prepared for experiments. For fixing

the blanks in the tools sheet metal screws were used because they are excellent fasteners for attaching metal hardware to wood. The fully threaded shank provides good retention in wood and eliminates any motion of the blank with respect to tool during rubber pad forming process.

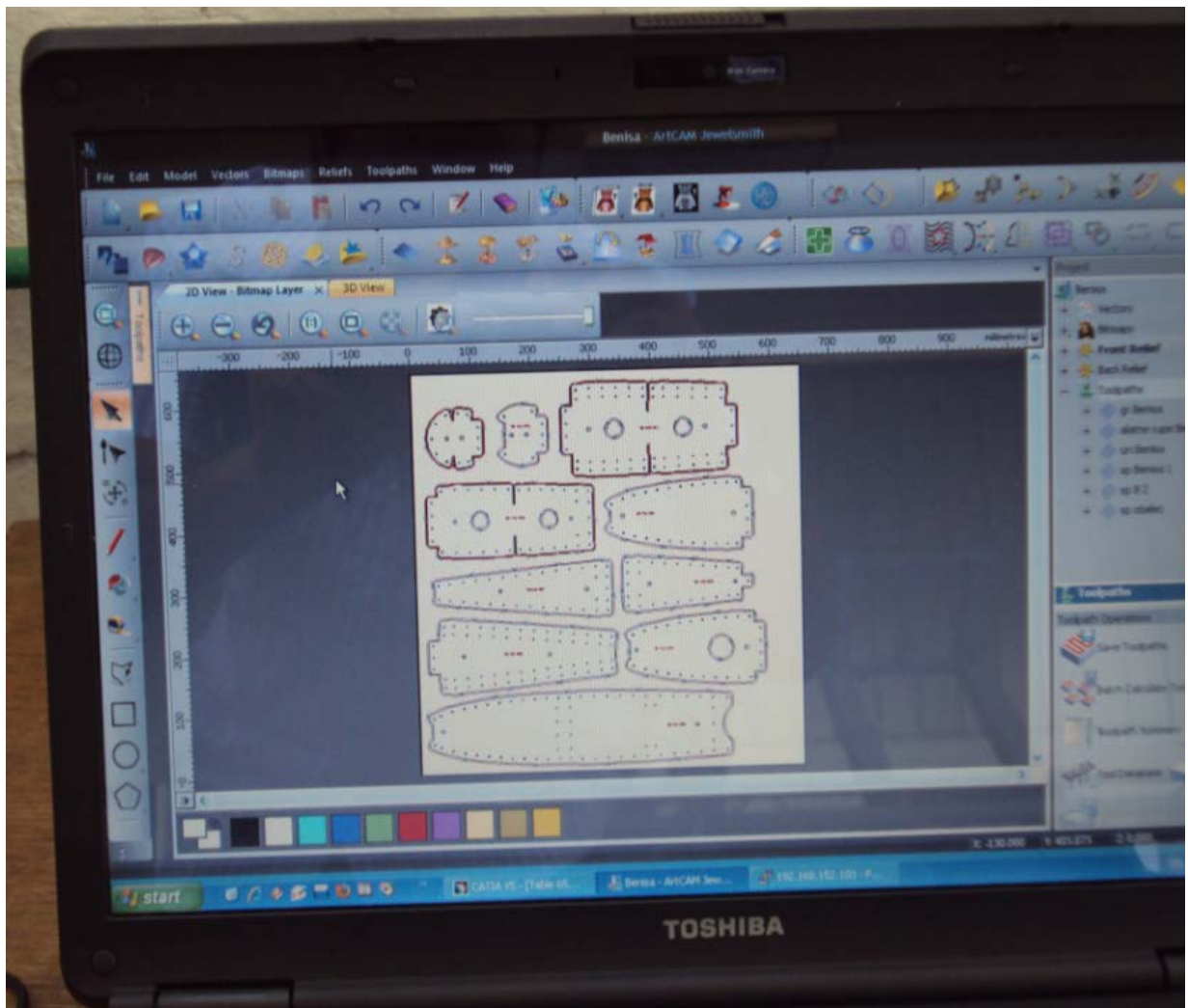


Figure8. 12:Unfolded ribs (blanks) prepared for cutting

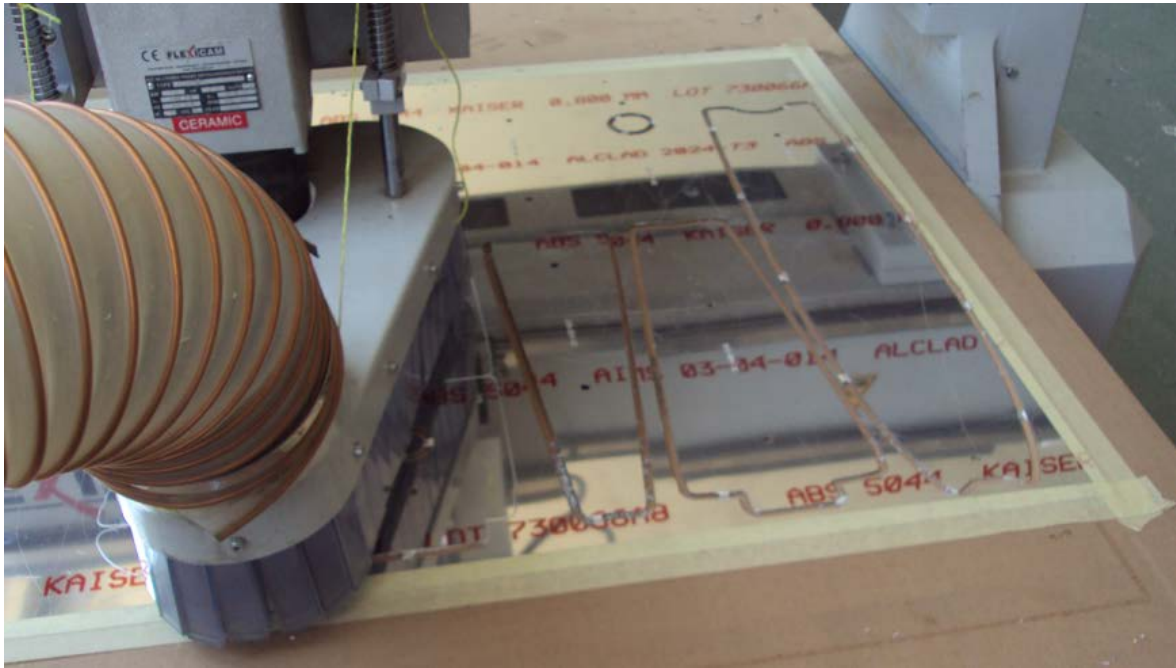


Figure8. 13: Cutting the blanks on FlexiCam machine

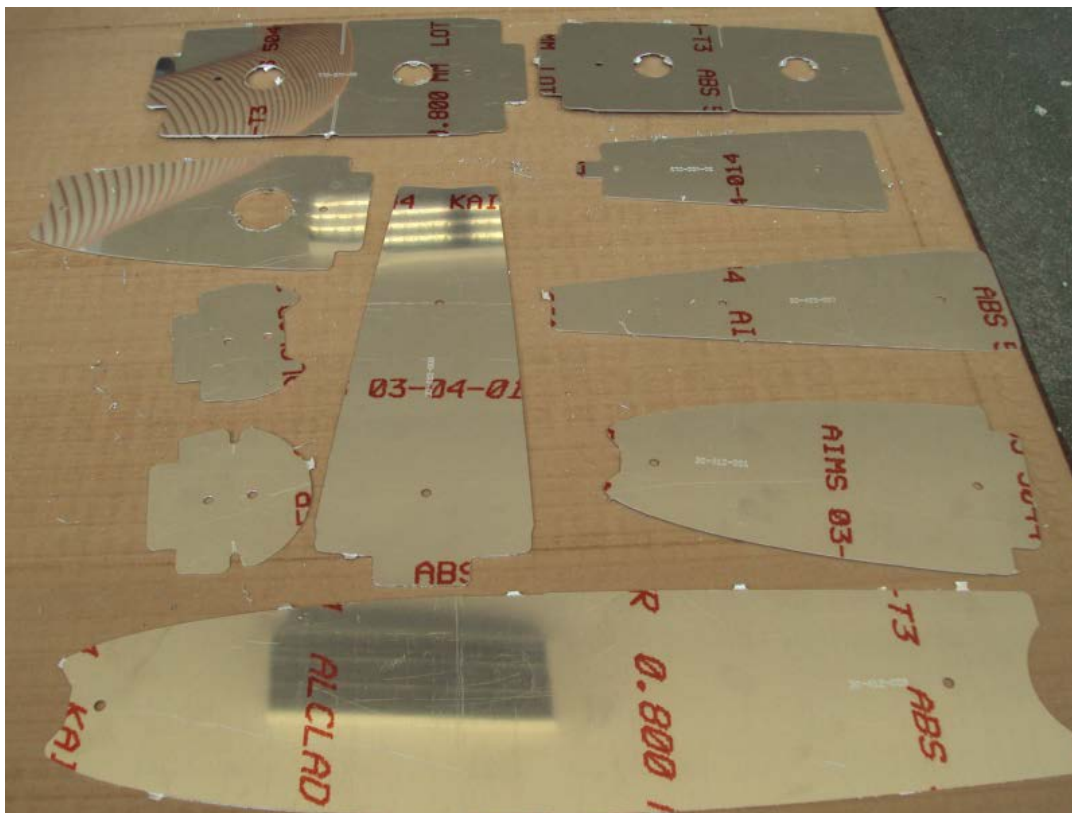


Figure8. 14: Blanks made of aluminum 2024-T3 used in experiments



Figure8. 15: Blanks fixed in tools for experiments

After all necessary tools and blanks had been prepared for investigation, experimental procedures have started. As mentioned above, one of the main aims of experiments was to verify results obtained in FEM simulations and to compare 3D shapes of ribs formed in Ansys (using nonlinear properties of aluminum) against shapes obtained in rubber pad forming. Other important aim of experiments (and numerical simulations, too) was improvement of the shape of dies in order to eliminate (or reduce) unwanted phenomena such as wrinkling, springback and crack initiation due to high values of plastic strain.

In previous chapters, where results of 2D and 3D numerical simulations were presented, we saw that FEA predicted wrinkling initiation and springback in almost all ribs and crack initiation in a few. Figure8.16 shows the shapes of eight different ribs of light aircraft tail formed in experiments with rubber pad on experimental set-up shown in Figures 1 and 2. As it can be seen, side-wall

wrinkling appeared on seven ribs, as predicted by 3D FEA performed in Ansys. On the other hand, springback appeared in all cases (two of them are shown in Figure 17).



Figure8. 16: Shapes of ribs formed by rubber pad on experimental set-up



Figure8. 17: Springback in two ribs formed by rubber pad

Comparing geometries of ribs obtained in simulations against geometries of ribs obtained in experiments, it was immediately noticeable that virtual and real springbacks were very similar. For example, Figure 18(a) shows springback on rib's wall obtained in experiment with rubber pad, while Figure 18(b) shows springback obtained in 3D simulation of rubber pad forming on rib with exactly the same geometry as rib formed in experiment. Difference between real and virtual springback angle was less than 10%. On other ribs these differences were both higher and lower than 10%, indicating that in each particular FEA of springback special attention must be paid to mesh quality and boundary conditions.

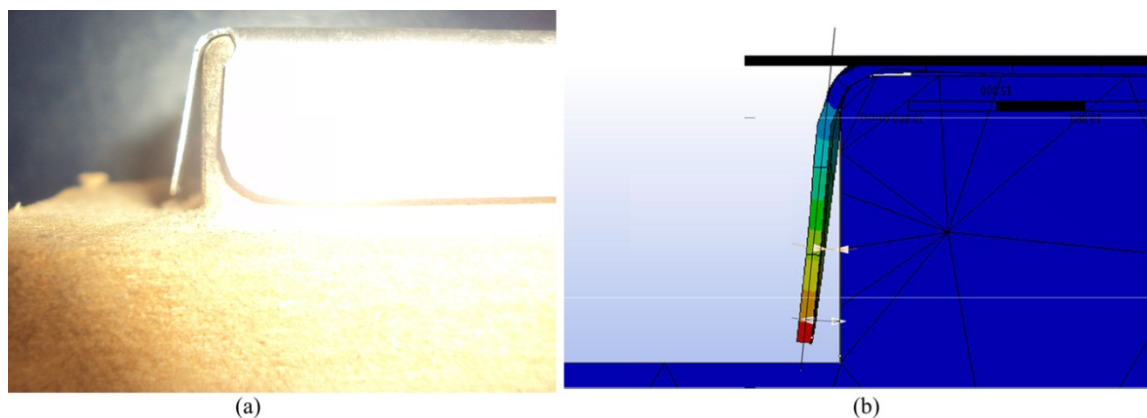


Figure8. 18: Springback obtained in (a) experiment and (b) FEM simulation

In a case of rib with lightening hole, formed on the wooden tool showed in Figure8.10, the value of springback angle was  $2.4^\circ$ , while FEA in Ansys predicted the appearance of springback angle equal to  $2^\circ$ . Percentage difference between predicted and actual value was 20%, but absolute value of difference was only  $0.4^\circ$  which was quite satisfactory. On the other hand, 2D simulations of rubber pad forming on tool for this rib predicted the crack initiation in the area with radius  $R_{II}=2\text{mm}$ , because the value of plastic strain obtained in this area was greater than  $0.186 \text{ mm/mm}$  (see previous chapter). The experiment with rib with lightening hole forming confirmed this prediction, because the small crack actually appeared in this area, which can be seen in Figures8.19 and8.20.



Figure8. 19: Small crack initiated in area with outer radius  $R_{II}$

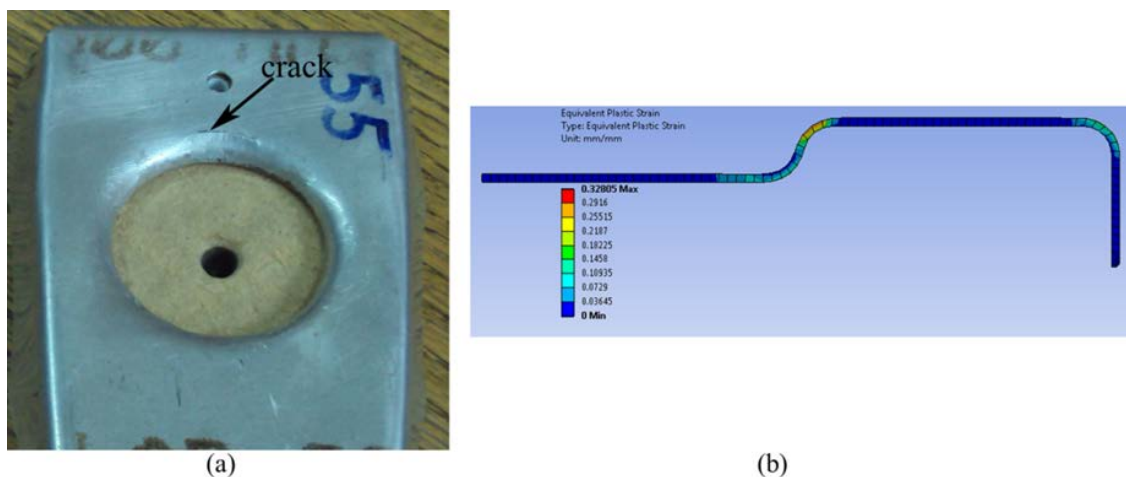


Figure 8. 20: The crack appeared in the area of radius  $R_{II}$  (a) Experimental, (b) as predicted by FE calculations

Based on experimental findings and FE calculations performed with other values of radius  $R_{II}$ , it was decided to make some corrections on the tool for rib with lightening hole. FE calculations led us to conclusion that the plastic strain was less than 0.186 mm/mm when  $R_I$  was greater than 2 mm and  $R_{II}$  was greater than 2.5mm, while springback would be significantly reduced if draft angle in the tool is at least  $2^\circ$ . Experiment showed that this angle was higher than  $2^\circ$ , so decision was made to increase this angle to  $3^\circ$  and, at the same time, to increase radius  $R_{II}$  to 4mm.

New tool with modified dimensions was made, but this time steel was used as a die material. Reason for that was very simple. This PhD thesis was part of the project of new light aircraft development and all researches have been done for the purpose of getting the best possible product and efficient design technologies. All tools for aircraft manufacturing must be made of steel and because all necessary studies have been done for rib with lightening hole, it was decided to make final tool which would be used in production. Figure 8.21 shows new steel tool, while Figure 8.22 shows the rib with lightening hole formed on this tool after the wrinkling on the flange was manually removed. Amount of springback on new tool was insignificant which confirmed all previously mentioned findings. Figure 8.23 shows other manufactured

horizontal tail ribs formed on steel tools where corrections for draft angles were also made. After rubber pad forming, the wrinkling of sheet metal material (generally in the ribs' flanges) was manually removed on the tool shown in Figure 8.24.



Figure 8. 21: New steel tool for rib with lightening hole



Figure 8. 22: Rib with lightening hole formed on steel tool



Figure8. 23: Several horizontal tail ribs manufactured on steel tools



Figure8. 24: Elimination of wrinkles on rib's flange

Figures from 8.25 to 8.28 illustrate other important aspects of successful 3D FEM simulations. As mentioned above, one of the primary defects that occurs in rubber pad forming operations is the wrinkling. The flange of the blank undergoes radial stress and tangential compressive stress during the forming process, which very often results in wrinkles (see Figure 8.16). In 2D FE analysis appearance of wrinkles cannot be detected, but in 3D environment this defect can be simulated efficiently. Wrinkling of ribs' flanges was simulated using two different Ansys modules: static-explicit and dynamic-explicit (LS-DYNA). It was found that several parameters could affect results of wrinkling simulation and the most important were the initial shape of the finite element mesh and definition of friction phenomena between the blank, punch and die.

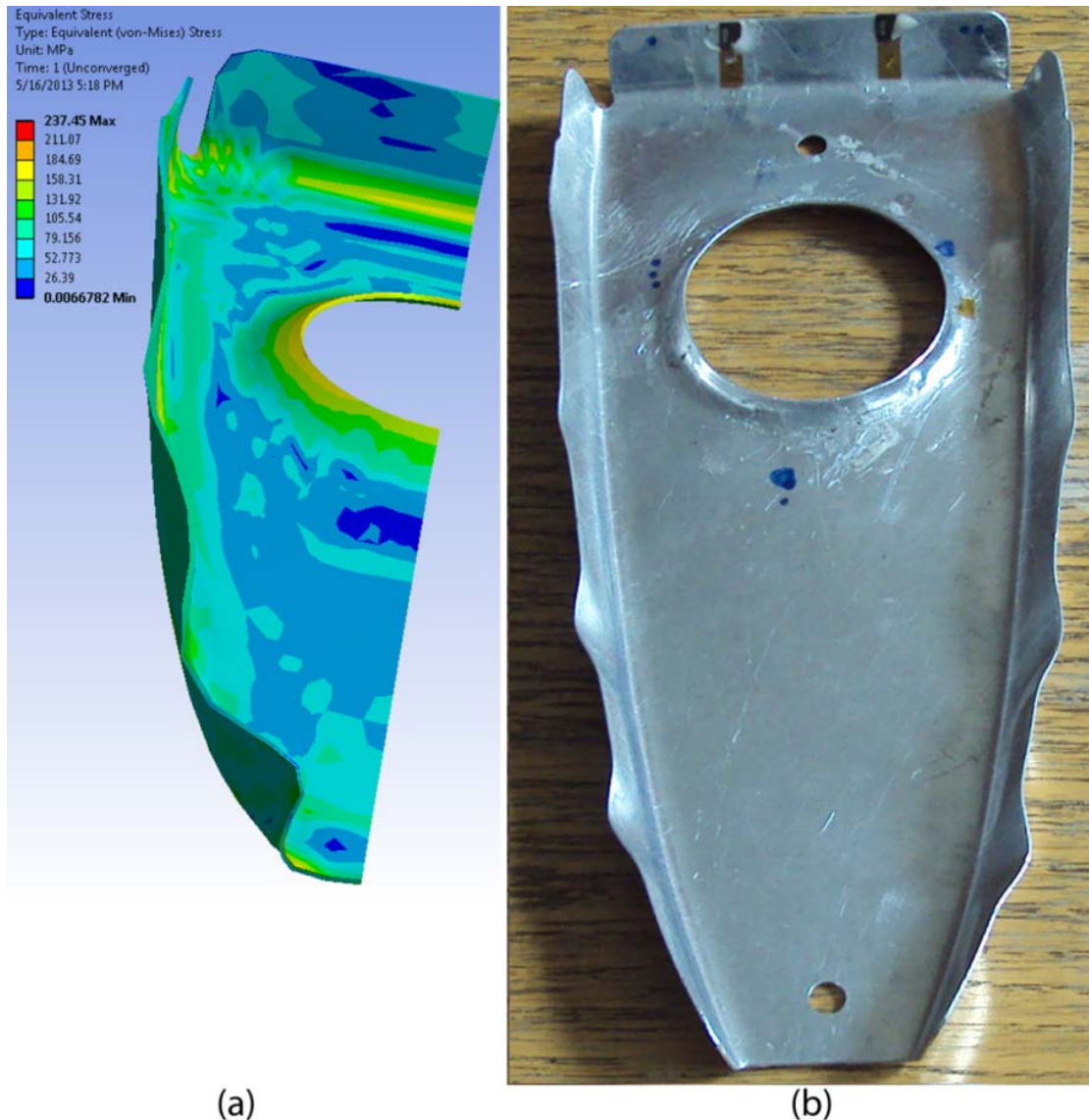


Figure 8.25: Comparison of the wrinkles obtained on rib with lightening hole in (a) FEM simulation and (b) experiment with rubber pad forming process

3D FE simulations of four different ribs forming showed that several wrinkles might be expected on long side walls of the ribs, which was confirmed in experiments. Both simulation and real forming process showed the wrinkling appearance in curved (surfacing) flanges, and the number of “waves” on curved flanges in simulations and real stamping was the same in all ribs. Also, positions of wrinkles on virtual and real ribs were almost identical (Figures 8.25 and 8.26). On the other hand, FE simulations didn’t predict the wrinkling on straight flanges of ribs and wrinkles actually didn’t appear on these parts in

experiment. To conclude, good matching of wrinkling phenomena in the simulations and real rubber pad forming process has definitely justified the use of FEM in predicting this type of defect.

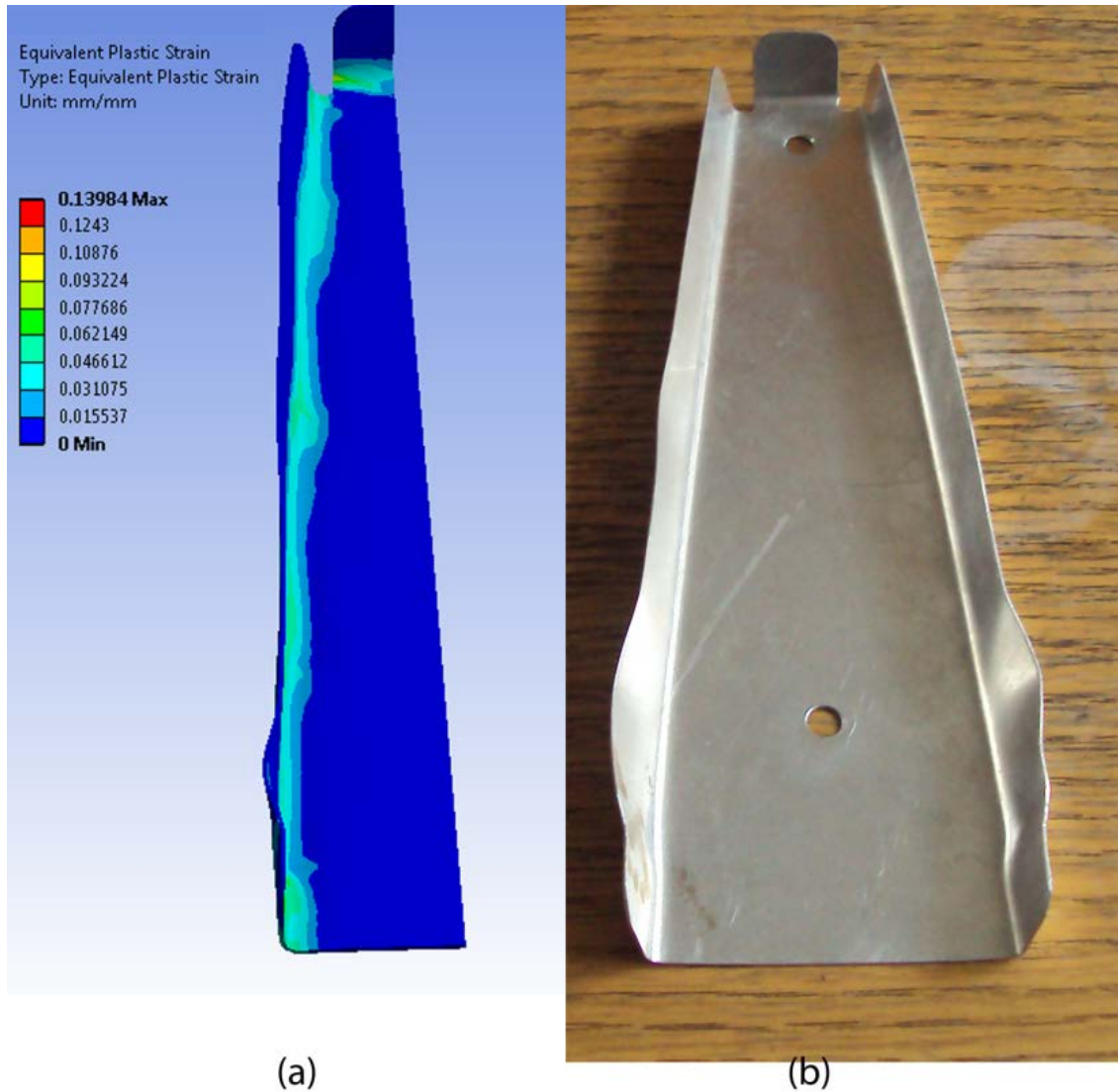
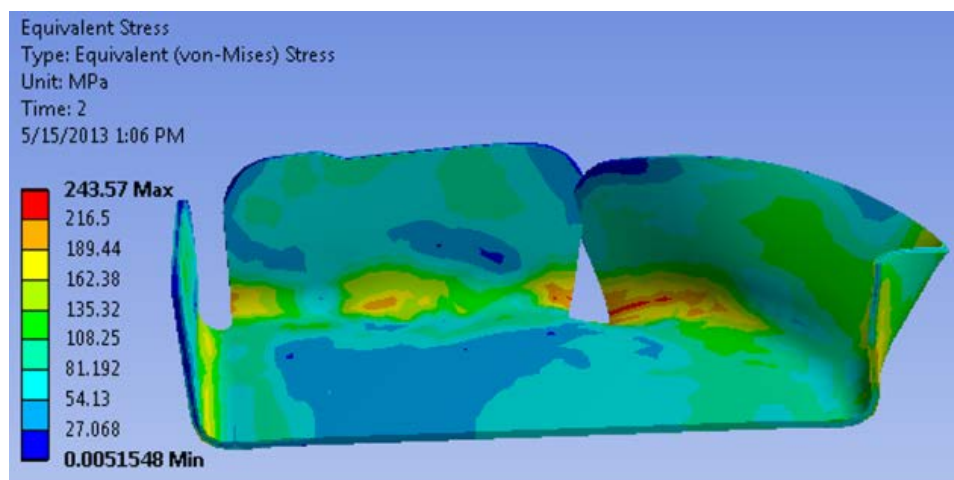


Figure 8.26 Comparison of the wrinkles obtained on straight rib in (a) FEM simulation and (b) experiment with rubber pad forming process

To reduce the probability of wrinkling, the design of the punch, die and blank must be optimized. Choosing a flange radius that is large enough and designing the blank geometry to minimize excess material can eliminate wrinkles, as explained in previous chapter. The sheet metal blank has an inherent grain structure, so the stresses can vary depending on the design of the

die and the orientation of the grain which may produce the wrinkling, too. But, investigation of grain structure influence wasn't the aim of this doctoral thesis.

Improving the shape of the part can also help and all improvements and changes may be tested with FEM first. Figure 4.5 in previous chapter showed bad design of one horizontal tail rib which experienced overlapping and high amount of wrinkling in curved flange during rubber pad forming simulation. The same defects appeared in experiment with wooden tool, as can be seen in Figure8.27.



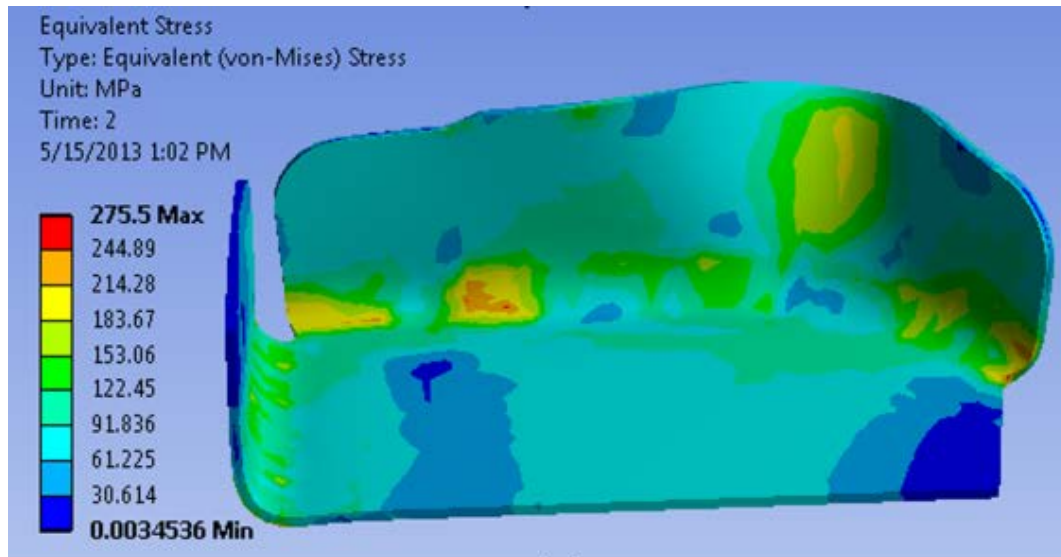
(a)



(b)

Figure8. 27: Material overlapping on rib in (a) FEM simulation and (b) experiment with rubber pad forming process. Some amount of springback is also noticeable.

This rib was redesigned and simulations with new shape of the blank were performed, showing acceptable wrinkling on surfacic flanges. Experiment with wooden tool confirmed this prediction, and as can be seen in Figure 28 wrinkle on surfacic flange appeared in the area suggested by FEA. Rib's straight wall didn't experience this defect in both virtual and real forming. This wrinkling was corrected by operator showing that rib with this amount of wrinkle can be used in aircraft tail assembly. At the same time, springbacks appeared in experiments (Figures 8.27 and 8.28) which were later eliminated by applying appropriate drift angle on steels tools.



(a)



(b)

Figure8. 28 Acceptable wrinkling on redesigned rib obtained in (a) FEM simulation and (b) experiment with rubber pad forming process. Some amount of springback is also noticeable

## 9. Conclusions and Recommendations:

### 9.1 Conclusions:

The theoretical modeling and experimental investigations of rubber pad forming process have been presented in the previous chapters. After considering all the facts listed throughout the thesis, the following conclusions may be drawn:

- Forming operations can be successfully optimized using the finite element simulation (FES) of the rubber-pad forming process. The most obvious benefit of utilizing FES is possibility of obtaining important data for determination of necessary parameters and operation times. The final shape of a manufactured product and possible defects (such as cracks) can be accurately predicted using appropriate FE models and method proposed in this thesis.
- The FE simulations demonstrated fact that locations of the higher-level stresses and strains were at the flanges and corners of ribs. On the other hand, the minimum stress and plastic strain were achieved in the straight rib (the rib with the simplest geometry), while the maximum stress and plastic strain appeared in the rib with the lightening hole (the most complex geometry).
- These results were confirmed in experiments, as well as the fracture criterion used for crack predictions. From conducted rubber pad experiments, it can therefore be ascertained that FE simulations are a satisfactorily accurate method of prediction. The FE simulations proved that the simpler tools would reduce lead times and would enable quicker production of small parts, while eradicating the chance of crack appearances during forming. For example, the FE simulation foresaw a crack that later appeared in the vicinity of the rib hole during the third stage of the forming process. This early detection of the crack can prompt a redesign

early in the process to remove further opportunity for defects to arise. However, more care must be taken when dealing with the geometry of more complicated tools, especially when determining the fillets' radii which minimizes the chance of fracture. FEM can facilitate radii determination, while opening the door to additional potential applications such as 3D model simulations and tool optimization. However, it must be noted that the optimization procedure of the press-forming processes should never be limited to simple numerical simulations. This is due to the presence of rarely reproducible phenomena like friction and lubrication. Rather, the latter phenomena could contribute to saving costs and reducing time-to-market, which at present is still delayed by empirical trial-and-error processes.

Considering the analysis of the fillet radius influence, two different cases were subsequently analyzed (shown in Chapter 7) and the following conclusions have been drawn:

- A high application of stress is placed on the  $R_I$  and  $R_{II}$  areas. The values of  $R_I$  and  $R_{II}$  (Figure 7.8) should be greater or equal to 2 mm in order to avoid the unnecessary stress concentration in those regions. However, the plastic strain will not reach an unacceptable value.
- To avoid the thinning phenomenon and to make an easy forming with complete rib tool cavity filling, the value of  $H$  should be less than  $R_{II}$  and the value of  $R_{III}$  should be greater than or equal to  $R_{II}$ .

An analysis of the springback and wrinkling phenomena were also conducted using 2D and 3D FEM simulations and results were compared with the experimental findings. Performed simulations proved to be a very valuable means of understanding and avoiding these phenomena during the forming operations. Developed FE models of the rubber pad forming process provided

an opportunity to alter and modify the final shape of the rib's tool for the purpose of minimizing defects that can appear during the forming process. Findings can be summarized as follows:

- The springback factor increases as the bend radius of straight rib increases.
- The correction angle of springback in a straight rib is  $2[^\circ]$  to get an approximate right angle. In the tests, however, the value of the springback angle was precisely  $2.40^\circ$  on the rib with a lightening hole that was formed on a wooden tool. There is disparity between the simulated and real angle value, but it is not excessive. While the FEA in ANSYS made a prediction of  $2^\circ$  (a deviation of 20% to the real value obtained from experimentation), the absolute value of the difference is still only  $0.40^\circ$ . Such a minor absolute value of difference is very acceptable.
- The 2D simulations predicted different type of results. When using a rubber pad forming on the tool for rib with a lightening hole, the simulations predicted a crack initiation in the area with radius  $R_{II}=2\text{mm}$ , because the value of plastic strain obtained in this area was greater than  $0.186 \text{ mm/mm}$ . The prediction was confirmed in the experiment with the rib with a lightening hole and during forming a small crack actually appeared in this area.
- The springback factor also increases as the  $R_I$  increases in the rib with a lightening hole, whereas there is no amount of springback when the value of this radius is equal to  $1\text{mm}$  and  $1.5 \text{ mm}$ . It means that these values are of great importance, and further indicative that the crack in  $R_I$  region can be expected.
- As the  $R_{II}$  increases in the rib with a lightening hole, the springback factor decreases; this is evidence that the rib's lightening hole works as stiffener. The value of  $R_{II}$  should be greater than  $1 \text{ mm}$  to

avoid critical value and therefore eliminate the possibility of crack appearance in the  $R_{II}$  region. Following various findings and FE calculations with other values of  $R_{II}$ , decision was made about changing the tool for this particular rib with a lightening hole. The FE simulations that ensued provided some parameters for the redesign. Firstly, they led to the conclusion that plastic strain was in an acceptable range when  $R_I$  was greater than 2 mm and  $R_{II}$  was greater than 2.5mm. Secondly, springback could be significantly reduced if the draft angle in the tool is at least  $2^\circ$ . However, experiments proved that this angle was, in fact, greater than  $2^\circ$ . Therefore, the resolution was to increase this angle to  $3^\circ$  and simultaneously increase the radius of  $R_{II}$  to 4mm.

- The wrinkling phenomena occurred in the 3D FEM in the surfacic flange. The amount of wrinkling increases as the curvature radius decreases, while straight flange regions had no detection of wrinkling in any 3D model. Both the simulation and real forming process had wrinkles on the curved (surfacic) flanges. Additionally, the amount of waves on the curved flanges was the same for the simulation and the real experiment for all ribs. Not only was the amount of waves coincidental, the actual position of the wrinkles on the real ribs matched those predicted by the simulation program. As for the absence of wrinkling in certain parts, the FE simulations did not predict the wrinkling on straight flanges of ribs and no wrinkles actually appeared on these parts during the experiment.

To conclude, comparisons of the wrinkling phenomena obtained in rubber pad forming simulations and those obtained in experiments, confirmed that FEM is a reliable detector of this particular type of defect.

In some cases it is useless to make corrections on the rib after production. Instead, to lessen the amount of wrinkling, it is easier to redesign the blank shape in the early design phase. With that in mind, the functionality of the product in its purpose after redesigning the blank piece must be retained. To conclude, the use of FEM in these circumstances can be considered reliable and accurate. The program proved it could estimate locations and levels of wrinkling when using the rubber pad in the forming process. Subsequent testing demonstrated the accuracy of FEM and proved its effectiveness for further trials.

## **9.2 Recommendations**

More simulations can be explored to optimize the process and results of rubber stamp experimentation. For example, further FEM simulation using rubber with varying thickness and hardness, as well as using multiple layers of rubber with different resistances in each (with progressive increases in hardness or softness). The question of how the rubber layer (hard or soft) which contacts the blank surface in the forming process effects the forming process and final shape of the product can also be answered. These parameters and their influence on the final shape can be investigated. FEM could be a useful means of reducing or eliminating defects that can appear on the final product.

In order to verify the theoretical results, further experimental work should be undertaken by measuring the stress, strain and reaction force and displacement during the forming process. Some of these results have been already obtained and will be used in further work.

### List of references:

- [1] ASM HANDBOOK VOL.14B METAL WORKING: SHEET FORMING, (2006)
- [2] THIRUVARUDCHELVAN, S., THE POTENTIAL ROLE OF FLEXIBLE TOOLS IN METAL FORMING, JOURNAL OF MATERIALS PROCESSING TECHNOLOGY 39 (1993), 55-82
- [3] SALA, G., A NUMERICAL AND EXPERIMENTAL APPROACH TO OPTIMIZE SHEET STAMPING TECHNOLOGIES: PART II - ALUMINUM ALLOYS RUBBER-FORMING MATERIAL AND DESIGN, 22 (4), (2001), 299-315.
- [4] BROWNE, D.J. AND BATTIKHA, E., OPTIMIZATION OF ALUMINIUM SHEET FORMING USING A FLEXIBLE DIE, JOURNAL OF MATERIALS PROCESSING TECHNOLOGY 55 (3-4) (1995),18-223
- [5] THIRUVARUDCHELVAN, S. (2002A) THE POTENTIAL ROLE OF FLEXIBLE TOOLS IN METAL FORMING. JOURNAL OF MATERIALS PROCESSING TECHNOLOGY 122 (2-3), PP. 293-300.
- [6] THIRUVARUDCHELVAN (2005) RECENT DEVELOPMENTS IN FRICTION-ASSISTED SHEET METAL FORMING PROCESSES. JOURNAL OF MATERIALS PROCESSING TECHNOLOGY 167 (2-3), PP. '161-166.
- [7] DIRIKOLU, M.H. AND AKDEMIR, E., COMPUTER AIDED MODELLING OF FLEXIBLE FORMING PROCESS, JOURNAL OF MATERIALS PROCESSING TECHNOLOGY, 148 (3) (2004), 376- 381
- [8] LINFAPENG, PENGHU,HINMIN LAI, DEQING, JUN NI, INVESTIGATION OF MICRO/MESO SHEET SOFT STAMPING PROCESS-SIMULATION AND EXPERIMENTS, MATERIAL AND DESIGN 30(2009)783-790
- [9] YANXIONG LIU AND LIN HUA, FABRICATION OF METALLIC BIPOLAR PLATE FOR PROTON EXCHANGE MEMBRANE FUEL CELLS BY RUBBER PAD FORMING, JOURNAL OF POWER SOURCE 195(2010)3529-3535
- [10] ANTONIO DEL PRETE, GABRIELE PANADIA AND BARBAREMANISI,COMPUTER AIDED MODELLING OF RUBBER FORMING PROCESS, KEY ENGINEERING MATERIAL VOL.473(2011) PP 637-644

- [11] M.W Fu,, H Li , J, LU, AND S. Q, LU., NUMERICAL STUDY ON THE DEFORMATION BEHAVIORS OF THE FLEXIBLE DIE FORMING BY USING VISCOPLASTIC PRESSURE-CARRYING MEDIUM , COMPUTATIONAL MATERIALS SCIENCE 46 (4): 1058-1068 (2009).
- [12] M. RAMEZANI, Z.M. RIPIN, R. AHMAD, SHEET METAL FORMING WITH THE AID FLEXIBLE PUNCH, NUMERICAL APPROACH AND EXPERIMENTAL VALIDATION ,CIRP OF JOURNAL OF MANUFACTURING SCIENCE AND TECHNOL.3(2010)196-203
- [13] FABRIZIO QUADRINI, LOREDANA SANTO .ERICA ANNA SQUEO, FLEXIBLE FORMING OF THIN ALUMINUM ALLOY SHEETS,ISSN2067-3604,VOL. II, No.1/2010
- [14] MAZIAR RAMEZANI, ZAIDI MODI RIPIN, ROSLAN AHMAD, COMPUTER AIDED MODELING OF FRICTION IN RUBBER -PAD FORMING PROCESS. JOURNAL OF MATERIAL PROCESSING TECHNOLOGY 209(2009) 4925-4934.
- [15] J. W. LEE , H.C. KWON . M.H. RHEE .Y.T.IM, DETERMINATION OF FORMING LIMIT OF A STRUCTURAL ALUMINUM TUBE IN RUBBER PAD BENDING. MATER.PROCESS. ECHNOL. 140 (2003) 487-493
- [16] MADOLIAT, R., NARIMANI, R. AND RAHROVAN, H., INVESTIGATION OF SHEET METAL FORMING USING RUBBER PAD FORMING, THE SMEIR 2005 INTERNATIONAL CONFERENCE IN MANUFACTURING ENGINEERING: 1-9, (2005).
- [17] YANXIONGLIU ,LINHUA , JIAN , XI WEI J., STUDIES OF THE DEFORMATION STYLES OF THE RUBBER-PAD FORMING PROCESS USED FOR MANUFACTURING METALLIC BIPOLAR PLATES, JOURNAL OF POWER SOURCES195 (2010)8177-8184
- [18] KWON H.C., IM, Y.T., AND RHEE D.C. Ji M.H.. THE BENDING OF AN ALUMINUM STRUCTURAL FRAME WITH A RUBBER PAD, JOURNAL OF MATERIALS PROCESSING TECHNOLOGY 113 (1-3) (2001), 786-791
- [19] MAZIAR RAMEZANI AND ZAIDI MOHD RIPIN,RUBBER PAD FORMING PROCESS,TECHNOLOGY AND APPLICATION, FIRST PUBLISHED 2012, WOOD PUBLISHING LIMITED ISBN 978-0-85709-2.

## References

- [20] S.J. HU, Z. MARCINIAK AND J.L. DUNCAN ,MECHANICS OF SHEET METAL FORMING, SECOND EDITION PUBLISHED BY BUTTERWORTH-HEINEMANN 2002, ISBN 0 75065300 0
- [21] SHEET METAL PROCESSES,CONSTITUTIVE MODLING AND NUMERICAL SIMULATION BANABIC, D. 2010,XV,350P.,HAREDCOVER ISBN 978-3-540-88112-4
- [22] DELADI, E.L., STATIC FRICTION RUBBER METAL CONTACT WITH APPLICATION TO RUBBER PAD FORMING PROCESS, PHD THESIS, UNIVERSITY OF TWENTE, (2006)
- [23]-METAL FABRICATION TECHNOLOGY, SYAMAL MUKHERJEE, ISBN-978-81-203-4090-9, PUBLISHED BY ASOKE K. GHOSH, PHI LEARING PRIVATE LIMITED ,M-97, CONNAUGHT CIRCUS, NEW DELHI-110001 AND PRINTED BY MUDRAK,30-A PATPARGANJ, DELHI-110091
- [24]MANUFACTURING PROPERTIES OF ENGINEERING MATERIALS LECTURE NOTES PROF.DR.AHMET ARAN 2007
- [25]: Z.J. WANG, J.G. LIU, X.Y. WANG, Z.Y. HU, B. GUO VISCOUS PRESSURE FORMING (VPF): STATE-OF-THE-ART AND FUTURE TRENDS. JOURNAL OF MATERIALS PROCESSING TECHNOLOGY 151 (2004) 80-87
- [26] ABMETOGLU, M., ALTAN, T. (2000) TUBE HYDROFORMING: STATE-OF-THE-ART AND FUTURE TRENDS. JOURNAL OF MATERIALS PROCESSING TECHNOLOGY 98 ( 1), PP. 25-33
- [27] KANG, B.H., LEE, M.Y., SHON, S.M., MOON, Y.H.(2007) FORMING VARIOUS SHAPES OF TUBULAR BELLOWS USING A SINGLE-STEP HYDROFORMING PROCESS. JOURNAL OF MATERIALS PROCESSING TECHNOLOGY 93 (1-3), PP.1- 6.
- [28] S.W. LEE, STUDY ON THE FORMING PARAMETERS OF THE METAL BELLOWS]JOURNAL OF MATERIALS PROCESSING TECHNOLOGY 130-131 (2002) 47-53
- [29] MERKLEIU, M., GEIGER, M., CELEGHIUI, M. (2005) COMBINED TUBE AND DOUBLE SHEET HYDROFORMING FOR THE MANUFACTURING OF COMPLEX PARTS. CIRP ANNALS - MANUFACTURING TECHNOLOGY 54 ( L), PP. 199-204.

## References

- [30] LIU, Y., WU, X. (2007) A MICROSTRUCTURE STUDY ON AN AZ31 MAGNESIUM ALLOY TUBE AFTER HOT METAL GAS FORMING PROCESS. JOURNAL OF MATERIALS ENGINEERING AND PERFORMANCE 16 (3), PP. 354-359.
- [31] HE ZHU-BIN, FAN XIAO-BO, SHAO FEI1,, ZHENG KAI-LUN, WANG ZHI-BIAO, YUAN SHI-JIAN FORMABILITY AND MICROSTRUCTURE OF AA6061 AL ALLOY TUBE FORHOT METAL GAS FORMING AT ELEVATED TEMPERATURE , TRANS. NONFERROUS MET. SOC. CHINA 22(2012) s364–s369
- [32] WANG, Z.J., WANG, X .Y., WANG, Z.R. (2004) VISCOUS PRESSURE FORMING (VPF) OF CORRUGATED THIN-WALLED SHEET PART WITH SMALL RADIUS. JOURNAL OF MATERIALS PROCESSING TECHNOLOGY 145 (3),PP. 345-35 L
- [33] AL-QURESHI, H.A. (2002), ANALYSIS OF SIMULTANEOUS SHEET METAL FORMING OPERATIONS USING ELASTOMER TECHNIQUE. JOURNAL OF MATERIALS PROCESSING TECHNOLOGY, 125- 126, PP. 751- 755.
- [34] OL.AZ, 1., RUBIO, L. (2003) DEVELOPMENTS TO MANUFACTURE STRUCTURAL AERONAUTICA PARTS IN CARBON FIBRE REINFORCED THERMOPLASTIC MATERIALS. JOURNAL OF MATERIALS PROCESSING TECHNOLOGY 143-144 (1), PP. 342-346.
- [35] ELLEN M. ARRUDA, MARY C. BOYCE .( 1993).A THREE-DIMENSIONAL CONSTITUTIVE MODEL FOR THE LARGE STRETCH BEHAVIOR OF RUBBER ELASTIC MATERIALS,JOURNAL OF THE MECHANICS AND PHYSICS OF SOLIDS, 41,( 2), , PP 389–412
- [36] MOONEY, M.(1940). A THEORY OF LARGE ELASTIC DEFORMATION, JOURNAL OF PPLIED PHYSICS, VOL. 11, PP.582-592
- [37] R. W. OGDEN (1986) RECENT ADVANCES IN THE PHENOMENOLOGICAL THEORY OF RUBBER ELASTICITY. RUBBER CHEMISTRY AND TECHNOLOGY: 1986, 59, (3), PP. 361-383.
- [38] L. R. G. TRELOAR (1975).THE PHYSICS OF RUBBER ELASTICITY, 3RD, CLARENDON PRESS, OXFORD.

## References

- [39] O. H. YEOH (1993) SOME FORMS OF THE STRAIN ENERGY FUNCTION FOR RUBBER. RUBBER CHEMISTRY AND TECHNOLOGY: NOVEMBER 1993, VOL. 66, NO. 5, PP. 754-771.
- [40] WANG, CHENG HUA AND BOURNE, DAVID A., "DESIGN AND MANUFACTURING OF SHEET METAL PARTS: USING FEATURES TO AID PROCESS PLANNING AND RESOLVE MANUFACTURABILITY PROBLEMS" (1997). ROBOTICS INSTITUTE. PAPER 96.
- [41] [HTTP://WWW.3DS.COM/PRODUCTS/CATIA](http://www.3ds.com/products/catia)
- [42] M. S. NIU, AIRFRAME STRUCTURAL DESIGN, CONMILIT PRESS LTD, HONG KONG, 1988.
- [43] [HTTP://WWW.AIRFOILTOOLS.COM/](http://www.airfoiltools.com/)
- [44] [HTTP://WWW.PDAS.COM/NACA456.HTML](http://www.pdas.com/naca456.html)
- [45] [HTTP://SEIT.UNSW.ADFA.EDU.AU/COURSEWORK/ZEIT4008/CATIA/DICKSON SHAM TUTORIALS/CATIA MOUSE.PDF](http://seit.unsw.adfa.edu.au/coursework/zeit4008/catia/dicksonsham_tutorials/catia_mouse.pdf)
- [46] M. TISZA, RECENT ACHIEVEMENTS IN COMPUTER AIDED PROCESS PLANNING AND NUMERICAL MODELLING OF SHEET METAL FORMING PROCESSES JOURNAL OF ACHIEVEMENTS IN MATERIALS AND MANUFACTURING ENGINEERING , 24 ,(1), 2007
- [47] MOAVENI SAEED, FINITE ELEMENT ANALYSIS: THEORY AND APPLICATION WITH ANSYS, 3RD EDITION, PEARSON PRENTICE HALL, 2008.
- [48] [HTTP://WWW.ANSYS.COM/](http://www.ansys.com/)
- [49] [HTTP://WWW.3DS.COM/PRODUCTS/SIMULIA/OVERVIEW/](http://www.3ds.com/products/simulia/overview/)
- [50] HUEI-HUANG LEE, FINITE ELEMENT SIMULATIONS WITH ANSYS WORKBENCH 12, SCHROFF DEVELOPMENT CORPORATION, 2010
- [51] HIROHIKO TAKUDA AND NATSUO HATTA, NUMERICAL ANALYSIS OF THE FORMABILITY OF ALUMINUM 2024 ALLOY SHEET AND ITS LAMINATES WITH STEEL SHEETS, METALLURGICAL AND MATERIAL TRANSACTION A , VOL 29A, NOVEMBER (1998), P2829-2834
- [52] JAYDEEP R. SHAH, S. K. SHARMA, B. C. PATEL, INVESTIGATING SPRINGBACK EFFECT IN U-DIE BENDING PROCESS BY VARYING DIFFERENT PARAMETERS,

- INSTITUTE OF TECHNOLOGY, NIRMA UNIVERSITY, AHMEDABAD,  
08-10 DECEMBER, 2011
- [53] VOLKAN ESAT, HALUK DARENDELILER, MUSTAFA ILHAN GOKLER, FINITE ELEMENT ANALYSIS OF SPRINGBACK IN BENDING OF ALUMINIUM SHEETS, MATERIALS AND DESIGN 23 (2002), PP. 223-229.
- [54] A.B. ABDULLAH, S.M. SAPUAN, Z. SAMAD AND N.A. AZIZ A COMPREHENSIVE REVIEW OF EXPERIMENTAL APPROACHES USED IN THE MEASUREMENT OF SPRINGBACK ADVANCES IN NATURAL AND APPLIED SCIENCES, 6(2): 195-205, 2012
- [55] V. NASROLLAHI , B. AREZOO, PREDICTION OF SPRINGBACK IN SHEET METAL COMPONENTS WITH HOLES ON THE BENDING AREA USING EXPERIMENTS, FINITE ELEMENT AND NEURAL NETWORKS , MATERIALS AND DESIGN 36(2012), PP331-336
- [56] Y.E. LING, H.P. LEE, B.T. CHEOK, FINITE ELEMENT ANALYSIS OF SPRINGBACK IN L-BENDING OF SHEET METAL, JOURNAL OF MATERIALS PROCESSING TECHNOLOGY 168 (2005), PP. 296-302.
- [57] A. FORCELLESE , L. FRATINI , F. GABRIELLI , F. MICARI, (1998). THE EVALUATION OF SPRINGBACK IN 3D STAMPING AND COINING PROCESSES, JOURNAL OF MATERIALS PROCESSING TECHNOLOGY 80-81, PP108-112
- [58] L. TAYLOR ; J. CAO, A.P. KARAFILLIS, M.C. BOYCE , NUMERICAL SIMULATIONS OF SHEET-METAL  
JOURNAL OF MATERIALS PROCESSING TECHNOLOGY 50 (1995) 168-179
- [59] KARAFILLIS, A.P., BOYCE, M.C., TOOLING AND BINDER DESIGN FOR 3-D SHEET METAL FORMING PROCESS USING SPRINGBACK CALCULATIONS, NUMIFORM '95, EDS. SHEN, S-F AND DAWSON, P., 581 (1995).
- [60] SIM, HB, BOYCE, MC, FINITE ELEMENT ANALYSES OF REAL-TIME STABILITY CONTROL IN SHEET FORMING PROCESSES, TO APPEAR TRANS. ASME, J. ENG. MAT. TECH., (1991
- [61] M.J. FINN, P.C. GALBRAITH, L. WU , J.O. HALLQUIST, L. LUM, T.-L. LIN , USE OF A COUPLED EXPLICIT-IMPLICIT SOLVER FOR CALCULATING SPRING-BACK IN

## References

- AUTOMOTIVE BODY PANELS JOURNAL OF MATERIALS PROCESSING TECHNOLOGY, VOLUME 50, ISSUES 1-4, MARCH 1995, PAGES 395-409
- [62] WEI GAN,R.H. WAGONER DIE DESIGN METHOD FOR SHEET SPRINGBACK, INTERNATIONAL JOURNAL OF MECHANICAL SCIENCES VOLUME 46, ISSUE 7, JULY 2004, PAGES 1097-1113
- [63] KARAFILLIS, A.P., BOYCE, M.C., TOOLING AND BINDER DESIGN FOR SHEET METAL FORMING PROCESSES COMPENSATING SPRINGBACK ERROR, INT. J. MACH. TOOLS MANUFACT., 503, 36 (1996).
- [64] NARKEERAN NARASIMHAN,MICHAEL LOVELL, PREDICTING SPRINGBACK IN SHEET METAL FORMING: AN EXPLICIT TO IMPLICIT SEQUENTIAL SOLUTION PROCEDURE, FINITE ELEMENTS IN ANALYSIS AND DESIGN 33, ISSUE 1,15 AUGUST 1999, PAGES 29-42
- [65] M. BAKHSHI-JOOYBARI , B. RAHMANI, V. DAEZADEH, A. GORJI, (2009). THE STUDY OF SPRING-BACK OF CK67 STEEL SHEET IN V-DIE AND U-DIE BENDING PROCESSES MATERIALS AND DESIGN 30 2410-2419
- [66] EUGENE A. AVALLONE, THEODORE BAUMEISTER, MARK'S STANDARD HANDBOOK FOR MECHANICAL ENGINEERS, MCGRAW-HILL PROFESSIONAL, 10TH EDITION, 1996
- [67] AMER SATTAR1 AND IRFAN A. MANARVI(2011), WRINKLING PREDICTION OF ALUMINUM 5456-H116SHEET METALS UNDER UNI-AXIAL AND BI-AXIALLOADING THROUGH FE SIMULATIONS, INTERNATIONAL JOURNAL OF MULTIDISCIPLINARY SCIENCES AND NGINEERING,. 2, NO. 5,
- [68] JIANGUANG LIU, ZHONHJIN WANG,(2010)PREDICTION OF WRINKLING AND FRACTURING IN VISCOUS PRESSURE FORMING (VPF) BY USING THE COUPLED DEFORMATION SECTIONAL FEM, COMPUTATIONAL MATERIAL SCIENCE 48,PP381-389
- [69] KARL BRIAN NIELSEN (2000), SHEET METAL FORMING SIMULATION USING EXPLICIT FINITE ELEMENT METHODS, ISBN 87-89767-69-6

## References

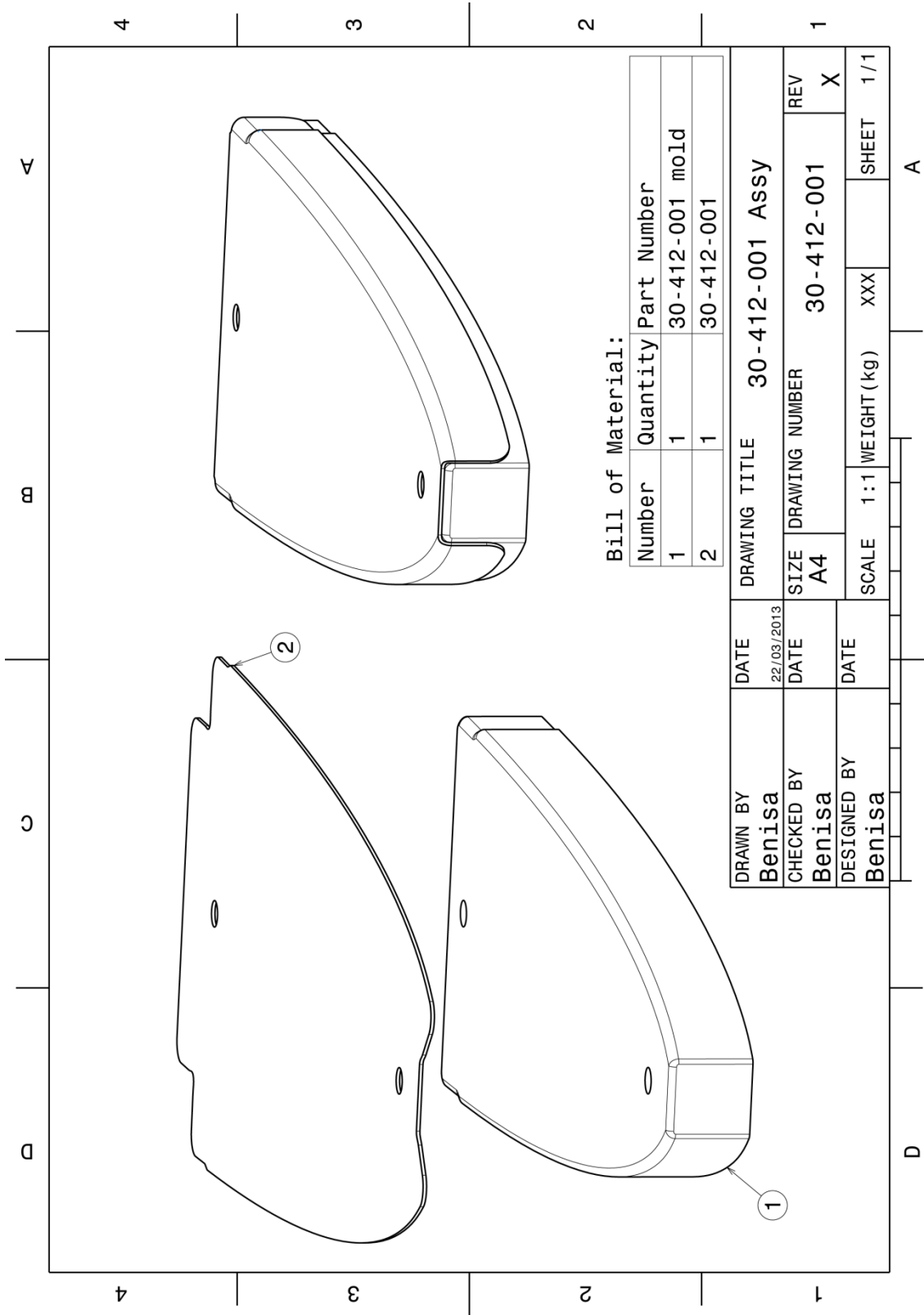
- [70] M. KAWKA, L. OLEJNIK, A. ROSOCHOWSKIC, H. SUNAGAD, A. MAKINOUCI,(2001), SIMULATION OF WRINKLING IN SHEET METAL FORMING, JOURNAL OF MATERIALS PROCESSING TECHNOLOGY 109 , 283-289

## Biography

Muamar M. Benisa was born on March 13, 1970 in Zliten Libya, he graduated in 1992 with BSc. and Engineering degrees in mechanical Engineering from Garyuons University, Faculty of mechanical Engineering. In 1994 started to work as responsible for workshop and welding lab at institute of technology and Training center till August 1996, and then moved to El-Mergeb University, Libya as assistant lecturer from the end of 1996 to August 2002. He enrolled in his master studies at faculty of mechanical Engineering and production, Budapest University of technology and Economic in Sep 2002. He graduated M.Sc. in filed production bulk nonstructural material in Sep 2005. Upon return back to Libya continued work at El-Margeb University, Faculty of mechanical Engineering Department as Latherer for the following subjects: production Engineering (I,II), workshop for mechanical Engineering department and straight of material I. PhD degree at the faculty of Mechanical Engineering in Belgrade University started in fall of 2008. Year, passed all exams by platform of these studies, with a potential mentor to work participated in two international scientific journals and international conference.

## Appendix A

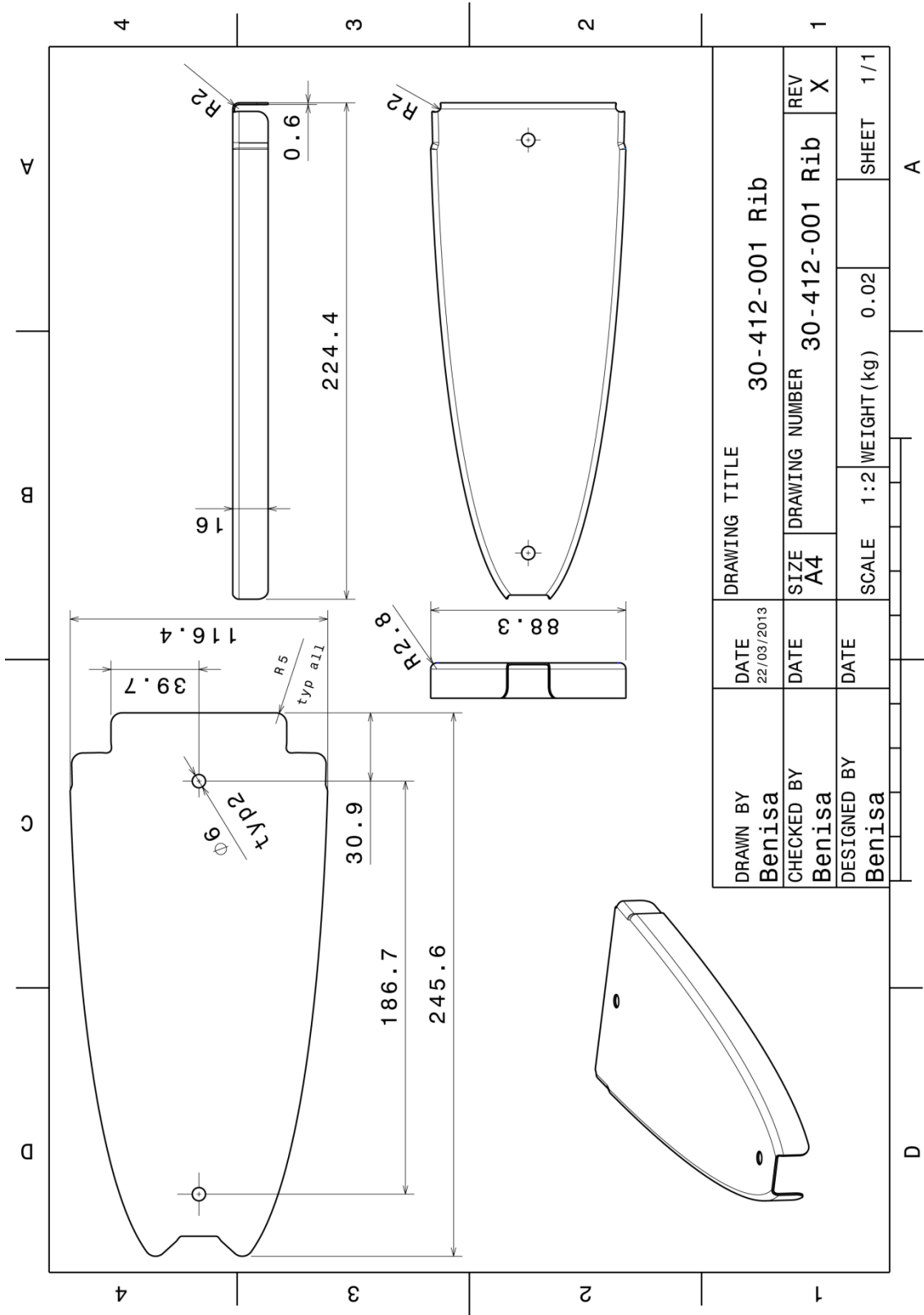
- Even pages show the different geometry of rib tools and blanks.
- Odd pages show the drawing of geometric shape design of different ribs



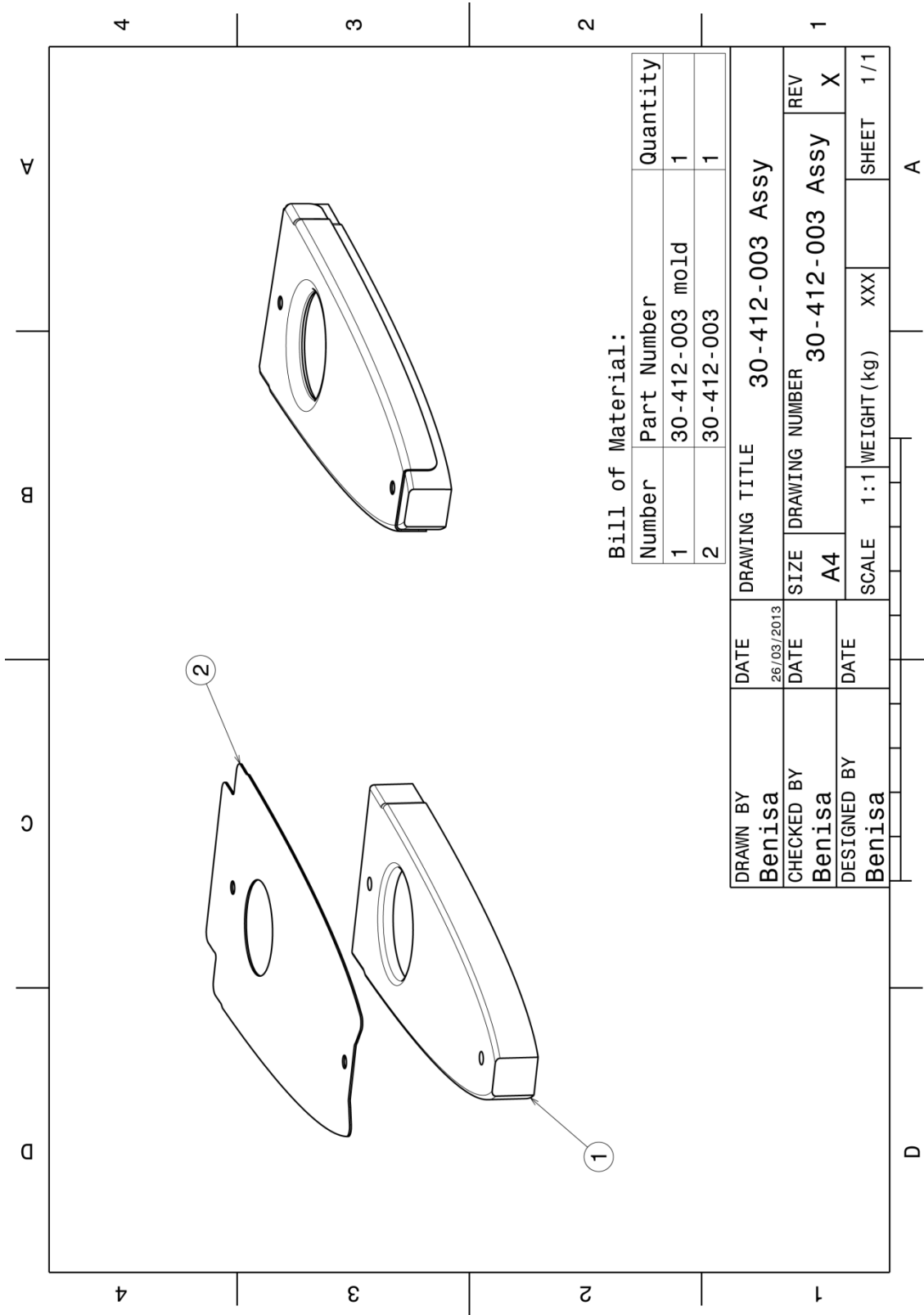
**Bill of Material:**

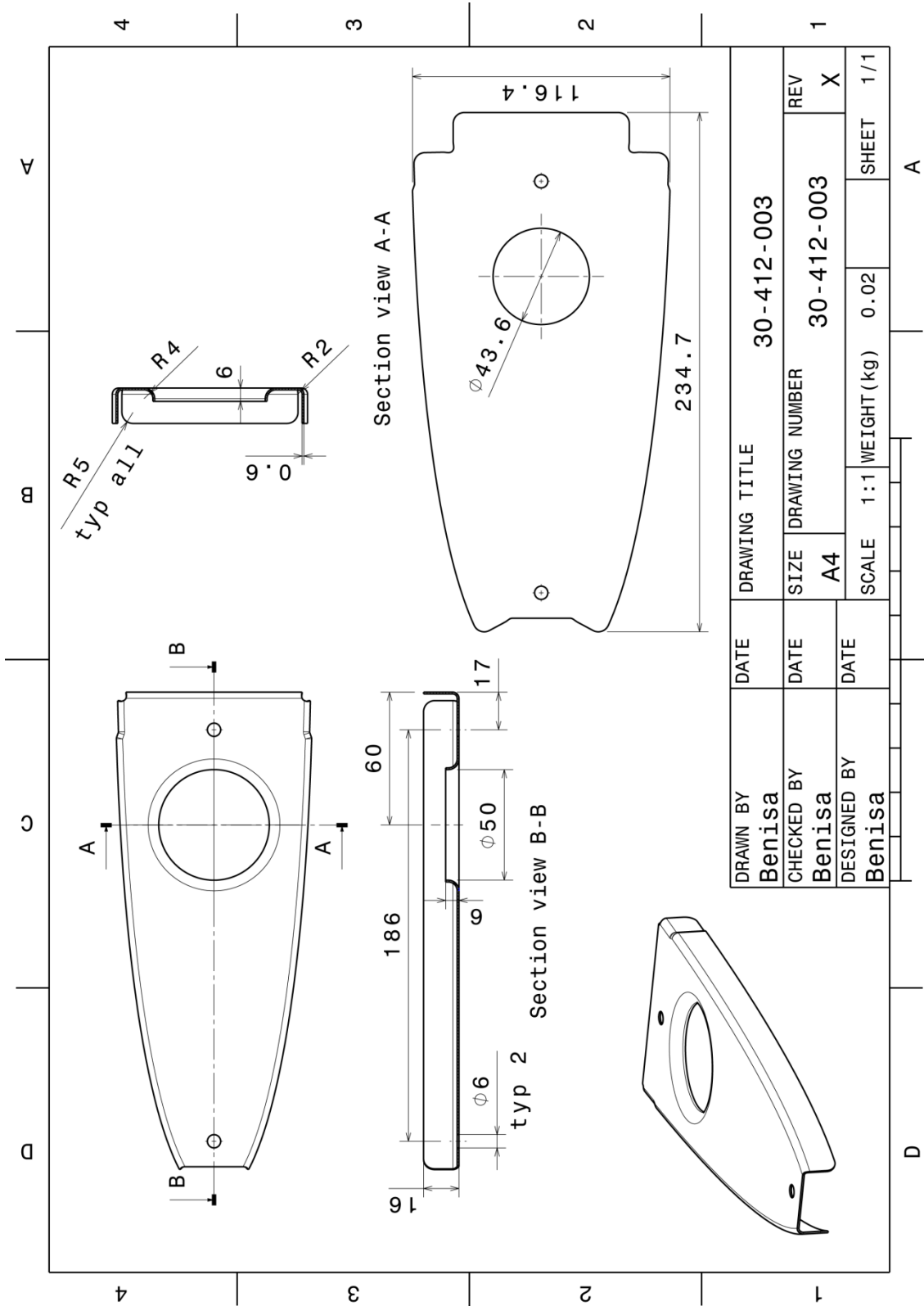
| Number | Quantity | Part Number     |
|--------|----------|-----------------|
| 1      | 1        | 30-412-001 mold |
| 2      | 1        | 30-412-001      |

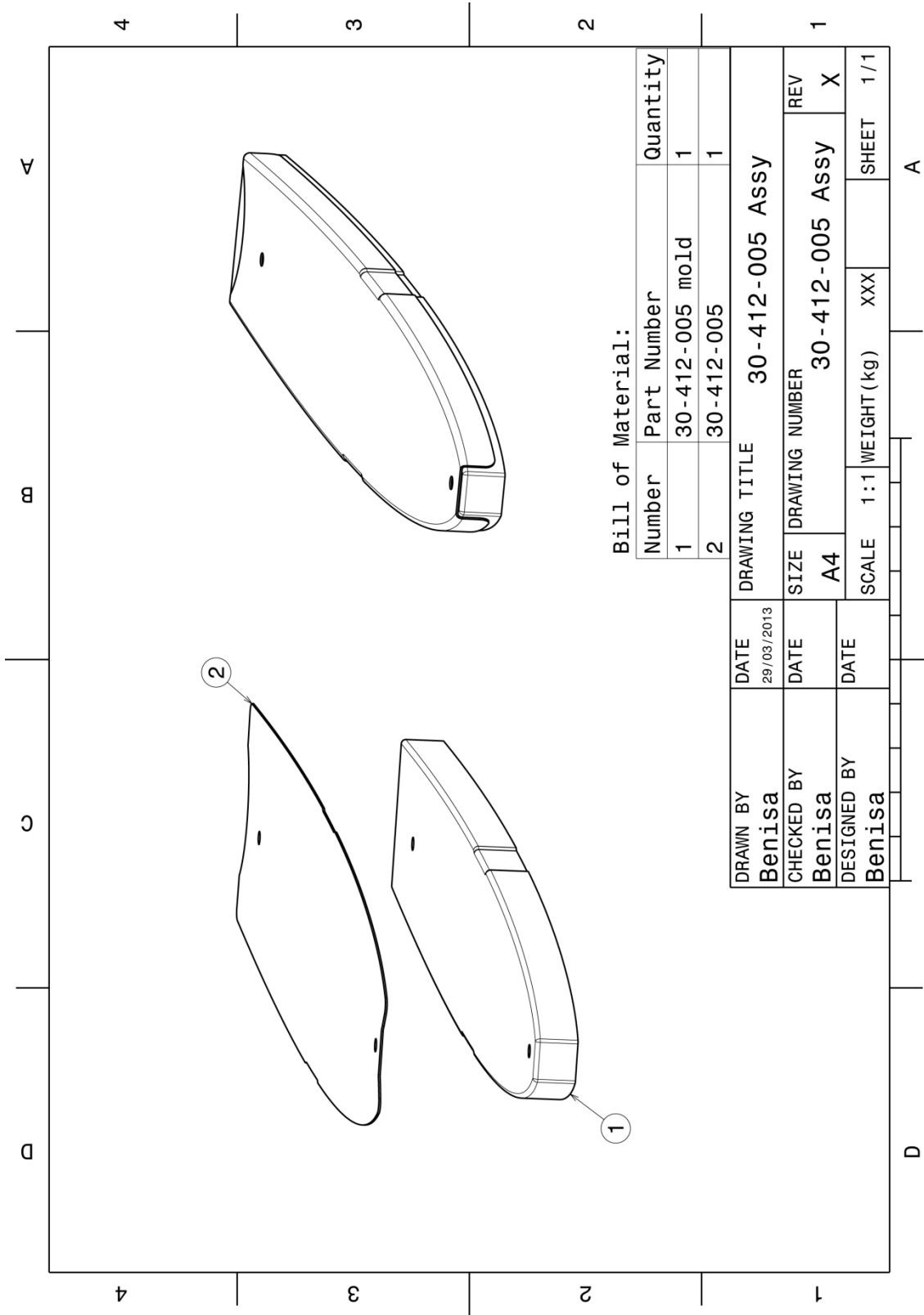
|                              |                           |   |                                     |                     |
|------------------------------|---------------------------|---|-------------------------------------|---------------------|
| <b>DRAWN BY</b><br>Benisa    | <b>DATE</b><br>22/03/2013 | <b>DRAWING TITLE</b><br>30-412-001 Assy |                                     |                     |
| <b>CHECKED BY</b><br>Benisa  | <b>DATE</b>               | <b>SIZE</b><br>A4                       | <b>DRAWING NUMBER</b><br>30-412-001 | <b>REV</b><br>X     |
| <b>DESIGNED BY</b><br>Benisa | <b>DATE</b>               | <b>SCALE</b><br>1:1                     | <b>WEIGHT (kg)</b><br>XXX           | <b>SHEET</b><br>1/1 |

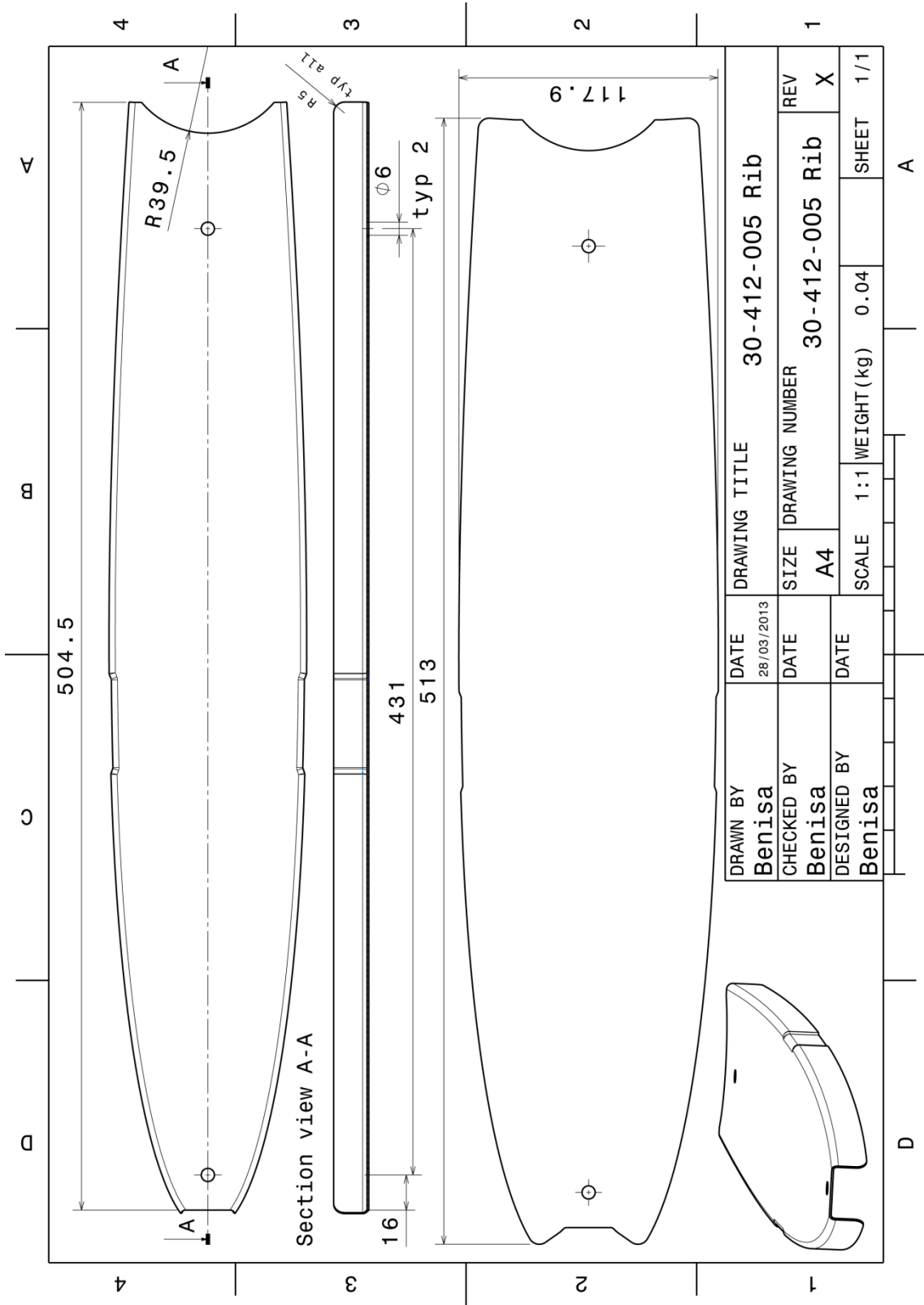


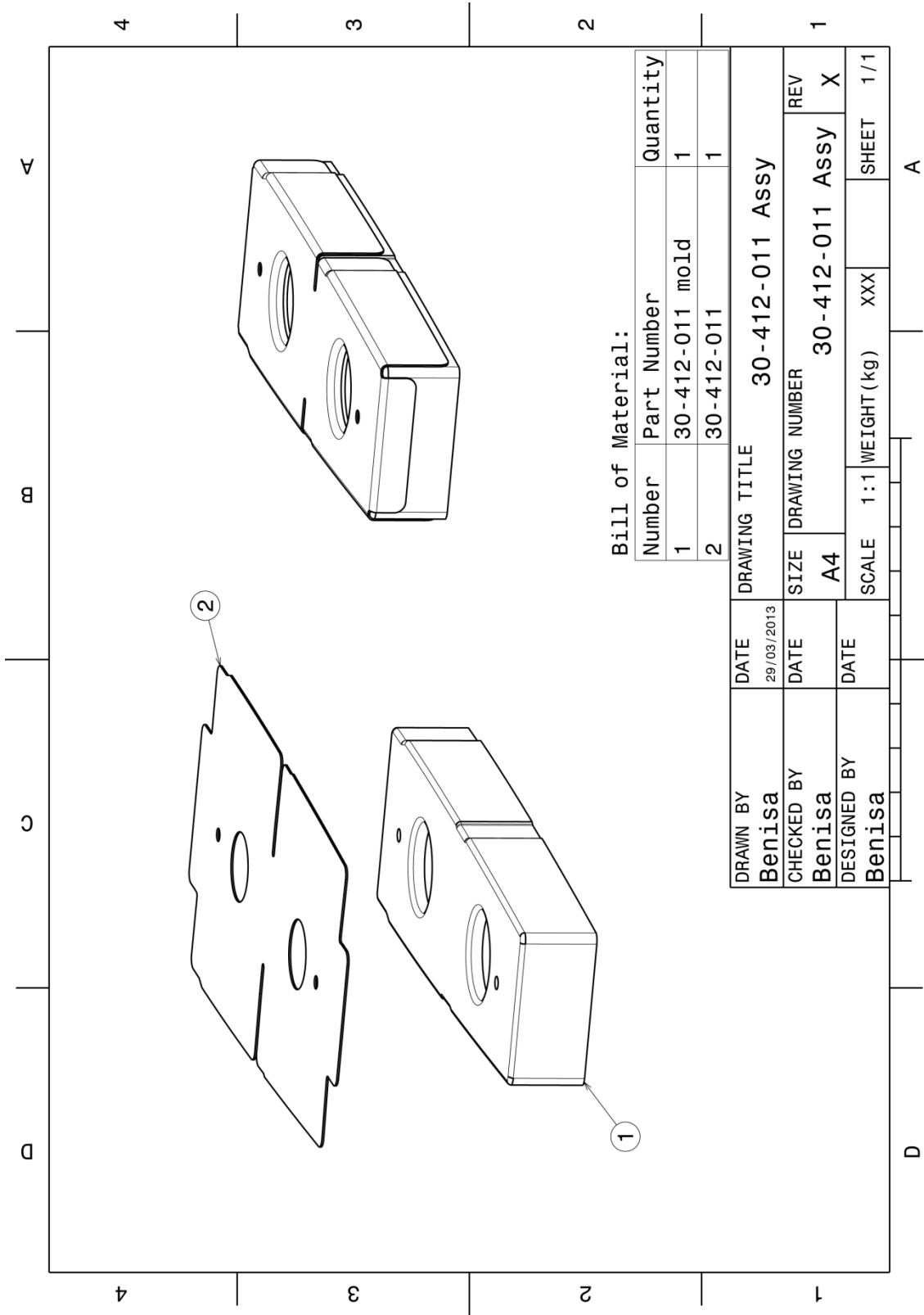
|             |            |                |       |                |       |
|-------------|------------|----------------|-------|----------------|-------|
| DRAWN BY    | DATE       | DRAWING TITLE  |       | DRAWING NUMBER | REV   |
| Benisa      | 22/03/2013 | 30-412-001 Rib |       | 30-412-001 Rib | X     |
| CHECKED BY  | DATE       | SIZE           | SCALE | WEIGHT (kg)    | SHEET |
| Benisa      |            | A4             | 1:2   | 0.02           | 1/1   |
| DESIGNED BY | DATE       |                |       |                |       |
| Benisa      |            |                |       |                |       |

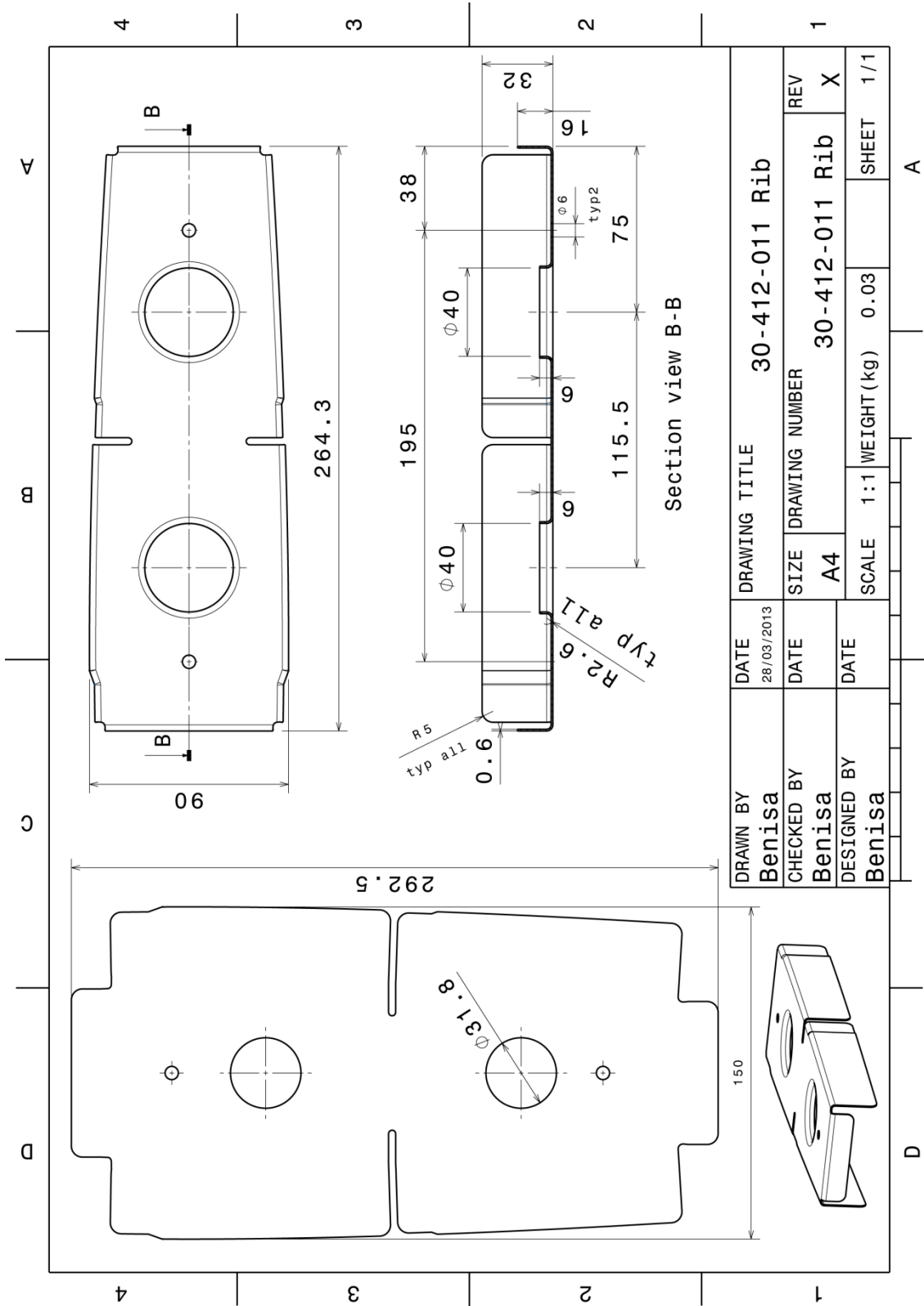


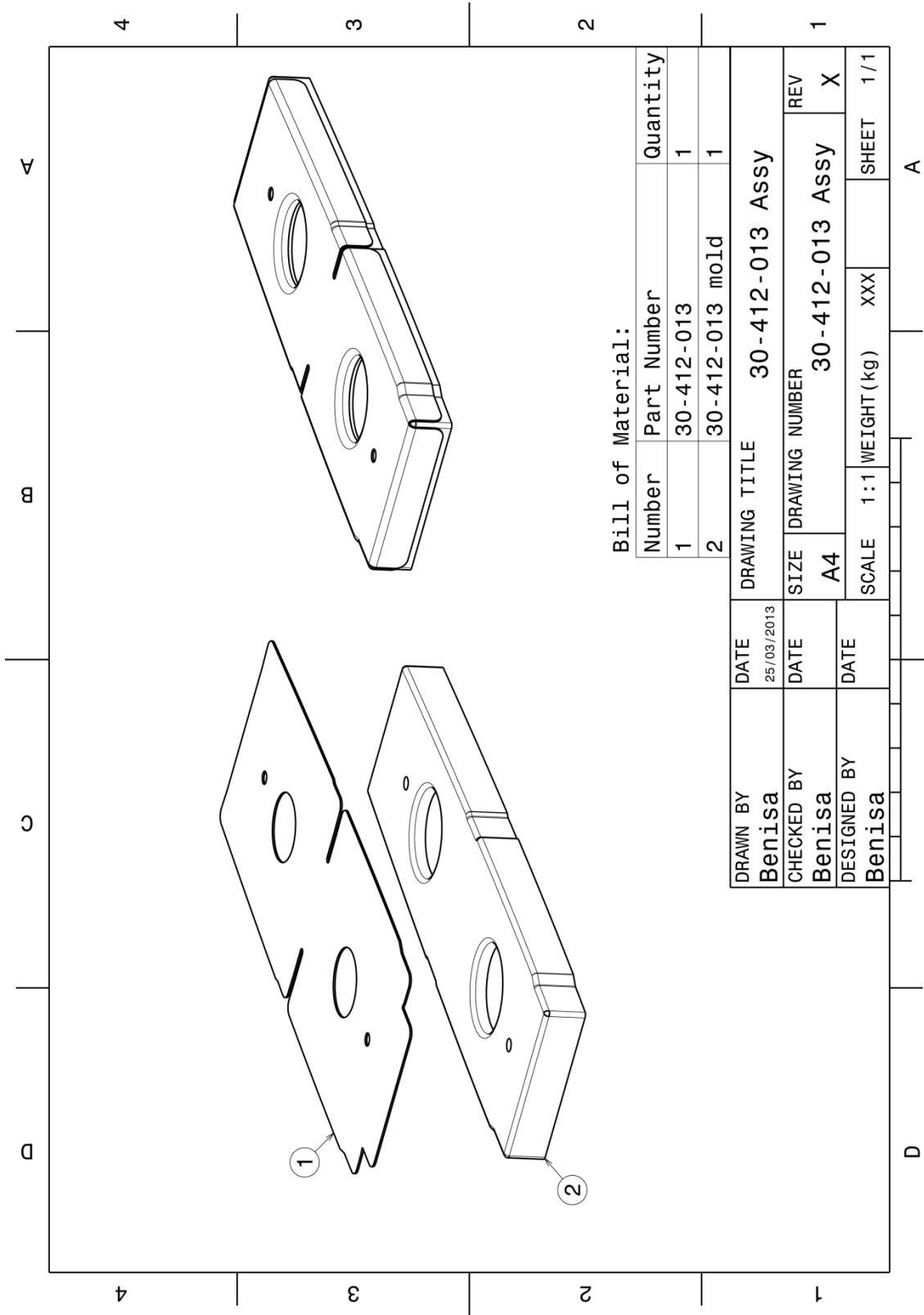










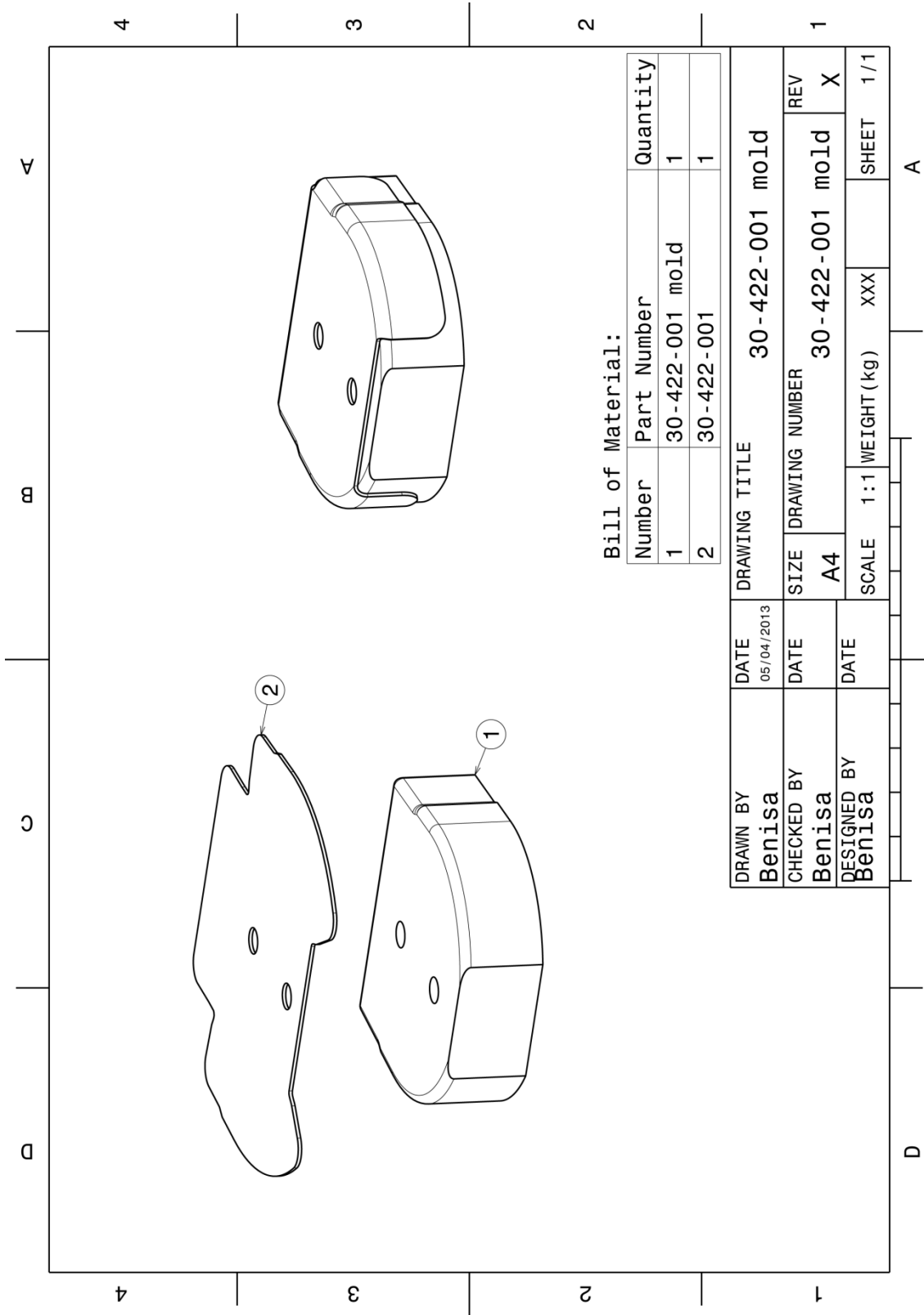


Bill of Material:

| Number | Part Number     | Quantity |
|--------|-----------------|----------|
| 1      | 30-412-013      | 1        |
| 2      | 30-412-013 mold | 1        |

|             |            |                 |                 |
|-------------|------------|-----------------|-----------------|
| DRAWN BY    | DATE       | DRAWING TITLE   |                 |
| Benisa      | 25/03/2013 | 30-412-013 Assy |                 |
| CHECKED BY  | DATE       | SIZE            | DRAWING NUMBER  |
| Benisa      |            | A4              | 30-412-013 Assy |
| DESIGNED BY | DATE       | SCALE           | WEIGHT (kg)     |
| Benisa      |            | 1:1             | XXX             |
|             |            |                 | SHEET           |
|             |            |                 | 1/1             |

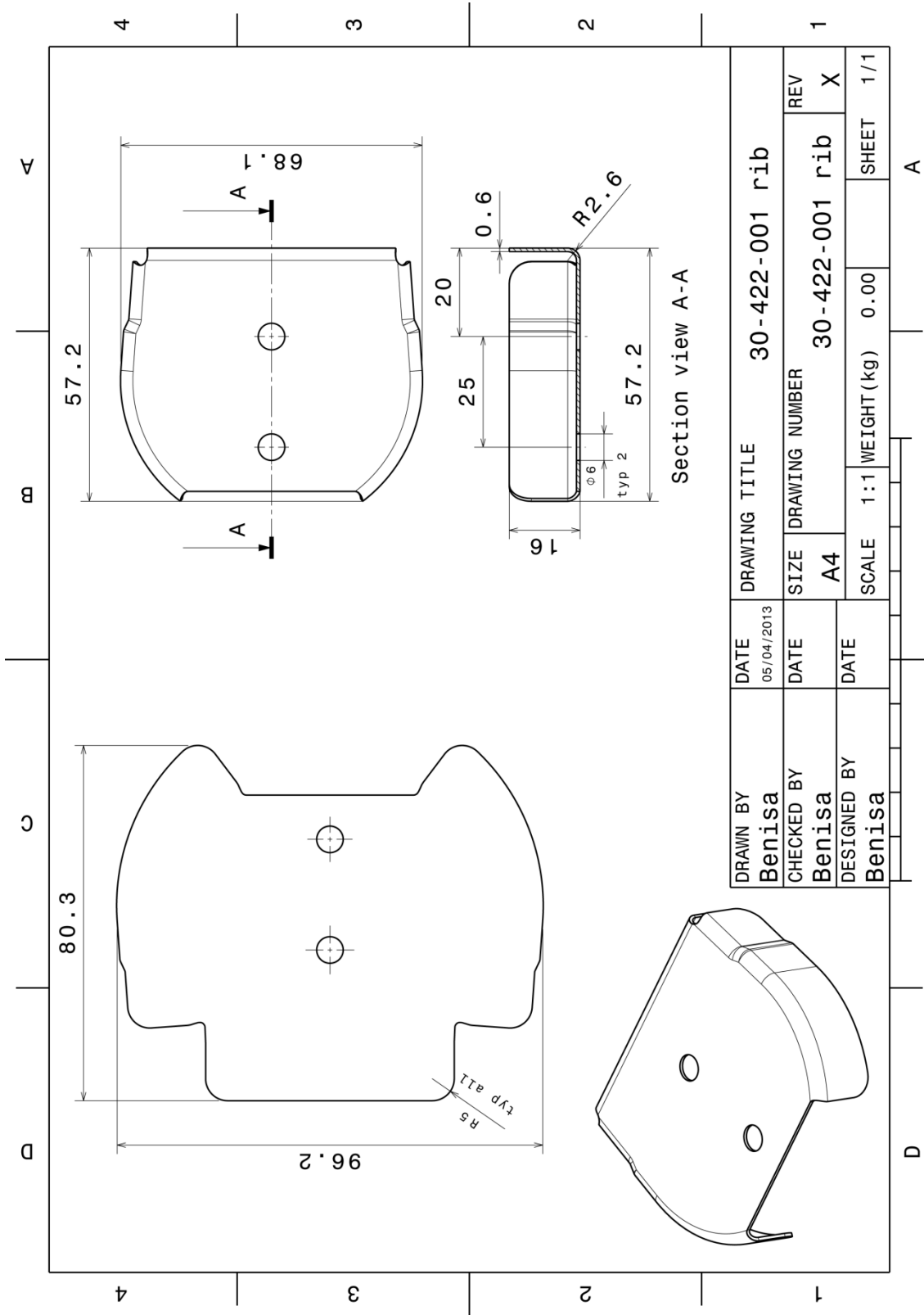


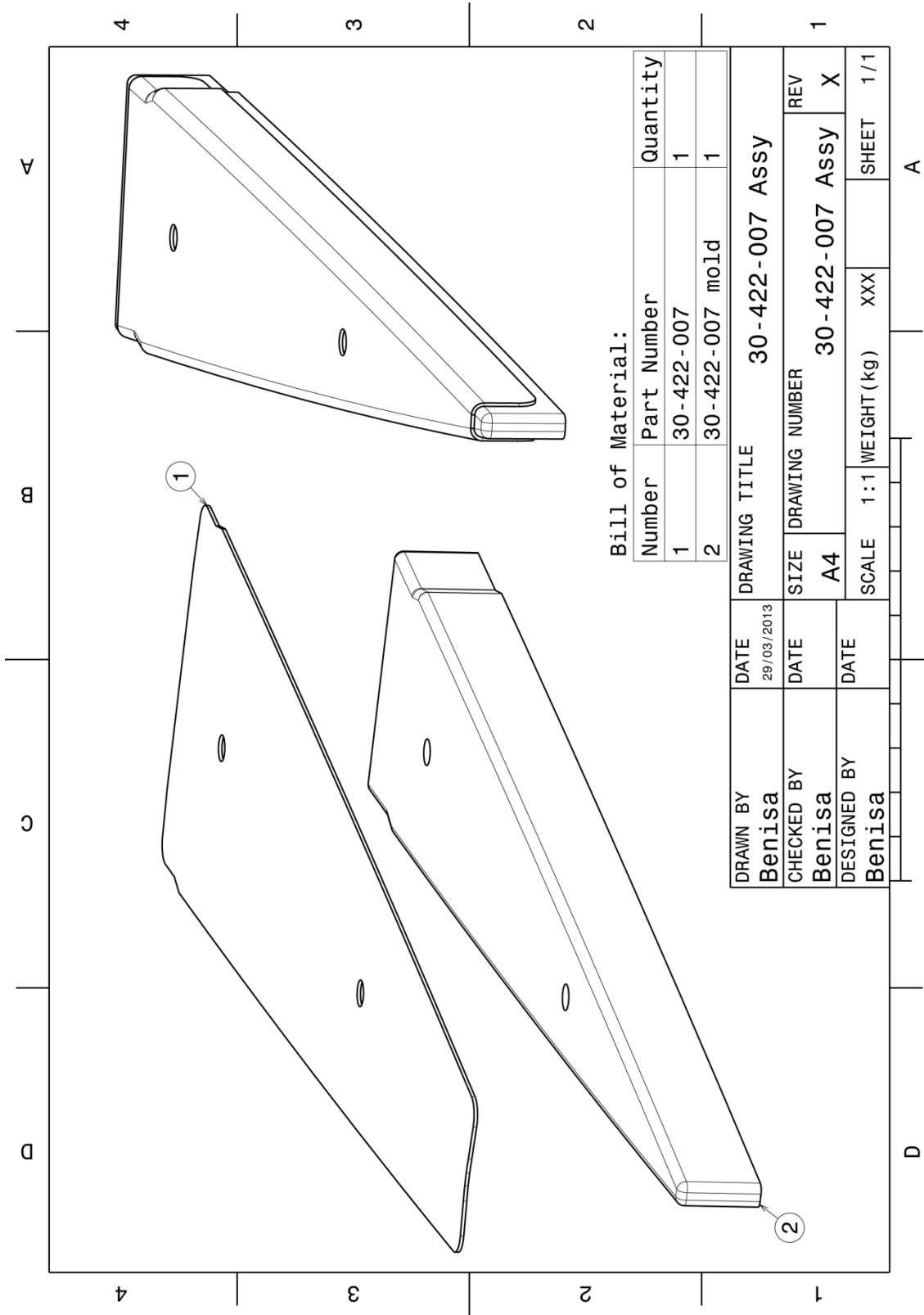


Bill of Material:

| Number | Part Number     | Quantity |
|--------|-----------------|----------|
| 1      | 30-422-001 mold | 1        |
| 2      | 30-422-001      | 1        |

|             |  |            |                 |                 |
|-------------|--|------------|-----------------|-----------------|
| DRAWN BY    |  | DATE       | DRAWING TITLE   |                 |
| Benisa      |  | 05/04/2013 | 30-422-001 mold |                 |
| CHECKED BY  |  | DATE       | SIZE            | DRAWING NUMBER  |
| Benisa      |  |            | A4              | 30-422-001 mold |
| DESIGNED BY |  | DATE       | SCALE           | WEIGHT (kg)     |
| Benisa      |  |            | 1:1             | XXX             |
|             |  |            | SHEET           | 1/1             |

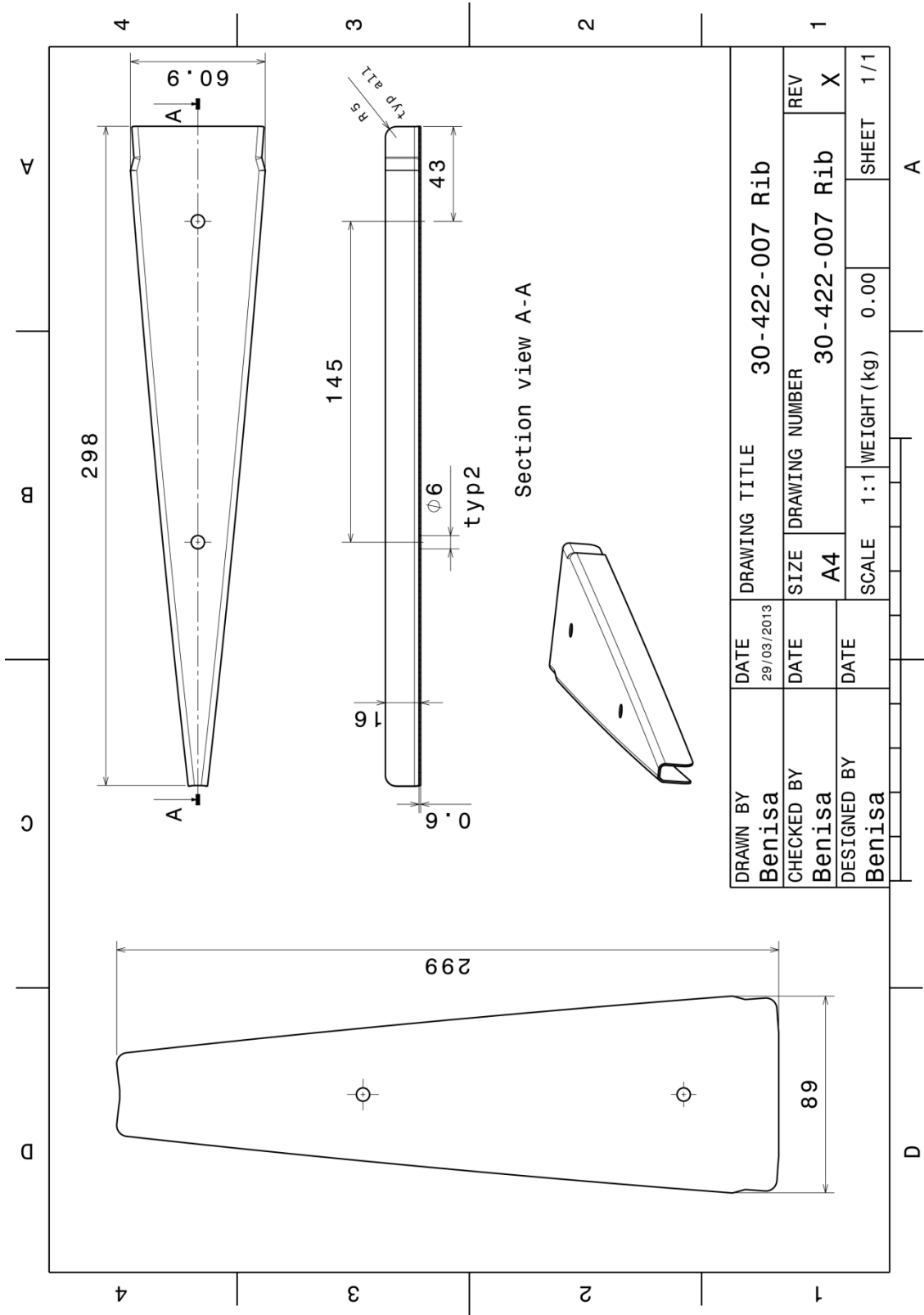


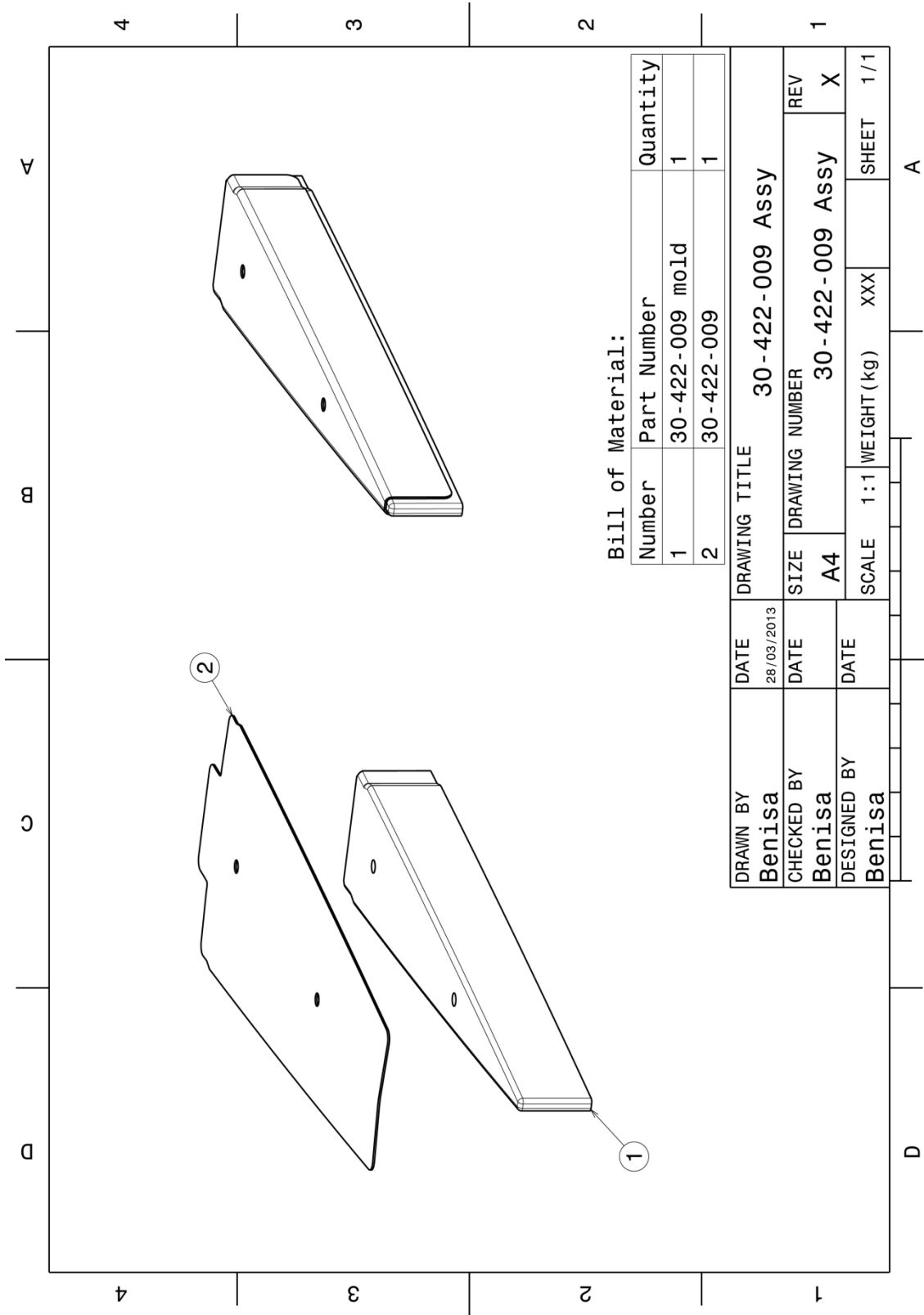


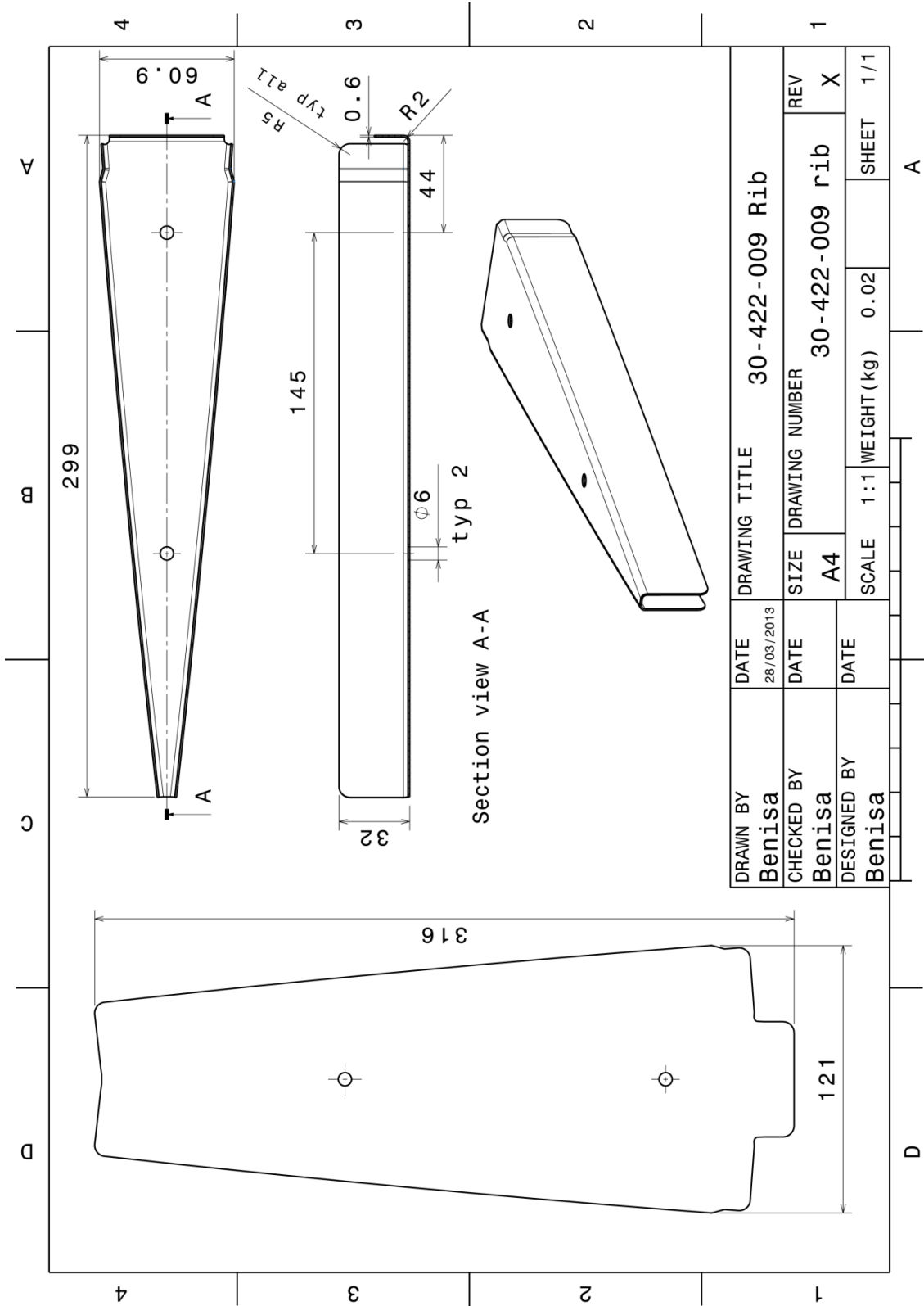
Bill of Material:

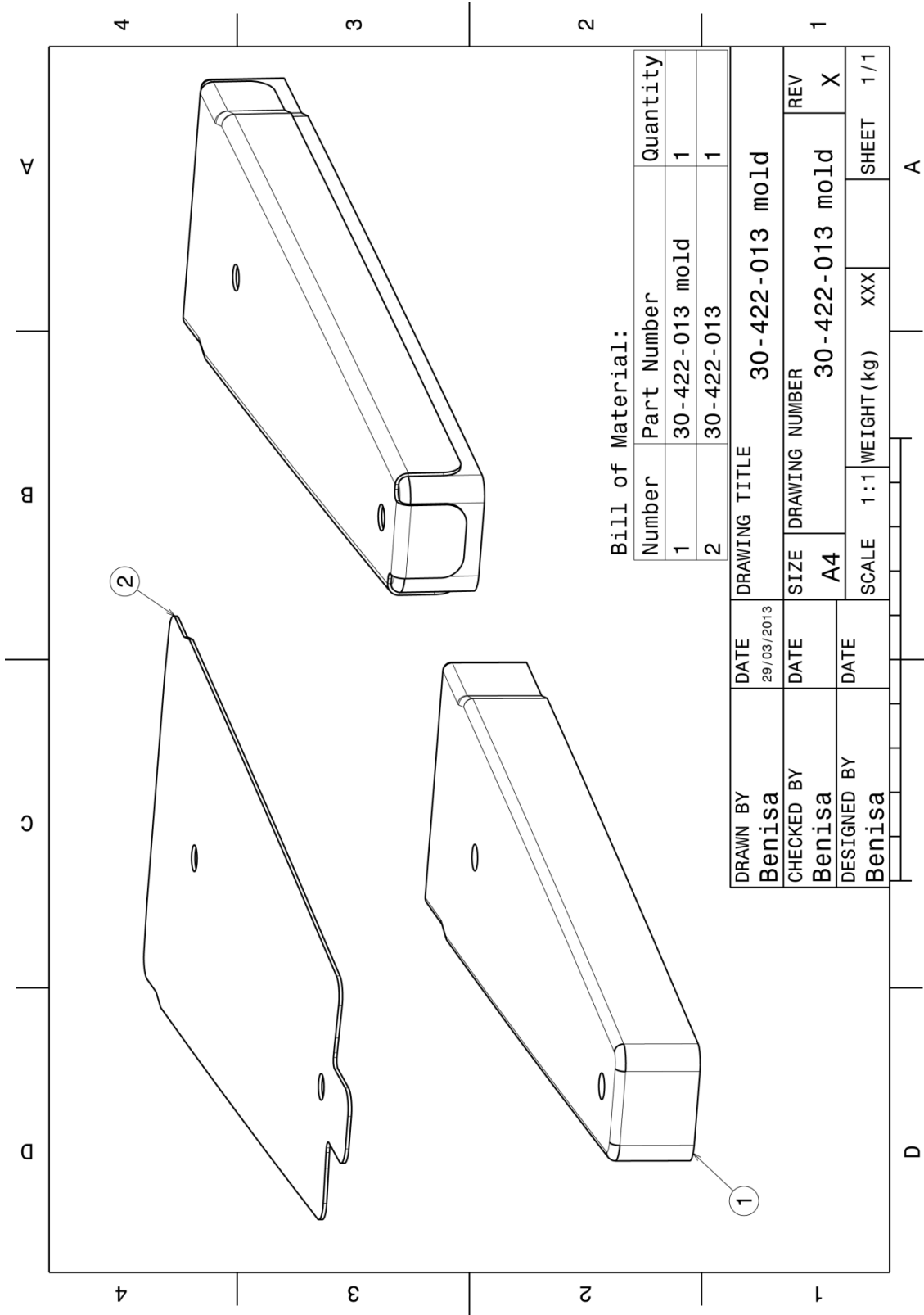
| Number | Part Number     | Quantity |
|--------|-----------------|----------|
| 1      | 30-422-007      | 1        |
| 2      | 30-422-007 mold | 1        |

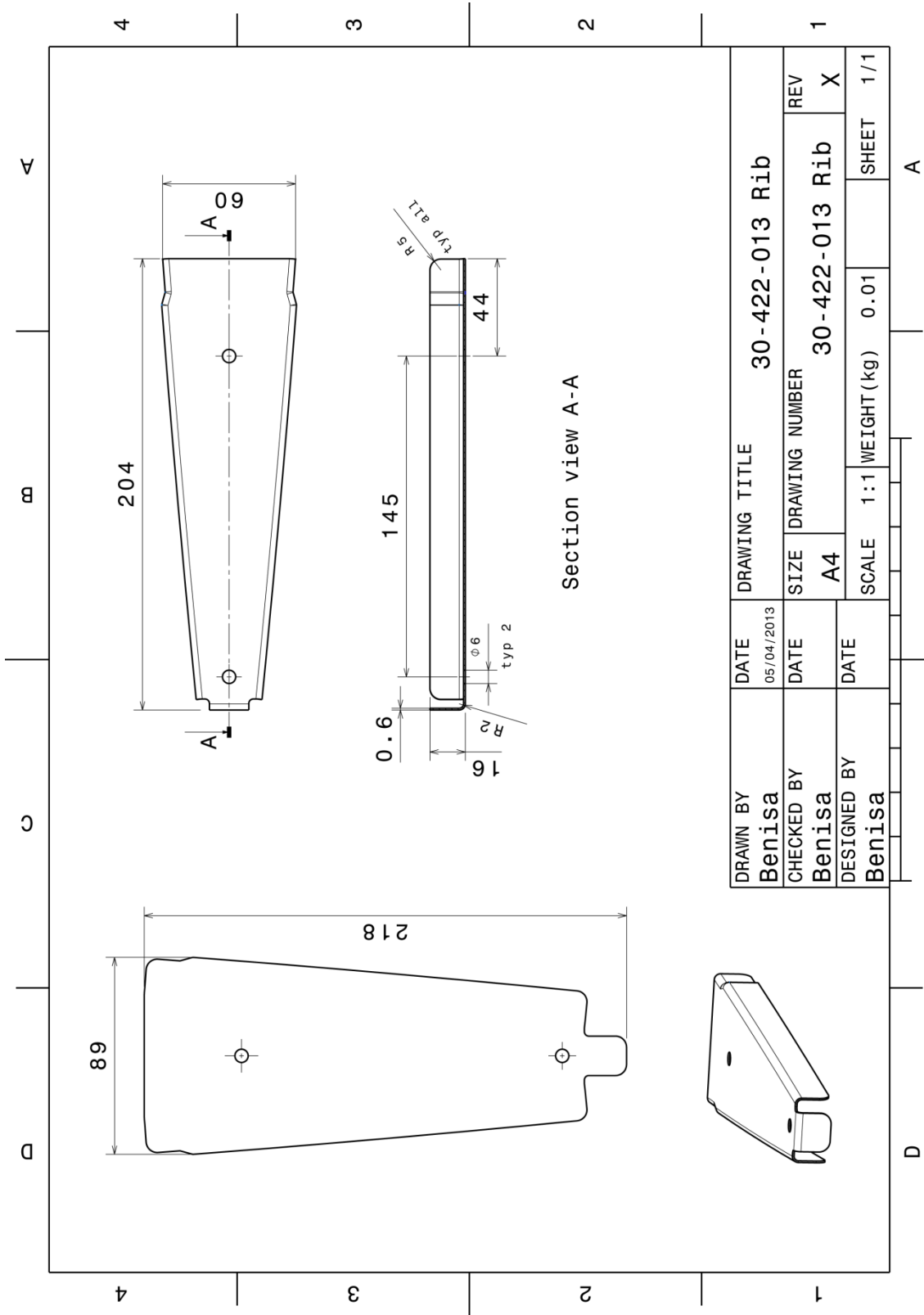
|             |            |                 |                 |
|-------------|------------|-----------------|-----------------|
| DRAWN BY    | DATE       | DRAWING TITLE   |                 |
| Benisa      | 29/03/2013 | 30-422-007 Assy |                 |
| CHECKED BY  | DATE       | SIZE            | DRAWING NUMBER  |
| Benisa      |            | A4              | 30-422-007 Assy |
| DESIGNED BY | DATE       | SCALE           | WEIGHT (kg)     |
| Benisa      |            | 1:1             | XXX             |
|             |            |                 | SHEET           |
|             |            |                 | 1/1             |







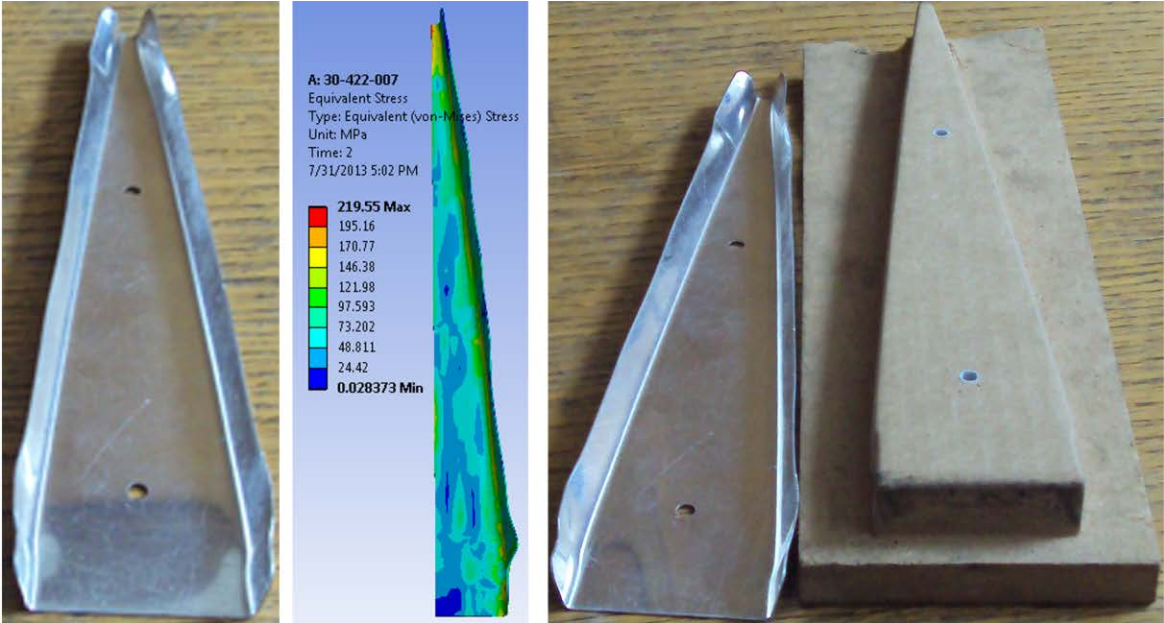




## Appendix B

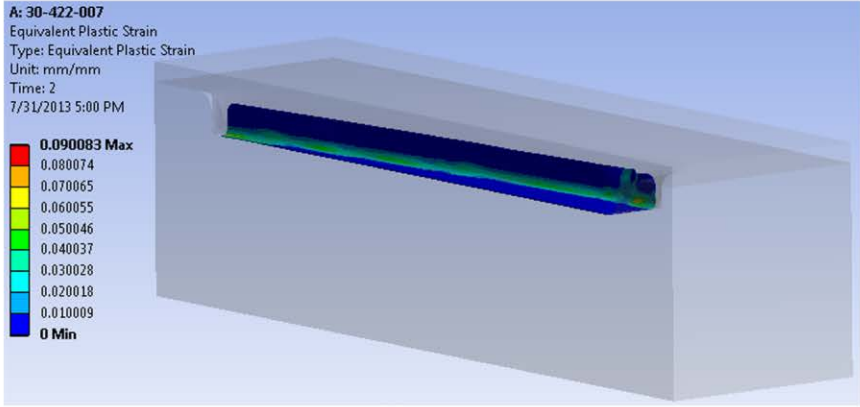
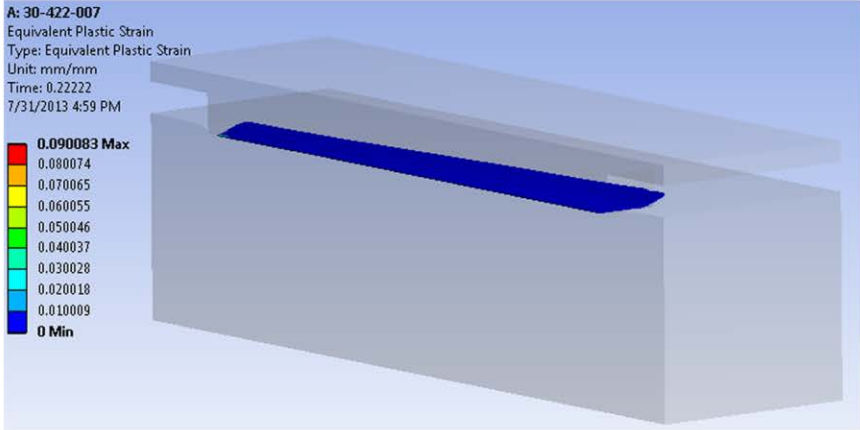
The appendix B shows the experimental and FEM simulations for different shape ribs (rib numbers) of forming samples using rubber pad forming process as following:

- a) Produced rib and FEM simulation,
- b) Produced rib and tool, and
- c) First and last step FEM simulations of rubber pad forming process



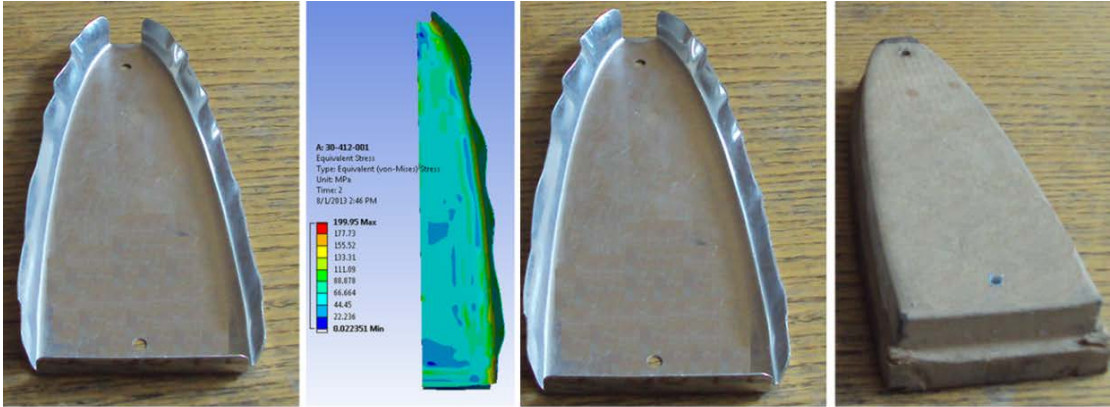
(a)

(b)



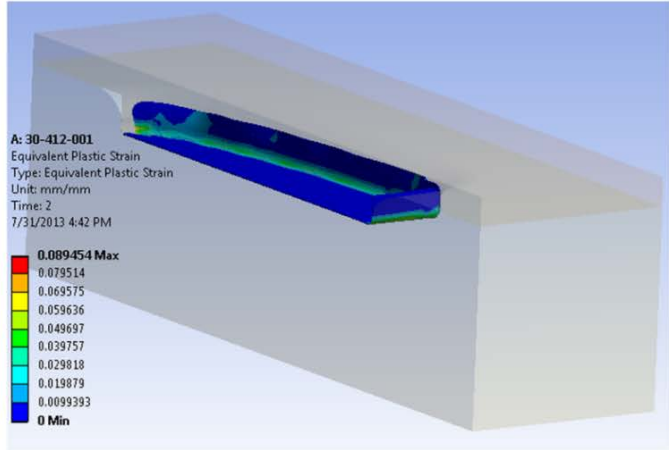
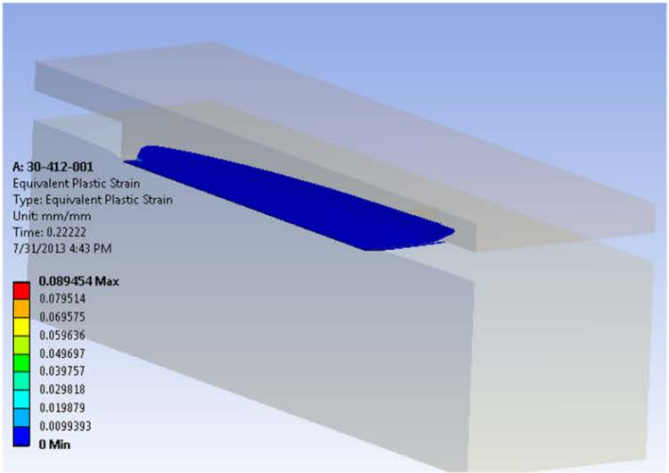
(c)

Figure B1 : Experimental and FEM simulations for rib number 30-422-007.



(a)

(b)



(c)

Figure B2 : Experimental and FEM simulations for rib number 30-412-001 .

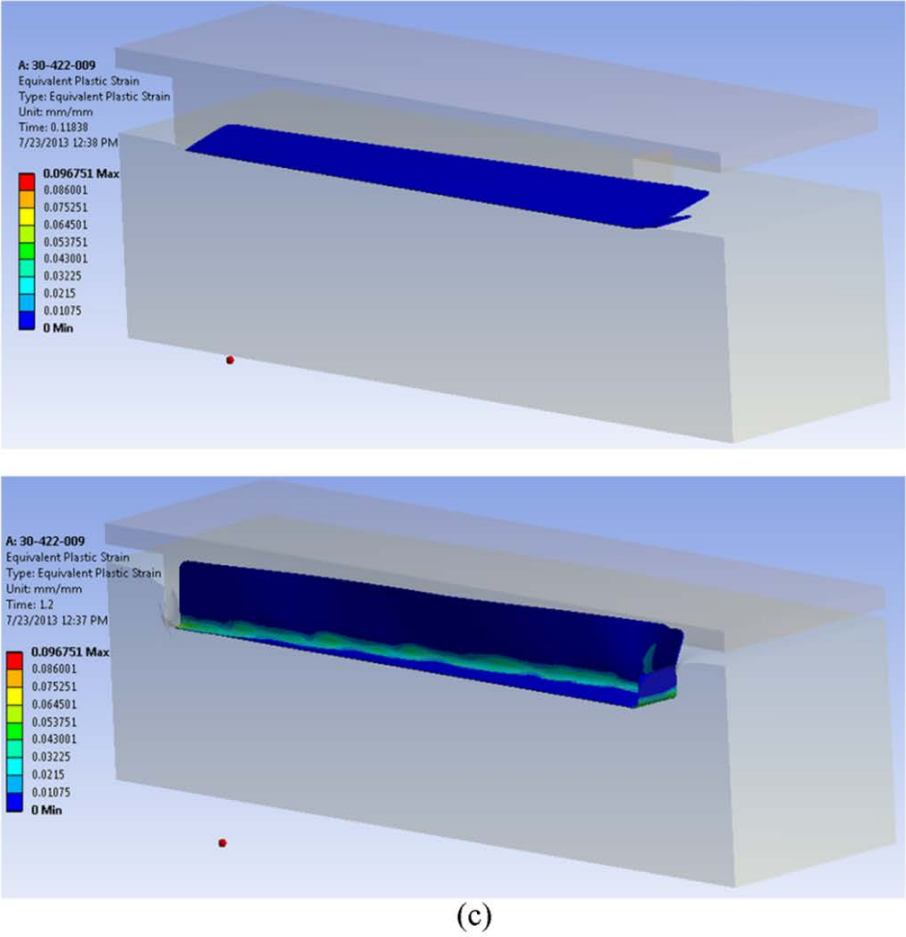
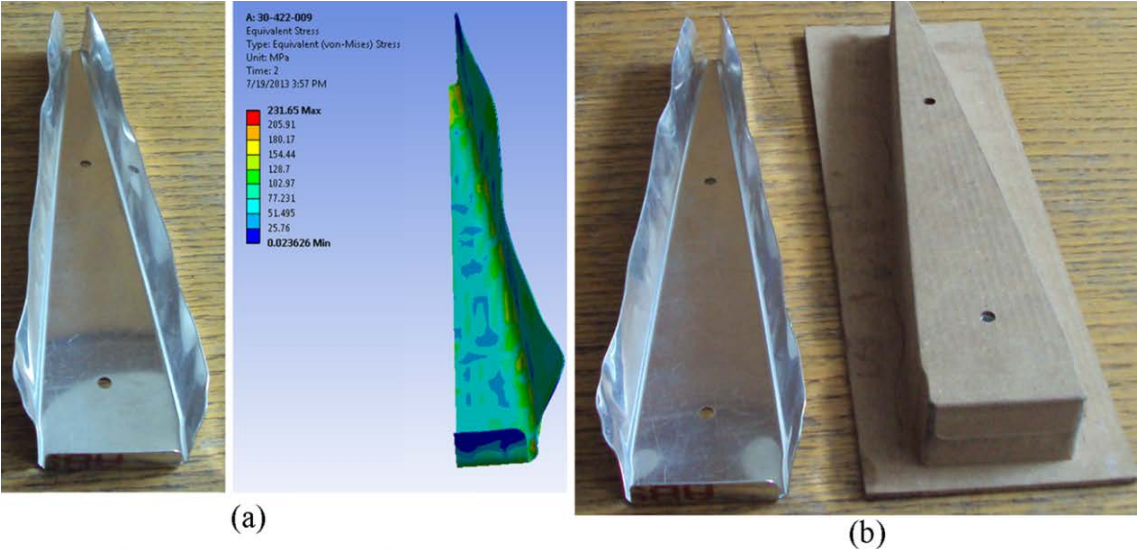
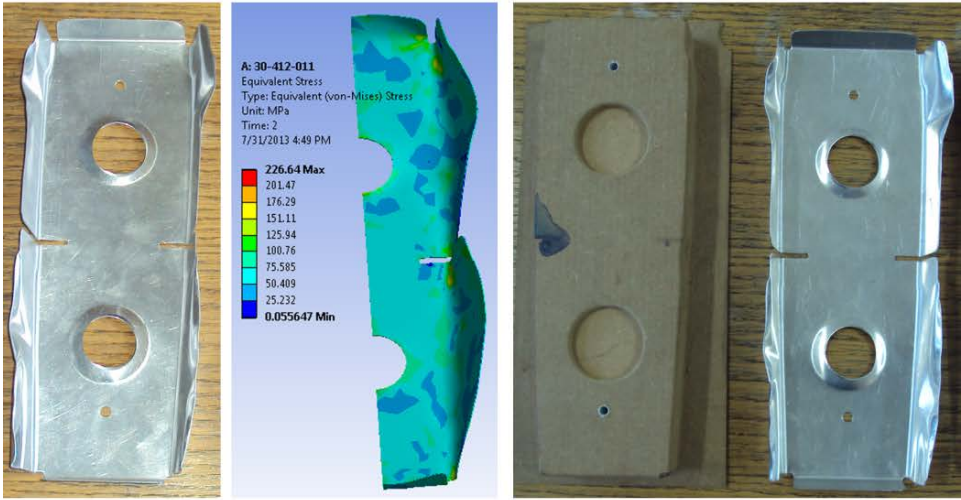
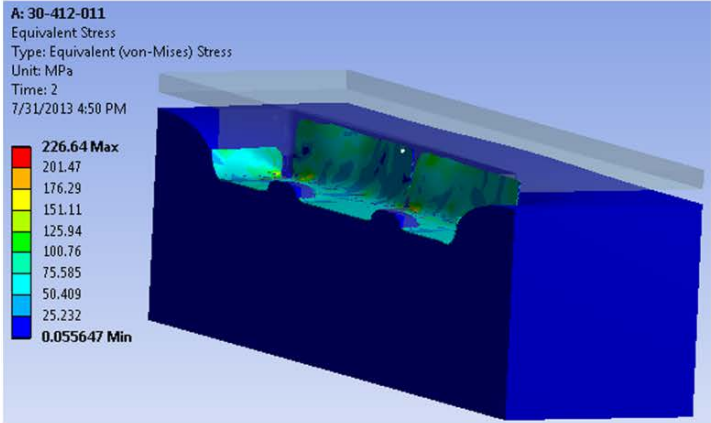
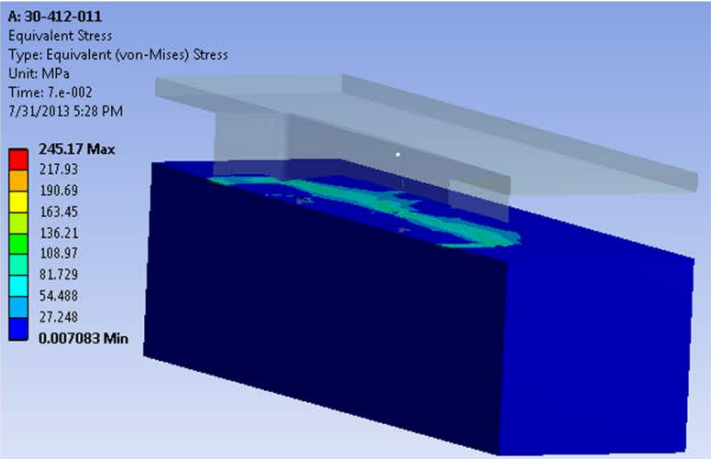


Figure B3 : Experimental and FEM simulations for rib number 30-422-009



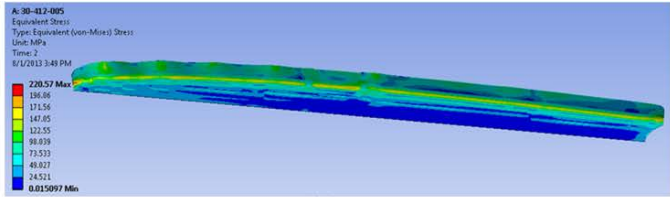
(a)

(b)

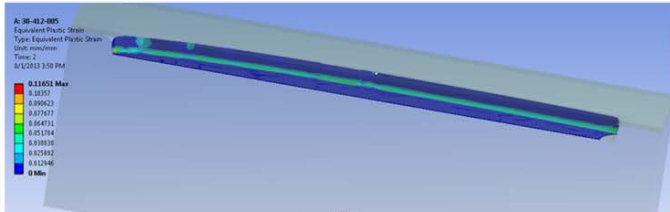
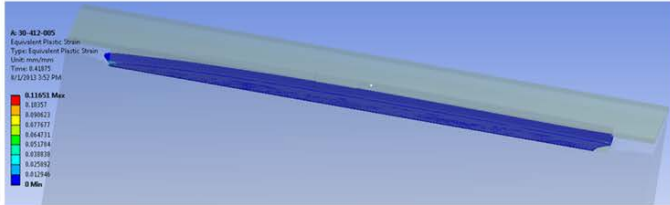


(c)

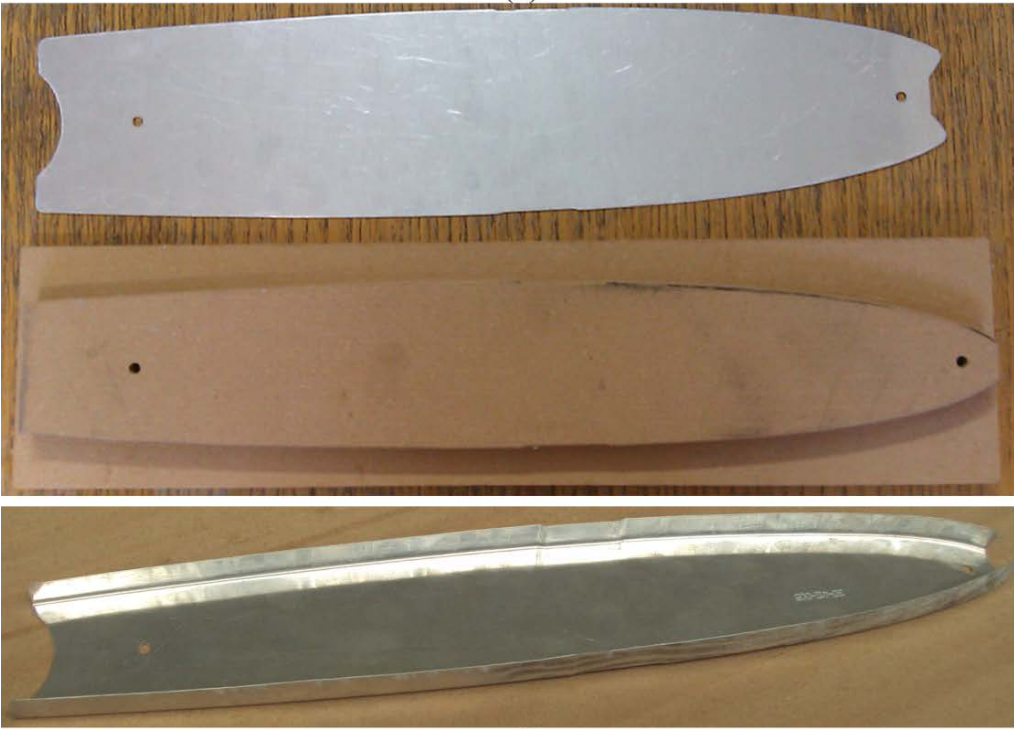
Figure B4 : Experimental and FEM simulations for rib number 30-412-011.



(a)



(b)



(c)

Figure B5 : Experimental and FEM simulations for rib number 30-412-005

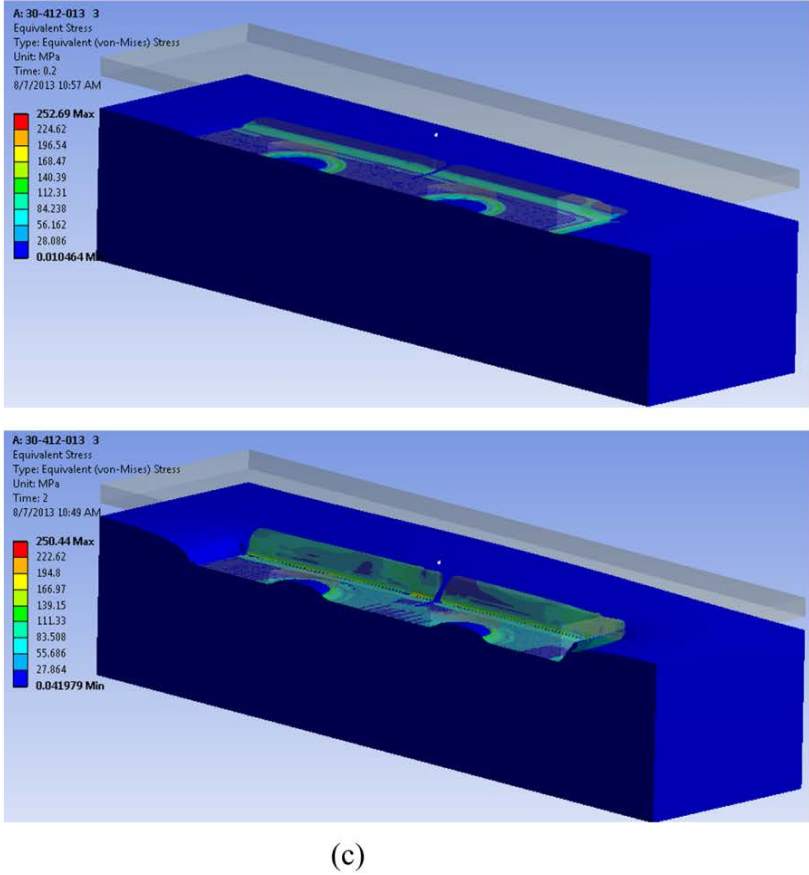
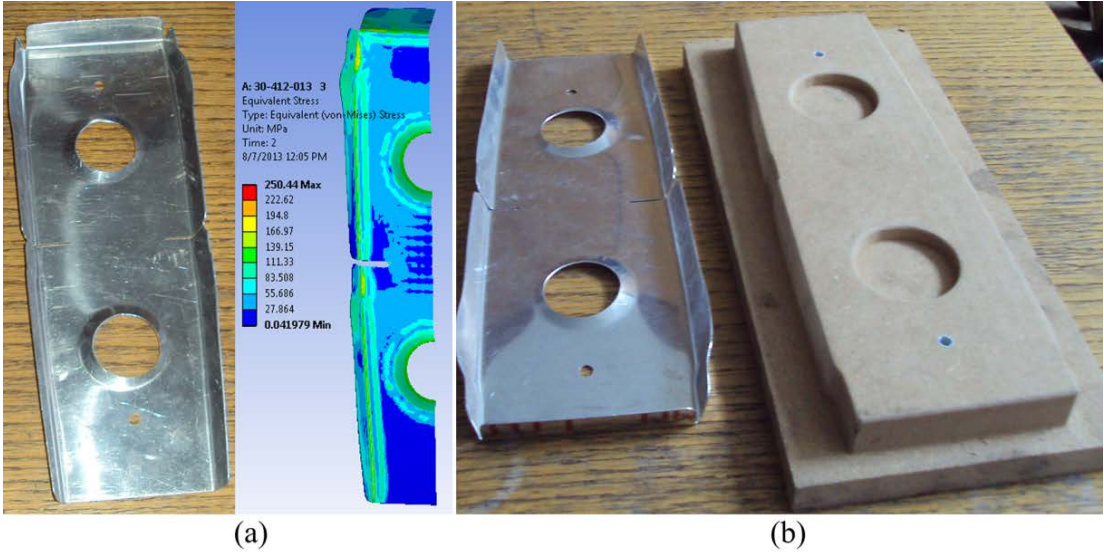


Figure B6 : Experimental and FEM simulations for rib number 30-412-013



## **Прилог 1.**

### **Изјава о ауторству**

Потписани-а Muamar M. Benisa

број уписа D29/08

### **Изјављујем**

да је докторска дисертација под насловом

#### **INTEGRATED PROCESS PLANNING, DIE-DESIGN AND SIMULATION IN SHEET METAL RUBBER FORMING**

- резултат сопственог истраживачког рада,
- да предложена дисертација у целини ни у деловима није била предложена за добијање било које дипломе према студијским програмима других високошколских установа,
- да су резултати коректно наведени и
- да нисам кршио/ла ауторска права и користио интелектуалну својину других лица.

### **Потпис докторанда**

У Београду, / /2013

## Прилог 2.

### Изјава о истоветности штампане и електронске верзије докторског рада

Име и презиме аутора: **Muamar M. Benisa**

Број уписа: D 29/08

Студијски програм: Doktorske studije

Наслов рада :

### **INTEGRATED PROCESS PLANNING, DIE-DESIGN AND SIMULATION IN SHEET METAL RUBBER FORMING**

Ментор : Dr Bojan Babić, professor

Потписани : Muamar M. Benisa

изјављујем да је штампана верзија мог докторског рада истоветна електронској верзији коју сам предао/ла за објављивање на порталу **Дигиталног репозиторијума Универзитета у Београду.**

Дозвољавам да се објаве моји лични подаци везани за добијање академског звања доктора наука, као што су име и презиме, година и место рођења и датум одбране рада.

Ови лични подаци могу се објавити на мрежним страницама дигиталне библиотеке, у електронском каталогу и у публикацијама Универзитета у Београду.

**Потпис докторанда**

У Београду, / /2013

### Прилог 3.

#### Изјава о коришћењу

Овлашћујем Универзитетску библиотеку „Светозар Марковић“ да у Дигитални репозиторијум Универзитета у Београду унесе моју докторску дисертацију под насловом:

#### **INTEGRATED PROCESS PLANNING, DIE-DESIGN AND SIMULATION IN SHEET METAL RUBBER FORMING**

која је моје ауторско дело.

Дисертацију са свим прилозима предао/ла сам у електронском формату погодном за трајно архивирање.

Моју докторску дисертацију похрањену у Дигитални репозиторијум Универзитета у Београду могу да користе сви који поштују одредбе садржане у одабраном типу лиценце Креативне заједнице (Creative Commons) за коју сам се одлучио/ла.

1. Ауторство
2. Ауторство - некомерцијално
3. Ауторство – некомерцијално – без прераде
4. Ауторство – некомерцијално – делити под истим условима
5. Ауторство – без прераде
6. Ауторство – делити под истим условима

(Молимо да заокружите само једну од шест понуђених лиценци, кратак опис лиценци дат је на полећини листа).

**Потпис докторанда**

У Београду, / /2013

1. Ауторство - Дозвољавате умножавање, дистрибуцију и јавно саопштавање дела, и прераде, ако се наведе име аутора на начин одређен од стране аутора или даваоца лиценце, чак и у комерцијалне сврхе. Ово је најслободнија од свих лиценци.
2. Ауторство – некомерцијално. Дозвољавате умножавање, дистрибуцију и јавно саопштавање дела, и прераде, ако се наведе име аутора на начин одређен од стране аутора или даваоца лиценце. Ова лиценца не дозвољава комерцијалну употребу дела.
3. Ауторство - некомерцијално – без прераде. Дозвољавате умножавање, дистрибуцију и јавно саопштавање дела, без промена, преобликовања или употребе дела у свом делу, ако се наведе име аутора на начин одређен од стране аутора или даваоца лиценце. Ова лиценца не дозвољава комерцијалну употребу дела. У односу на све остале лиценце, овом лиценцом се ограничава највећи обим права коришћења дела.
4. Ауторство - некомерцијално – делити под истим условима. Дозвољавате умножавање, дистрибуцију и јавно саопштавање дела, и прераде, ако се наведе име аутора на начин одређен од стране аутора или даваоца лиценце и ако се прерада дистрибуира под истом или сличном лиценцом. Ова лиценца не дозвољава комерцијалну употребу дела и прерада.
5. Ауторство – без прераде. Дозвољавате умножавање, дистрибуцију и јавно саопштавање дела, без промена, преобликовања или употребе дела у свом делу, ако се наведе име аутора на начин одређен од стране аутора или даваоца лиценце. Ова лиценца дозвољава комерцијалну употребу дела.
6. Ауторство - делити под истим условима. Дозвољавате умножавање, дистрибуцију и јавно саопштавање дела, и прераде, ако се наведе име аутора на начин одређен од стране аутора или даваоца лиценце и ако се прерада дистрибуира под истом или сличном лиценцом. Ова лиценца дозвољава комерцијалну употребу дела и прерада. Слична је софтверским лиценцама, односно лиценцама отвореног кода.